

THREE DIMENSIONAL PRINTED CONTROLLED RELEASE TRITHERAPEUTIC TABLET (3D CRTT) FOR THE DELIVERY OF ANTI-HIV DRUGS

MARGARET SIYAWAMWAYA

A thesis submitted to the Faculty of Health Sciences, University of the Witwatersrand, Johannesburg, in fulfilment of the requirements for the degree of Doctor of Philosophy




Supervisor:
Professor Viness Pillay
Department of Pharmacy and Pharmacology, University of the Witwatersrand,
South Africa

Co-Supervisors:
Professor Yahya E. Choonara, Doctor Pradeep Kumar and Doctor Pierre P.D. Kondiah
Department of Pharmacy and Pharmacology, University of the Witwatersrand,
South Africa

Johannesburg, 2017

DECLARATION

I, Margaret Siyawamwaya, declare that this thesis is my own work. It has been submitted for the degree of Doctor of Philosophy in the Faculty of Health Sciences in the University of the Witwatersrand, Johannesburg. It has not been submitted before for any degree or examination at this or any other University.

.....

Signed this ..15th... day of September 2017

RESEARCH OUTPUTS

PUBLICATIONS

1. Siyavamwaya, M., Choonara, Y.E., Bijukumar, D., Kumar, P., du Toit, L.C., Pillay, V., 2015. A review: overview of novel polyelectrolyte complexes as prospective drug bioavailability enhancers. *International Journal of Polymeric Materials and Polymeric Biomaterials*, 65(11), 955–68.
2. Siyavamwaya, M., Choonara, Y.E., Kumar, P., Kondiah, P.P.D., du Toit, L.C., Pillay, V., 2016. A humic acid-polyquaternium-10 stoichiometric self-assembled fibrilla polyelectrolyte complex: Effect of pH on synthesis, characterization, and drug release. *Int Journal of Polymeric Materials and Polymeric Biomaterials*, 65(11), 550-60.
3. Siyavamwaya, M., Choonara, Y.E., Kumar, P., Kondiah, P.P.D., du Toit, L.C., Pillay, V., Synthesis, Comparison and Optimization of a Humic Acid-Quat10 Polyelectrolyte Complex by Complexation-Precipitation vs. Extrusion-Spheronization. *AAPS PharmSciTech*, November 2016.
4. Siyavamwaya, M., Choonara, Y.E., Kumar, P., Kondiah, P.P.D., du Toit, L.C., Pillay, V., Fabrication and comparison of humic acid and polyquaternium 10 tablets implementing 3D-Printing and direct tablet compression. Submitted to *International Journal of Pharmaceutics*.
5. Siyavamwaya, M., Choonara, Y.E., Kumar, P., Kondiah, P.P.D., du Toit, L.C., Pillay, V., Formulation of an anti-HIV 3D-Printed 'Controlled Release Tritherapeutic Tablet'. To be submitted to *Pharmaceutical Research*.

CONFERENCE PROCEEDINGS

1. Margaret Siyavamwaya, Viness Pillay, Yahya E. Choonara, Pradeep Kumar, Pierre P.D. Kondiah and Lisa C. du Toit. Humic acid/polyquaternium-10 novel stoichiometric self-assembled fibrous polyelectrolyte complex. **(Poster Presentation)**. The Academy of Pharmaceutical Sciences of the Pharmaceutical Society of South Africa (APSSA) Conference, Cedar Woods of Sandton, Conference Centre, Johannesburg, South Africa, 2015.
2. Margaret Siyavamwaya, Viness Pillay, Yahya E. Choonara, Pradeep Kumar, Pierre P.D. Kondiah and Lisa C. du Toit. The influence of complexation-precipitation and benchtop extrusion techniques on polyelectrolyte complex fabrication. **(Poster Presentation)**. The 7th Cross Faculty Post Graduate Symposium, University of the Witwatersrand, Johannesburg, South Africa, 2016.

3. Margaret Siyawamwaya, Viness Pillay, Yahya E. Choonara, Pradeep Kumar, Pierre P.D. Kondiah and Lisa C. du Toit. The use of a novel polyelectrolyte complex to enhance the aqueous solubility of a BCS class II anti-HIV drug. **(Poster Presentation)**. The Faculty of Health Sciences Research Day, University of the Witwatersrand, Johannesburg, South Africa, 2016.

4. Margaret Siyawamwaya, Viness Pillay, Yahya E. Choonara, Pradeep Kumar, Pierre P.D. Kondiah and Lisa C. du Toit. 3D printing of a novel humic acid and polyquaternium-10 polyelectrolyte complex for controlled oral drug release application. **(Poster Presentation)**. The International AAPS Annual Meeting and Exposition, Colorado Convention Centre, Denver, Colorado, USA, 2016.

PATENT FILED

Siyawamwaya M, Viness Pillay, Yahya E. Choonara, Pradeep Kumar P, Pierre P.D. Kondiah and Lisa C. du Toit. Polyelectrolyte complex-based oral drug delivery system for enhancing solubility and permeability properties of drugs in BCS class II/IV: SA Provisional Patent Application made.

ABSTRACT

Numerous pharmaceutical solid dosage form manufacturing techniques have emerged over the years and among them, 3D-Printing (3DP) has emerged as a highly attractive and versatile approach. 3DP is a cutting edge technology set to expand and revolutionize tablet manufacturing among various other applications in industry. The study reported in this thesis focuses on developing a humic acid-polyquaternium-10 (HA-PQ10) 3D-Printable ink for the delivery of three anti-HIV bioactives, efavirenz (EFV), tenofovir (TDF) and emtricitabine (FTC). HA was strategically employed based on its capability of entrapping both hydrophilic and hydrophobic drugs. PQ10 contributed towards the system's swellability in aqueous media. The HA-PQ10 PEC was responsible for retarding drug release therefore it behaved as a drug reservoir. Validation of HA-PQ10 complexation was carried out by synthesizing the HA-PQ10 polyelectrolyte complex (PEC) in aqueous media at pH 6, 7 and 8. The complexation yielded fibrilla and porous PECs. The PEC formation was attributed to ionic interactions between the quaternary ammonium centres (PQ10) and carboxylic groups (HA). The PECs were determined to be amorphous in nature and exhibited good biocompatibility when tested for cytotoxicity in human adenocarcinoma cell line (Caco2). The model drug, efavirenz (EFV) was loaded into HA-PQ10 using the complexation-precipitation (C-P) technique. The resultant EFV-loaded HA-PQ10 was compared to benchtop extrudates manufactured using the extrusion-spheronization (E-S) process. Assessment of the EFV saturation solubility and intestinal permeability showed EFV solubility and permeability enhancement of $14.14\pm 2.81\%$ and $61.24\pm 6.92\%$ respectively. The properties were compared to those of a marketed comparator product. Loading RTV into the optimized HA-PQ10 further validated the solubility and permeability enhancing properties in the BCS class IV drug as well. The extrudates performed superiorly compared to the formulation synthesized by C-P. The E-S technique was utilized to optimize HA-PQ10 based on drug release and intestinal permeation enhancement. The optimal HA-PQ10 was employed for 3DP of EFV-loaded HA-PQ10 into an oral tablet formulation. It was imperative to add cellulose acetate phthalate (CAP) to enhance the 3D-Printability of the HA-PQ10. CAP made the synthesized delivery system pH responsive and drug release results showed that most of the release occurred under intestinal conditions. The EFV-loaded 3DP tablet was compared to a tablet synthesized by direct compression. 3DP was more porous, less dense and more swellable than the direct compression tablet. These remarkable differences were attributed to the tableting method. 3DP leads to the formation of solid bridges between particles as the sludge (ink) undergoes extrusion and drying process. The direct compression technique involves axial powder compaction at high pressures which force particles to interact through Van der Waals forces or hydrogen bond formation. High drug loading of EFV was achieved and the tablet was further optimized to manufacture the 'controlled release tritherapeutic tablet', CRTT, a fixed dose combination (FDC) consisting of EFV, TDF and FTC. *In vivo* studies were conducted in large white pigs and CRTT absorption was compared to a marketed FDC, Atripla®. There was sustained release of EFV, TDF and FTC from CRTT and this was validated by the long residence times determined from pharmacokinetic analysis. EFV was maintained within the therapeutic index of the drug during the 24 hour study. Through this study, 3DP proved to be a technology with potential for manufacturing novel formulations. As more research is underway in the 3DP field, it can only be appreciated that its scope of use will continue to grow and restructure pharmaceutical manufacturing processes.

ACKNOWLEDGEMENTS

I would like to thank God for being with me always throughout this journey and giving me the strength to run the race to the end.

To my supervisor, Prof. Viness Pillay, I am most grateful for allowing me the great opportunity to join your research group where I have learnt many invaluable lessons and grown as a researcher. My heartfelt gratitude goes to my co-supervisors, Prof. Yahya Choonara, Mr Pradeep Kumar and Dr. Pierre Kondiah for providing guidance with my research project.

To Prof. Lisa du Toit and Dr. Thashree Marimuthu. I am grateful for your advice, support and always being available to help throughout the years. I would also like to thank Mr Sello Ramarumo, Mr Kleinbooi Mohlabi, Mr Bafana Temba, Ms Pride Mothobi, and Ms Phumzile Madondo for their technical assistance.

To my colleagues Poornima Ramburrun, Karmani Murugan, Fatema Bibi Choonara, Mpho Ngoepe, Gillian Mahumane, Sunaina Inderman, Mershen Govender, Latavia Singh, Pride Mothobi, Pakama Mahlumba, Johnel Giliomee, Priyamvada Pradeep, Lara Freidus, Lusanda Mapela, Avirup Chakraborty, Az-Zamakhshariy Zardad, Simphiwe Mavuso, Pariksha Kondiah, Steven Mufamadi, Nonhlanhla Masina, Felix Mashingaidze, Ahmed Seedat, Angus Hibbins, Samson Adeyemi, Khadija Rhoda, , Teboho Kgesa, Martina Manyikana, Kealeboga Mokolobate, Khadija Rhoda, Fatema Mia, Jonathan Pantshwa, Pierre Kondiah, Olufemi Akilo, Khuphukile Madida, Zikhona Hayiyana, Mduduzi Sithole, Patrick Komane and Gretta Mbityi-Ibouily thank you for all your help and support, I would not have made it without you.

I would like to acknowledge Prof. Kennedy Erlwanger and the staff at Central Animal Services (CAS), University of Witwatersrand for their dedication and assistance with *in vivo* studies.

This research would not have been successfully completed without financial assistance from the National Research Foundation (NRF).

I am more than grateful to my parents Ms Elizabeth Picardo, Mr Shepherd Siyawamwaya, Mrs Ruth Siyawamwaya and my siblings for their encouragement and for believing in me.

DEDICATION

This thesis is dedicated to my parents, Mr Shepherd Siyawamwaya and Ms Elizabeth Picardo, the giants on whose shoulders I stand.

ANIMAL ETHICS DECLARATION

I, Margaret Siyawamwaya, confirm that the study entitled “*In vivo* analysis of the 3DP CRTT in comparison to a marketed formulation in a large white pig” received the approval from the Animal Ethics Committee of the University of the Witwatersrand with ethics clearance number 2014/38/C (see Appendix C)

TABLE OF CONTENTS

DECLARATION.....	i
RESEARCH OUTPUTS	ii
PATENT FILED	iv
ABSTRACT	v
ACKNOWLEDGEMENTS	vi
DEDICATION	vii
LIST OF TABLES.....	xxv
LIST OF EQUATIONS	xxvi
LIST OF COMMONLY USED ABBREVIATIONS.....	xxvii

CHAPTER 1

INTRODUCTION AND MOTIVATION FOR THE STUDY	1
1.1. BACKGROUND TO THE STUDY	1
1.2. RATIONALE AND MOTIVATION FOR THE STUDY.....	3
1.3. OUTLINE OF THE SYSTEM.....	5
1.4. AIM AND OBJECTIVES OF THE STUDY	6
1.5. Overview of Thesis.....	7
1.6. REFERENCES	9

CHAPTER 2

2.1. INTRODUCTION	11
2.1.1. Polymeric polyelectrolyte complexes.....	13
2.2. METHODS OF SYNTHESIS OF POLYMERIC POLYELECTROLYTE COMPLEXES..	13
2.2.1. The solution method.....	13
2.2.2. Melt extrusion.....	14
2.2.3. Layer-by-layer self-assembly.....	14
2.3. FORMATION OF POLYELECTROLYTE COMPLEXES.....	16
2.3.1. Stoichiometric complexes.....	17
2.3.2. Non-stoichiometric complexes.....	18
2.4. POLYMERS USED IN POLYELECTROLYTE COMPLEXATION.....	20
2.5. MECHANISM OF DRUG RELEASE BY PECS	22
2.6. BIOAVAILABILITY ENHANCING TECHNIQUES ASSOCIATED WITH PECS	25
2.6.1. Techniques implemented to improve bioavailability	27
2.6.1.1. <i>Permeation enhancers</i>	28
2.6.1.2. <i>Microparticles</i>	29
2.6.1.3. <i>Nanoparticles</i>	30
2.6.1.4. <i>Gastroretentive controlled release systems</i>	32
2.6.2. Combination systems.....	33
2.7. CONCLUDING REMARKS	33
2.8. REFERENCES	34

CHAPTER 3

3.1. INTRODUCTION	44
3.2. MATERIALS AND METHODS	46
3.2.1. Materials	46
3.2.2. Determination of the humic acid concentration and functional group profiling.....	46
3.2.3. Determination of the self-assembly of humic acid and polyquaternium-10 to form the fibrilla PEC	47
3.2.4. Physicochemical characterization of the PEC and native components	47
3.2.4.1. Determination polyquaternium-10 concentration for stoichiometric ratio reaction with humic acid.....	47
3.2.4.2. Determination of polyquaternium-10 and humic acid electrostatic interactions	47
3.2.4.3. Assessment of the influence of simulated gastrointestinal fluids on the swelling and degradation of the PEC.....	48
3.2.4.4. Degree of crystallinity of polyquaternium-10, humic acid and the PEC	48
3.2.4.5. Determination of thermodynamic properties of the PEC	48
3.2.4.6. Analysis of the surface morphology and elemental quantification of the PEC and native components.....	48
3.2.4.7. In vitro drug release studies and drug loading capacity of the PEC	49
3.2.4.8 Determination of impact of the PEC on viability of Caco2 cell line	49
3.3. RESULTS AND DISCUSSION	50
3.3.1. Self-assembly nature of humic acid and polyquaternium-10 to form a fibrilla PEC	50
3.3.2. Evaluation of the humic acid concentration and presence of functional groups	51
3.3.3. Analysis of the polyquaternium-10 concentration for stoichiometric reactivity with humic acid.....	52
3.3.4. Elucidation of the polyquaternium-10 and humic acid electrostatic interactions.....	52
3.3.5. The influence of simulated gastrointestinal fluid on swelling and degradation of the PEC	53
Figure 3.5: PEC degradation and % swelling degree profiles of (a) F1, (b) F2 and (c) F3 in SGF and SIF.....	55
3.3.6. Degree of crystallinity of polyquaternium-10, humic acid and the PEC	55

3.3.7. Analysis of the thermodynamic properties of the PEC	57
3.3.8. Assessment of the surface morphology and elemental quantification	59
3.3.9. Evaluation of <i>in vitro</i> drug release and drug-loading within the PEC	61
3.3.10. Elucidation of the impact of HA, PQ10 and PEC on viability of Caco2 cells	63
3.4. CONCLUDING REMARKS	64
3.5. REFERENCES	65

CHAPTER 4

4.1. INTRODUCTION	69
4.2. MATERIALS AND METHODS	70
4.2.1. Materials	70
4.2.2. Synthesis of the drug-loaded Polyelectrolyte Complex (PEC)	70
4.2.2.1. <i>Complexation-Precipitation (C-P) via solution-blending of HA and PQ10</i>	70
4.2.2.2. <i>Extrusion-spheronization (E-S) via benchtop extruder and spheronizer</i>	71
4.2.3. Physicochemical and mechanical characterization of the drug-free HA-PQ10 PEC ..	71
4.2.3.1. <i>Assessment of the surface morphology</i>	71
4.2.3.2. <i>Complexation validation via PEC solubility testing in varying solvents</i>	71
4.2.3.4. <i>Determination of polyelectrolyte complex cytotoxicity</i>	71
4.2.4. Characterization of EFV-loaded HA-PQ10 PECs produced by E-S and C-P	72
4.2.4.1. <i>Influence of PEC synthesis method on the interaction of HA and PQ10</i>	72
4.2.4.2. <i>Determination of the thermal properties of PECs and physical mixture</i>	72
4.2.4.3. <i>Determining the extent of supersaturation and in vitro EFV release</i>	72
4.2.4.4. <i>Ex vivo permeability studies employing porcine small intestinal tissue</i>	73
4.2.5. PEC optimization via a Design of Experiments (DoE) approach.....	74
4.2.5.1. <i>Implementation of a randomized Box-Benkehn experimental design</i>	74
4.2.5.2. <i>Evaluation of extrudate flow properties of the HA-PQ10 PEC</i>	75
4.2.5.3. <i>Establishing the surface morphology and porosity of the optimized PEC</i>	75
4.3. RESULTS AND DISCUSSION.....	76
4.3.1. Outcome of PEC synthesis and physical variances between PEC(E-S) and PEC(C-P)	76
4.3.1.1. <i>Analysis of surface morphology of the PEC in compacted and powdered form</i>	76
4.3.1.2. <i>Validation of drug-free PEC complexation via solubility testing in varying solvents media</i>	77
4.3.1.3. <i>Assessment of the cytotoxicity of the PEC</i>	77
4.3.2. Characterization of EFV-loaded PEC synthesized by C-P and E-S	78
4.3.2.1. <i>The influence of complexation method on EFV, HA and PQ10 interactions</i>	78

4.3.2.2. Elucidation of the thermodynamic properties of the EFV-loaded PEC compared to drug-free PEC and physical drug/polymer mixtures	79
4.3.2.3. Evaluation of the extent of supersaturation and EFV release	81
4.3.2.4. Assessment of ex vivo intestinal tissue permeability of EFV from the PEC.....	82
4.3.3. Analysis of the experimental design and optimized PEC formulations	84
4.3.3.1. Analysis of the physical properties of the experimental design formulations.....	84
4.3.3.2. Analysis of PEC formulation variables on MDT and ex vivo drug permeability.....	86
4.3.4. Characterization of the optimized PEC formulation	88
4.3.4.1. Analysis of surface morphology and quantification of porosity of the extrudates.....	88
4.3.4.2. Evaluation of saturation solubility, drug release and permeability of the optimized PEC formulation.....	89
4.4. CONCLUDING REMARKS	91
4.5. REFERENCES	92

CHAPTER 5

5.1. INTRODUCTION	97
5.2. MATERIALS AND METHODS	98
5.2.1. Materials	98
5.2.2. Preparation and characterization of a 3D-Printable (HA-PQ10)-EFV sludge	98
5.2.2.1. <i>Determination of ideal excipients and solvents for 3DP sludge synthesis</i>	98
5.2.2.2. <i>Determination of polymer-drug interactions in EFV and the 3D-Printable sludges</i> ..	99
5.2.2.3. <i>Determination of thermal properties of EFV and 3D-Printable sludges</i>	99
5.2.2.4. <i>Determination of (HA-PQ10)-EFV sludge consistency</i>	99
5.2.3. Manufacture and physicochemical characterization of 3DP and direct compression tablets	100
5.2.3.1. <i>Synthesis of cylindrical tablets using 3DP and direct compression</i>	100
5.2.3.2. <i>Measurement of mechanical strength and polymer-EFV packing of 3DP and direct compression tablets</i>	100
5.2.3.3. <i>Porosimetric analysis undertaken on the 3DP and direct compression tablets</i> ..	101
5.2.3.4. <i>Mapping of matrix hydration kinetics and gravimetric analysis of the 3DP and direct compression tablets</i>	101
5.2.3.5. <i>Analysis of in vitro drug release of 3DP and direct compression tablets</i>	101
5.3. RESULTS AND DISCUSSION	102
5.3.1. Analysis of the synthesized 3D-Printable (HA-PQ10)-EFV sludge.....	102
5.3.1.1. <i>Assessment of the synthesis of a 3D-Printable sludge</i>	102
5.3.1.1. <i>Assessment of chemical and physical interactions in (HA-PQ10)-EFV sludge</i>	104
5.3.1.2. <i>Analysis of thermodynamic properties of (HA-PQ10)-EFV sludge</i>	105
5.3.1.3. <i>Assessment of the (HA-PQ10)-EFV sludge consistency</i>	106
5.3.2. Analysis of the tablet manufacturing process and physicochemical characterization of 3DP and direct compression tablets	107
5.3.2.1. <i>Determination of the tableting parameters for 3DP and direct compression</i>	107
5.3.2.2. <i>Assessment of mechanical strength and (HA-PQ10)-EFV packing in 3DP and direct compression tablets</i>	108

5.3.2.3. <i>Assessment of porositometric analysis of the 3DP and direct compression tablets</i>	108
5.3.2.4. <i>MRI mapping and gravimetric analysis of the 3DP and direct compression tablets</i>	110
5.3.2.5. <i>In vitro drug release profiles</i>	113
5.4. CONCLUDING REMARKS	115
5.5. REFERENCES	116

CHAPTER 6

6.1. INTRODUCTION	120
6.2. MATERIALS AND METHODS	121
6.2.1. Materials	121
6.2.2. Synthesis of 3DP fixed dose combination tablet.....	121
6.2.3. Determination of electrostatic stability between formulation components	122
6.2.4. Surface morphology characterization of 3DP tablet.....	122
6.2.5. Prediction of tablet matrix strength in simulated gastric and intestinal fluid.....	122
6.2.6. Determination of drug loading and the <i>in vitro</i> dissolution of CRTT and the conventional tablet.....	123
6.3. RESULTS AND DISCUSSION.....	123
6.3.1. Assessment of synthesis of the 3DP tablet.....	123
6.3.2. Analysis of any electrostatic interactions between the HA-PQ10 and the drugs	124
6.3.3. Analysis of CRTT surface morphology	125
6.3.4. Evaluation of the CRTT matrix strength prediction in gastric and intestinal fluid	126
6.3.5. Analysis of drug loading and the <i>in vitro</i> drug release profiles of 3DP CRTT and the conventional tablet.....	128
6.4. CONCLUDING REMARKS	130
6.5. REFERENCES	131

CHAPTER 7

7.1. INTRODUCTION	133
7.2. MATERIALS AND METHODS	134
7.2.1. Materials	134
7.2.2. Habituation of pigs at the animal unit.....	134
7.2.3. Experimental design and procedures on the white pigs.....	134
7.2.4. Administration of the 3DP CRTT and conventional via gastric gavage	135
7.2.5. Drug Quantification by Ultra Performance Liquid Chromatography Analysis	137
7.2.6. Ultra Performance Liquid Chromatography Parameters	138
7.2.7. Preparation of Standard Calibration Curve and the Liquid-Liquid Extraction Process	138
7.2.8. Determination of the pharmacokinetic profiles of drugs and 3DP CRTT <i>IVVC</i>	139
7.3. RESULTS AND DISCUSSION.....	139
7.3.1. Post-surgical and post-gavage evaluation of pigs.....	139
7.3.2. <i>In vivo</i> drug release profiles of 3DP CRTT and Atripla®.....	139
7.3.3. Evaluation of <i>in vivo</i> pharmacokinetics of EFV, TDF and FTC and their <i>IVVC</i> analysis	142
7.3.4. Assessment of <i>IVVC</i> of EFV, TDF and FTC in CRTT.....	146
7.4. CONCLUDING REMARKS	147
7.5. REFERENCES	148

CHAPTER 8

8.1. CONCLUSIONS.....	150
8.2. RECOMMENDATIONS AND FUTURE OUTLOOK.....	151

APPENDICES

9.1. APPENDIX A	152
9.1.1. Research Publications.....	152
9.1.1.1. <i>Review Paper</i>	152
9.1.1.2. <i>Research Paper 1</i>	153
9.1.1.3. <i>Research Paper 2</i>	154
9.2. APPENDIX B	155
9.2.1. Abstracts of Research Outputs at Conference Proceedings	155
9.2.1.1. <i>The Academy of Pharmaceutical Sciences of the Pharmaceutical Society of South Africa (APSSA) Conference, Cedar Woods of Sandton, Conference Centre, Johannesburg, South Africa, 2015. (Poster Presentation)</i>	155
9.2.1.2. <i>The 7th Cross Faculty Post Graduate Symposium, University of the Witwatersrand, Johannesburg, South Africa, 2016. (Poster Presentation)</i>	156
9.2.1.3. <i>The Faculty of Health Sciences Research Day, University of the Witwatersrand, Johannesburg, South Africa, 2016. (Poster Presentation)</i>	157
9.2.1.4. <i>The International AAPS Annual Meeting and Exposition, Colorado Convention Centre, Denver, Colorado, USA, 2016. (Poster Presentation)</i>	158
9.3. APPENDIX C	159
9.3.1. Animal Ethics Approval	159

LIST OF FIGURES

Figure 1.1: Schematic depicting the behaviour of CRTT in gastric and intestinal environments.....	6
Figure 2.1: Classification of polyelectrolyte complexes based on molecular architecture, composition and origin	12
Figure 2.2: Schematic representation of drug loading in a PEC and instability as a result of the presence of electrolytes (Kindermann <i>et al.</i> , 2011).....	14
Figure 2.3: Schematic representation of a) PEC formation in solution from oppositely charged polymers b) Melt extrusion and c) Layer-by- layer self-assembly.....	15
Figure 2.4: Carboxymethylcellulose and chitosan polyelectrolyte hydrogel and calcium phosphate biomimetic mineralization (Rodríguez <i>et al.</i> , 2011).	18
Figure 2.5: Illustrates classification of polymers based on source, charge, aqueous solubility and bio-adhesive force.....	22
Figure 2.6: Profile illustrating the drug release profile of Chitosan, Ghatti gum and Chitosan/Ghatti gum PEC (Reddy <i>et al.</i> , 2011)	23
Figure 2.7: Showing schematic representation of different steps involved in achieving bioavailability of a solid dosage form.....	27
Figure 2.8: Schematic illustrations of the presumed mechanism of the paracellular transport of insulin released from test nanoparticles (Sonaje <i>et al.</i> , 2009).....	29
Figure 2.9: Schematic representation of Insulin- chitosan PEC (Jintapattanakit <i>et al.</i> , 2007)	32
Figure 3.1: (a) Model structure of humic acid as proposed by Stevenson (Peña-Méndez <i>et al.</i> , 2005) and (b) general structure of polyquaternium-10 (Yang <i>et al.</i> , 2008)	46
Figure 3.2: (a) Digital pictures of the self-assembly of HA and PQ10 and the fibrous PECs collected by filtration before drying; (b) a schematic depicting the self-assembly process of the HA and PQ10.....	51
Figure 3.3: Viscosities of supernatants from complexes synthesized by adding different quantities of PQ10 to HA.....	52
Figure 3.4: FTIR spectra of (a) F1, F2 and F3 and (b) a comparison of F2 with HA and PQ10	53
Figure 3.5: PEC degradation and % swelling degree profiles of (a) F1, (b) F2 and (c) F3 in SGF and SIF.....	55
Figure 3.6: Powder X-Ray diffraction patterns for (a) F1, F2 and F3 and (b) a comparison of F2 with HA and PQ10	56
Figure 3.7: DSC thermograms for (a) F1, F2 and F3 and (b) a comparison of F2, HA and PQ10	57
Figure 3.8: TGA thermograms for (a) F1, F2 and F3 and (b) a comparison of F2, HA and PQ10	59
Figure 3.9: SEM images of (a) HA, (b) PQ10, (c) F1, (d) F2, (e) F3 at 2000x magnification	60
Figure 3.10: Elemental composition of (a) F1, (b) F2 and (c) F3 in comparison to HA and PQ10	61
Figure 3.11: EFV calibration curve	62
Figure 3.12: Drug release profiles of EFV-loaded F1, F2 and F3 in (a) SGF and (b) SIF.....	63
Figure 4.1: SEM images of drug-free PECs (a) PEC _(E-S) , (b) PEC _(E-S) (powdered), (c) PEC _(C-P) and (d) PEC _(C-P) (powdered) at x2000 magnification.....	77

Figure 4.2: Cell viability analysis of HA, PQ10 and drug-free PECs	78
Figure 4.3: FTIR spectra for (a) PEC-E _(E-S) and (b) PEC-E _(C-P)	79
Figure 4.4: DSC thermograms for (a) PEC-E _(E-S) and (a) PEC-E _(C-P)	81
Figure 4.5: (a) Drug release profiles and (b) porcine intestinal tissue permeation profiles for EFV formulations	83
Figure 4.6: Intestinal integrity analysis of EFV-loaded formulations (TEER in $\Omega \cdot \text{cm}^2 \times 10^4$) .	84
Figure 4.7: Schematic of the optimization desirability plots	87
Figure 4.8: Contour plots depicting the influence of granulating fluid and HA: PQ10 on (a) MDT and (b) flux	87
Figure 4.9: Surface morphology images of the EFV (a-c) and RTV (d-f) extrudates	88
Figure 4.10: Calibration curve for RTV	90
Figure 4.11: Graphs depicting (a) drug release profiles of EFV and RTV optimized formulations and (b) permeability profiles of EFV and RTV optimized formulations	91
Figure 5.1: 3D-Printing of HA-PQ10 sludge using the 3D-Bioplotter®	102
Figure 5.2: FTIR spectra depicting (HA-PQ10)-EFV interactions in 3D-Printable sludges at (HA-PQ10) : EFV ratios of 1:2, 1:1 and 2:1	105
Figure 5.3: DSC thermograms of 3D-Printable sludges at (HA-PQ10) : EFV ratios of 1:2, 1:1 and 2:1.....	106
Figure 5.4: Graphs depicting one-deformation tests of sludges (a) 3DP _{1:2} , (b) 3DP _{1:1} and (c) 3DP _{2:1}	107
Figure 5.5: Printing speed and extrusion pressure tuning to detect strand width using a 0.61mm injection nozzle.....	108
Figure 5.6: Isotherm linear plots of (a) 3DP _{1:1} tablet and (b) direct compression tablet depicting N ₂ adsorption (blue) and desorption (red) with inserts of SEM micrographs of tablets at x2000 magnification.....	110
Figure 5.7: MRI coronal plane imaging of (a) 3DP tablet and (b) direct compression tablet in SIF over 8 hours	111
Figure 5.8: Digital images of the dry 3DP and direct compression tablets before MRI and the hydrated tablets after MRI analysis	112
Figure 5.9: Gravimetric analysis of (a) 3DP and (b) direct compression tablets in SIF.....	113
Figure 5.10: Drug release profiles of 3DP tablet and direct compression tablet in 900mL SIF at 37°C over 8 hours	114
Figure 5.11: Proposed EFV-polymer particle arrangement in 3DP tablet and direct compression tablet.....	115
Figure 6.1: Digital images of results from two design attempts implemented.....	124
Figure 6.2: FTIR spectra of CRTT in relation to EFV, TDF, FTC and HA-PQ10	125
Figure 6.3: SEM images of CRTT at (a) surface of a strand at 80x magnification, (b) surface of a strand at 500x magnification, (c) inner pattern alignment of strands at 90° and (d) inner pattern alignment of strands at 60°.....	126
Figure 6.4: Digital Biotester images of CRTT, corresponding strains and Y-force graphs in (a) SGF and (b) SIF	127
Figure 6.5: Stress-strain graphs of (a) CRTT submerged in SGF, (b) initial linear curve in SGF, (C) CRTT submerged in SIF and (d) initial liner curve in SIF.....	128
Figure 6.6: UV calibration curves of (a) EFV, (b) TDF and (c) FTC	129
Figure 6.7: Drug release profiles of (a) EFV, (b) TDF and (c) FTC in CRTT compared to Atripla®.....	130
Figure 7.1: Digital images depicting the surgical procedure followed during catheterization	135

Figure 7.2: Digital images of gastric administration of CRTT and Atripla®.....	136
Figure 7.3: Flow diagram showing the <i>in vivo</i> study outline.....	137
Figure 7.4: Representative chromatogram of stock solution showing the UPLC detection and selectivity of EFV, TDF, FTC and DS.....	140
Figure 7.5: Calibration curves for (a) EFV, (a) TDF and (c)FTC.....	141
Figure 7.6: <i>In vivo</i> plasma drug concentrations for (a) EFV, (b) TDF and (c) FTC.....	142
Figure 7.7: Predicted <i>in vitro</i> release profiles and mean observed <i>in vivo</i> CRTT drug release profiles of (a) EFV, (b) TDF and (c) FTC.....	147

LIST OF TABLES

Table 2.1: Advantages and disadvantages of the methods of polyelectrolyte complex synthesis.....	16
Table 2.2: Examples of stoichiometric and non-stoichiometric polyelectrolyte complexes from previous studies.....	20
Table 2.3: Previous studies on drug-loaded polyelectrolyte complexes and their effect on drug release.....	26
Table 3.1: 2θ positions and % crystallinity obtained from XRD.....	56
Table 3.2: Viability of Caco2 cells treated with PECs and native polymers.....	64
Table 4.2: Flow properties of extrusion and spheronization of experimental design formulations.....	85
Table 4.3: Flux and permeability coefficient results of experimental design and optimized formulations.....	86
Table 4.4: BET and BJH analysis of optimized PECs.....	89
Table 5.1: screening formulation template for 3D-Printable sludge.....	103
Table 5.2: Pore volume and BET surface areas of 3DP and direct compression formulations.....	109
Table 7.1: Ultra Performance Liquid Chromatography gradient elution conditions.....	138
Table 7.2: Efavirenz extravascular compartmental model with Tlag.....	143
Table 7.3: Tenofovir disoproxil fumarate extravascular compartmental model with Tlag ...	144
Table 7.4: Emtricitabine extravascular compartmental model with Tlag.....	145

LIST OF EQUATIONS

Equation 3.1.....	48
Equation 3.2.....	49
Equation 3.3.....	50
Equation 4.1.....	73
Equation 4.2.....	74
Equation 4.3.....	74
Equation 4.4.....	75
Equation 4.5.....	75
Equation 4.6.....	75
Equation 4.7.....	76
Equation 4.8.....	76
Equation 4.9.....	90
Equation 5.1.....	100
Equation 5.2.....	101
Equation 5.3.....	112
Equation 7.1.....	139

LIST OF COMMONLY USED ABBREVIATIONS

3DP	Three dimensional printing
AESC	Animal ethics screening committee
ANOVA	Analysis of variance
ATR-FTIR	Attenuated Total Reflectance Fourier Transform Infrared Spectroscopy
AUC	Area under the curve
BCS	Biopharmaceutics Classification System
BET	Brunauer-Emmett-Teller
BHN	Brinell Hardness Number
CAP	Cellulose acetate phthalate
CAS	Central Animal Service
cE	Efavirenz comparator product
cR	Ritonavir comparator product
C-P	Complexation-precipitation
DC	Direct compression
DSC	Differential Scanning Calorimetry
EFV	Efavirenz
E-S	Extrusion-spheronization
FDC	Fixed dose combination
FTC	Emtricitabine
HA	Humic acid
MCC	Microcrystalline cellulose
MDT	Mean dissolution time
MRI	Magnetic Resonance Imaging
pE	Physical mixture of efavirenz and polymers
PEC	Polyelectrolyte complex
PEC _{C-P}	Polyelectrolyte complex synthesized by complexation-precipitation
PEC-E _{C-P}	Efavirenz-loaded polyelectrolyte complex synthesized by complexation-precipitation
PEC _{E-S}	Polyelectrolyte complex synthesized by extrusion-spheronization
PEC-E _{E-S}	Efavirenz-loaded polyelectrolyte complex synthesized by extrusion-spheronization
PEC-R _{E-S}	Ritonavir-loaded polyelectrolyte complex synthesized by extrusion-spheronization

PQ10	Polyquaternium-10
RTV	Ritonavir
SEM	Scanning Electron Microscopy
SGF	Simulated gastric fluid
SIF	Simulated intestinal fluid
TDF	Tenofovir
TGA	Thermal Gravimetric Analysis
UPLC	Ultra Performance Liquid Chromatography

CHAPTER 1

INTRODUCTION AND MOTIVATION FOR THE STUDY

1.1. BACKGROUND TO THE STUDY

Polyelectrolyte complexes (PECs) are increasingly being used to advance drug delivery. Their significant swellability in aqueous medium provides controlled drug release. PECs are formed by strong, but reversible ionic interactions between a cationic and anionic polymer (Lankalapalli and Kolapalli, 2009). Formation of PECs and their stability is determined by factors such as the polymer concentration, molecular weight, mixing ratio, nature of ionic groups, as well as temperature and pH of the reaction medium. The mechanism of drug release from PECs encompasses solution equilibration, ion exchange, charge interaction, gradual decomplexation or breakdown and dissolution (Moustafine *et al.*, 2008). The benefits of using PECs include protection of the drug from degradation in the gastrointestinal tract (GIT), reduced frequency of dosing due to controlled drug release, improved bioavailability of poorly soluble drugs and a subsequent reduction of both drug toxicity and side-effects. Controlled release of drug provides a steady plasma drug concentration which is essential to patients, reducing frequency of dosing improving patient compliance with least drug related toxicity.

Various polymers have been used to date, to manipulate the release kinetics of drug-loaded systems. However, it is more prudent to use PECs to achieve this since the properties of PECs have greater advantage over those of native polymers. For example, with a chitosan and polyacrylic acid (Carbopol®) complex, the presence of ammonium ion in the chitosan enables the formation of a PEC. Polyacrylic acid has limited use as a controlled release polymer due to its sensitivity to ionic environments and high water solubility while chitosan has rapid gastric acid dissolution. These challenges can be resolved when two polymers are combined to form a PEC (Sabar *et al.*, 2011). Polymeric drug delivery systems also prevent the crystallization of drugs within their matrices. This property is particularly essential for solid dispersions where the amorphous form of the drug is liable to recrystallization over time, thus reducing the solubility of the drug (Qian and Bogner, 2012).

PECs may be synthesised by the titration method. However, the main drawback is the dilution of the solution into which the other polymer is titrated, therefore changing the concentration of the solution. Another method that has been used is jet mixing where the jet mixer generates two opposing jets which collide in a mixing chamber at high velocity and

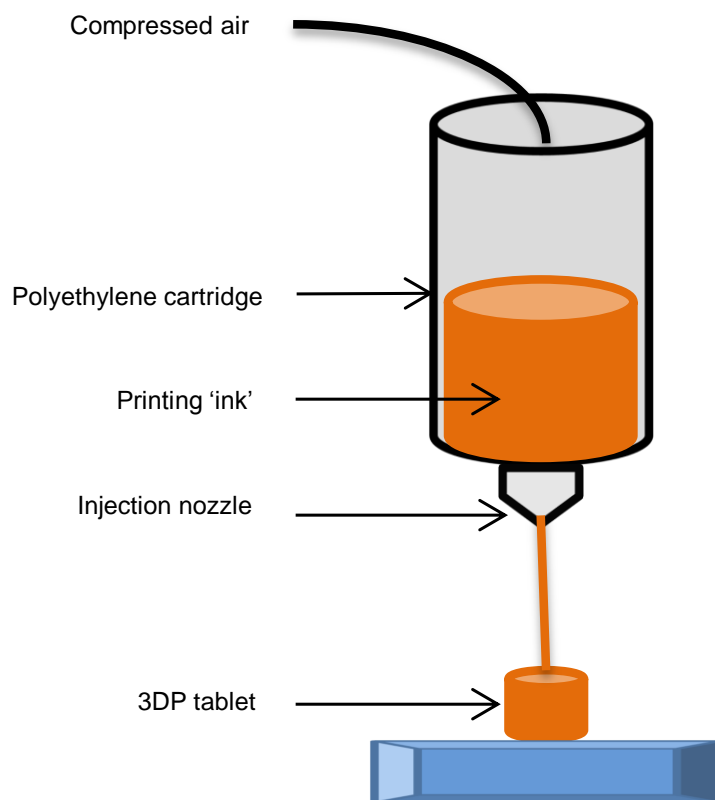
pressure resulting in brief mixing times (Ankerfors *et al.*, 2010). Drug-loaded PECs can also be prepared by extrusion where pressure and agitation are applied that mixes the materials by forcing them through a die (Wilson and Williams, 2012). This process has been used to improve the solubility of drugs through the formation of amorphous or crystalline dispersions. After extrusion, drug particle size is reduced which leads to faster dissolution rate. Extrusion can also be combined with heating, resulting in melt extrusion technique (Shah *et al.*, 2012).

The solvent evaporation method is a highly attractive method employed for preparing drug-loaded solid dispersions. The drug and polymers are dissolved in a common solvent which is then evaporated leaving a homogenous solid dispersion of the drug in the polymeric matrix. Allowing the continuous evaporation of the common solvent, maximizes the drug loading efficiency due to the elimination of drug-solvent interaction which could be stronger than drug-polymer interaction (Preisig *et al.*, 2014). This method has successfully been used to synthesize PECs due to the ionization of individual polymers in the selected common solvent (Yusif *et al.*, 2014; Zhao *et al.*, 2011).

The Biopharmaceutics Classification System (BCS) is used to classify drugs based on their aqueous solubility and intestinal permeability. It is used to set drug product dissolution standards so as to determine any *in vitro-in vivo* correlations (IVIVC). Class I drugs have high solubility and permeability, class II drugs exhibit low solubility and high permeability, class III drugs exhibit high solubility but poor permeability while class IV drugs have both poor solubility and permeability (FDA, 2000). Examples of drugs within this class (class IV) include anti-HIV drugs, specifically protease inhibitors (PIs) and non-nucleoside reverse transcriptase inhibitors (NNRTIs) (Breckenridge, 2005). Some of the novel drug delivery approaches developed to improve the delivery of BCS class II and IV anti-HIV drugs are slow release, bio-adhesive and enteric coated systems (Ojewole *et al.*, 2008).

This study utilized the PEC system that enhances the solubility and permeability of drugs to synthesize a 3D-Printed (3DP) tablet containing a fixed dose combination (FDC) of anti-HIV drugs with the aid of 3D Bioplotter® (EnvisionTEC GmbH, Gladbeck, Germany). FDCs are one of the contemporary principal ways that have been implemented to simplify as well as to improve the effectiveness of anti-HIV regimens. FDCs offer advantages such as improved patient compliance to medication, lower medication costs, the circumvention of inaccurate dosing by patients, and reduced risks of side-effects (Chrysant, 2008). Application of the humic acid/ polyquaternium-10 polyelectrolyte complex (HA-PQ10 PEC) will be extended to drugs falling within any BCS class.

3DP is a recent revolutionary and advanced rapid prototyping technique which is highly beneficial to the pharmaceutical industry. It produces solid three dimensional objects such as tablets of any shape using additive layer manufacturing instructed by computer aided design (CAD) (Goyanes *et al.*, 2015; Wu *et al.*, 2009). Drawing on this technology leads to simplified, yet improved quality of drug formulations that are manufactured at increased speed and lower costs. Figure 1.1 depicts the manufacture of a 3DP tablet using an extrusion based 3D-Bioplotter®.



3DP tablet manufacture by sludge extrusion from cartridge onto the build platform

Figure 1.1: Schematic representation of 3DP process

1.2. RATIONALE AND MOTIVATION FOR THE STUDY

FDC drugs presently available have eliminated the pill burden associated with the oral administration of anti-HIV drugs (Nachegea *et al.*, 2014). However, there are still challenges associated with these drugs, and these include: **1)** the drugs in the FDC which fall in BCS class II, III and IV exhibit poor bioavailability due to poor solubility and/or permeability, **2)** patients experience difficulties in swallowing the single dose tablet due to the size of the formulation, **3)** formulations with ideal solubility and permeability properties (BCS class I drugs) still present with short half-lives and require multiple daily dosing and **4)** there is

degradation and less than optimal absorption of the anti-HIV drugs exposed to the gastric environment. The complexation-precipitation and extrusion-spheronization methods were utilized to synthesize the drug-loaded HA-PQ10 complex. However, a feasible technique which further reduced the unnecessary use of excipients and yet maintained enhanced drug solubility and permeation while supporting the use of natural polymers had to be implemented hence the use of the 3D Bioplotter®. The 3D Controlled Release Tritherapeutic Tablet (3D-CRTT) led to the fabrication of a novel system with the following applications:

- Effective delivery of drugs with poor solubility and poor permeability and therefore increasing their bioavailability.
- Effective treatment of chronic conditions such as HIV where reduced dosing frequency encourages patient compliance.
- Formulation of multiple drugs into one delivery system.
- Lowering the pill burden by combining a multi-drug regimen into an FDC.
- Effective delivery of drugs, regardless of BCS classification which leads to reduced toxicity due to the administration of lower drug concentrations *in vivo*.
- Facilitating the stability of solid dispersions.
- Site-specific delivery of gastro-sensitive drugs including proteins and peptides.
- Fabrication of a delivery system that will provide sustained drug release; this is beneficial in preventing subtherapeutic drug levels as well as toxicity from drugs with a narrow therapeutic index.

Two polymers of opposite net charges were utilized to fabricate a PEC in order to investigate the possibility of superior controlled release of the drug molecules. It was imperative to select polymers that would improve drug wettability therefore increasing drug solubility (Conte *et al.*, 2005; Hossel *et al.*, 2000). Both hydrophilic and hydrophobic drugs were loaded into the novel complex due to the presence of a hydrophilic PQ10 and amphiphilic HA. Entrapment of the drugs would occur in the hydrophobic core of HA. PQ10, being more hydrophilic attracted more fluid to the system therefore creating a microenvironment that enhanced the solubility of the molecularly dispersed drugs. Entrapment of the drugs in the aromatic core of HA would improve their permeation across the pig intestinal tissue when undertaking animal studies.

3DP of HA-PQ10 targeted at designing a delivery system which would successfully encapsulate drugs from all the BCS classes. The extended release of BCS class III drugs is a challenge due to poor permeability (Chakraborti *et al.*, 2014). Unlike conventional methods which offer a singular drug release profile, 3DP allows for the formulation of various

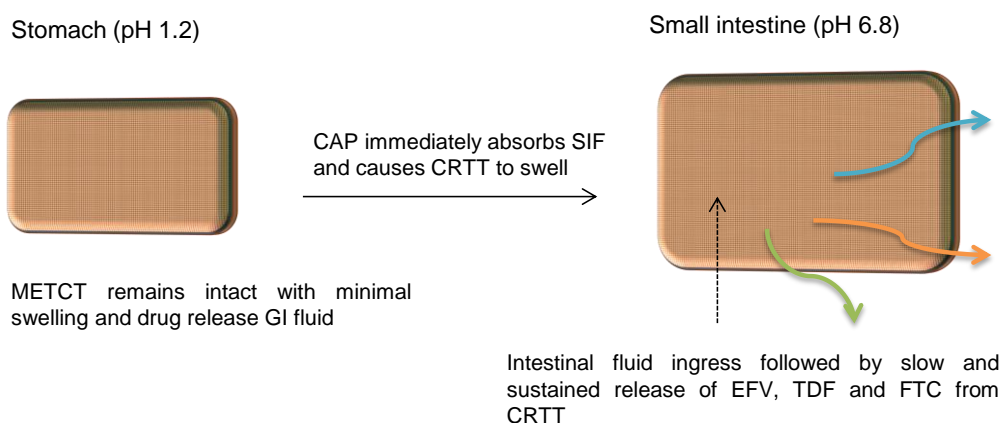
polymeric systems with sophisticated and reproducible drug release profiles with the benefit of reduced risk of inter-subject variation. It offers flexible tableting with customized shapes according to the desired design making it ideal for purposes such as chronotherapy. Precise location, distribution and dosage of the desired drug can be achieved. 3DP facilitates the synthesis of a multilayered formulation which is resistant to delamination. The production steps can be consolidated into one technique and enteric polymers included into the outer layer of the tablet eliminating procedures such as coating (Yu *et al.*, 2008). The novel aspects of this study are as follows:

1. The system was formulated using a novel polyelectrolyte complex of two natural and cost-effective polymers.
2. Drug-loaded HA-PQ10 PEC has proven its effectiveness in enhancing aqueous solubility and intestinal permeability of BCS class II and IV drugs. The PECs will cause the same effect on drugs in BCS class I and III.
3. The use of heat is not necessary with the bioplotter. This makes it possible to synthesize delivery systems with HA-PQ10 PEC which are natural polymers. These polymers melt at very high temperatures and are unsuitable for methods requiring heat. Thermolabile drugs may be safely formulated.
4. Utilizing the unique pharmacotechnical properties of 3DP will allow for the formulation of an FDC, regardless of drug compatibilities, with each drug loaded into a separate layer. An FDC that will be explored includes tenofovir (BCS class III) /emtricitabine (BCS class I)/ efavirenz (BCS class II).
5. An additional polymer, cellulose acetate phthalate (CAP) was included to facilitate the 3DP process. This thermoplastic and enteric polymer has good mechanical compatibility with natural polymers.
6. Incorporating a 'smart' polymer such as CAP served the purpose of making a viscous binder paste of the materials for printing. The polymer facilitates gastroprotection and enteric release of the drugs.
7. The tablet mainly released the drugs in the small intestine, the largest portion for effective drug absorption.

1.3. OUTLINE OF THE SYSTEM

The anti-HIV drugs, EFV, TDF and FTC were combined into an FDC and formulated as a 3DP tablet. Figure 1.2 depicts the mechanism of action of CRTT. This was achieved by synthesizing a sludge which made the drug-loaded HA-PQ10 PEC 3D-Printable. The sludge was a smooth homogenous consistency capable of being extruded out of the sample holder. The optimized tablet shape and design took into consideration the loading capacity of the

drugs encapsulated and the ability to contain pores for ease of significant fluid ingress. The 3DP tablet remained structurally intact with minimal swelling and drug release in gastric conditions. This property was attributed to the inclusion of a smart polymer, CAP which is an enteric polymer. Drugs were protected from gastric degradation and most of the release occurred in the small intestine, the site for maximum absorption. Once the system reached the small intestine, CAP allowed more fluid into the system hence increasing wettability of drugs and leading to increase in solubility and consequently enhancing drug bioavailability. Use of HA-PQ10 PEC ensured that the drugs are released in a controlled manner, a highly attractive feature for drugs falling in BCS class I and class III. The selected polymers, HA and PQ10 contributed to enhancing the bioavailability by increasing the permeability of the drugs.



Mechanism of action of CRTT: CRTT will pass through the stomach intact due to gastroprotection from the pH-sensitive CAP. Increase in pH as the tablet enters the small intestine leads to more intestinal fluid entering the tablet and causing swelling. Efavirenz (EFV), tenofovir (TDF) and emtricitabine (FTC) will simultaneously be gradually released from the drug-loaded HA-PQ10. The presence of pores included in the tablet design will lead to greater contact of the delivery system with enteric fluid.

Figure 1.2: Schematic depicting the behaviour of CRTT in gastric and intestinal environments

1.4. AIM AND OBJECTIVES OF THE STUDY

The aim of this study was to develop a 3DP Controlled Release Tritherapeutic Tablet (3D-CRTT), synthesized with a novel polyelectrolyte complex to achieve programmed and targeted enteric release of an anti-HIV FDC over 24 hours. The system was capable of extending the stability of the drugs embodied in the solid dispersions and enhancing their bioavailability as an FDC.

Objectives achieved:

1. Determination of the elemental composition of the individual polymers and the PECs. The complex was expected to contain elements from both polymers; however, the complexation process was affected by the pH of the surrounding medium with alkaline media being the ideal one for complexation. Implementation of 3DP for formulating CRTT provided for exposure of the PEC in enteric fluid.
2. Validation of the complexation process by determining dissolution of the complexes in various solvents. Stoichiometric PECs do not easily dissolve in solvents therefore the different types of solvents were tested to validate that a stoichiometric PEC had been synthesized.
3. Selection of appropriate polymers (HA and PQ10) of opposite charges that could form a polyelectrolyte complex as well enhance the solubility and permeability of drugs.
4. Determination of an ideal technique for synthesizing the FDC. Different methods of fabricating a drug-loaded PEC were explored such as complexation-precipitation technique and benchtop extrusion-spheronization. 3DP emerged superior to all these methods and was therefore utilized to formulate the FDC.
5. Determination of appropriate thermoplastic polymer and solvents as well their quantities to be used as the 3D-Printable biomaterial. Ideal parameters such as speed and pressure of extrusion were determined.
6. Design of CRTT shape and dimensions considering doses of the three drugs as well as desired release pattern.
7. Characterization of the 3DP tablets employing tests such as the determination of electrostatic interactions (FTIR), mechanical tensile strength (BioTester), Magnetic Resonance Imaging (MRI), surface morphological properties (SEM), thermal and thermodynamic properties (DSC and TGA), tablet hardness (Textural profiling), and presence and quantity of pores on tablets (Porosity analysis).
8. Conduction of *in vitro* drug release studies in biorelevant media to assess the controlled release behaviour of HA-PQ10 PEC.
9. Undertaking *in vivo* studies using a pig model to ascertain the pharmacokinetic and pharmacodynamic properties of the drug delivery system.
10. Ascertainning *in vitro-in vivo* (IVIVC) correlation of the drug release profiles utilizing statistical analysis to determine the predictable release characteristics of HA-PQ10.

1.5. OVERVIEW OF THESIS

Chapter One of this thesis highlights the background of the study and rationale. The aim and objectives of the study are discussed in detail.

Chapter Two is a detailed literature review of the synthesis and applications of polyelectrolyte complexes (PECs) in drug delivery. The review provides a background to classification of PECs and an insight to common methods and polymers used in their synthesis. The advantages and disadvantages of utilizing these methods are also highlighted. There is an in-depth explanation of the formation of PECs and important factors that should be present for this process to take place. The mechanism of drug release and bioavailability enhancing techniques of PECs are further highlighted.

Chapter Three is a preformulation study focussing on the validation of complexation between humic acid and polyquaternium-10. The complexation-precipitation method is discussed with reference to the concentrations of the polymers required for stoichiometric complexation. The biocompatibility of the system was ascertained using Caco2 cell line. Drug release evaluation of the PEC was tested utilizing efavirenz as a model drug.

Chapter Four explores another complexation technique, the benchtop extrusion-spheronization. The outcome from the extrusion process was compared to the complexation-precipitation method. The extrusion method gave superior results and was selected for optimization implementing a Box-Benkehn design of experiments (DoE).

Chapter Five outlines procedures undertaken for synthesis of 3DP HA-PQ10 tablet. This chapter emphasizes on various parameters for EFV-loaded HA-PQ10 3DP. A list of unsuccessful formulations is also provided. The 3DP tablets are further compared to tablets synthesized by a traditional method, direct compression to ascertain any need for 3DP. The superior nature of 3DP is discussed.

Chapter Six underscores the design and fabrication of the fixed dose combination. This chapter provides a prediction of the mechanical properties of the tablet *in vivo*. The *in vitro* performance of the tablet in comparison to a similar commercial product is also discussed.

Chapter Seven focusses on the *in vivo* study of CRTT in comparison to a marketed FDC with the same drug combination. A pig model was selected for this study describing pharmacokinetic and pharmacodynamic properties of the CRTT. Pharmacokinetic modelling analysis and (*IV/VC*) correlation of the results are further provided in this chapter.

Chapter Eight is a conclusion to the study. Future recommendations based on findings of this study are highlighted.

1.6. REFERENCES

- Ankerfors, C., Ondaral, S., Wågberg, L., Ödberg, L., 2010. Using jet mixing to prepare polyelectrolyte complexes: Complex properties and their interaction with silicon oxide surfaces. *Journal of Colloid and Interface Science*, 351(1), 88–95.
- Breckenridge, A., 2005. Pharmacology of drugs for HIV. *Medicine*, 33(6), 30-1.
- Chakraborti, C.K., Sahoo, S., Behera, P.K., 2014. Role of different biodegradable polymers on the permeability of ciprofloxacin. *Journal of Advanced Pharmaceutical Technology and Research*, 5(3), 140.
- Chrysant, S.G., 2008. Using fixed-dose combination therapies to achieve blood pressure goals. *Clinical Drug Investigation*, 28(11), 713-34.
- Conte, P., Agretto, A., Spaccini, R., Piccolo, A., 2005. Soil remediation: humic acids as natural surfactants in the washings of highly contaminated soils. *Environmental Pollution*, 135 (5), 515-522.
- Goyanes, A., Buanz, A.B., Hatton, G.B., Gaisford, S., Basit, A.W., 2015. 3D printing of modified-release aminosalicylate (4-ASA and 5-ASA) tablets, *European Journal of Pharmaceutics and Biopharmaceutics*, 89, 157-162.
- Hossel, P., Dieing, R., Norenberg, R., Pfau, A., Sander, R., 2000. Conditioning polymers in today's shampoo formulations-efficacy, mechanism and test methods. *International Journal of Cosmetic Science*, 22(1), 1-10.
- Lankalapalli, S., Kolapalli, V.M., 2009. Polyelectrolyte complexes: A review of their applicability in drug delivery technology. *Indian Journal of Pharmaceutical Sciences*, 71(5), 481.
- Moustafine, R.I., Margulis, B.E., Sibgatullina, L.F., Kemenova, V.A., Van den Mooter, G., 2008. Comparative evaluation of inter-polyelectrolyte complexes of chitosan with Eudragit L100 and Eudragit L100-55 as potential carriers for oral controlled drug delivery. *European Journal of Pharmaceutics and Biopharmaceutics*, 70(1), 215–25.
- Nachega, J.B., Parienti, J.J., Uthman, O.A., Gross, R., Dowd, D.W., Sax, P.E., Giordano, T.P., 2014. Lower pill burden and once-daily dosing antiretroviral treatment regimens for HIV infection: a meta-analysis of randomized controlled trials. *Clinical Infectious Diseases*, eiu046.
- Ojewole, E., Mackraj, I., Naidoo, P., Govender, T., 2008. Exploring the use of novel drug delivery systems for antiretroviral drugs. *European Journal of Pharmaceutics and Biopharmaceutics*, 70(3), 697–710.
- Preisig, D., Haid, D., Varum, F.J., Bravo, R., Alles, R., Huwyler, J., Puchkov, M., 2014. Drug loading into porous calcium carbonate microparticles by solvent

evaporation. *European Journal of Pharmaceutics and Biopharmaceutics*, 87(3), 548-58.

- Qian, K.K., Bogner, R.H., 2012. Application of mesoporous silicon dioxide and silicate in oral amorphous drug delivery systems. *Journal of Pharmaceutical Sciences*, 101(2), 444-63.
- Sabar, M.H., Samein, L.H., Sahib, H.B., 2011. Some Variables Affecting the Formulation of Ketoprofen Sustained Release Tablet using Polyelectrolyte Complex as a Matrix Former. *Journal of Pharmacy and Allied Health Sciences*, 1, 1-15.
- Shah, S., Maddineni, S., Lu, J., Repka, M.A., 2013. Melt extrusion with poorly soluble drugs. *International journal of pharmaceutics*, 453(1):233-52.
- U.S. Department of Health and Human Services, Food and Drug Administration Center for Drug Evaluation and Research (CDER), Waiver of *In Vivo* Bioavailability and Bioequivalence Studies for Immediate-Release Solid Oral Dosage Forms Based on a Biopharmaceutics Classification System, Guidance for Industry, 2000.
- Wilson, M., Williams, M.A., Jones, D.S., Andrews, G.P., 2012. Hot-melt extrusion technology and pharmaceutical application. *Therapeutic delivery*, 3(6), 787-97.
- Wu, W., Zheng, Q., Guo, X., Sun, J., Liu, Y., 2009. A programmed release multi-drug implant fabricated by three-dimensional printing technology for bone tuberculosis therapy. *Biomedical Materials*, 4(6), 06500.
- Yu, D.G., Zhu, L.M., Branford-White, C.J., Yang, X.L., 2008. Three-dimensional printing in pharmaceutics: Promises and problems. *Journal of pharmaceutical sciences*, 97(9), 3666-90.
- Yusif, R.M., Abu Hashim, I.I., El-Dahan, M.S., 2014. Some variables affecting the characteristics of Eudragit E-sodium alginate polyelectrolyte complex as a tablet matrix for diltiazem hydrochloride. *Acta Pharmaceutica*, 64(1), 89-104.
- Zhao, Q., An, Q., Qian, J., Wang, X., Zhou, Y., 2011. Insight into fractal self-assembly of poly (diallyldimethylammonium chloride)/sodium carboxymethyl cellulose polyelectrolyte complex nanoparticles. *The Journal of Physical Chemistry B*, 115(50), 14901-11.

CHAPTER 2

A REVIEW: OVERVIEW OF NOVEL POLYELECTROLYTE COMPLEXES AS PROSPECTIVE DRUG BIOAVAILABILITY ENHANCERS

2.1. INTRODUCTION

Polymeric materials which are sensitive to specific conditions such pH, temperature, magnetic and electric fields have become highly attractive in the field of drug delivery (Liechty and Kryscio, 2010; Torchilin 2009). These transitions are primarily due to the alterations in the charged groups by the interaction of oppositely charged polymers, changes in the efficiency of hydrogen bonding at higher temperature or ionic strength, etc., and they lead to the development of a new pharmaceutical platform with improved physico-chemical properties. The interaction of two oppositely charged polymers leads to the formation of a complex system, generally called a polyelectrolyte complex (PEC).

In PEC formation, strong electrostatic attractions occur without the aid of reaction initiators, catalysts or crosslinkers. The elimination of these additives renders most PECs non-toxic and easy to make and this lowers the cost in research and development of drug formulations (Lee *et al.*, 1999). Furthermore, some polymers cannot be effectively used for drug delivery unless they form a complex. For example, the use of a polyacrylic acid matrix usually results in immediate drug release and this property is attributed to its sensitivity to ionic environments and high water solubility. Chitosan is another polymer which has fast gastric acid dissolution. However, these challenges are resolved when the two polymers form a PEC. The presence of the positively charged ammonium ions in chitosan facilitates the formation of the PEC (Sabar *et al.*, 2011; Chen *et al.*, 2010; Risbud *et al.*, 2000).

In recent years, polyelectrolyte complexes have obtained considerable attention in the field of drug delivery because of their biocompatibility, biodegradability and their ability to improve the bioavailability of the active molecule (Heinen *et al.*, 2013). *In situ*, PECs are hydrogel in nature and this property closely resembles biological tissue hence their safety *in vivo* (Chang *et al.*, 2014; Calija *et al.*, 2013). Plasma drug concentrations can be increased thereby improving the cost-effectiveness of drugs and it will also become possible to administer lower doses of drugs (Thanou *et al.*, 2001).

There are various types of polyelectrolyte complexes such as, but are not limited to, polymer-polymer, polymer-drug, polymer-drug-polymer and polymer-protein complexes

(Petzold and Simona, 2014). In order to form the complex, one component has to be positively charged while the other is negatively charged. PECs are generally classified based on origin, composition and molecular architecture as shown in Figure 2.1 (Lankalapalli and Kolapalli, 2009).

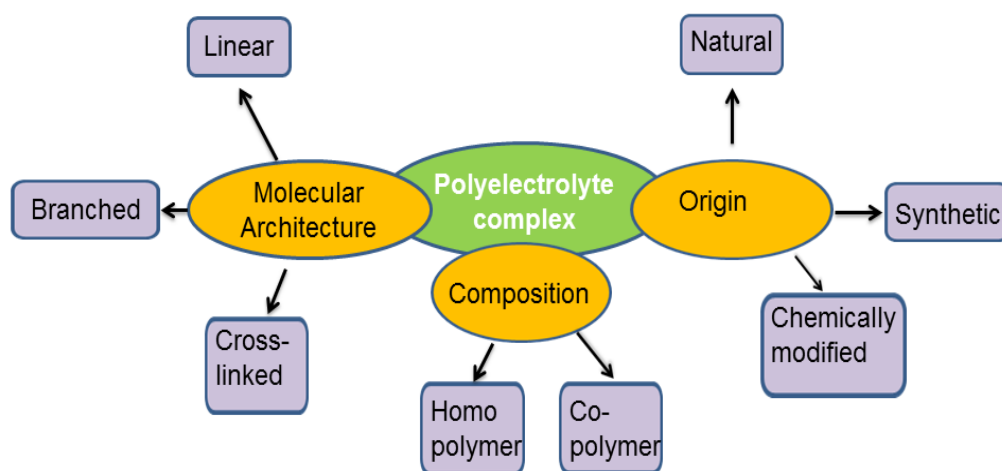


Figure 2.1: Classification of polyelectrolyte complexes based on molecular architecture, composition and origin

Polymer-drug together with polymer-drug-polymer complexes have been used to improve the encapsulation efficiency of drugs as well as to control the rate of drug release due to the bonds that form between the polymer and the drug (Cheow and Hadinoto, 2012). High encapsulation efficiency will lower the amount of excipients required in a formulation. Polymers are being widely used in drug delivery since they can achieve drug delivery at the intended site thus reducing unwanted side effects (Soppimath *et al.*, 2001). On the other hand, proteins can form strong electrostatic bonds with polymers regardless of their isoelectric point and they form either soluble, insoluble or amorphous complexes (Vries *et al.*, 2003). These complexes are useful for purposes such as protein separation, immobilization or enzyme stabilization (Xu *et al.*, 2011).

The aim of this review is to report on the vast research in literature that has been carried out and which centres on PECs formed by means of self-assembly between oppositely charged polymers and their contribution towards enhancing the bioavailability of drugs. The specific mechanism of drug release by PECs will also be highlighted. An increase in the amount of drug reaching the systemic circulation in systems utilizing PECs has been noted and this article seeks to clarify whether this increase is entirely as a result of encapsulating the drug in PECs or whether it is also due to any other mechanisms present in the system.

2.1.1. Polymeric polyelectrolyte complexes

PECs generally present with the advantage of combining unique physicochemical properties from the polymers involved and this property attributes to their novelty. Consequently, they form delivery systems with gradual drug release and good swelling capacity (Argin-Soysal *et al.*, 2009). It has been stipulated that the high pH-sensitive swelling of PECs renders them applicable for oral drug delivery (Li *et al.*, 2013). Polymeric PECs have biomedical applications as powders, membranes, sponges, spheres, fibers, gels or in solution depending on their intended use (Bernabe *et al.*, 2005).

2.2. METHODS OF SYNTHESIS OF POLYMERIC POLYELECTROLYTE COMPLEXES

2.2.1. The solution method

This is a widely used method of PEC synthesis where the polymers are completely dissolved in solvents or water before they are mixed together. In most cases, water is the solvent of choice and minimizing the use of organic solvents gives impetus for using PECs in pharmaceutical industries. The polymers have to be charged in order to facilitate PEC formation which occurs by the electrostatic interaction between oppositely charged polyions in solution. Incorporation of the drug into a PEC may occur by one of the following ways:

- 1) Adding the drug as the PEC precipitates out of the solution
- 2) Addition of the drug into the PEC that has already formed
- 3) Addition of the drug to either of the polymers with the same charge before the PEC forms (Lankalapalli and Kolapalli, 2009).

Drug entrapment is influenced by the polymer ratios or whether the resulting PEC is loosely or tightly clustered (Vries *et al.*, 2003). Figure 2.2 below illustrates how an active pharmaceutical ingredient (API) can be incorporated into a PEC. The PEC can be solubilized by the presence of an electrolyte (sodium chloride) in solution.

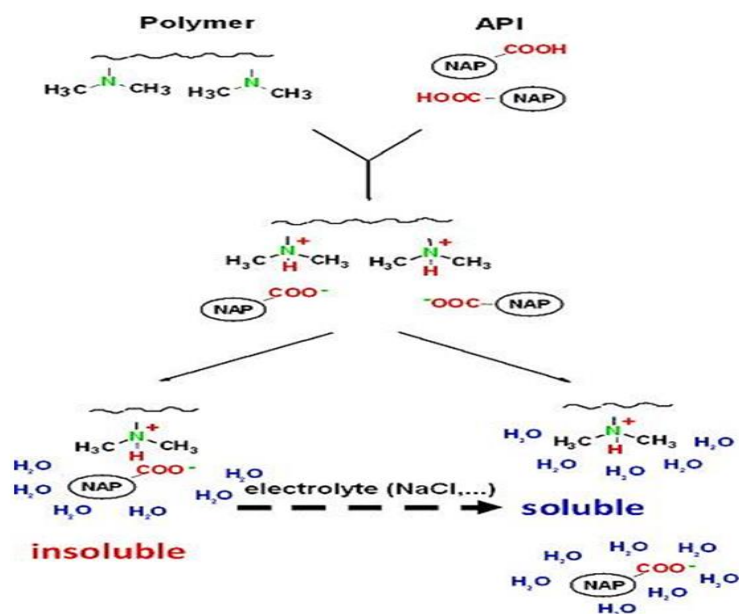


Figure 2.2: Schematic representation of drug loading in a PEC and instability as a result of the presence of electrolytes (Kindermann *et al.*, 2011)

2.2.2. Melt extrusion

Melt extrusion involves the use of an extruder that melts and mixes the polymers and excipients together using heat, pressure and agitation. This mixture is then forced out through a die in the form of soft rods. The drug, polymers and other excipients are mixed physically before being loaded into the extruder. This is illustrated in Figures 2.3(a) and (b) below. This method does not require the use of solvents to make the complexes containing the drug. The drug is molecularly dispersed within the polymers and this leads to the enhancement of its solubilization since the crystal lattice does not need to be broken (Kindermann 2012; Vasconcelos *et al.*, 2007). Miscibility of the drug with the polymers determines the extent of the formation of intermolecular interactions. It has been noted that the melt extrusion process leads to an increase in the bioavailability of drugs since it forms amorphous and stable solid dispersions of the drug within a polymer matrix. Controlled release together with improved solubility of the drug can be achieved (Janssens and Van den Mooter, 2009).

2.2.3. Layer-by-layer self-assembly

With this method, successive layers of cationic and anionic polymers are deposited onto a solid substrate such as silica particles (Mihai *et al.*, 2013). The multilayers are therefore stabilized by the electrostatic forces in the PEC. Charged compounds such as drugs and proteins can be incorporated in the multilayers which are amorphous in nature. Antunes and

co-workers (2011) successfully demonstrated formation of the PEC of chitosan and poly (γ -glutamic acid) by *layer-by-layer assembly* (Figure 2.3(c)).

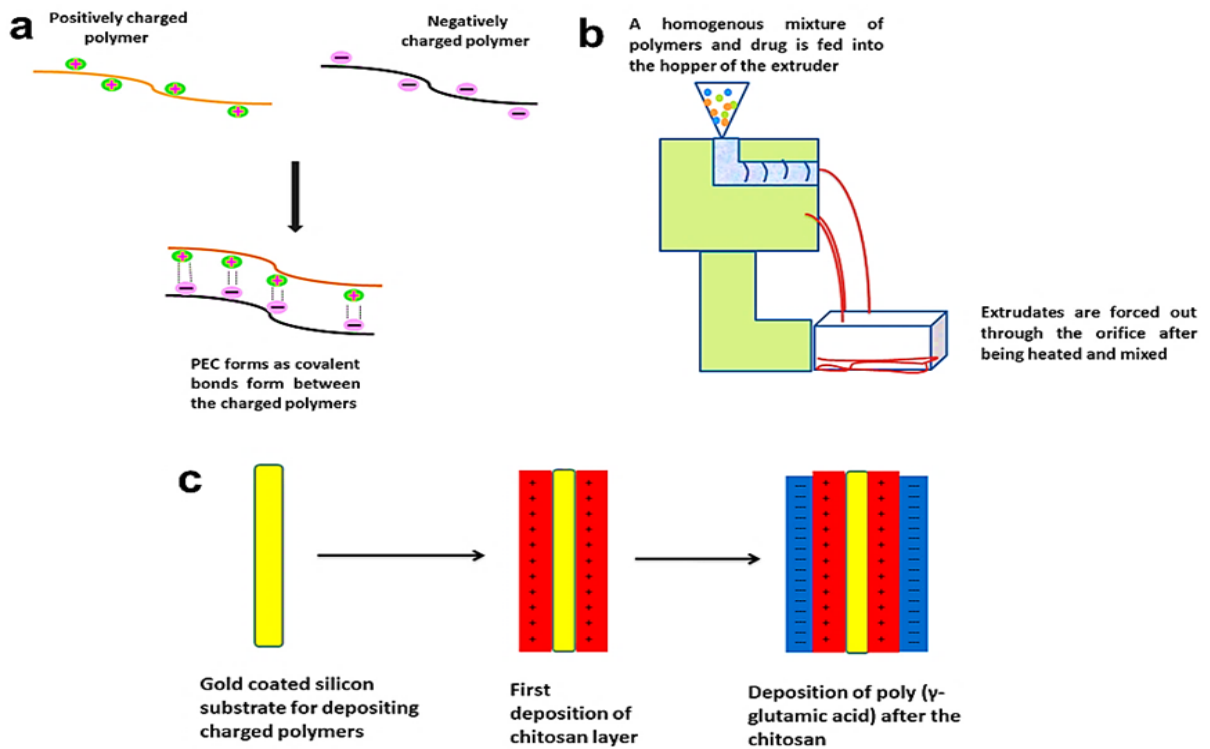


Figure 2.3: Schematic representation of a) PEC formation in solution from oppositely charged polymers b) Melt extrusion and c) Layer-by-layer self-assembly

Based on the description of the methods given above, Table 2.1 below highlights the advantages and disadvantages of implementing these methods for PEC synthesis.

Table 2.1: Advantages and disadvantages of the methods of polyelectrolyte complex synthesis

Method of synthesis	Advantage	Disadvantage
Solution	Ease of synthesis and collection due to the PEC precipitating out immediately after formation (Lankalapalli and Kolapalli, 2009; Vries <i>et al.</i> , 2003).	Some of the polymers and drug are lost in supernatant solution during synthesis (Lankalapalli and Kolapalli, 2009; Vries <i>et al.</i> , 2003).
Melt extrusion	Synthesis is continuous and does not require addition of solvents (Kindermann 2012; Vasconcelos <i>et al.</i> , 2007).	Generally its use requires the polymers with low melting points (Janssens and Van den Mooter, 2009).
Layer-by-layer	Stable PECs are formed and application of the layers includes coating substances (Antunes <i>et al.</i> , 2011).	Slow process and a uniform surface is needed for the deposition of the next polymer layer (Mihai <i>et al.</i> , 2013; Antunes <i>et al.</i> , 2011).

2.3. FORMATION OF POLYELECTROLYTE COMPLEXES

In PEC formation, there is initially the formation of a random primary complex which might either become an ordered complex or form fibrils but that is not constant (Dakhara and Anajwala, 2010). PECs can form within the pH range where both the cationic and the anionic polymers are charged (Boddohi *et al.*, 2009). This is the pH around their pKa values (Cranford *et al.* 2010; Sarmiento *et al.*, 2007). However, monitoring the pH value is vital for polymers possessing a weak charge density otherwise those with a strong charge density maintain their charges regardless of the pH of the reaction medium (Mihai *et al.*, 2011). PECs have been renowned for their ability to maintain the stability of polymers. Generally, polymers are not easily dissolved in water due to their low entropy values (Feng *et al.*, 2007; Jintapattanakit *et al.*, 2007). The addition of chitosan to alginate in making a carboplatin-containing PEC stabilizes the alginate pre-gel nucleus which then forms nanoparticles (Nanjwade *et al.*, 2011). Similarly, the stability of theophylline and alginate beads was enhanced by the electrostatic interactions between the alginate and chitosan. The two polymers formed a PEC by the coating of alginate with chitosan (Colinet *et al.*, 2011).

Various parameters affecting PEC formation include:

- pH of the reaction medium
- ionic strength of the reaction medium
- density of the charges
- charge distribution over the polymers
- mixing ratio of the polymers
- order of mixing
- duration of the interaction
- the position of the ionic groups on the polymer
- degree of ionization
- polymer chain flexibility (Hamman, 2010; Dinu *et al.*, 2010; Petrov *et al.*, 2003).

Polyelectrolyte complexes can be formed using either the *stoichiometric* or *non-stoichiometric polymer ratios*. These ratios influence the polycationic and polyanionic densities and they determine the physicochemical properties of the complexes that are formed (Le Cerf *et al.*, 2014; Petrov *et al.*, 2003). Table 2.2 below provides examples of stoichiometric and non-stoichiometric PECs from studies previously conducted by various groups.

2.3.1. Stoichiometric complexes

Stoichiometric ratios of polymers yield PECs that are electroneutral and they usually precipitate out of solution. Their formation is characterized by the strong electrostatic forces between the polymers which are in a 1:1 molar ratio (Vasconcelos *et al.*, 2007; Berger *et al.*, 2004). The complexes do not dissolve in water and organic solvents but are capable of swelling in water. Their rigidity and hydrophobic nature is attributed to their lack of free charges (Kabanov and Zezin, 1984). There has been intensive research in the use of PECs as matrices that slowly release the API over time. Tapia and co-workers (2004) developed and characterized chitosan–alginate and chitosan–carrageenan matrices for the prolonged release of diltiazem clorhydrate. The amounts of polymers were varied in order to ascertain how much of each polymer was required to obtain a complete reaction and therefore the synthesis of stoichiometric PECs. They concluded that the chitosan-alginate matrix performed better since it resulted in prolonged release of the drug at lower polymeric ratios (Tapia *et al.*, 2004). According to a study conducted by Ngwuluka *et al.* (2013) computational as well as *in vitro* data validated the formation of an interpolyelectrolyte complex in stoichiometric ratios between methacrylate copolymer and sodium carboxymethylcellulose. This has the potential to be employed in controlled drug delivery (Ngwuluka *et al.*, 2013). The use of stoichiometric complexes is limited in fields such as biomimetic mineralization

where the PEC would act as a template with free charges that can bind to minerals such as Ca^{2+} in order to form crystals. These crystals lead to the formation of hybrids with unique properties. However, non-stoichiometric PECs are eligible for this application but their use has not been explored much. Figure 2.4 illustrates the formation of a BSA entrapped in carboxymethyl cellulose and chitosan polyelectrolyte hydrogel and its use in biomimetic mineralization. The PEC acts as a template by providing carboxylate ions for the calcium ions to attach and therefore making a biodegradable scaffold that can be utilized in tissue engineering. Sustained release of the BSA also shows that the PEC has drug delivery applications (Salama and El-Sakhawy, 2014).

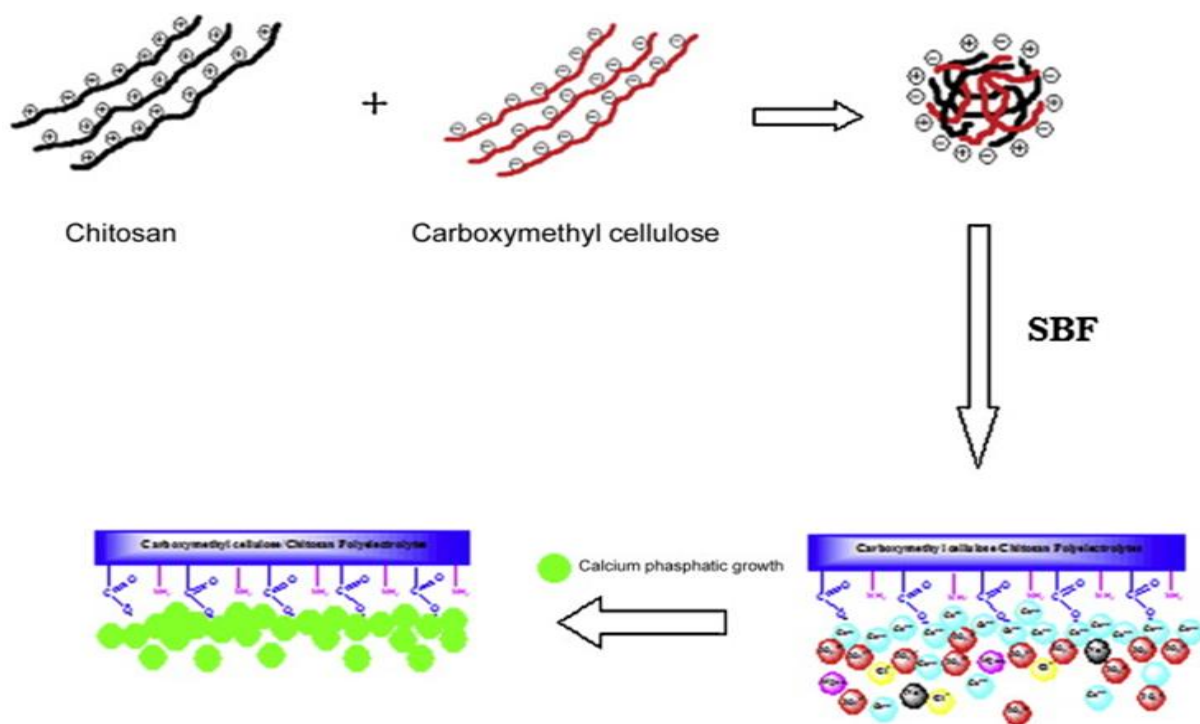


Figure 2.4: Carboxymethylcellulose and chitosan polyelectrolyte hydrogel and calcium phosphate biomimetic mineralization (Rodríguez *et al.*, 2011).

2.3.2. Non-stoichiometric complexes

Non-stoichiometric ratios of polymers result in the formation of water soluble complexes and the level of turbidity determines the concentration of the PEC in the solution (Kramarenko *et al.*, 2006; Kabanov and Zezin, 1984). Formation of this type of PEC is facilitated by the presence of a 'host' and a 'guest' polymer. The 'host' polymer possesses a longer chain and has to be present in larger amounts compared to the 'guest' polymer. The excess charges which are not participating in the complex formation therefore interact with the aqueous medium and are responsible for the stability of the complex as well as its net charge. The resulting PEC is homogeneously dispersed in the aqueous solution and its formation is

reversible. Other factors leading to the formation of hydrophilic PECs are differences in molecular weights between the participating polymers and the presence of salt and weak ionic groups in the polymers. However, if the conditions of formation are not maintained by decreasing the amount or the level of ionization of the host polymer, clustering of complexes occurs. This may eventually lead to the formation of stoichiometric complexes (Shovsky *et al.*, 2009; Sotiropoulou *et al.*, 2004; Kabanov and Zezin, 1984). Shovsky *et al.*, (2009) noted that the formation of non-stoichiometric PECs between block ionomers and enzymes or oligonucleotides is beneficial in drug delivery for purposes such as enzyme entrapment or gene therapy. They reported on the effect of adding poly [ethylene oxide] ether methacrylate, (poly [PEO MEMA]), a non-ionic compound, to a cation, poly (methacryloxyethyltrimethylammonium) chloride (poly [METAC]). The poly [METAC] formed a water soluble PEC with poly sodium styrene sulfonate (NaPSS) at both stoichiometric and non-stoichiometric ratios. Both ratios yielded colloidal dispersions that did not precipitate in 5mM of sodium chloride. The PECs were able to form aqueous dispersions due to the steric hindrance caused by the presence of at least 25% poly (METAC) (Pollexe and Delair, 2013) PECs that form in non-stoichiometric ratios can form colloids which exhibit the Tyndall effect. Recently, Pollexe and Delair (2013) effectively entrapped an antibody (anti-ovalbumin) onto chitosan and hyaluronic acid colloidal PEC nanoparticles. These PECs maintained their colloidal stability.

Moreover, there is a group of PECs that forms regardless of the nature of the polymeric ratios and *coacervates* fall into this category. Being fluid in nature, their formation can be reversed. The polyelectrolyte complex-rich fluid is immiscible with the supernatant but it does not precipitate out of the solution and can be collected by further centrifugation (Berger *et al.*, 2009; Bohida 2008). It has been noted that non-stoichiometric, water-soluble PECs can eventually form coacervates if the charge density of the polymers increases. The highest yield of coacervates is achieved at or near their stoichiometric ratios (Kizilay *et al.*, 2011). Aguero and co-workers (2013) provided an example of biomedical application of coacervates where they reported the potential of using drug loaded poly(acryloxyethyl-trimethylammonium chloride-co-2-hydroxyethyl methacrylate) copolymer (poly(Q-co-H)) and alginate PEC as a scaffold for effective oral drug delivery.

There are theories that have been proposed to explain how coacervation in PEC formation occurs and these include but are not limited to the Overbeek-Voorn, Veis-Aranyi and Tainaka theories. These theories have been adequately reviewed by Burgess (1990). According to the Overbeek-Voorn theory, the level of clustering is minimized when the concentration of salt ions is increased in the polyelectrolyte solution. The salt ions would

neutralize the charges and thus lower the charge density. Minimization of clustering also occurs when non-stoichiometric binding occurs between the molecules involved (Dinu *et al.*, 2010; Burgess 1990). In the case of the Veis-Aranyi model, the first step towards co-acervation is the self-assembly of molecules which is then followed by the slow rearrangement of co-acervates. As re-arrangement takes place, entropy value increases. The Tainaka theory is based on how the respective negatively and positively charged molecules initially assemble without any charge interactions between them. These aggregates will then precipitate out due to the attractive forces between them thereby forming co-acervates. Higher molecular weights lead to better precipitate formation and the ionic interaction then occurs in the precipitate to form PECs (Dinu *et al.*, 2010; Burgess 1990).

Table 2.2: Examples of stoichiometric and non-stoichiometric polyelectrolyte complexes from previous studies

Stoichiometric PECs	Non-stoichiometric PECs
chitosan–alginate and carrageenan (Tapia <i>et al.</i> , 2004)	chitosan–poly(methacrylic acid) and poly(N-ethyl-4-vinyl-pyridinium bromide) (Dainiak <i>et al.</i> , 1998-1999)
methacrylate copolymer and sodium carboxymethylcellulose (Ngwuluka <i>et al.</i> , 2013)	chloride–co–2–hydroxyethyl methacrylate copolymer (poly(Q–co–H)) and alginate (Aguero <i>et al.</i> , 2013)
carboxymethyl cellulose and chitosan (Salama and El-Sakhawy 2014)	polyvinylsulfate and poly-diallyldimethylammonium chloride (Chen <i>et al.</i> , 2003)
Na-carboxymethyl cellulose and chitosan hydrochloride (Shtompel <i>et al.</i> , 2011)	carboxymethylcellulose and N-methylated poly(2-vinylpyridine) (Vishalakshi and Ghosh, 2003)
poly(styrenesulfonate) and poly(diallyldimethylammonium) (Wang and Schlenoff, 2014)	chitosan with poly(sodium 2-acrylamido-2-methylpropanesulfonate) (Mihai and Dragan, 2009)
Eudragit E PO kappa-carrageenan (Prado <i>et al.</i> , 2008)	chitosan and hyaluronic acid (Pollexe and Delair, 2013)

2.4. POLYMERS USED IN POLYELECTROLYTE COMPLEXATION

Generally, polymers can be classified according to their source, charge, aqueous solubility and bioadhesive properties as illustrated in (Figure 2.5) (Majumdar *et al* 2010; Roy and Prabhakar, 2010; Chickering *et al.*, 1996). In order to form a PEC, the constituent polymers should be charged enough to form ionic interactions between the polymers. Polymers used for PEC synthesis are either natural, synthetic or chemically modified polymers or a

combination of different types of polymers. These three types of polymers may be in various forms such as linear, branched, crosslinked, polyacids, polybases, polyampholytes and copolymers (Lankalapalli and Kolapalli, 2009). Advantages of using natural polymers are that they are biocompatible, biodegradable, cheap and ubiquitous in nature. Synthetic polymers present with the advantage of thermal stability due to their strong mechanical properties as well as minimal batch to batch variations (Dang and Leong, 2006). This stability would make them more suitable for use in methods such as melt extrusion. They are polymers of choice for applications such as implants. The natural and synthetic polymers can be modified to achieve a desired outcome which in most cases is the optimization of a specific property. This will expand the applicability of polymers. Chemical surface treatments are implemented in order to alter the charge density, the pH or hydrophilicity/hydrophobicity of the polymer (Hoffman 1995). A comparative study on insulin-loaded chitosan/ γ -poly (glutamic acid) and trimethyl chitosan (TMC-chemically modified form of chitosan)/ γ -poly (glutamic acid) nanoparticles for the stability of drug molecule reported that TMC-containing PEC had a significantly superior stability across a wider pH range compared to the chitosan-containing PEC (Mi *et al.*, 2008). Examples of cationic polymers that have been explored for complexation include chitosan, poly (ethyleneimine), and poly-L-(lysine). Anionic polymers include carboxymethyl cellulose, alginate, dextran sulfate and poly acrylic acid. Some of the charged polymers exhibit additional beneficial properties such penetration enhancing effects and pH-specific disintegration. Polymers such as chitosan and alginate improve the residence time of the system thus improving drug permeation at the site of action (Arora *et al.*, 2011). Chitosan retains its bioadhesive properties even after the PEC has disintegrated. Polymer disintegration under a certain pH facilitates targeted drug release. For example, Eudragit L100-55 and Eudragit L-100 are insoluble in acidic pH but soluble in alkaline pH and this makes it suitable for targeted drug delivery to the small intestines (Cetin *et al.*, 2010).

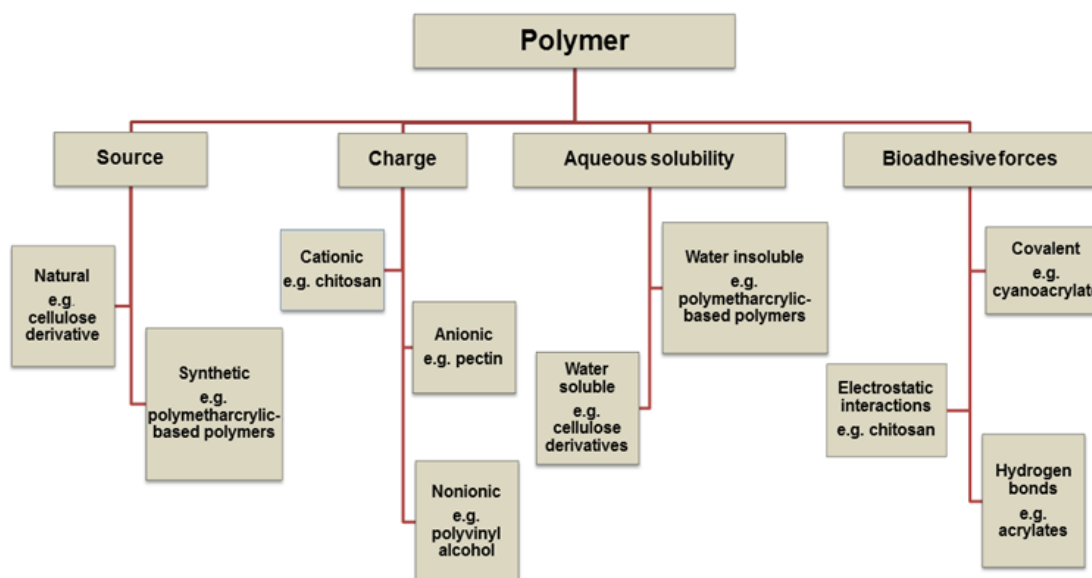


Figure 2.5: Illustrates classification of polymers based on source, charge, aqueous solubility and bio-adhesive force

2.5. MECHANISM OF DRUG RELEASE BY PECS

The use of PECs provides controlled release of the drug with spatial and temporal distribution. This changes the pharmacokinetic and pharmacodynamic properties of the drug. PECs are also known to retain a large amount of water and therefore have a good swelling capacity which helps with the mechanism of drug release (Kim *et al.*, 2004; Tapia *et al.*, 2004). Drug release is generally by means of diffusion (if PECs have a porous structure) and degradation. The degradation of the PEC structure leads to swelling as free charges become available for interaction with water. Swelling is caused by the charge repulsion within the PEC and also by the neutralisation of free charges by water and other counter ions. The degree of swelling is dependent on the flexibility of the PEC (Berger *et al.*, 2004). Alternatively, drug release may occur by pH-sensitive shrinking. In this case, the maximum level of swelling is reached then shrinkage occurs as the inter-polyelectrolyte reaction is completed. The release of dextran from dextran sulfate/chitosan PEC was observed at neutral pH when the PEC shrunk (Berger *et al.*, 2004; Sakiyama *et al.*, 2001). The swelling or shrinking is therefore responsible for the diffusion of the drug out of the matrix (Alba *et al.*, 2014; Ngwuluka *et al.*, 2013). Drug release by hydrolysis of the PECs occurs to a very small extent (Hamman 2010). However, with regards to PECs having a high water absorption capacity, drug release occurs by means of disintegration of the polymer, instead of swelling (Tapia *et al.*, 2004). Upon dissolution, a viscous solution of the PEC will form and this helps in extending the drug release. In addition, polymers such as poly-L-lysine and polyethyleneimine can be used to block the pores in gel networks and thereby retarding the

drug release. Alginate-Polyethyleneimine complex led to prolonged release of furosemide, a hydrophobic drug. The extra alginate layer helped achieve controlled release by blocking the matrix pores. PEC formation delayed the swelling of the system (Mallikarjuna *et al.*, 2005). (Figure 2.6) shows the timed-release of the drug profile by the chitosan/ghatti gum PEC in comparison to the individual polymers, chitosan and ghatti gum (Reddy *et al.*, 2011).

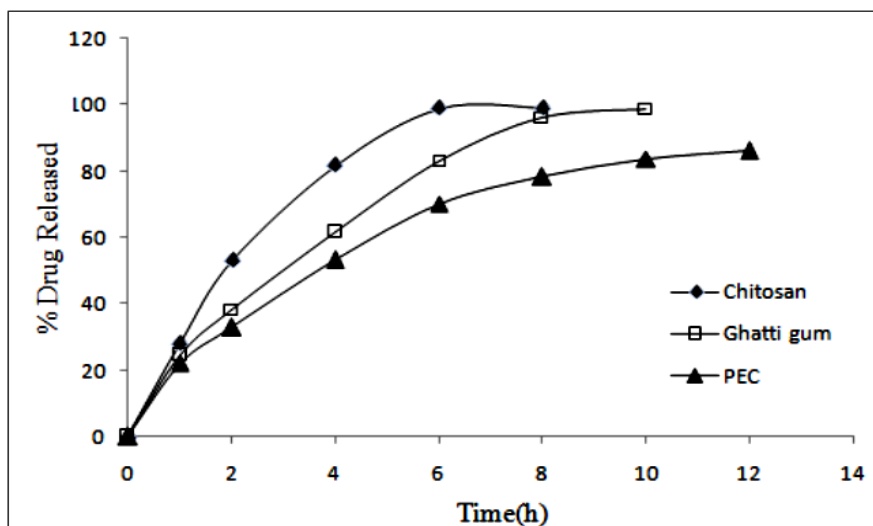


Figure 2.6: Profile illustrating the drug release profile of Chitosan, Ghatti gum and Chitosan/Ghatti gum PEC (Reddy *et al.*, 2011)

The controlled release mechanism includes extended release where a certain predetermined amount of drug is released at a certain time and sustained release where an unpredictable amount of drug is slowly released to maintain plasma concentrations. Polyelectrolyte complexes, unlike polymer blends, provide a modified drug release profile. This mechanism is believed to facilitate the accumulation of higher drug levels at the site of action (Bani-Jaber *et al.*, 2011). This accumulation leads to a higher saturation solubility which leads to enhanced drug absorption (Martinez and Amidon, 2002). This type of drug release facilitates continuous treatment particularly in the nocturnal phase and it helps to improve the stability of the drug (Bani-Jaber *et al.*, 2011; Ahn *et al.*, 2002). The accumulation of toxic amounts of the drug in the body is therefore prevented as well as the accumulation of sub-therapeutic levels of the drug which may result in the emergence of resistance to treatment (Shu *et al.*, 2009; Liao *et al.*, 2005). In addition, the drugs possessing a short *in vivo* half-life may become long acting drugs after being incorporated into PECs. Sufficient maintenance of plasma drug levels is achieved. Attempts to obtain gradual release of ibuprofen have been made by embedding the drug within a Eudragit E 100/Eudragit L 100 polyelectrolyte complex (Moustafine *et al.*, 2006). This was successfully achieved. A similar effect on ibuprofen was seen with Eudragit EPO/Eudragit L 100-55 complex. The drug was embedded within the

matrix without any drug-polymer covalent interactions (Moustafine *et al.*, 2006). Studies conducted by Prado and co-workers showed the different polyelectrolyte complexes that can be used to achieve the slow release of ibuprofen over time. Cationized starch/K-carrageenan, *Polysiphonia nigrescens* and cationized agaroses/Eudragit E and Eudragit E/K-carrageenan complexes gave zero order release kinetic with Fickian diffusion (Prado *et al.*, 2012, 2009, 2008).

Lipophilic drugs pose the challenge of poor plasma drug concentrations due to their low aqueous solubility. Ai and co-workers (2003), demonstrated the enhanced bioavailability of furosemide, when incorporated in the layer-by-layer PEC of polystyrene sulfonate and poly (dimethyldiallyl ammonium chloride) in the form of drug loaded gelatin microcrystals (Ai *et al.*, 2003). The use of PECs as bioenhancers of active pharmaceutical agents is not only limited to hydrophobic substances. A hydrophilic moiety such as fluorescein isothiocyanate conjugate bovine serum albumin was embedded into a chondroitin sulfate/chitosan nanoparticle complex with significant improvement in the amount of drug that reached the target site (Yeh *et al.*, 2011). Another example is of a study conducted by Bawa *et al.*, (2011) who investigated the use of a PEC (pectin, chitosan and hydrolyzed polyacrylamide) to modify the release of diphenhydramine, a highly water-soluble API. They concluded that the delivery system is applicable for targeted release specifically to the small intestines and the colon because of its pH-sensitivity. PECs also exhibit a potential in gastroprotection and sustaining the release of bioactives that are prone to degradation such as proteins. Liao *et al.* (2005) investigated the ability of interfacial chitosan/alginate polyelectrolyte complexation for high drug encapsulation efficiency, sustained release kinetics, and capacity to retain the bioactivity of bovine serum albumin (BSA), dexamethasone, platelet derived growth factor (PDGF) and avidin. This study achieved the successful incorporation of positively charged (PDGF and avidin), negatively charged (BSA) and neutral (dexamethasone) molecules in a PEC. It was stipulated that the PEC has the potential for releasing the active ingredient slowly over time while retaining the activity (Liao *et al.*, 2005).

The rate of extended drug release is directly proportional to the strength of the PEC. For example with the chitosan/pectin PEC loaded with resveratrol, formation of the PEC in low pH results in a strong complex which exhibits little swelling and erosion thus retarding drug release until it reaches the colon. In the colon, enzymes are responsible for breaking down the complex. *In-vivo* studies in rats revealed that little amounts of resveratrol were detected in the plasma in the first 5 hours and these amounts gradually increased with time (Das *et al.*, 2011).

2.6. BIOAVAILABILITY ENHANCING TECHNIQUES ASSOCIATED WITH PECS

Numerous studies have been carried out to enhance the bioactivity of drugs by incorporating them into polymers (Table 2.3). Making use of PECS is one of the ways that this has been done with the ultimate result being the formation of a modified release system which can combat the problem of short duration of action of drugs. The drug is either imbedded within the complex or it interacts with either of the polymers in the complex (Martinez and Amidon, 2002). The controlled release mechanism has been explained previously. Other methods of enhancing bioavailability such as, the use of nanoparticles or microparticles may also be used together with the PECs. The steps involved as well as the suggested ways to improve each step for the solid dosage form to reach the systemic circulation are shown in (Figure 2.7).

Table 2.3: Previous studies on drug-loaded polyelectrolyte complexes and their effect on drug release

Polymers	MOS ^{*1}	Drug	LE ^{*2}	EODS ^{*3}
N-Trimethyl chitosan and poly (γ -glutamic acid) nanoparticles	Ionic-gelation	Insulin	73.8 \pm 2.9%	Sustained release along the entire intestinal tract (Mi <i>et al.</i> , 2008).
Alginate-Polyethyleneimine beads	Solution and incubation	Furosemide	97.16%-100.49%,	Sustained release of the drug with reduced initial swelling and erosion of the complex (Mallikarjuna <i>et al.</i> , 2005).
Polystyrene sulfonate and poly (dimethyldiallyl ammonium chloride)	Layer-by-layer assembly	Furosemide	-	Sustained release of furosemide (Ai <i>et al.</i> , 2003).
Dextran sulfate and chitosan nanoparticles	Solution	Curcumin	~74%	The drug release pattern showed a burst release in the first 3 h followed by a controlled release over a period of one week (Anitha <i>et al.</i> , 2011).
Eudragit E and carrageenan	Solution	Metronidazole	-	Less than 9% burst release followed by controlled release over 10 hours (Bani-Jaber <i>et al.</i> , 2011).
Chitosan and gum kondagogu	Solution	Diclofenac sodium	64.40-85.71%	5.3 to 5.8 times increase compared to the free drug (Naidu <i>et al.</i> , 2009).
Chitosan and poly (γ -glutamic acid) nanoparticles	Ionic-gelation	Insulin	71.8 %	Significant increase in bioavailability compared to the free insulin 15.1% (Sonaje <i>et al.</i> , 2009).
Chitosan and alginate microsphere beads	Solution	Anti-tuberculosis drugs (rifampicin, isoniazid and pyrazinamide)	65 - 85%	Increase in bioavailability attributed to increase in the half life and mean residence time of the drugs (Pandey and Khuller, 2004).
Chitosan and dextran sulfate microspheres	Solution	Ibuprofen	At least 80%	Expected increase in bioavailability since solubility of the drug was enhanced by colon specific drug delivery (Lin <i>et al.</i> , 2005).
Chitosan and alginate-g-PCL/Ca ²⁺	Coating	Theophylline	87-91%	Stable in gastric conditions and achieved controlled release of the drug over 7 hours (Colinet <i>et al.</i> , 2010).
Chitosan and pectin microparticles	Solution	Resveratrol	>97%	Steady increase in blood drug concentrations after 5 hours (Das <i>et al.</i> , 2011).
Chitosan and xanthan gum	Extrusion	Chlorpheniramine maleate	100%	Controlled release due to the formation of a hydrogel upon dissolution (Fukuda <i>et al.</i> , 2006).
Polydiallyldimethylammonium chloride (PDADMAC) and polystyrene sulfonate	Layer-by-layer	Daunorubicin	88.3%-93.95%	Higher drug release in alkaline pH with an initial burst release of 65% in the first hour followed by sustained release (Kainourgios <i>et al.</i> , 2013).

*¹ MOS: method of synthesis

*² LE: loading efficiency

*³ EODS: effect on drug release

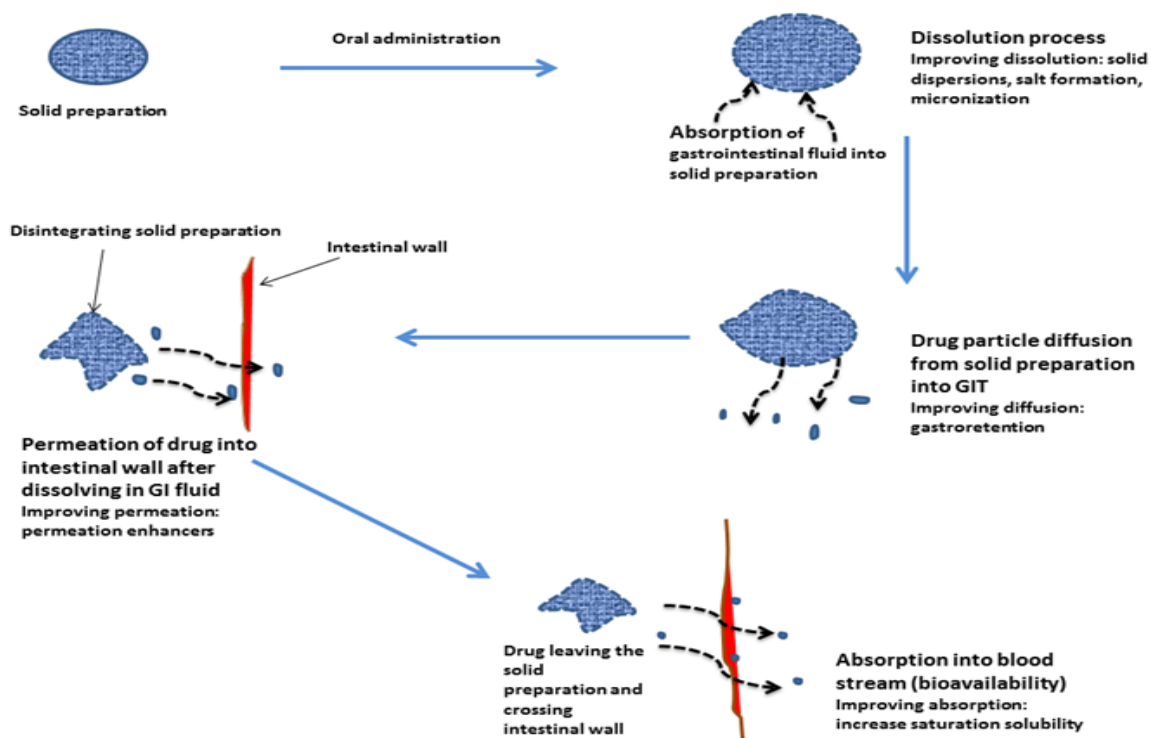


Figure 2.7: Showing schematic representation of different steps involved in achieving bioavailability of a solid dosage form

2.6.1. Techniques implemented to improve bioavailability

Different approaches that exploit polyelectrolyte complexes and are believed to enhance the amount of drugs reaching their intended sites of action include permeation enhancers, nanoparticles, microparticles and gastroretentive systems, etc. These techniques are further described below and the examples given are mainly of PECs containing chitosan and its derivatives. There are replete studies in literature based on chitosan and its derivatives and their use in PEC synthesis. Chitosan PECs shrink in acidic pH but start to swell in alkaline pH and therefore drug release starts to occur. This is opposed to the use of chitosan alone which is readily soluble in gastric pH. Naidu *et al.*, (2009) concluded that gum kondagogu and chitosan polyelectrolyte complex led to an increase in relative bioavailability of diclofenac sodium by 5.3 to 5.8 times compared to the free drug. The study was conducted in rats where, modified drug release was achieved and the PEC was a barrier to gastric drug release (Naidu *et al.*, 2009). Diclofenac sodium served as an ideal model because it is associated with drawbacks such as poor solubility, short duration of action and liability to be degraded in the gastrointestinal tract (GIT). Use of the PEC resolved these limitations. Other polymers have been utilized for PEC formation without the inclusion of chitosan. When metronidazole was loaded into eudragit E and carrageenan IPEC, the gastric residence time was prolonged by use of the floating matrix tablet and this property was attributed to

controlled release. There was an increase in the amount of metronidazole absorbed in the GIT (Bani-Jaber *et al.*, 2011). As mentioned earlier, furosemide loaded in calcium alginate and polyethyleneimine (Arora *et al.*, 2011) as well as the polystyrene sulfonate and poly (dimethyldiallyl ammonium chloride) PECs (Ai *et al.*, 2003) led to the fulfilment of retarded drug release.

2.6.1.1. Permeation enhancers

Lipophilic molecules can cross the intestinal wall down a concentration gradient in contrast to hydrophilic ones which require a selective transport system such as the active transport or facilitated diffusion in order for them to cross the wall. The integrity of the wall along the GIT may be breached to enhance permeation of molecules. However, there is a risk of toxicity when unwanted pathogens enter through the intestinal wall. It is believed that some of these permeation enhancers cause irritation to the gastrointestinal (GI) wall (Muheem *et al.*, 2011; Gaucher *et al.*, 2010). Generally, polymeric permeation enhancers are hydrophilic in nature and are therefore not absorbed. Thiolates and polyacrylates are examples of polymers that can be used for permeation enhancement (Bernkop-Schnurch, 2009). Chitosan and its derivatives have known excellent bioadhesive properties and therefore increase the residence time of substances in the GIT. It is stipulated that chitosan binds to the mucin on the mucosa thus facilitating permeation of substances across the wall (Balabushevich *et al.*, 2011). Protonated chitosan interacts with the tight junctions found on the intestinal wall thus facilitating paracellular permeation of macromolecular drugs (Figure 2.8). It has been noted that chitosan has minimal effects on the integrity of the cells of the intestinal wall (Zakhem *et al.*, 2012). This makes it ideal for enhancing the permeation of drugs. In addition, it is broken down by the enzyme beta-glucosidase and therefore is useful in targeted colon delivery of drugs. For example, the targeted delivery of vancomycin to the colon was achieved using a chitosan/pectin PEC (Pendekal and Tegginamat, 2013). Similarly, Moodley and co-workers (2011) formulated the same PEC for colonic delivery of mesalamine. PECs can help solve the problem associated with colonic drug delivery due to its distal position in the gastrointestinal tract (Moodley *et al.*, 2011). Enhanced permeation and prolonged release of 5-Fluorouracil was achieved by incorporating it in chitosan and alginate inter-polyelectrolyte complex (IPEC). The mucoadhesive nature of chitosan might prevent the presystemic metabolism of molecules such as peptides thus enhancing their oral absorption (Pendekal and Tegginamat, 2013).

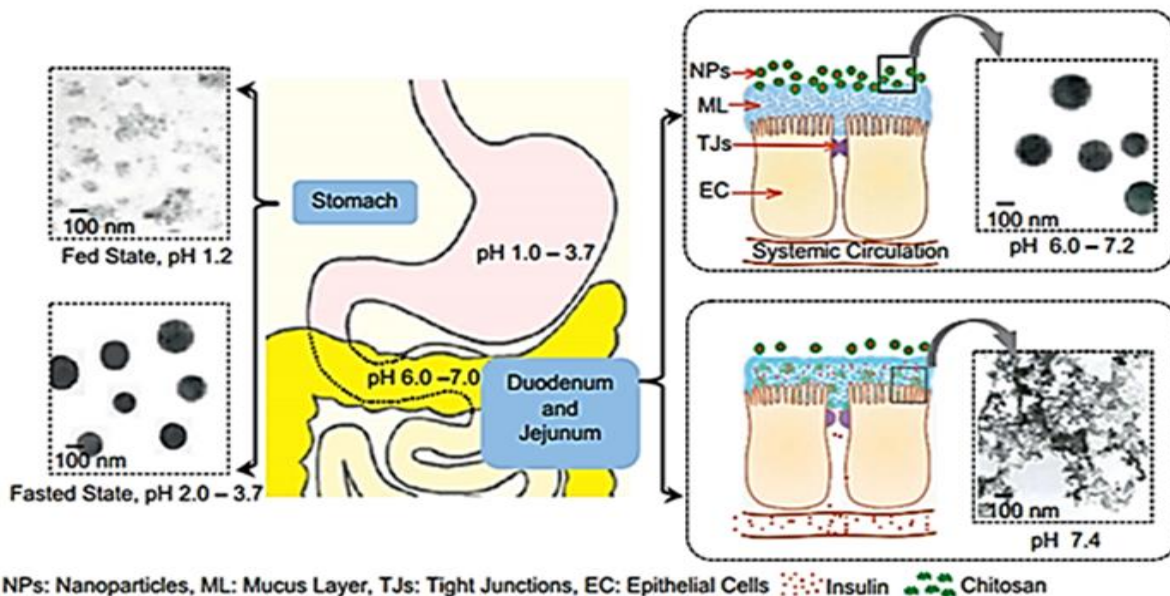


Figure 2.8: Schematic illustrations of the presumed mechanism of the paracellular transport of insulin released from test nanoparticles (Sonaje *et al.*, 2009)

2.6.1.2. Microparticles

The microparticle size is of great importance in relation to drug release kinetics, where, the larger the particle size, the slower the drug release will be. The specific rate of release may be controlled by aiming to use a defined range of microsphere size (Yujie and Pack, 2015). This drug delivery method has been found to be applicable in insulin delivery where gastroprotection is essential as well as the timely release of the drug for effective glucose monitoring (Balabushevich *et al.*, 2013). Chitosan crosslinked with tripolyphosphate formed microspheres with dextran sulfate for the delayed release of ibuprofen. Almost 100% drug release was observed in intestinal fluid within 6 hours (Lin *et al.*, 2005). Chitosan coated alginate and dextran sulfate microspheres were used to develop a system that protects insulin from gastric degradation. In addition, it reduced the burst release of insulin (Martins *et al.*, 2007). Attempts were also made by Mao and co-workers (2005) who encapsulated ciprofloxacin hydrochloride into polystyrene sulfonate and poly (allyl amine hydrochloride) microcapsule complex for prolonged release. This type of release has been proven to improve drug release and therefore preventing toxicity associated with poorly water-soluble drugs (Mao *et al.*, 2005). Another application for microparticles was demonstrated when anti-tuberculosis drugs (rifampicin, isoniazid and pyrazinamide) were encapsulated into chitosan/alginate microspheres. Results revealed bioenhancement, increase in half-life by threefold and a significant thirteen times elevation in the mean residence time. Furthermore, the release of the drugs in the blood plasma of guinea pigs occurred over 7 days. Frequency of dosing would have to decrease thus encouraging patient compliance to treatment

(Pandey and Khuller, 2004). Good bioavailability of antibiotics through the oral route is beneficial for the treatment of local infections in the GIT such as Crohn's disease besides being a more favourable method of drug administration by patients.

2.6.1.3. Nanoparticles

Nanoparticle-containing PECs are believed to potentially deliver protein and peptide drugs orally. The PEC will shield the drug from GI degradation and will eventually undergo enzymatic degradation particularly in the colon. This facilitates site-specific drug delivery to either the small intestines or the colon (Morishita and Peppas, 2006). The main problem with parenteral delivery is that the protein or peptide drug is not efficiently absorbed and hence the need to maximize oral delivery of these drugs (Anitha *et al.*, 2011). Nanoparticulate carriers that are resistant to gastric degradation have been used to deliver drugs prone to chemical degradation before absorption takes place as well as those which are poorly permeable across the GI wall (Lopes *et al.*, 2010). When insulin was encapsulated into alginate and chitosan nanoparticulate polyelectrolyte complex, efficacy of the bioactive was improved threefold compared to that of the free insulin. Permeation through the intestinal wall was increased and the drug was shielded from gastric degradation (Morishita and Peppas, 2006; Sakiyama *et al.*, 2001).

Nanotechnology has provided an efficient way to enhance bioactivity therefore showing significant differences with conventional systems (Sarmiento *et al.*, 2007). For example, curcumin-loaded nanoparticles of dextran sulphate and chitosan PEC showed better controlled drug delivery and bioavailability in comparison to curcumin-loaded *O*-carboxymethyl chitosan (Anitha *et al.*, 2011). The advantage of using nanoparticles over microparticles is the additional reduction in size which allows for more complete drug absorption within the intestinal transit time which is estimated to be 3-4 hours (Porter *et al.*, 2008). The particles have improved accessibility to most parts of the body. This further reduction in particle size also aids in stabilizing the formulation. The residence time of the system increases by making use of nanoparticles and this helps in lowering the drug doses used. Permeation of the drug through the GI wall and the duration of drug delivery can be enhanced (Wilczewska *et al.*, 2012; Williams *et al.*, 2012). Nanoparticles serve as drug reservoirs since they are not easily excreted from the body. They can also access most of the body parts (Shu *et al.*, 2009). However, some studies have reported on the design of delivery systems that combine both nanoparticles and microparticles to achieve multiple drug release profiles (Lee *et al.*, 2013).

Techniques for forming nanoparticles include dispersion into preformed polymers, polymerization of monomers and ionic gelation. The chosen method will influence properties of the resulting nanoparticles and are therefore selected based on the desired outcome (Fasano, 1998). The ionic gelation technique is the most common one and can be achieved by solvent evaporation or nanoprecipitation. The technique can be implemented where beads result from the reaction of the polyelectrolyte solution and a counterion solution. The beads can swell extensively and form a gel in simulated biological fluids thus releasing the drug. Nanoparticles range in size from 10 to 1000 nm and have efficient absorption due to their size and lipophilicity (Fan *et al.*, 2012). In the case of nanocapsules, the drug is coated with the polymer and its release entails diffusion across the polymeric barrier. Drug release is expected to be of zero order. Another type of nanoparticles is nanospheres and these are formed by the monodispersion of the drug within the matrix (Mora-Huertas *et al.*, 2010). Figure 2.9 illustrates the formation of an insulin-containing chitosan and alginate PEC. pH-sensitive nanoparticles improve the stability of a delivery system since they respond to changes in pH. This is beneficial in the delivery of sensitive bioactives such as insulin which presents with complexity of absorption of inadequate amounts into the blood stream via the oral route (Mudassir *et al.*, 2015). Various studies have explored the delivery of insulin by nanocomplexes with successful outcomes. A marked increase in bioavailability was noted when it was loaded into poly- γ -glutamic acid and chitosan nanocomplex in the presence of magnesium sulfate and tripolyphosphate (Sonaje *et al.*, 2009). It has been observed that the nanoencapsulation of insulin in a chitosan/alginate PEC reduces blood glucose by 40% in diabetic rats. This occurs 12 hours after administration with a hypoglycemic effect of 45% in 24 hours whereas; the free form reduced the blood glucose by 15% in 3 hours with a 42% hypoglycemic effect (Wilson *et al.*, 2012).

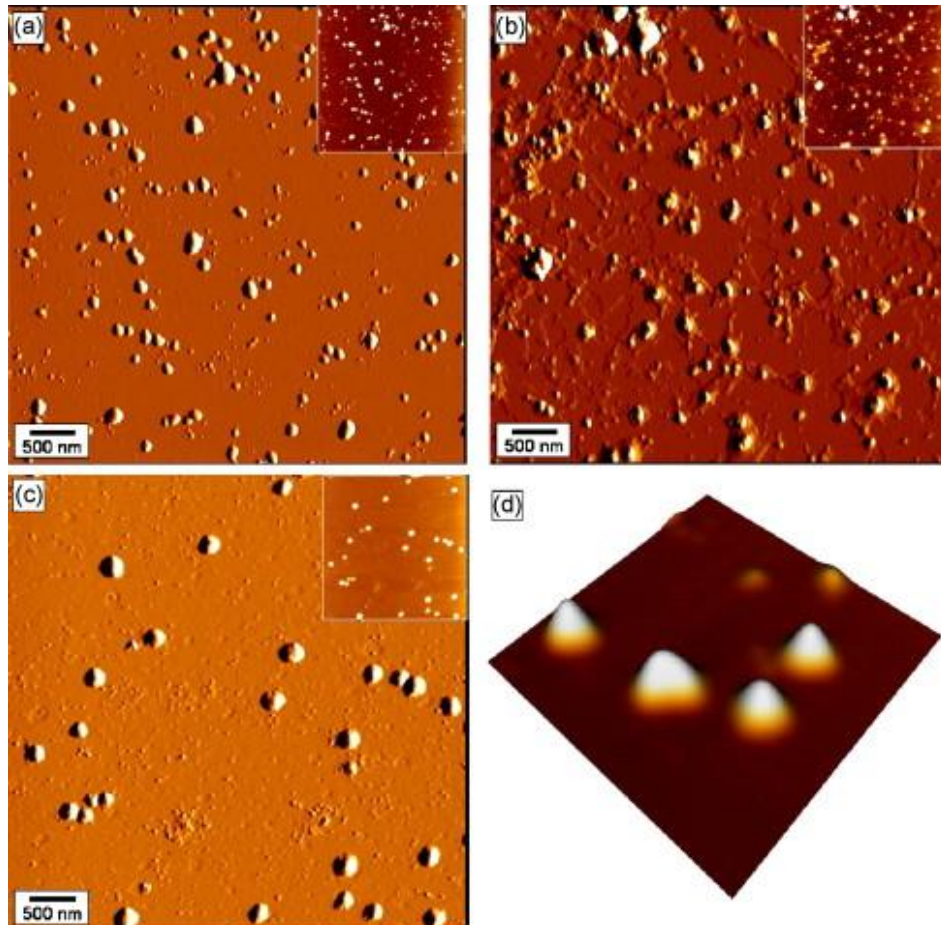
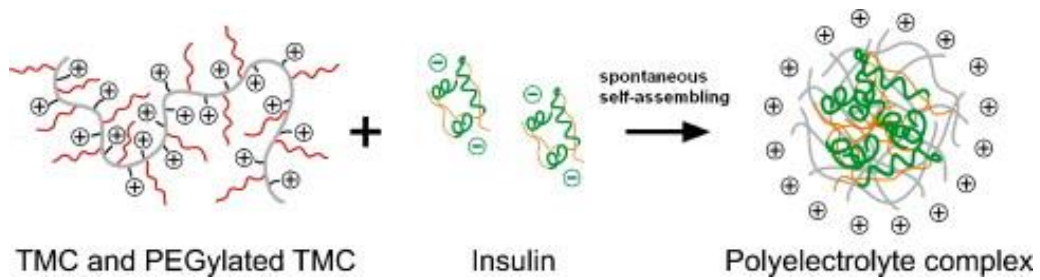


Figure 2.9: Schematic representation of Insulin- chitosan PEC (Jintapattanakit *et al.*, 2007)

2.6.1.4. Gastroretentive controlled release systems

Intragastric floating systems aid in achieving controlled drug release. These systems have a lower density compared to the stomach contents and can therefore float in the stomach without affecting the gastric motility. The retention of the system is prolonged in the fed state. The residence time may be prolonged by bioadhesive systems as well as swelling and expanding systems. This will allow for a more targeted drug release (Bani-Jaber *et al.*, 2011). The intragastric floating system may be used to improve the gastric absorption of drugs such as furosemide.

Recent studies of a Eudragit E100/Sodium carboxymethylcellulose PEC successfully achieved a release-modulating matrix for the delivery of levodopa. Based on the *in vitro* data, such a system is anticipated to be gastroretentive while providing a zero-order and controlled release of the drug *in vivo*. It is believed to have the potential to enhance absorption and subsequently the bioavailability of the psychoactive drug. These results have therapeutic benefits since the drug is known to possess an inherent narrow therapeutic index (Ngwuluka *et al.*, 2013).

2.6.2. Combination systems

The above mentioned approaches to enhance bioavailability of drugs can also be combined with the result of further improving the effectiveness of the PEC-containing delivery system. Amoxicillin-loaded chitosan/alginate complex utilized both properties of nanoparticles and the penetration enhancing system. The amoxicillin-loaded PEC may be successfully used in the eradication of *Helicobacter pylori* (Arora *et al.*, 2011).

2.7. CONCLUDING REMARKS

Polyelectrolyte complex-mediated drug delivery befits an imminent area of research in the field of pharmaceuticals with the aim of developing novel and more effective delivery systems for safe, targeted delivery of bioactives *in vivo*. One major advantage of polyelectrolyte complexes is that they can combine properties of different polymers by maintaining their individual characteristics. The controlled and site-specific delivery of drugs by PECs is attributed to their swelling capability in gastrointestinal fluids as well as their pH dependent degradation. From the literature review provided in this chapter, it can be inferred that the field of polyelectrolyte complexes can be expanded more by combining systems containing the complexes with other bioavailability enhancing techniques such as nanoparticles and permeation enhancers for more effective multiple drug delivery applications.

2.8. REFERENCES

- Agüero, L., Garcia, J., Valdés, O., Fuentes, G., Zaldivar, D., Blanco MD., Katime I., 2013. Synthesis and characterization of polyelectrolyte complex microparticles for drug release. *Journal of Applied Polymer Science*, 128(6), 3548–54.
- Ahn, J.S., Choi, H.K., Chun, M.K., Ryu, J.M., Jung, J.H., Kim, Y.U., Cho C.C., 2002. Release of triamcinolone acetonide from mucoadhesive polymer composed of chitosan and poly(acrylic acid) *in vitro*. *Biomaterials*, 23(6), 1411–6.
- Ai, H., Jones, S.A., de Villiers, M.M., Lvov, Y.M., 2003. Nano-encapsulation of furosemide microcrystals for controlled drug release. *Journal of Controlled Release*, 86(1), 59–68.
- Alba, M., Formentín, P., Ferré-Borrull, J., Pallarès, J., Marsal L. F., 2014. pH-responsive drug delivery system based on hollow silicon dioxide micropillars coated with polyelectrolyte multilayers. *Nanoscale Research Letters*, 9(1), 1-8.
- Anitha, A., Deepagan, V.G., Rani, V.D., Menon, D., Nair, S.V., Jayakumar, R., 2011. Preparation, characterization, *in vitro* drug release and biological studies of curcumin loaded dextran sulphate–chitosan nanoparticles. *Carbohydrate Polymer*, 84(3), 1158–64.
- Antunes, J.C., Pereira, C.L., Molinos, M., Ferreira-da-Silva, F., Dessì, M., Gloria, A., Ambrosio, L., Gonçalves, R.M., Barbosa, M.A., 2011. Layer-by-layer self-assembly of chitosan and poly(γ -glutamic acid) into polyelectrolyte complexes. *Biomacromolecules*, 12(12), 4183-4195.
- Argin-Soysal, S., Kofinas, P., Lo, Y.M., 2009. Effect of complexation conditions on xanthan–chitosan polyelectrolyte complex gels. *Food Hydrocolloids*. 23(1), 202–9.
- Arora, S., Gupta, S., Narang, R.K., Budhiraja, R.D., 2011. Amoxicillin Loaded Chitosan-Alginate Polyelectrolyte Complex Nanoparticles as Mucopenetrating Delivery System for H. Pylori. *Scientia Pharmaceutica*, 79(3), 673–94.
- Balabushevich, N.G., Pechenkin, M.A., Shibanova, E.D., Volodkin, D.V., Mikhailchik, E.V., 2013. Multifunctional polyelectrolyte microparticles for oral insulin delivery. *Macromolecular Bioscience*, 13(10), 1379–88.
- Balabushevich, N.G., Pechenkin, M.A., Zorov, I.N., Shibanova, E.D., Larionova, N.I., 2011. Mucoadhesive polyelectrolyte microparticles containing recombinant human insulin and its analogs aspart and lispro *Biochemistry Moscow*, 76(3), 327–31.
- Bani-Jaber, A., Al-Aani, L., Alkhatib, H., Al-Khalidi, B., 2011. Prolonged Intra-gastric Drug Delivery Mediated by Eudragit® E-Carrageenan Polyelectrolyte Matrix Tablets *AAPS PharmSciTech*, 12(1), 354–61.

- Bawa, P., Pillay, V., Choonara, Y.E., du Toit, L.C., Ndesendo, V.M.K., Kumar, P.A., 2011. Composite Polyelectrolytic Matrix for Controlled Oral Drug Delivery. *AAPS PharmSciTech*, 12(1), 227-38.
- Berger, J., Reist, M., Mayer, J.M., Felt, O., Gurny, R., 2004. Structure and interactions in chitosan hydrogels formed by complexation or aggregation for biomedical applications. *European Journal of Pharmaceutics and Biopharmaceutics*, 57(1), 35–52.
- Berger, J., Reist, M., Mayer, J.M., Felt, O., Gurny, R., 2004. Structure and interactions in chitosan hydrogels formed by complexation or aggregation for biomedical applications. *European Journal of Pharmaceutics and Biopharmaceutics*, 57(1), 35–52.
- Bernabé, P., Peniche, C., Argüelles-Monal, W., 2005. Swelling behavior of chitosan/pectin polyelectrolyte complex membranes. Effect of thermal cross-linking. *Polymer Bulletin*, 55(5), 367–75.
- Boddohi, S., Moore, N., Johnson, P.A., Kipper, M.J., 2009. Polysaccharide-Based Polyelectrolyte Complex Nanoparticles from Chitosan, Heparin, and Hyaluronan. *Biomacromolecules*, 10(6), 1402–9.
- Bohidar, H.B., 2008. Coacervates: a novel state of soft matter: an overview. *Journal of Surface Science and Technology*, 24, 105–24.
- Burgess, D.J., 1990. Practical analysis of complex coacervate systems. *Journal of Colloid and Interface Science*, 140(1), 227–38.
- Čalija, B., Cekić, N., Savić, S., Daniels, R., Marković, B., Milić, J., 2013. pH-sensitive microparticles for oral drug delivery based on alginate/oligochitosan/Eudragit® L100-55 "sandwich" polyelectrolyte complex. *Colloids and Surfaces B: Biointerfaces*, 110, 395–402.
- Cetin, M., Alptug, A., Yucel, K., 2010. Formulation and *In vitro* Characterization of Eudragit® L100 and Eudragit® L100-PLGA Nanoparticles Containing Diclofenac Sodium. *AAPS PharmSciTech*, 11(3), 1250-6.
- Chang, H.H., Wang, Y.L., Chiang, Y.C., Chen, Y.L., Chuang, Y.H., Tsai, S.J., Heish, K.H., Lin, F.H., Lin, C.P., 2014. Autism and Sensory Processing Disorders: Shared White Matter Disruption in Sensory Pathways but Divergent Connectivity in Social-Emotional Pathways. *Public Library of Science one*, 9(7), e92362.
- Chen, J., Heitmann, J.A., Hubbe, M.A., 2003. Dependency of polyelectrolyte complex stoichiometry on the order of addition. 1. Effect of salt concentration during streaming current titrations with strong poly-acid and poly-base 2003. *Colloids and Surfaces A: Physicochemical and Engineering Aspects*, 223(1), 215–30.

- Chen, P.H., Kuo, T.Y., Kuo, J.Y., Tseng, Y.P., Wang, D.M., Lai, J.Y., 2010. Novel chitosan–pectin composite membranes with enhanced strength, hydrophilicity and controllable disintegration. *Carbohydrate Polymer*, 82(4), 1236–42.
- Cheow, W.S., Hadinoto, K., 2012. Self-assembled amorphous drug–polyelectrolyte nanoparticle complex with enhanced dissolution rate and saturation solubility. *Journal of Colloid and Interface Science*, 367(1), 518–26.
- Chickering, D., Jacob, J., Mathiowitz, E., 1996. Poly(fumaric-co-sebacic) microspheres as oral drug delivery systems. *Biotechnology and Bioengineering*, 52(1), 96-101.
- Colinet, I., Dulong, V., Mocanu, G., Picton, L., Le Cerf, D., 2010. Effect of chitosan coating on the swelling and controlled release of a poorly water-soluble drug from an amphiphilic and pH-sensitive hydrogel. *International Journal of Biological Macromolecules*, 47(2), 120–5.
- Cranford, S.W., Ortiz, C., Buehler, M.J., 2010. Mechanomutable properties of a PAA/PAH polyelectrolyte complex: rate dependence and ionization effects on tunable adhesion strength *Soft Matter*, 6(17), 4175–88.
- Dainiak, M.B., Izumrudov, V.A., Muronetz, V.I., Galaev, I.Y., Mattiasson, B., 1998. Affinity precipitation of monoclonal antibodies by nonstoichiometric polyelectrolyte complexes. *Bioseparation*, 7(4-5), 231–40.
- Dakhara, S.L., Anajwala, C.C., 2010. Polyelectrolyte Complex: A Pharmaceutical Review. *Systematic Reviews in Pharmacy*, 1(2), 121–7.
- Dang, J.M., Leong, K.W., 2006. Natural polymers for gene delivery and tissue engineering. *Advanced drug delivery reviews*, 58(4), 487–99.
- Das, S., Chaudhury, A., Ng, K.Y., 2011. Preparation and evaluation of zinc–pectin–chitosan composite particles for drug delivery to the colon: Role of chitosan in modifying *in vitro* and *in vivo* drug release. *International Journal of Pharmaceutics*, 406(1), 11–20.
- De Vries, R., Weinbreck, F., De Kruif, C.G., 2003. Theory of polyelectrolyte adsorption on heterogeneously charged surfaces applied to soluble protein–polyelectrolyte complexes. *The Journal of Chemical Physics*, 118(10), 4649–59.
- Dinu, I.A., Mihai, M., Dragan, E.S., 2010. Comparative study on the formation and flocculation properties of polyelectrolyte complex dispersions based on synthetic and natural polycations. *Chemical Engineering Journal*, 160(1), 115-121.
- Fan, W., Yan, W., Xu, Z., Ni, H., 2012. Formation mechanism of monodisperse, low molecular weight chitosan nanoparticles by ionic gelation technique. *Colloids and Surfaces B: Biointerfaces*, 90, 21-27.
- Fasano, A., 1998. Innovative strategies for the oral delivery of drugs and peptides *Trends in Biotechnology*, 16(4), 152–7.

- Feng, X., Pelton, R., Leduc, M., Champ, S., 2007. Colloidal Complexes from Poly(vinyl amine) and Carboxymethyl Cellulose Mixtures. *Langmuir*, 23(6), 2970–6.
- Fukuda, M., Peppas, N.A., McGinity, J.W., 2006. Properties of sustained release hot-melt extruded tablets containing chitosan and xanthan gum. *International Journal of Pharmaceutics*, 310(1), 90–100.
- Gaucher, G., Satturwar, P., Jones, M.C., Furtos, A., Leroux, J.C., 2010. Polymeric micelles for oral drug delivery. *European Journal of Pharmaceutics and Biopharmaceutics*, 76(2), 147–58.
- Hamman, J.H., 2010. Chitosan Based Polyelectrolyte Complexes as Potential Carrier Materials in Drug Delivery Systems. *Marine Drugs*, 8(4), 1305–22.
- Heinen, C., Reuss, S., Saaler-Reinhardt, S., Langguth, P., 2013. Mechanistic basis for unexpected bioavailability enhancement of polyelectrolyte complexes incorporating BCS class III drugs and carrageenans. *European Journal of Pharmaceutics and Biopharmaceutics*, 85(1), 26–33.
- Hoffman, A.S., 1995. Surface modification of polymers. *Chinese Journal of Polymer Science*, 13(3), 195–203
- Janssens, S., Van den Mooter, G., 2009. Review: physical chemistry of solid dispersions. *Journal of Pharmacy and Pharmacology*, 61(12), 1571–86.
- Jintapattanakit, A., Junyaprasert, V.B., Mao, S., Sitterberg, J., Bakowsky, U., Kissel, T., 2007. Peroral delivery of insulin using chitosan derivatives: A comparative study of polyelectrolyte nanocomplexes and nanoparticles. *International Journal of Pharmaceutics*, 342(1), 240–9.
- Kabanov, V.A., Zezin, A.B., 1984. A new class of complex water-soluble polyelectrolytes. *Die Makromolekulare Chemie*, 6(S19841), 259–76.
- Kainourgiou, P., Efthimiadou, E.K., Tziveleka, L.A., Pappas, G.S., Boukos, N., Kordas, G., 2013 Comparative study of LbL and crosslinked pH sensitive PEGylated LbL microspheres: Synthesis, characterization and biological evaluation. *Colloids Surfaces B: Biointerfaces*, 104, 91–8.
- Kim, S.J., Lee, K.J., Kim, S.I., 2004. Swelling behavior of polyelectrolyte complex hydrogels composed of chitosan and hyaluronic acid. *Journal of Applied Polymer Science*, 93(3), 1097–101.
- Kindermann, C., Matthée, K., Sievert, F., Breitzkreutz, J., 2012. Electrolyte-stimulated biphasic dissolution profile and stability enhancement for tablets containing drug-polyelectrolyte complexes. *Pharmaceutical Research*, 29(10), 2710-2721.
- Kindermann, C., Matthée, K., Strohmeyer, J., Sievert, F., Breitzkreutz, J., 2011. Tailor-made release triggering from hot-melt extruded complexes of basic polyelectrolyte and

poorly water-soluble drugs. *European Journal of Pharmaceutics and Biopharmaceutics*, 79(2), 372-381.

- Kizilay, E., Kayitmazer, A.B., Dubin, P.L., 2011. Complexation and coacervation of polyelectrolytes with oppositely charged colloids. *Advances in Colloid and Interface Science*, 167(1), 4–37.
- Kramarenko, E.Y., Khokhlov, A.R., Reineker, P., 2006. Stoichiometric polyelectrolyte complexes of ionic block copolymers and oppositely charged polyions. *The Journal of Chemical Physics*, 25(19), 194902.
- Lankalapalli, S., Kolapalli, V.R.M., 2009 Polyelectrolyte Complexes: A Review of their Applicability in Drug Delivery Technology. *Indian Journal of Pharmaceutical Science* 71(5), 481–7.
- Le Cerf, D., Pepin, A.S., Niang, P.M., Cristea, M., Karakasyan-Dia, C., Picton, L., 2014. Formation of polyelectrolyte complexes with diethylaminoethyl dextran: Charge ratio and molar mass effect. *Carbohydrate Polymers*, 113, 217–24.
- Lee, J.W., Kim, S.Y., Kim, S.S., Lee, Y.M, Lee, K.H., Kim, S.J., 1999. Synthesis and characteristics of interpenetrating polymer network hydrogel composed of chitosan and poly(acrylic acid). *Journal of Applied Polymer Science*, 73(1), 113–20.
- Lee, Y.S., Johnson, P.J., Robbins, P.T, Bridson. R.H., 2013. Production of nanoparticles-in-microparticles by a double emulsion method: a comprehensive study. *European Journal of Pharmaceutics and Biopharmaceutics*, 83(2), 168–73.
- Li, C., Hein, S., Wang, K., 2012. Chitosan-Carrageenan Polyelectrolyte Complex for the Delivery of Protein Drugs. *ISRN Biomaterials* Available from: <http://www.hindawi.com/journals/isrn.biomaterials/2013/629807/abs/>
- Liao, I.C., Wan, A.C.A., Yim, E.K.F., Leong, K.W., 2005, Controlled release from fibers of polyelectrolyte complexes. *Journal of Controlled Release*, 104(2), 347–58.
- Liechty, W.B., Kryscio, D.R., Slaughter, B.V., Peppas NA., 2010. Polymers for Drug Delivery Systems. *Annual Review of Chemical and Biomolecular Engineering*, 1, 149–73.
- Lin, W.C., Yu, D.G., Yang, M.C., 2005. pH-sensitive polyelectrolyte complex gel microspheres composed of chitosan/sodium tripolyphosphate/dextran sulfate: swelling kinetics and drug delivery properties. *Colloids Surfaces B: Biointerfaces*, 44(2), 143–51.
- Lopes, C.M., Martins-Lopes, P. 7 Souto, E.B., 2010. Nanoparticulate carriers (NPC) for oral pharmaceutics and nutraceutics. *Die Pharmazie-An International Journal of Pharmaceutical Sciences*, 65(2), 75–82.

- Majumdar, S., Ray, P.S., Kargupta, K., Ganguly, S., 2010. Ionic ingress and charge-neutralization phenomena of conducting-polymer films. *ChemPhysChem*, 11(1), 211-219.
- Mallikarjuna, Setty, C., Sahoo, S.S., Sa, B., 2005. Alginate-Coated Alginate-Polyethyleneimine Beads for Prolonged Release of Furosemide in Simulated Intestinal Fluid. *Drug Development and Industrial Pharmacy*, 31(4-5), 435–46.
- Mao, Z., Ma, L., Gao, C., Shen, J., 2005. Preformed microcapsules for loading and sustained release of ciprofloxacin hydrochloride. *Journal of Controlled Release*, 104(1), 193–202.
- Martinez, M.N., Amidon, G.L., 2002. A Mechanistic Approach to Understanding the Factors Affecting Drug Absorption: A Review of Fundamentals. *Journal of Clinical Pharmacology*, 42(6), 620–43.
- Martins, S., Sarmiento, B., Souto, E.B., Ferreira, D.C., 2007. Insulin-loaded alginate microspheres for oral delivery – Effect of polysaccharide reinforcement on physicochemical properties and release profile. *Carbohydrate Polymer*, 69(4), 725–31.
- Mi, F.L., Wu, Y.Y., Lin, Y.H., Sonaje, K., Ho, Y.C., Chen, C.T., Juang, J.H., Sung, H.W., 2008. Oral delivery of peptide drugs using nanoparticles self-assembled by poly (γ -glutamic acid) and a chitosan derivative functionalized by trimethylation. *Bioconjugate Chemistry*, 19(6), 1248-55.
- Mihai, M., Dragan, E.S., 2009. Chitosan based nonstoichiometric polyelectrolyte complexes as specialized flocculants. *Colloids and Surfaces A: Physicochemical and Engineering Aspects*, 346(1), 39–46.
- Mihai, M., Ghiorghită, C.A., Stoica, I., Niță, L., Popescu, I., Fundueanu, G., 2011. New polyelectrolyte complex particles as colloidal dispersions based on weak synthetic and/or natural polyelectrolytes. *Express Polym Letters*, 5(6), 506–15.
- Mihai, M., Schwarz, S., Janke, A., Ghiorghită, C.A., Drăgan, E.S., 2013. Silica microparticles surface coating by layer-by-layer or polyelectrolyte complex adsorption. *Journal of Polymer Research*, 20(2), 1–9.
- Moodley, K., Pillay, V., Choonara, Y. E., du Toit, L. C., Ndesendo, V. M., Kumar, P., Bawa, P., 2011. Oral drug delivery systems comprising altered geometric configurations for controlled drug delivery. *International Journal of Molecular Sciences*, 13(1), 18-43.
- Mora-Huertas, C.E., Fessi, H., Elaissari, A., 2010. Polymer-based nanocapsules for drug delivery. *International Journal of Pharmaceutics*, 385(1), 113–42.
- Morishita, M., Peppas, N.A., 2006. Is the oral route possible for peptide and protein drug delivery? *Drug Discovery Today*, 11(19), 905–10.

- Moustafine, R.I., Kabanova, T.V., Kemenova, V.A., Van den Mooter, G., 2005. Characteristics of interpolyelectrolyte complexes of Eudragit E100 with Eudragit L100. *Journal of Controlled Release*, 103(1), 191–8.
- Moustafine, R.I., Zaharov, I.M., Kemenova, V.A., 2006. Physicochemical characterization and drug release properties of Eudragit® E PO/Eudragit® L 100-55 interpolyelectrolyte complexes. *European Journal of Pharmaceutics and Biopharmaceutics*, 63(1), 26-36.
- Mudassir, J., Darwis, Y., Khiang, P. K., 2015. Prerequisite Characteristics of Nanocarriers Favoring Oral Insulin Delivery: Nanogels as an Opportunity. *International Journal of Polymeric Material*, 64(3), 155-167.
- Muheem, F., Shakeel, M.A., Jahangir, M., Anwar, N., Mallick, G.K., Jain, M.H., Warsi, F.J., Ahmad, F.J., 2014. A review on the strategies for oral delivery of proteins and peptides and their clinical perspectives. *Saudi Pharmaceutical Journal* (adapted from <http://dx.doi.org/10.1016/j.jsps.2014.06.004>).
- Naidu, V.G.M., Madhusudhana, K., Sashidhar, R.B., Ramakrishna, S., Khar, R.K., Ahmed, F.J., Diwan P.V., 2009. Polyelectrolyte complexes of gum kondagogu and chitosan, as diclofenac carriers. *Carbohydrate Polymer*, 76(3), 464–71.
- Nair, L.S., Laurencin, C.T., 2007. Biodegradable polymers as biomaterials. *Progress in Polymer Science*, 32(8), 762–98.
- Nanjwade, B.K., Singh, J., Parikh, K.A., Manvi, F.V., 2010. Preparation and evaluation of carboplatin biodegradable polymeric nanoparticles. *International Journal of Pharmaceutics*, 385(1), 176–80.
- Ngwuluka, N. C., Choonara, Y. E., Kumar, P., Modi, G., Toit, L. C. D., Pillay, V., 2013. A Hybrid Methacrylate-Sodium Carboxymethylcellulose Interpolyelectrolyte Complex: Rheometry and *in Silico* Disposition for Controlled Drug Release. *Materials*, 6(10), 4284-4308
- Ngwuluka, N.C., Choonara, Y.E., Modi, G., du Toit, L.C., Kumar, P., Ndesendo, V.M., Pillay, V., 2013. Design of an interpolyelectrolyte gastroretentive matrix for the site-specific zero-order delivery of levodopa in Parkinson's disease. *AAPS PharmSciTech*, 14, 605-619.
- Pandey, R., Khuller, G.K., 2004. Chemotherapeutic potential of alginate-chitosan microspheres as anti-tubercular drug carriers. *Journal of Antimicrobial Chemotherapy*, 53(4), 635–40.
- Pendekal, M.S., Tegginamat, P.K., 2013. Hybrid drug delivery system for oropharyngeal, cervical and colorectal cancer - *in vitro* and *in vivo* evaluation. *Saudi Pharmaceutical Journal*, 21(2), 177–86.

- Petrov, A.I., Antipov, A.A., Sukhorukov, G.B., 2003. Base-acid equilibria in polyelectrolyte systems: from weak polyelectrolytes to interpolyelectrolyte complexes and multilayered polyelectrolyte shells. *Macromolecules*, 36(26), 10079–86.
- Petzold, G., Simona, S., 2014. *Polyelectrolyte Complexes in Flocculation Applications*. Springer Berlin Heidelberg, 256, 25-65.
- Polexe, R.C., Delair, T., 2013. Elaboration of Stable and Antibody Functionalized Positively Charged Colloids by Polyelectrolyte Complexation between Chitosan and Hyaluronic Acid. *Molecules*, 18(7), 8563–78.
- Porter, C.J.H., Pouton, C.W., Cuine, J.F., Charman, W.N., 2008. Enhancing intestinal drug solubilisation using lipid-based delivery systems. *Advanced Drug Delivery Reviews*, 60(6), 673–91.
- Prado, H.J., Matulewicz, M.C., Bonelli, P., Cukierman, A.L., 2008. Basic butylated methacrylate copolymer/kappa-carrageenan interpolyelectrolyte complex: Preparation, characterization and drug release behaviour. *European Journal of Pharmaceutics and Biopharmaceutics*, 70(1), 171–8.
- Prado, H.J., Matulewicz, M.C., Bonelli, P.R., Cukierman, A.L., 2009. Preparation and characterization of a novel starch-based interpolyelectrolyte complex as matrix for controlled drug release. *Carbohydrate Research*, 344(11), 1325–31.
- Prado, H.J., Matulewicz, M.C., Bonelli, P.R., Cukierman, A.L., 2012. Preparation and characterization of controlled release matrices based on novel seaweed interpolyelectrolyte complexes. *International Journal of Pharmaceutics*, 429(1), 12–21.
- Reddy, M.M., Reddy, D.J., Moin, A., Shivakumar, H.G., 2011. Formulation of sustained release matrix tablet using Chitosan/Ghatti gum polyelectrolyte complex *Der Pharmacia Lettre* 3, 119–28.
- Risbud, M.V., Hardikar, A.A., Bhat, S.V., Bhonde, R.R., 2000. pH-sensitive freeze-dried chitosan-polyvinyl pyrrolidone hydrogels as controlled release system for antibiotic delivery. *Journal of Control Release*, 68(1), 23–30.
- Rodríguez, K., Renneckar, S., Gatenholm, P., 2011. Biomimetic calcium phosphate crystal mineralization on electrospun cellulose-based scaffolds. *ACS Applied Materials and Interfaces*, 3(3), 681-9.
- Roy, S., Prabhakar, B., 2010. Bioadhesive polymeric platforms for transmucosal drug delivery systems—a review. *Tropical Journal of Pharmaceutical Research*, 9(1), 91-104.
- Sabar, M.H., Samein, L.H., Sahib, H.B., 2011. Some *Variables* Affecting the Formulation of Ketoprofen Sustained Release Oral Tablet using Polyelectrolyte Complex as a Matrix Former. *Journal of Pharmacy and Allied Health*, 1, 1–15.

- Sakiyama, T., Takata, H., Toga, T., Nakanishi, K., 2001. pH-sensitive shrinking of a dextran sulfate/chitosan complex gel and its promotion effect on the release of polymeric substances. *Journal of Applied Polymer Science*, 81(3), 667–74.
- Salama, A., El-Sakhawy, M., 2014. Preparation of polyelectrolyte/calcium phosphate hybrids for drug delivery application. *Carbohydrate polymers*, 113, 500-506.
- Sarmiento, B., Ferreira, D.C., Jorgensen, L., van de Weert, M., 2007. Probing insulin's secondary structure after entrapment into alginate/chitosan nanoparticles. *European Journal of Pharmaceutics and Biopharmaceutics*, 65(1), 10–7.
- Shovsky, A., Varga, I., Makuška, R., Claesson, P.M., 2009. Formation and Stability of Water-Soluble, Molecular Polyelectrolyte Complexes: Effects of Charge Density, Mixing Ratio, and Polyelectrolyte Concentration. *Langmuir*, 25(11), 6113–21.
- Shtompel, V.I., Sasa, B.S., Polischuk, T.A., Ryabov, S.V., 2011. Structure of stoichiometric polyelectrolyte complexes based on Na-carboxymethyl cellulose and chitosan hydrochloride. *Polymer Journal* (18181724), 33(1).
- Shu, S., Zhang, X., Teng, D., Wang, Z., Li, C., 2009. Polyelectrolyte nanoparticles based on water-soluble chitosan–poly(L-aspartic acid)–polyethylene glycol for controlled protein release. *Carbohydrate Research*, 344(10), 1197–204.
- Sonaje, K., Lin, Y.H., Juang, J.H., Wey, S.P., Chen, C.T., Sung, H.W., 2009. *In vivo* evaluation of safety and efficacy of self-assembled nanoparticles for oral insulin delivery. *Biomaterials*, 30(12), 2329–39.
- Soppimath, K.S., Aminabhavi, T.M., Kulkarni, A.R., Rudzinski, W.E., 2001. Biodegradable polymeric nanoparticles as drug delivery devices. *Journal of Controlled Release*, 70(1), 1–20.
- Sotiropoulou, M., Cincu, C., Bokias, G., Staikos, G., 2004. Water-soluble polyelectrolyte complexes formed by poly(diallyldimethylammonium chloride) and poly(sodium acrylate-co-sodium 2-acrylamido-2-methyl-1-propanesulphonate)-graft-poly(N,N-dimethylacrylamide) copolymers. *Polymer*, 45(5), 1563–8.
- Tapia, C., Escobar, Z., Costa, E., Sapag-Hagar, J., Valenzuela, F., Basualto, C., Gai, M.N., Yazdani-Pedram, M., 2004. Comparative studies on polyelectrolyte complexes and mixtures of chitosan–alginate and chitosan–carrageenan as prolonged diltiazem clorhydrate release systems. *European Journal of Pharmaceutics and Biopharmaceutics*, 57(1), 65-75.
- Thanou, M., Verhoef, J.C., Junginger, H.E., 2001. Oral drug absorption enhancement by chitosan and its derivatives. *Advanced Drug Delivery Reviews*, 52(2), 117–26.
- Torchilin, V., 2009. Multifunctional and stimuli-sensitive pharmaceutical nanocarriers. *European Journal of Pharmaceutics and Biopharmaceutics*, 71(3), 431-44.

- Vasconcelos, T., Sarmiento, B., Costa, P., 2007. Solid dispersions as strategy to improve oral bioavailability of poor water soluble drugs. *Drug Discovery Today*, 12(23), 1068–75.
- Vishalakshi, B., Ghosh, S., 2003. Nonstoichiometric polyelectrolyte complex of carboxymethylcellulose and N-methylated poly (2-vinylpyridine): Formation of a gel-like structure. *Journal of Polymer Science Part A: Polymer Chemistry*, 41(14), 2288-95.
- Wang, Q., Schlenoff, J.B., 2014. The Polyelectrolyte Complex/Coacervate Continuum. *Macromolecules*, 47(9), 3108–16.
- Wilczewska, A.Z., Niemirowicz, K., Markiewicz, K.H., Car, H., 2012. Nanoparticles as drug delivery systems. *Pharmacological Reports*, 64(5), 1020–37.
- Williams, R. O., Watts, A.B., Miller, D.A., 2012. Formulation of poorly soluble drug. 1st edition Springer, New York, USA 228.
- Wilson, M., Williams, M.A., Jones, D.S., Andrews, G.P., 2012. Hot-melt extrusion technology and pharmaceutical application. *Therapeutic Delivery*, 3(6), 787–97.
- Woodley, J., Bernkop-Schnürch, A., 2009. Oral Delivery of Macromolecular Drugs: Barriers, Strategies and Future Trends. Springer, 249.
- Xu, Y., Mazzawi, M., Chen, K., Sun, L., Dubin, P.L., 2011. Protein purification by polyelectrolyte coacervation: influence of protein charge anisotropy on selectivity. *Biomacromolecules*, 12(5), 1512-1522.
- Yeh, M., Cheng, K., Hu, C., Huang, Y., Young, J., 2011. Novel protein-loaded chondroitin sulfate-chitosan nanoparticles: preparation and characterization. *Acta Biomaterialia*, 7(10), 3804–12.
- Yujie, X., Pack, D.W., 2015. Uniform biodegradable microparticle systems for controlled release. *Chemical Engineering Science*, 125, 129–143.
- Zakhem, E., Raghavan, S., Gilmont, R.R., Bitar, K.N., 2012. Chitosan-based scaffolds for the support of smooth muscle constructs in intestinal tissue engineering. *Biomaterials*, 33(19), 4810–7.

CHAPTER 3

A HUMIC ACID-POLYQUATERNIUM-10 STOICHIOMETRIC SELF-ASSEMBLED FIBRILLA POLYELECTROLYTE COMPLEX: EFFECT OF PH ON SYNTHESIS, CHARACTERIZATION AND DRUG RELEASE

3.1. INTRODUCTION

Polyelectrolyte complexes (PECs) utilize unique properties of polymers involved in the complex and are formed by electrostatic binding between a cation and an anion (Nath *et al.*, 2015; Ankerfors *et al.*, 2010). As previously reported by our group (Siyawamwaya *et al.*, 2015), polymers that are readily charged or those that become charged under specific conditions such as certain pH values are a prerequisite for PEC formation. This study utilized the solution mixing method to investigate the possibility of a stoichiometric PEC formation between humic acid (HA) and polyquaternium-10 (PQ10) with emphasis on the effect of pH of the solution medium on synthesis. It is a well-known fact that pH of the solution medium is one of the parameters which significantly impacts on the PEC formation (Kumar and Ahuja, 2013; Lin *et al.*, 2005). Stoichiometric polymeric ratios yield insoluble and neutrally charged PECs (Tapia *et al.*, 2004; Kabanov and Zezin, 1984).

PQ10 is a cationic cellulose derivative which is also known as quaternized hydroxyethylcellulose ethoxylate. It is stipulated that polymers containing quaternary amino groups are promising candidates for biomedical applications since they exhibit diverse chemical properties (Bierbrauer *et al.*, 2014). They are soluble in both aqueous and aqueous-alcoholic media. The ammonium group in PQ10 is situated at the end of the poly (ethylene glycol) chains therefore it possesses a very high affinity for negatively charged groups. During the aggregation process, as the PEC forms, these hydroxyethyl substituents may be included in the complex and thereby contributing to the self-assembly process (Rodríguez^a *et al.*, 2003).

Advantages of using PQ10 include non-toxicity, mucoadhesion, biocompatibility, stability against gastrointestinal enzymes and the ability to attain a high viscosity upon swelling (Mazoniene *et al.*, 2011). An example of a similar polymer is chitosan by which the cationic nature is also attributed to the presence of the ammonium substituents. The ionization of PQ10 is pH independent unlike that of chitosan. PQ10 exhibits efficient solubility properties in water and upon dissolving, there is thickening of the medium (Rodríguez *et al.*, 2003^a 2003^b). PQ10 has been known to form stable complexes with anionic surfactants and this

combination is believed to possibly enhance the solubility of hydrophobic drugs (Cumming *et al.*, 2008; Rodríguez^a *et al.*, 2003). Additionally, polyquaternium compounds exhibit antibacterial properties which are facilitated by their penetration enhancing effects (Carmona-Ribeiro and de Melo Carrasco, 2013; Rodríguez^a *et al.*, 2003).

Humic acid (HA) belongs to a family of humic substances which are weakly acidic and heterogeneous compounds. Its acidic behavior is exhibited by the ionization of carboxylic and phenolic groups and it has been shown to exhibit good complexing properties with cations. HA contains both a supramolecular and macromolecular structure with a significant aromatic character. The quantity of the aromatic groups is directly proportional to the more carboxylic acid groups present in the HA structure (Baigorri *et al.*, 2009). HA is a mixture of different components and therefore it is not associated with a distinct structure.

HAs are partially soluble in water and the solubility increases with increase in pH. The alkaline medium will cause deprotonization of some HA molecules and therefore peptization occurs as the molecules repel each other (Klučáková and Pekař, 2005). In the study undertaken, commercial brown HA was used. The brown colour emanates from the aromatic carbon moieties derived from plant precursor materials (Coble *et al.*, 2014). Brown HA is known to dissolve in alkaline solution and dissolution is independent of ionic strength unlike gray HA which dissolves in low ionic strength. The condensed aromatic structures and oxygen containing groups are responsible for the molecular aggregates formed in solution by the brown HA as well as its high affinity for hydrophobic substances (Baigorri *et al.*, 2009). HA also exhibits amphiphilic properties (Bahvalov *et al.*, 2010). The negative charges take part in complex formation with cationic groups and the hydrophobic site becomes exposed thus forming a water insoluble complex (Stepanov 2008; Yee *et al.*, 2006).

A HA and PQ10 polyelectrolyte complex was synthesized in aqueous solutions at pH 6.0 (F1), 7.0 (F2) and 8.0 (F3). To the best of our knowledge, this complex has not been reported in literature thus far. The main aim of this study was to confirm formation of the novel PEC. Currently, there is extensive research on the use of natural polymers for biomedical and industrial application largely due to their biocompatibility, biodegradability and ubiquitous availability (Thakur *et al.*, 2016; Thakur and Thakur, 2014; Tsai *et al.*, 2014). Additionally, properties such as simulating natural tissues and extemporaneous self-healing enable biopolymers to be applicable for properties such as synthesis of hydrogels for extended release of bioactives (Thakur and Kessler, 2015; Thakur and Thakur, 2015). A lipophilic drug, efavirenz (EFV), was chosen as the model prototype drug to determine the drug release profile from this complex. EFV is a long-established drug in HIV treatment due

to the fact that at least two mutations are required in the reverse transcription for any drug resistance to materialize in patients (Hofman *et al.*, 2004). Figure 3.1 depicts the model structures of HA and PQ10.

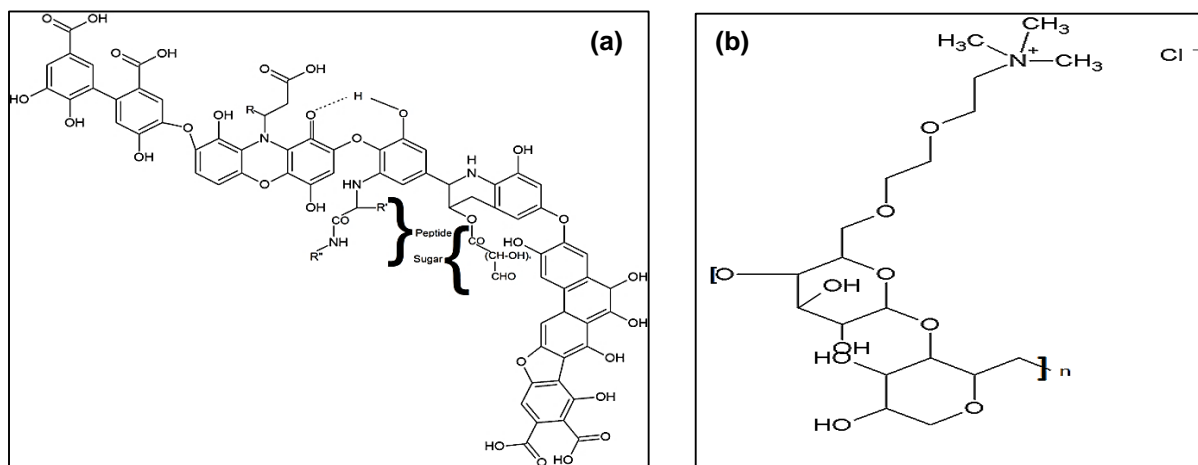


Figure 3.1: (a) Model structure of humic acid as proposed by Stevenson (Peña-Méndez *et al.*, 2005) and (b) general structure of polyquaternium-10 (Yang *et al.*, 2008)

3.2. MATERIALS AND METHODS

3.2.1. Materials

Brown humic acid, polyquaternium-10 (quaternized hydroxyethylcellulose ethoxylate), methyl thiazoyl tetrazolium bromide (MTT) and the solubilizing solution (10% sodium dodecyl sulfate in 0.01M hydrochloric acid) were purchased from Sigma-Aldrich® (St. Louis, MO, USA). Pure efavirenz powder was purchased from Xingcheng Chemphar Co., Ltd. (Taizhou, Zhejiang, China) and was used as received. pH of solutions was adjusted to the desired pH using 1M sodium hydroxide (NaOH) solution and 0.1M solution of hydrochloric acid (HCl). The Caco2 human adenocarcinoma cell line, Dulbecco's Modified Eagle's Medium (DMEM), foetal bovine serum and all other cell culture reagents were acquired Promolab Pty Ltd T/A Separations (Johannesburg, South Africa). All other reagents were of analytical grade.

3.2.2. Determination of the humic acid concentration and functional group profiling

HA (2.3g) was added to 400mL of deionized water and the pH was adjusted accordingly using 1M NaOH/HCl to pH 6.0, 7.0 and 8.0. The solution was left to stir for 2 hours after which it was filtered using 90mm filter paper. Filtration was repeated to ensure that only the dissolved HA remained in the solution (Klučáková and Pekař, 2005). The filtrate (0.5mL) was measured out and left to dry overnight. After drying, the samples were re-weighed to determine the amount of HA that dissolved in deionized water. The titration method was implemented to determine the amount of carboxylic acid groups present in the HA sample.

Titration gave an indication of the exact number of moles of HA that reacted with the PQ10. The automatic pipette was used to measure the phenolphthalein and NaOH volumes. Brown HA solution (0.5mL) was diluted in 500mL of water and 150 μ l of phenolphthalein was added to the solution. The solution was left to stir for a minute. Titration of the solution was carried out by adding a known amount of the NaOH from the micropipette until the end point was reached (Klučáková and Pekař, 2005).

3.2.3. Determination of the self-assembly of humic acid and polyquaternium-10 to form the fibrilla PEC

PQ10 powder (600mg) was dissolved in deionized water (100mL). The PQ10 solution was slowly titrated into HA solution (100mL) under constant magnetic stirring (Piyakulawat *et al.*, 2007). The solution was left to stand to allow the supernatant to separate from the PECs. The PECs were then soaked in distilled water and filtered using the 90mm filter paper. Drug loading in the complexes was conducted by adding the drug solution (200mg of drug dissolved in 20mL methanol) to the HA solution prior to adding the PQ10 solution. The PEC strands were filtered as soon as they separated from the supernatant. The PEC was dried in an oven at 40°C for at least 12 hours, when a constant mass was obtained. The powder containing 200mg drug was thereafter filled into hard gelatin capsule shells size 00 for drug release studies after determination of percentage drug loading of PECs (Heinen *et al.*, 2013).

3.2.4. Physicochemical characterization of the PEC and native components

3.2.4.1. Determination polyquaternium-10 concentration for stoichiometric ratio reaction with humic acid

Rheology was performed to determine the viscosities of the supernatants that separated out from the complex. Measurement was conducted with the aid of a Modular Advanced Rheometer (ThermoHaake MARS Modular Advanced Rheometer, Thermo Electron, Karlsruhe, Germany). Viscosity measurements were taken over 360 seconds at 25°C.

3.2.4.2. Determination of polyquaternium-10 and humic acid electrostatic interactions

Intermolecular interactions between HA and PQ10 were determined utilizing a PerkinElmer Spectrum 2000 ATR-FTIR (PerkinElmer 100, Llantrisant, Wales, UK). Wavelength for analysis ranged from 650 to 4000 cm^{-1} with a resolution of 4 cm^{-1} . A direct force of 115N was applied and 25 scans/spectrum were taken.

3.2.4.3. Assessment of the influence of simulated gastrointestinal fluids on the swelling and degradation of the PEC

Pre-weighed PECs were placed in 100mL of USP buffers at pH 1.2 and 6.8 to mimic gastrointestinal conditions. These were incubated in an orbital shaker bath (37°C, 50rpm) and the weights were recorded every 2 hours for 8 hours thereafter, at 24 hours. Percentage swelling degree (% SD) was calculated for each PEC using Equation 3.1. Any changes to the initial structures of the PECs were determined by conducting FTIR on PECs that had been left to dry in an oven at 50°C until a constant mass was obtained.

$$\% SD = \frac{W_s - W_D}{W_D} \times 100$$

Equation 3.1

Where, W_s is weight of swollen PEC and W_D is the weight of the dry PEC.

3.2.4.4. Degree of crystallinity of polyquaternium-10, humic acid and the PEC

Dried and powdered samples of the PECs were analysed using a powder X-Ray diffractometer (Rigaku Miniflex 600 XRD) (Rigaku Corporation, Tokyo, Japan) to compare the crystallinity of the PECs to that of the native polymers. Measurements were taken from 0°-90° at 10°/min. The incident and receiving slits were both at 2.5°. No monochromator was used during the analysis process. Operation of the XRD was done at 40kV and 15mA.

3.2.4.5. Determination of thermodynamic properties of the PEC

Differential scanning calorimetry (DSC) was conducted for the determination of the thermal behavior of HA, PQ10 and PECs. A Mettler-Toledo TC15, TA controller System (Mettler Toledo, DSC1, STARe System, Schwerzenback, Switzerland) was utilized. A maximum of 10mg of sample was filled into each pan which was then closed and perforated. Temperature was set at 10°C-300°C with a heating rate of 10°C/min. Thermal degradation was carried out using thermogravimetric analysis, Perkin Elmer TGA 4000, (Perkin Elmer Inc. Waltham, USA). The heating range utilized was 30°C–900°C with a 10°C/min heating rate.

3.2.4.6. Analysis of the surface morphology and elemental quantification of the PEC and native components

Surface morphology was analysed with the aid of a scanning electron microscope. FEI Nova NanoLab™ 600 DualBeam (FEI, Hillsboro, OR, USA) was used. Preparation of samples was undertaken by sputter coating them with gold and palladium using the SPI-Module Sputter coater (Structure Probe Inc. West Chester, USA). Scanning was conducted under 30kV with

a beam current of 0.63nA. The working distance was set at 5mm and a dwell time of 3μs was utilized. Compositions of the samples were determined using Energy Dispersive X-ray spectroscopy which is installed as part of the FIB/SEM. Element mapping was conducted with an accelerating voltage of 30kV and an image resolution of 512μm x 448μm. EDS utilizes a focused beam of electrons to measure X-ray emissions from charged particles of a solid sample.

3.2.4.7. *In vitro* drug release studies and drug loading capacity of the PEC

Acetonitrile (50%, 80mL) was added to a 100mg powder sample of the PECs. The amount of drug in the sample was determined using a calibration curve constructed using an ultraviolet (UV) spectrophotometer (LAMBDA 25 UV/Vis spectrophotometer, PerkinElmer, MA, USA) at 248nm. A series of dilutions of EFV in simulated intestinal fluid (SIF) (pH=6.8) with 1% sodium lauryl sulfate (SLS) were prepared. Percentage drug loading was calculated using Equation 3.2.

$$\% \text{ drug loading} = \frac{\text{amount of drug in 100mg powder sample}}{\text{total amount of powder sample}} \times 100$$

Equation 3.2

Drug release studies were conducted utilizing the USP apparatus II paddle stirrer (Erweka DT 700, Erweka GmbH, Heusenstamm, Germany) with a rotation of 50rpm (Ngwuluka *et al.*, 2012). Temperature was set at 37°C and 900mL of simulated gastric fluid at pH 1.2 and intestinal fluid at pH 6.8 were used respectively. SLS was added to the dissolution media due to the low solubility of EFV. Sample aliquots (5mL) were collected and immediately replaced with fresh buffer at 0.5, 1, 1.5, 2, 3, 4, 5, 6, 7 and 8 hours. Quantification of the drug was carried out after drying the samples and reconstituting the dry powder with acetonitrile. Preliminary studies showed that the polymers potentially interfered with UV analysis. Dilution of the samples was done separately with deionized water before filtration and UV analysis at 248nm. All data was obtained in triplicate.

3.2.4.8. *Determination of impact of the PEC on viability of Caco2 cell line*

Ex vivo cytotoxicity of HA-PQ10 PEC was conducted on the human colorectal adenocarcinoma (Caco2) cell line. The growth medium consisted of Dulbecco's Modified Eagle's Medium (DMEM) with 4.0mM L-Glutamine and 10% sodium pyruvate foetal bovine serum (FBS). Cytotoxicity was measured with the aid of the methyl tetrazolium (MTT) cell proliferation assay. The tetrazolium ring of 3-[4,5-dimethylthiazol-2-yl]-2,5-diphenyl tetrazolium bromide is reduced by the cell mitochondrial dehydrogenases yielding MTT

formazan crystals which were quantified spectrophotometrically to obtain the optical density with the aid of a microplate reader (Power Wave XS, BIO-TEK®, USA) (Palamà *et al.*, 2011). Caco2 cells (100µl) with a density of $(6 \times 10^4)/100\mu\text{l}$ were seeded in a 96 well plate and incubated in a CO₂ incubator (RS Biotech Galaxy, Irvine, UK). After 24 hours, 0.375mg/mL powdered PEC samples (100µl) dispersed in the cell culture medium were added to the well plates in triplicate and incubated for another 24 hours. The test solution was replaced with culture medium (100µl) and MTT solution (10µl) before incubation for 3 hours. Solubilization solution was added before absorbance from the wells was measured at 570nm with a background absorbance of 690nm. Cell viability was calculated using Equation 3.3.

$$\text{Cell viability (\%)} = \frac{OD_{\text{treated}}}{OD_{\text{control}}} \times 100$$

Equation 3.3

Where OD_{treated} is the optical density of the cells treated with the PEC sample and OD_{control} is the optical density of the untreated cells.

3.3. RESULTS AND DISCUSSION

3.3.1. Self-assembly nature of humic acid and polyquaternium-10 to form a fibrilla PEC

As the PQ10 solution was slowly added to the HA solution, the PEC was instantly formed and it was observed as brown strands that precipitated out and settled at the bottom of the beaker. Figure 3.1(a) represents the stages of formation and the strands that formed which is generally characteristic to PEC formation. The PECs were synthesized in stoichiometric ratios at pH 6.0 (F1), pH 7.0 (F2) and pH 8.0 (F3). When the PECs were soaked in distilled water, they did not dissolve but collected at the bottom of the beaker possibly due to the intramolecular interactions being more superior to the PEC-water interactions. Upon filtering, they were washed with deionized water to ensure that all untrapped drug was removed from the fibrous PEC sample. Complexation between the polycation (PQ10) and the anionic amphiphile (HA) transpired through the formation of electrostatic bonds between the functional groups. When the PQ10 solution was titrated into the HA solution, the ammonium groups bonded with the carboxylic groups therefore exposing the less hydrophilic cellulose backbone to the aqueous environment (Figure 3.1(b)). The HA macromolecule was engulfed by the PQ10 molecules in a stoichiometric ratio that facilitated the self-assembly of the polymers into a strong and stable system, devoid of crosslinking. Drug loading was conducted by adding the dissolved drug into the HA solution prior to titration of the PQ10 into the solution. EFV was encapsulated into the polymer through hydrophobic interactions with the large aromatic core present in HA.

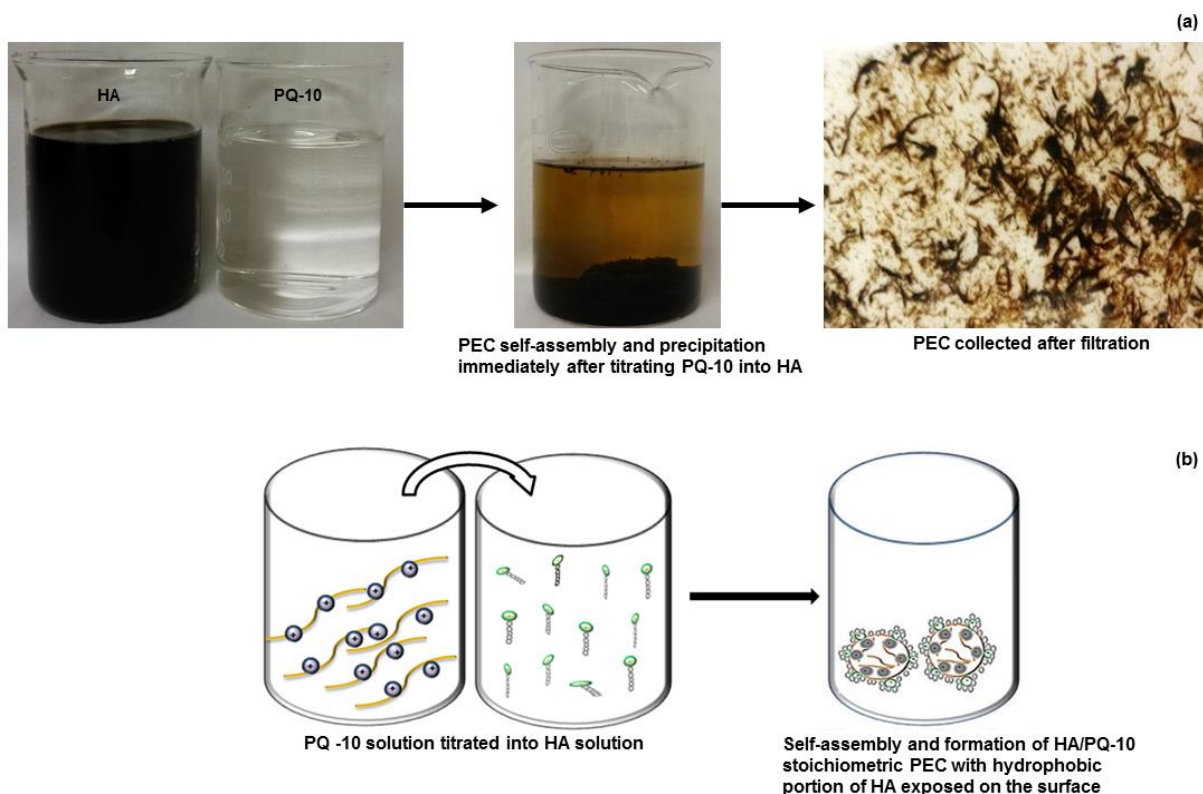


Figure 3.2: (a) Digital pictures of the self-assembly of HA and PQ10 and the fibrous PECs collected by filtration before drying; (b) a schematic depicting the self-assembly process of the HA and PQ10

3.3.2. Evaluation of the humic acid concentration and presence of functional groups

Since HA is known to dissolve in alkaline conditions, a pH of 7.0 was found to be ideal for dissolving the polymer with 100mL of this solution being utilized for PEC formation. Preliminary rheology results for HA in solution showed a viscosity of 1.0735mPa.s at pH 6.0, 1.406mPa.s at pH 7.0 and 1.348mPa.s at pH 8.0. A higher viscosity value indicated an increase in the amount of humic acid that completely dissolved in water at that particular pH. Consequently, using a pH >8.0 meant that phenolic groups would become ionized as well since they possess an estimated pKa of 9. The phenoxide ion is however less stable and can therefore easily reform the phenol group unlike the ionized carboxylic group. The carboxyl groups are the more dominant ones in number in HA compared to the phenolic groups (Ritchie and Perdue, 2003). Re-weighing the dry HA samples indicated that an average amount of 2.8mg of HA was present in 0.5mL of HA solution. Concentration of HA was determined to be 5.6mg/mL. Six titrations were carried out and an average of 150 μ l was obtained for the complete reaction of 0.5mL of HA. It was thus confirmed that 0.3mmols of COO⁻ groups were present in 5.6mg of HA.

3.3.3. Analysis of the polyquaternium-10 concentration for stoichiometric reactivity with humic acid

Rheology of supernatants was carried out as a means of quantifying the amount of PQ10 required to react completely with 25mL (140mg) of HA. The solution containing the PECs was allowed to stand for 30 minutes so that the supernatant could be collected after the PEC settled. The viscosities steadily decreased as the amount of PQ10 increased from 0.1g. The increase was due to a more complete reaction occurring between the polymers. Simultaneously, the colour of the supernatants changed and became lighter from a brown colour with the decrease in viscosity. Complete reaction was determined after adding 0.141g of PQ10 because the viscosity of the supernatant was lowest (1.066mPa.s) at this weight. 0.141g of PQ10 was required to completely react with 0.140g of HA. Thereafter, the viscosity values started increasing when 0.142g or more of PQ10 were added. This increase was probably due to the presence of the unreacted PQ10 since complete reaction was achieved with 0.141g. Results from rheology are illustrated in Figure 3.2.

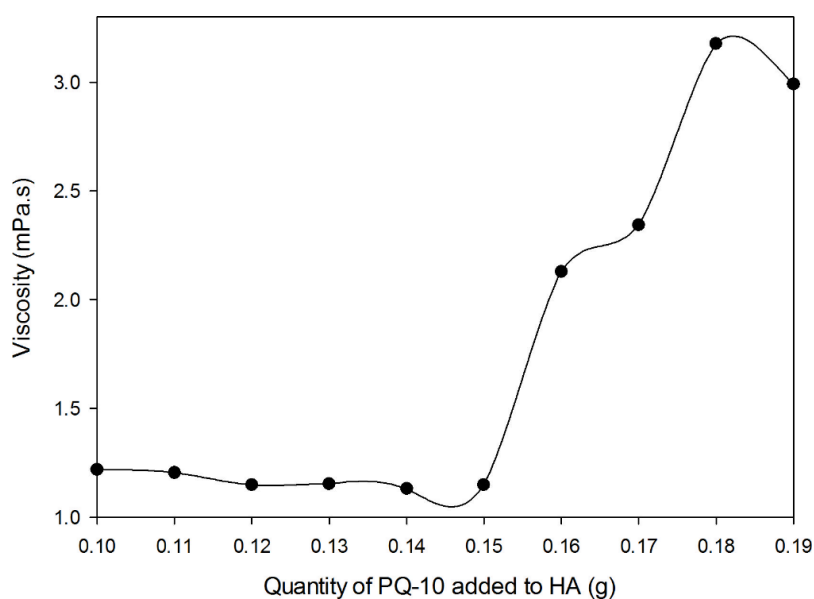


Figure 3.3: Viscosities of supernatants from complexes synthesized by adding different quantities of PQ10 to HA

3.3.4. Elucidation of the polyquaternium-10 and humic acid electrostatic interactions

The FTIR spectra for all PECs synthesized at different pH values showed that all the samples had the same peaks at similar wavelengths thus implying that they did not possess distinct qualitative differences. The main difference was with the percentage transmittances (%T) peaks. The FTIR spectra are shown in Figure 3.3(a) and Figure 3.3(b). In comparison to the HA spectrum, the F2 spectrum shows a shift in the position of the broad peak at

3323.54 cm^{-1} to 3329.63 cm^{-1} as well as a decrease in intensity of absorption. This peak is attributed to the free carboxylic acid groups. F3 contained the most of these free groups. Two bonds in HA at 1030.28 cm^{-1} and 1008.07 cm^{-1} which correspond to C-O bonds and Si-O bonds respectively were destroyed. Between 1080 cm^{-1} and 1300 cm^{-1} , the C-O bonds of primary alcohols and ether linkages in the PQ10 were destroyed.

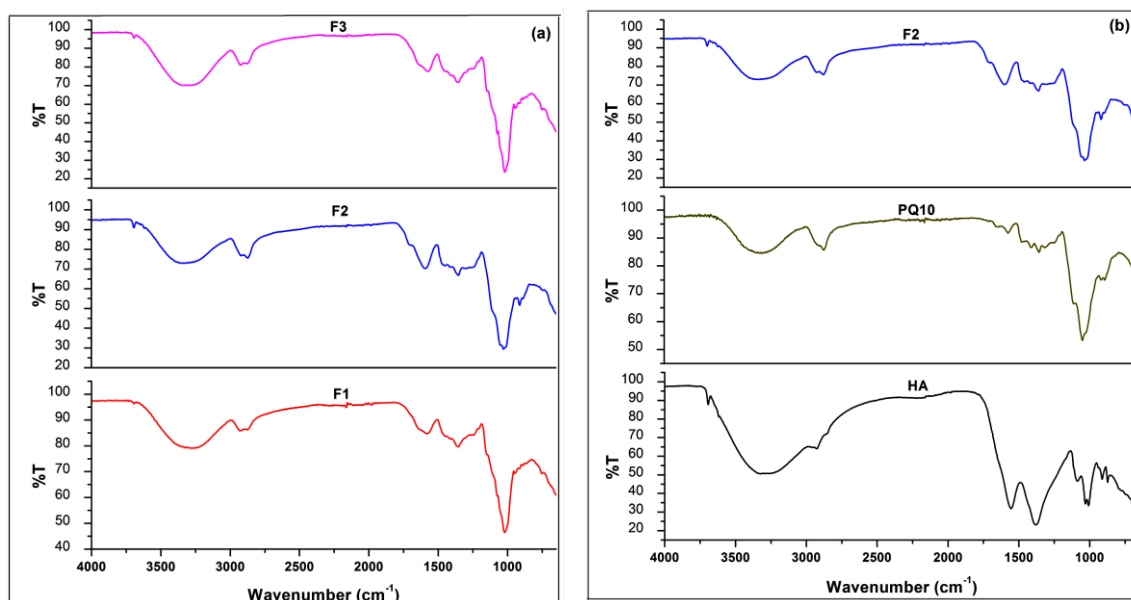


Figure 3.4: FTIR spectra of (a) F1, F2 and F3 and (b) a comparison of F2 with HA and PQ10

The absorption in HA at 1379.59 cm^{-1} is due to the COOH groups and this peak was still detected in the PECs though at a much lower absorbance. The shift in the position of the unreacted COOH in the PECs at around 1353 cm^{-1} was caused by the changes that occurred as complexation took place (Bigucci *et al.*, 2008; Amir *et al.*, 2004). This peak significantly decreased in intensity in the complex. Unreacted NH_3^+ which is expected to absorb around 1640 cm^{-1} was not detected in the PECs (Heinen *et al.*, 2013). C-H bonds at 2927.52 cm^{-1} and 2862.49 cm^{-1} in PQ10 were also present in the PECs at 2924.67 cm^{-1} . The analysis confirmed formation of a new compound and the region of interaction is depicted by the new peak that formed at 1592 cm^{-1} which is present in all the PECs. Detection of the new peak at this wavelength is congruous with the FTIR results of chitosan and alginate complexation reported by Ribeiro and co-workers (2005).

3.3.5. The influence of simulated gastrointestinal fluid on swelling and degradation of the PEC

Percentage swelling degree (%SD) of the PECs generally increased with time although swelling was limited by the lack of or low amounts of free charges within the PECs (Li *et al.*,

2009). There was a rapid increase in %SD in the first 2 hours with the PECs swelling most in pH 6.8 medium which was followed by a steady increase over time. F1 swelled more in pH 1.2 medium due to the presence of the free ammonium groups in PQ10. F2 reached equilibrium of %SD in both buffers due to the lack of free ions within the PEC. The pH at which F2 was synthesized ensured that almost all the charged groups from both polymers were exhausted. The complete neutralization of the charges in the polymers resulted in a decrease in the internal osmotic pressure of F2. The swelling behaviour was consistent with a study conducted by Li *et al* (2009) in which it was concluded that the chitosan/alginate PEC lacking free charged ions would swell the least. F3 exhibited the most %SD after 24 hours in both simulated media with the most swelling occurring in pH 6.8. The swelling was attributed to the abundance of ionized COO^- groups and therefore suboptimal reaction with the NH_3^+ groups at pH 8.0 so that more water could interact with the PEC. The free ions were present in the PEC before the experiment was conducted which explains the high %SD even in acidic medium. These results are shown in Figure 3.4. FTIR was also utilized to determine any pH degradation of the PECs after 24 hours. F1 and F3 formed new bonds at 912cm^{-1} (C-H bending) and this bond was already present in F2 before the experiment was conducted. The characteristic peak in F2 was altered in both media. F1 and F3 notably had this bond (around 1590cm^{-1}) altered in pH 1.2 and this behavior can be attributed to the aforementioned fact that there were free ammonium and carboxylic groups in these PECs. The behavior of all the PECs signified their potential to interact with the aqueous media and their capability of degrading *in vivo*.

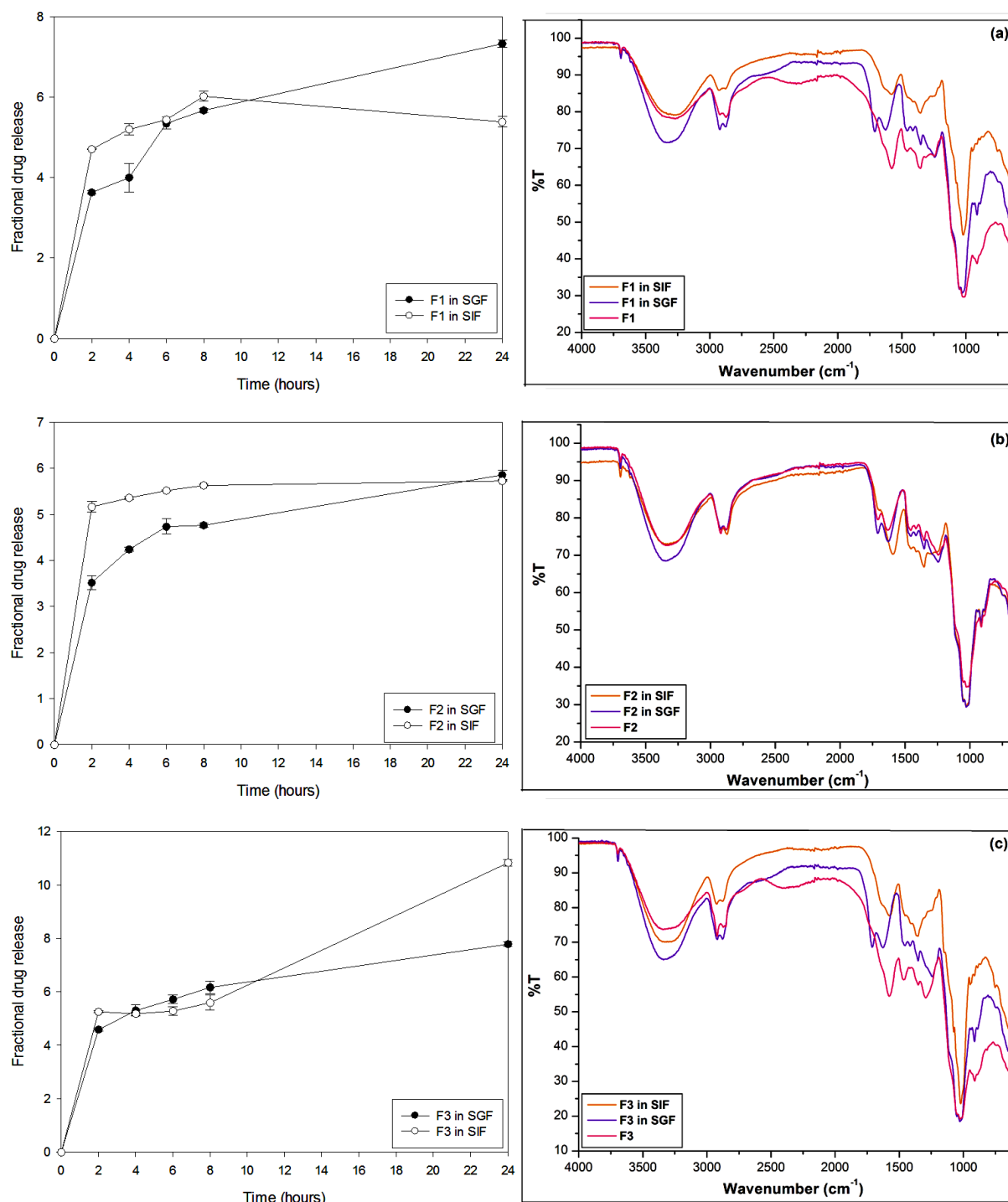


Figure 3.5: PEC degradation and % swelling degree profiles of (a) F1, (b) F2 and (c) F3 in SGF and SIF

3.3.6. Degree of crystallinity of polyquaternium-10, humic acid and the PEC

PQ10 exhibited a strong and broad reflection at about 22° which signified the amorphous nature of the polymer (Figure 3.5). The presence of minerals such as calcium, aluminium and sodium in the polymers are responsible for lowering the intensities of the XRD spectra for the native polymers. These elements scatter the X-rays thus leading to a reduction in

their absorption by the samples (Rupiasih and Vidyasagar, 2009). This reflection is present in all the PEC formulations which are largely amorphous. The intensities of the formulations are reduced in comparison to the polymers and F2 exhibits the least value in this regard. The differences between the PECs and native polymers validate the formation of a new complex.

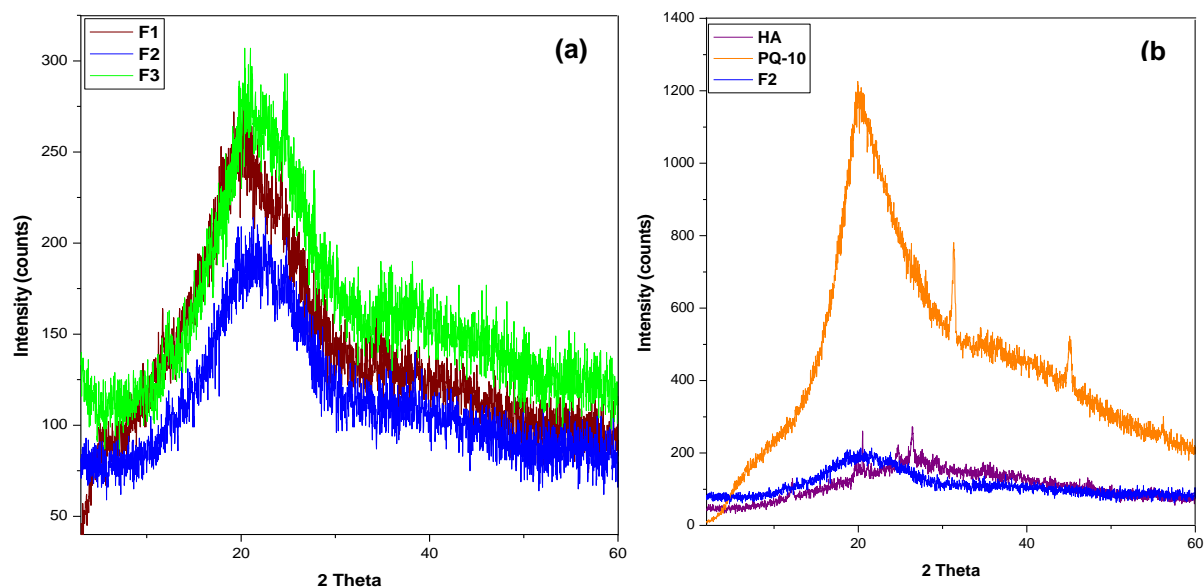


Figure 3.6: Powder X-Ray diffraction patterns for (a) F1, F2 and F3 and (b) a comparison of F2 with HA and PQ10

From the results in Table 3.1, it can be noted that all the formulations were amorphous with no trace of crystallinity. F2 lacked any significant peaks that could be detected while the ones in F1 and F3 fell in similar positions and corresponded to some of the peaks in the individual polymers ($2\theta = 20$ for PQ10 and $2\theta = 24$ for HA). The lack of crystallinity in F1, F2 and F3 signifies good compatibility between the polymers at these pH values. The diffraction pattern of HA was similar to that reported by Mirza and co-workers (2011) in being largely amorphous although showing a few crystalline peaks.

Table 3.1: 2θ positions and % crystallinity obtained from XRD

Polymer/PEC	2θ positions	% Crystallinity
F1	19.54°; 23.8°	0
F2	-	0
F3	20.68°; 23.7°	0
PQ10	20.06°; 31.37°; 45.14°; 76.19°; 80.60°	3.5
HA	12.18°; 20.69°; 24.64°; 26.462°	0

3.3.7. Analysis of the thermodynamic properties of the PEC

All the PECs (F1, F2, F3) had single broad peak melting points which fell between 60°C and 80°C (Figure 3.6(a)). These endothermic peaks were followed by another set of endothermic peaks. The onset of the second endothermic event was at 188.10°C and 220°C for F2 and F3 PECs respectively. F1 showed this change at 244.50°C. The onsets of these peaks are an indication of the stability of the compounds analyzed, where early onset reflects instability. It therefore can be concluded that F2, the most amorphous formulation of the three formulations, was most stable. Compared to those of HA and PQ10, the thermal behavior of the PEC did not correspond to that of either HA or PQ10 (Figure 3.6(b)). A single melting point was obtained for all the PECs and these were lower than those of HA (91°C) and PQ10 (80.25°C). PQ10 had a second endothermic peak at 264.73°C. This reflects the formation of a single new complex different to either of the individual polymers and whose melting point is a contribution of the polymers (HA and PQ10). All the thermograms for the individual polymers as well as for F1, F2 and F3 showed broad peaks which are characteristic of macromolecules. The second endothermic event falls between 150°C and 290°C and this finding is compliant with the DSC results on a chitosan and sodium alginate PEC from a study conducted by Shao and co-workers (2015). Similar to the HA-PQ10 PEC, the chitosan/sodium alginate PEC is formed by electrostatic bonds between ammonium groups in chitosan and carboxylic acid groups in the alginate salt. The bizarre-shaped peak shown by HA between 40°C and 140°C in Figure 3.6(b) was due to its macromolecular nature.

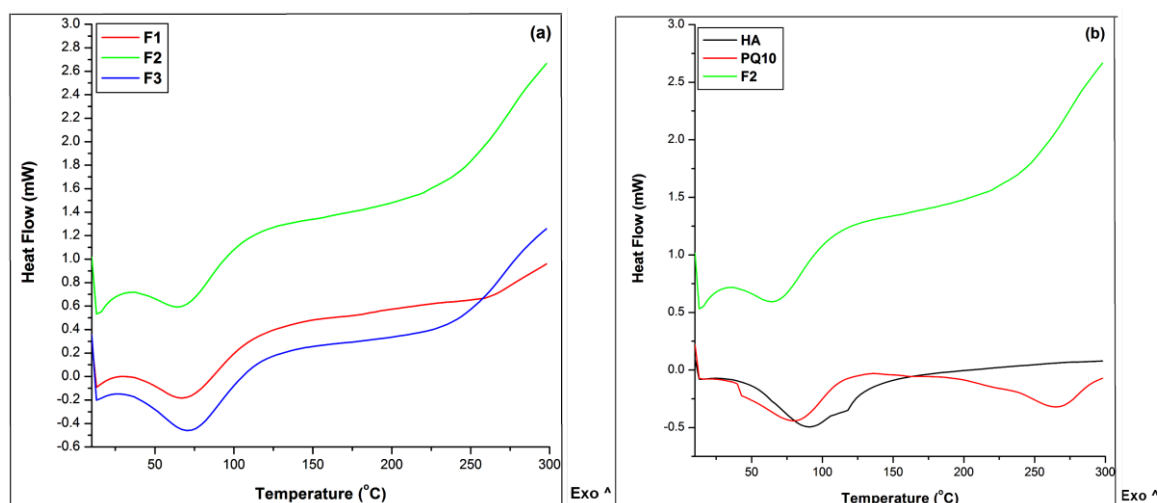


Figure 3.7: DSC thermograms for (a) F1, F2 and F3 and (b) a comparison of F2, HA and PQ10

TGA analysis revealed that the PECs were characterized by some initial weight loss beginning around 30°C which was probably caused by dehydration of the samples as they

were heating up. The thermal degradation behavior of the PECs is shown as inserts in the graphs in Figure 3.7. The PECs showed one degradation event; however, the first derivative revealed that the degradation was a two-step process in which the first step occurred at a temperature range of 300°C-350°C and the second step at 400°C-550°C. F2 degrades first at 506.13°C followed by F1 at 529.91°C and lastly F3 at 542.51°C. Mass loss was more than 90% for all the PECs with F2 exhibiting the most mass loss and F3 the least loss. Total degradation of HA and PQ10 did not occur within the 30°C–700°C range. The PECs degraded at lower temperatures than the two polymers. The mass loss for PQ10 and HA was about 4% and 30% respectively. The degradation results from TGA are similar to the DSC ones where F2 melts and degrades first followed by F1 and F3. Both sets of results suggest loss of organisation within the PECs due to the complexation process as similarly observed by Pandey *et al* (2013) in the study of a chitosan/pectin PEC. These differences are as a result of the effect of pH on PEC formation. The degradation of the PECs at lower temperatures can also be attributed to this loss of organization.

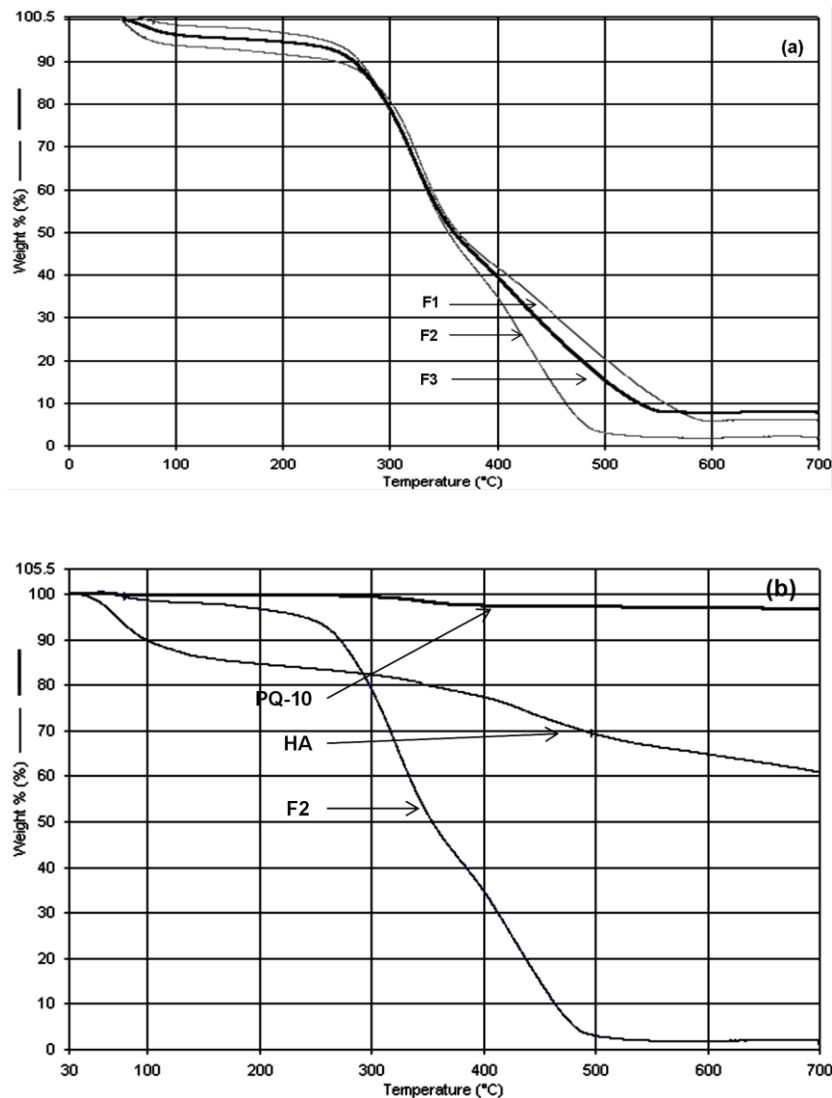


Figure 3.8: TGA thermograms for (a) F1, F2 and F3 and (b) a comparison of F2, HA and PQ10

3.3.8. Assessment of the surface morphology and elemental quantification

The physical structures of the PECs were different to those of the individual polymers as shown by the images in Figure 3.8 where HA and PQ10 are different to F1, F2 and F3. The images reveal that the surface of PQ10 is characterized by ridges and that of HA is compact and speckled by smaller crystals. SEM images of the PECs showed self-assembled fibrils. F1 PEC had fewer and smaller pores while F2 and F3 had larger and more numerous pores. Increase in pH of synthesis resulted in PECs which were more porous. With regards to the use of PECs in drug delivery, pore diameter and number has an influence on the rate of drug release (Bawa *et al.*, 2011). It is apparent from the SEM images below that complexation occurred because the “fibrilla” appearance of the PECs does not resemble the appearances of the individual polymers.

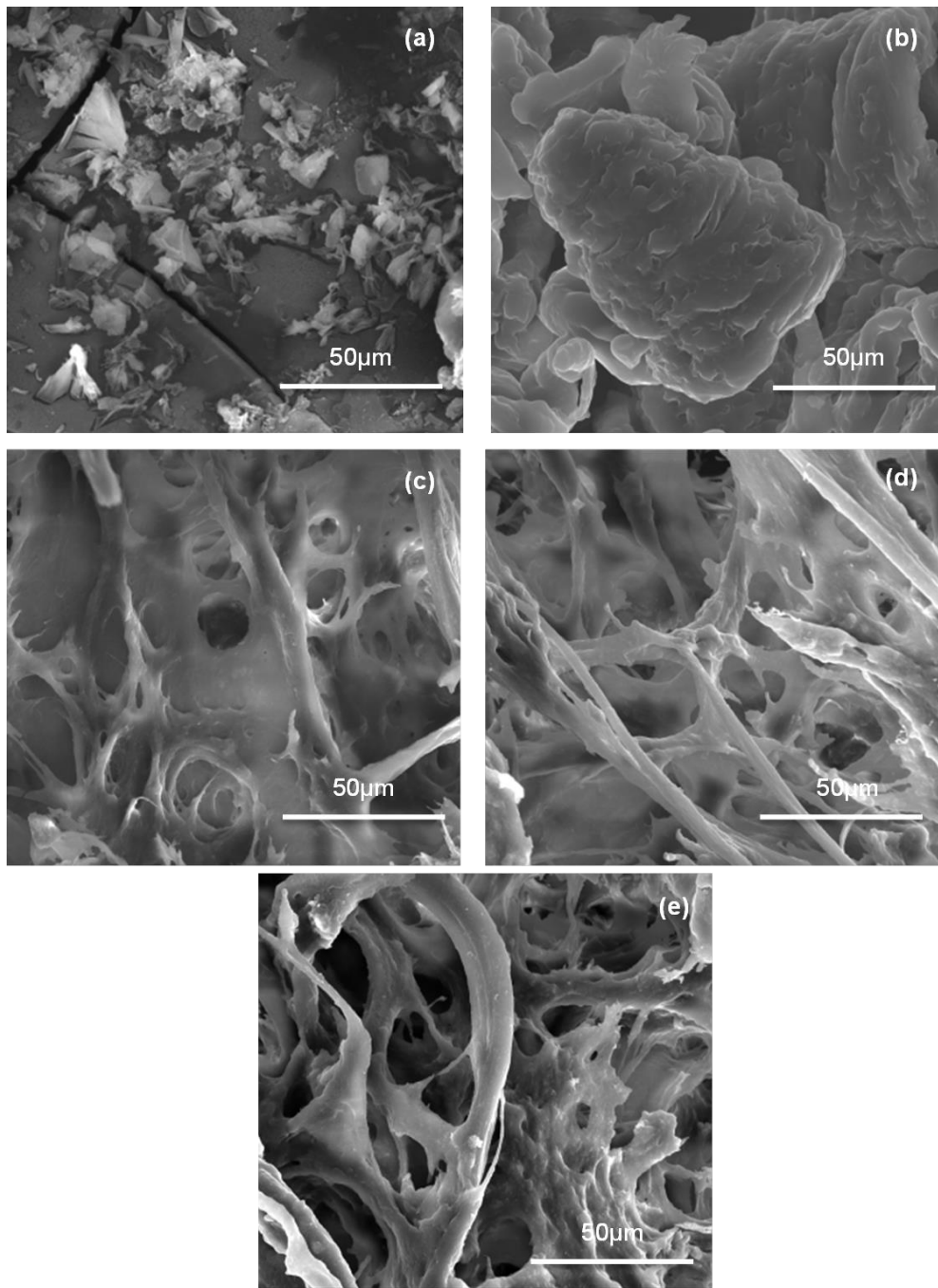


Figure 3.9: SEM images of (a) HA, (b) PQ10, (c) F1, (d) F2, (e) F3 at 2000x magnification

The quantitative results of PQ10 and HA were compared to those of all the PECs and these are shown in Figure 3.9. F1 has the least elements while F2 contains the most. Both F2 and F3 exhibit a mixture of elements in PQ10 and HA. This finding is consistent with SEM results where F2 and F3 are more porous than F1 containing the least elements.

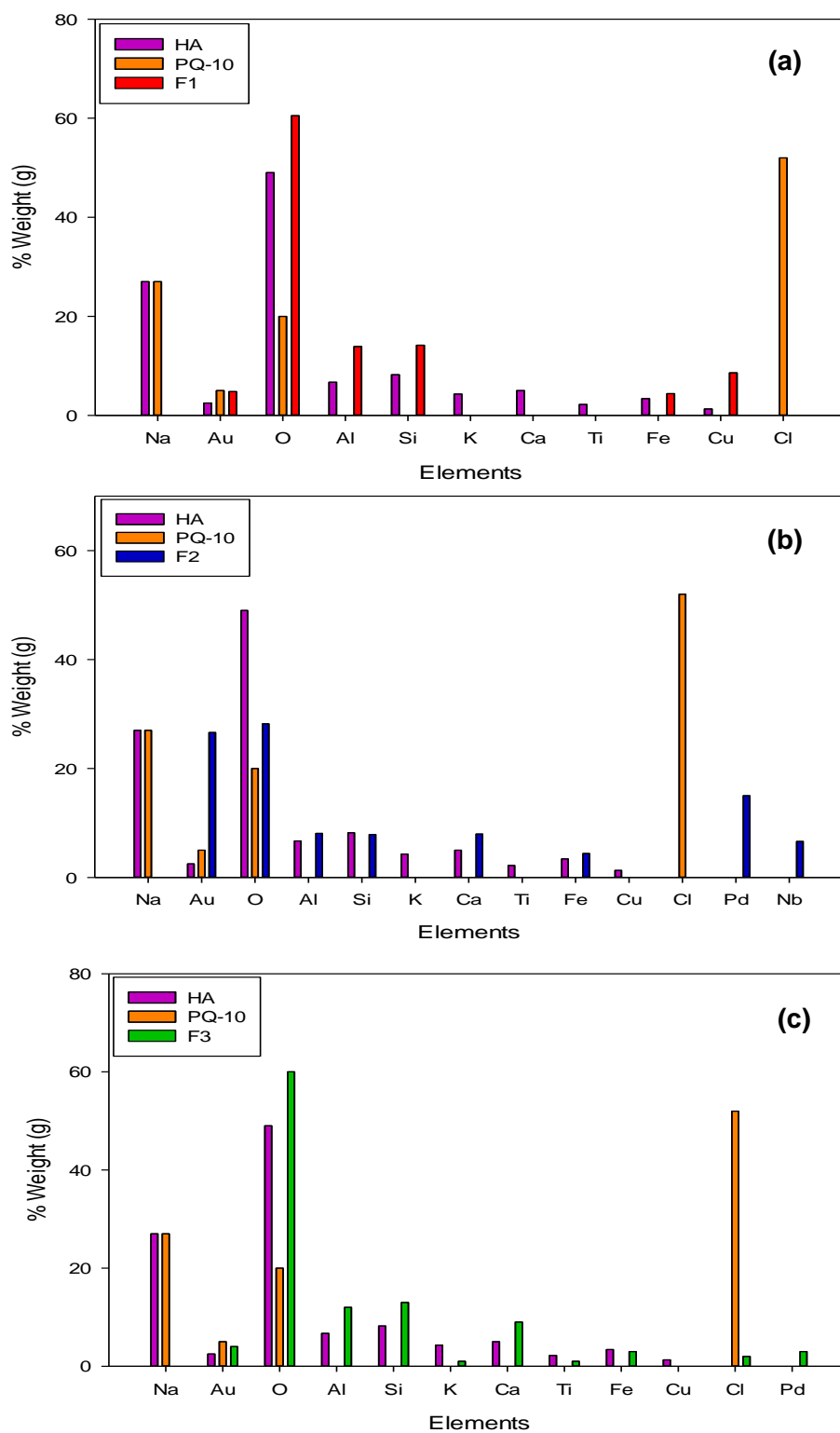


Figure 3.10: Elemental composition of (a) F1, (b) F2 and (c) F3 in comparison to HA and PQ10

3.3.9. Evaluation of *in vitro* drug release and drug-loading within the PEC

The calibration curve in Figure 3.10 was determined spectrophotometrically at 248nm. A stock solution of 0.3mg/mL was used from which a series of dilutions were prepared. SigmaPlot 12.0 (Systat Software Inc, San Jose, California, USA) was employed to plot a

liner curve of the UV absorbance of EFV as the dependent variable against the drug concentration. The R^2 value obtained was 0.99.

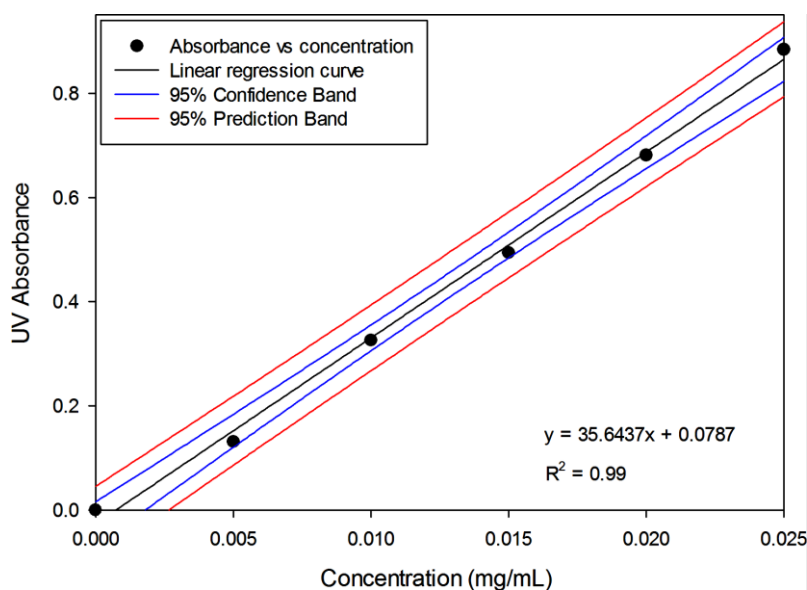


Figure 3.11: EFV calibration curve

The percentage drug loading (%DL) had to be determined prior to filling capsules for use in the drug release studies. Huang and Dai (2014) have noted that the ideal %DL should be >20% and F1 showed the ideal %DL of 23.91% while F2 and F3 had %DLs of 14.27% and 11.9% respectively. The decrease in %DL with increase in pH of synthesis can be attributed to the presence of COO^- ions which reduced the hydrophobicity of the HA. A high %DL will lower the amount of matrix materials to be included in a formulation. On the other hand, very high quantities of the drug in the dissolution medium could lead to recrystallization due to the thermodynamic instability of the drug in such quantities. The lack of protection from the polymeric matrix causes this instability (Six *et al.*, 2004). With the solution mixing method, the %DL depends on the self-assembly that occurs when the dissolved polymers and the drug are mixed together. Percentage DL can be affected by the inevitable loss of some of the polymers and drug in solution during PEC synthesis.

According to the release profiles in Figure 3.11, F2 and F3 exhibited immediate drug release over the 2 hours in SGF while a slower drug release pattern was achieved in SIF. The release pattern of F1 was different from F2 and F3 in that only 20% of the drug was released in SGF while at least 85% was released in SIF over the test period. F1 contained excess NH_3^+ ions and in SGF charge repulsion might have occurred therefore limiting the swelling ability of the PEC and decreasing the rate of drug release in acidic media. This behaviour was due to the ability of the PEC to control the drug release in its swollen state as also

reported by Saleem and co-workers (2012) on CMe_3^+ and COO^- interactions. In SIF, the excess charge increased the charge density in the PEC leading to faster drug dissolution.

F2 and F3 showed similar drug release profiles in both SGF and SIF. Both PECs exhibit low charge densities in acidic medium therefore they are liable to rearrangement leading to breakages of the complexes and rapid drug release. However it must be noted that EFV dissolves better in acidic SGF compared to the alkaline SIF (Singh *et al.*, 2013) and this might have contributed to the faster release rate from F2 and F3 in SGF. F3 contained excess ions (COO^-) in SIF which retarded PEC swelling due to charge repulsion.

The drug was released from the PECs when the complexes interacted with the aqueous environment leading to the gradual breakage of the electrostatic bonds between HA and PQ10. The hydrophilic polymer, PQ10, would form a layer rich with the aqueous medium around the drug-loaded HA thus enhancing the wetting of the amphiphile, HA, which ultimately leads to better wetting of the drug entrapped in the hydrophobic core of HA (De Paolis and Kukkonen, 1997). The PEC therefore serves as a drug reservoir. This PEC may be utilized for drug delivery with the release pattern being programmed to a desired profile such as once daily dosing. This is beneficial for HIV patients so as to improve their compliance to medication as well as provide them with more effective treatment.

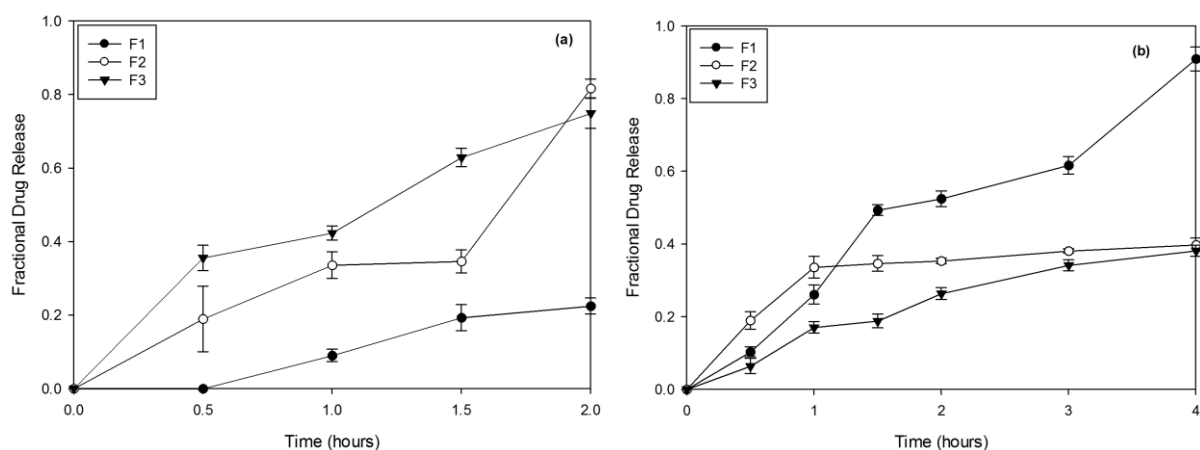


Figure 3.12: Drug release profiles of EFV-loaded F1, F2 and F3 in (a) SGF and (b) SIF

3.3.10. Elucidation of the impact of HA, PQ10 and PEC on viability of Caco2 cells

The optical densities of cells treated with the PECs and native polymers were compared to the optical density of the untreated cells. The PEC concentration utilized was similar to the one implemented in the drug release studies. All the polymer and PEC samples yielded cell viabilities above 90% (Table 3.2). Palamà and co-workers (2011) established that cell viabilities above 90% indicated non-cytotoxicity. Complexation did not drastically alter the

non-cytotoxicity of the biopolymers therefore the native polymers and the PEC were biocompatible with the Caco2 cells. The least value (96.8%) was noted for both F2 and F3 and this decrease in viability was probably due to the presence of excess COO⁻ ions in the PECs. These findings validate that the polymers and PEC possess the potential for safe *in vivo* drug delivery application.

Table 3.2: Viability of Caco2 cells treated with PECs and native polymers

Sample	Cell viability (%)
HA	100
PQ10	98.4
F1	98.9
F2	96.8
F3	96.8

3.4. CONCLUDING REMARKS

This study corroborated the formation of a novel polyelectrolyte complex between the HA and PQ10. The complexation ability of the two polymers can be attributed to their complementary charges that facilitated spontaneous formation of the electrostatic bonds between quaternary amino groups in PQ10 and carboxylic groups in the HA leading to the formation of a self-assembled “fibrilla” architecture. The use of both polymers has been previously established to be safe and HA and PQ10 are readily available at low costs. Characterization of the mechanical properties of these biomaterials was essential to validate if they are possible candidates for use in drug delivery. Generally, polyelectrolyte complex use can be implemented for purposes such as drug delivery particularly to achieve controlled drug release. This was validated by the drug release studies and for future uses, different polymer ratios or changes in drug loading can be explored in order to achieve a specific desired outcome in drug delivery. pH degradation studies revealed the possibility of biodegradation of the PECs and also drug release as these PECs break down upon interaction with simulated gastrointestinal fluid. This system has significant potential in the field of drug delivery for its application in the delivery of lipophilic drugs such as EFV and therefore improving the effectiveness of anti-HIV drugs. Other pharmaceutical methods of HA-PQ10 complexation will be explored.

3.5. REFERENCES

- Amir, S., Hafidi, M., Merlina, G., Hamdi, H., Revel, J.C., 2004. Elemental analysis, FTIR and ¹³C-NMR of humic acids from sewage sludge composting. *Agronomie*, 24(1), 13-8.
- Ankerfors, C., Ondaral, S., Wågberg, L., Ödberg, L., 2010. Using jet mixing to prepare polyelectrolyte complexes: Complex properties and their interaction with silicon oxide surfaces. *Journal of Colloid and Interface Science*, 351(1), 88–95.
- Bahvalov, A.V., Rozanova, M.S., Trofimov, S.Y., 2010. The elemental composition and amphiphilic properties of humic acids in southern taiga soils. *Moscow University Soil Science Bulletin*, 65(4), 168-71.
- Baigorri, R., Fuentes, M., González-Gaitano, G., García-Mina, J.M., Almendros, G., González-Vila, F.J., 2009. Complementary multianalytical approach to study the distinctive structural features of the main humic fractions in solution: gray humic acid, brown humic acid, and fulvic acid. *Journal of Agricultural and Food Chemistry*, 57(8), 3266-72.
- Bawa, P., Pillay, V., Choonara, Y.E., du Toit, L.C., Ndesendo, V.M.K., Kumar, P.A., 2011. Composite Polyelectrolytic Matrix for Controlled Oral Drug Delivery. *AAPS PharmSciTech*, 12(1), 227-38.
- Bierbrauer, K.L., Alasino, R.V., Muñoz, A., Beltramo, D.M., Strumia, M.C., 2014. Characterization and bacterial adhesion of chitosan-perfluorinated acid films. *Colloids and Surfaces B: Biointerfaces*, 114, 201-8.
- Bigucci, F., Luppi, B., Cerchiara, T., Sorrenti, M., Bettinetti, G., Rodriguez, L., Zecchi, V., 2008. Chitosan/pectin polyelectrolyte complexes: selection of suitable preparative conditions for colon-specific delivery of vancomycin. *European Journal of Pharmaceutical Sciences*. 35(5), 435-41.
- Carmona-Ribeiro, A.M., de Melo Carrasco, L.D., 2013. Cationic antimicrobial polymers and their assemblies. *International Journal of Molecular Sciences*, 14(5), 9906-46.
- Coble, P.G., Lead, J., Baker, A., Reynolds, D.M., Spencer, R.G., (editors), 2014. *Aquatic organic matter fluorescence*. Cambridge University Press, 2014.
- Cumming, J.L., Hawker, D.W., Nugent, K.W., Chapman, H.F., 2008. Ecotoxicities of polyquaterniums and their associated polyelectrolyte-surfactant aggregates (PSA) to *Gambusia holbrooki*. *Journal of Environmental Science and Health Part A*, 43(2), 113-7.
- De Paolis, F., Kukkonen, J., 1997. Binding of organic pollutants to humic and fulvic acids: influence of pH and the structure of humic material. *Chemosphere*, 34(8), 1693-704.
- Heinen, C., Reuss, S., Saaler-Reinhardt, S., Langguth, P., 2013. Mechanistic basis for unexpected bioavailability enhancement of polyelectrolyte complexes incorporating BCS

class III drugs and carrageenans. *European Journal of Pharmaceutics and Biopharmaceutics*, 85(1), 26-33.

- Hofman, M.J., Higgins, J., Matthews, T.B., Pedersen, N.C., Tan, C., Schinazi, R.F., North, T.W., 2004. Efavirenz therapy in rhesus macaques infected with a chimera of simian immunodeficiency virus containing reverse transcriptase from human immunodeficiency virus type 1. *Antimicrobial Agents and Chemotherapy*, 48(9), 3483-90.
- Huang, Y., Dai, W.G., 2014. Fundamental aspects of solid dispersion technology for poorly soluble drugs. *Acta Pharmaceutica Sinica B*, 4(1), 18-25.
- Kabanov, V.A., Zezin, A.B., 1984. A new class of complex water-soluble polyelectrolytes. *Macromolecular Chemistry and Physics*, 6(S19841), 259-76.
- Klučáková, M., Pekař, M., 2005. Solubility and dissociation of lignitic humic acids in water suspension. *Colloids and Surfaces A: Physicochemical and Engineering Aspects*, 252(2), 157-63.
- Kumar, A., Ahuja, M., 2013. Carboxymethyl gum kondagogu–chitosan polyelectrolyte complex nanoparticles: Preparation and characterization. *International Journal of Biological Macromolecules*, 62, 80-4.
- Li, X., Xie, H., Lin, J., Xie, W., Ma, X., 2009. Characterization and biodegradation of chitosan–alginate polyelectrolyte complexes. *Polymer Degradation and Stability*, 94(1):1-6.
- Lin, W.C., Yu, D.G., Yang, M.C., 2005. pH-sensitive polyelectrolyte complex gel microspheres composed of chitosan/sodium tripolyphosphate/dextran sulfate: swelling kinetics and drug delivery properties. *Colloids and Surfaces B: Biointerfaces*, 44(2), 143-51.
- Mazoniene, E., Joceviciute, S., Kazlauske, J., Niemeyer, B., Liesiene, J., 2011. Interaction of cellulose-based cationic polyelectrolytes with mucin. *Colloids and Surfaces B: Biointerfaces.*, 83(1), 160-4.
- Mirza, M.A., Ahmad, N., Agarwal, S.P., Mahmood, D., Anwer, M.K., Iqbal, Z., 2011. Comparative evaluation of humic substances in oral drug delivery. *Results in Pharma Sciences*, 1(1):16-26.
- Nath, S.D., Abueva, C., Kim, B., Lee, B.T., 2015. Chitosan–hyaluronic acid polyelectrolyte complex scaffold crosslinked with genipin for immobilization and controlled release of BMP-2. *Carbohydrate Polymers*, 115, 160-9.
- Ngwuluka, N.C., Choonara, Y.E., Modi, G., du Toit, L.C., Kumar, P., Ndesendo, V.M., Pillay, V., 2013. Design of an interpolyelectrolyte gastroretentive matrix for the site-specific zero-order delivery of levodopa in Parkinson's disease. *AAPS PharmSciTech*, 14(2), 605-19.

- Palamà, I.E., Musarò, M., Coluccia, A.M., D'Amone, S., Gigli, G., 2011. Cell uptake and validation of novel PECs for biomedical applications. *Journal of Drug Delivery*.
- Pandey, S., Mishra, A., Raval, P., Patel, H., Gupta, A., Shah, D., 2013. Chitosan–pectin polyelectrolyte complex as a carrier for colon targeted drug delivery. *Journal of Young Pharmacists*, 5(4):160-6.
- Peña-Méndez, E.M., Havel, J., Patočka, J., 2005. Humic substances—compounds of still unknown structure: applications in agriculture, industry, environment, and biomedicine. *J. Appl. Biomed*, 3, 13-24.
- Piyakulawat, P., Praphairaksit, N., Chantarasiri, N., Muangsin, N., 2007. Preparation and evaluation of chitosan/carrageenan beads for controlled release of sodium diclofenac. *AAPS PharmSciTech*, 8(4), 120-30.
- Ribeiro, A.J., Silva, C., Ferreira, D., Veiga, F., 2005. Chitosan-reinforced alginate microspheres obtained through the emulsification/internal gelation technique. *European Journal of Pharmaceutical Sciences*, 25(1), 31-40.
- Ritchie, J.D., Perdue, E.M., 2003. Proton-binding study of standard and reference fulvic acids, humic acids, and natural organic matter. *Geochimica et Cosmochimica Acta*, 67(1), 85-96.
- Rodríguez^a, R., Alvarez-Lorenzo, C., Concheiro, A., 2003. Cationic cellulose hydrogels: kinetics of the cross-linking process and characterization as pH-/ion-sensitive drug delivery systems. *Journal of Controlled Release*, 86(2), 253-65.
- Rodríguez^b, R., Alvarez-Lorenzo, C., Concheiro A., 2003. Influence of cationic cellulose structure on its interactions with sodium dodecylsulfate: implications on the properties of the aqueous dispersions and hydrogels. *European Journal of Pharmaceutics and Biopharmaceutics*, 56(1), 133-42.
- Rupiasih, N,N,, Vidyasagar, P.B., 2009. Analytical Study Of Humic Acid From Various Sources Commonly Used As Fertilizer: Emphasis On Heavy Metal Content. *International Journal of Design and Nature and Ecodynamics*, 4(1), 32-41.
- Saleem, M.A., Kotadia, D.R., Kulkarni, R.V., 2012. Effect of formulation variables on dissolution of water-soluble drug from polyelectrolyte complex beads. *Dissolution Technology*, 19, 21-8.
- Shao, Y., Li, L., Gu, X., Wang, L., Mao, S., 2015. Evaluation of chitosan–anionic polymers based tablets for extended-release of highly water-soluble drugs. *Asian Journal of Pharmaceutical Sciences*, 10(1):24-30.
- Singh, A., Majumdar, S., Deng, W., Mohammed, N.N., Chittiboyina, A.G., Raman, V., Shah, S., Repka, M.A., 2013. Development and characterization of taste masked

- Efavirenz pellets utilizing hot melt extrusion. *Journal of Drug Delivery Science and Technology*, 23(2), 157-63.
- Six, K., Verreck, G., Peeters, J., Brewster, M., Mooter, G.V., 2004. Increased physical stability and improved dissolution properties of itraconazole, a class II drug, by solid dispersions that combine fast-and slow-dissolving polymers. *Journal of Pharmaceutical Sciences*, 93(1), 124-31.
 - Siyawanwaya, M., Choonara, Y.E., Bijukumar, D., Kumar, P., Du Toit, L.C., Pillay, V., 2015. A review: overview of novel polyelectrolyte complexes as prospective drug bioavailability enhancers. *International Journal of Polymeric Materials and Polymeric Biomaterials*, 64(18), 955-68.
 - Stepanov, A.A., 2008. Separation and characterization of amphiphilic humic acid fractions. *Moscow University Soil Science Bulletin*, 63(3), 125-9.
 - Tapia, C., Escobar, Z., Costa, E., Sapag-Hagar, J., Valenzuela, F., Basualto, C., Gai, M.N., Yazdani-Pedram, M., 2004. Comparative studies on polyelectrolyte complexes and mixtures of chitosan–alginate and chitosan–carrageenan as prolonged diltiazem clorhydrate release systems. *European Journal of Pharmaceutics and Biopharmaceutics*, 57(1), 65-75.
 - Thakur, M.K., Thakur, V.K., Gupta, R.K., Pappu, A., 2015. Synthesis and applications of biodegradable soy based graft copolymers: a review. *ACS Sustainable Chemistry and Engineering*, 4(1), 1-7.
 - Thakur, V.K., Kessler, M.R., 2015. Self-healing polymer nanocomposite materials: A review. *Polymer*, 69,369-83.
 - Thakur, V.K., Thakur, M.K., 2014. Recent advances in graft copolymerization and applications of chitosan: a review. *ACS Sustainable Chemistry and Engineering*, 2(12), 2637-52.
 - Thakur, V.K., Thakur, M.K., 2015. Recent advances in green hydrogels from lignin: a review. *International journal of biological macromolecules*, 72, 834-47.
 - Tsai, R.Y., Chen, P.W., Kuo, T.Y., Lin, C.M., Wang, D.M., Hsien, T.Y., Hsieh, H.J., 2014. Chitosan/pectin/gum Arabic polyelectrolyte complex: Process-dependent appearance, microstructure analysis and its application. *Carbohydrate Polymers*, 101, 752-9.
 - Yang, X., Chen, X., Zhang, X., Yang, W., Evans, D.G., 2008. Direct electrochemistry and electrocatalysis with horseradish peroxidase immobilized in polyquaternium-manganese oxide nanosheet nanocomposite films. *Sensors and Actuators B: Chemical*, 134, 182-8.
 - Yee, M.M., Miyajima, T., Takisawa, N., 2006. Evaluation of amphiphilic properties of fulvic acid and humic acid by alkylpyridinium binding study. *Colloids and Surfaces A: Physicochemical and Engineering Aspects*, 272(3), 182-8.

CHAPTER 4

SYNTHESIS, COMPARISON AND OPTIMIZATION OF A HUMIC ACID-QUAT10 POLYELECTROLYTE COMPLEX BY COMPLEXATION-PRECIPITATION VS. EXTRUSION-SPHERONIZATION

4.1. INTRODUCTION

The humic acid (HA) and polyquaternium-10 (PQ10) polyelectrolyte complex (PEC) was explored in order to benefit from the synergistic effect of using a polymeric complex contrary to the individual polymers. The novel HA-PQ10 PEC, previously reported (Siyawamwaya *et al.*, 2016), was investigated further for the purposes of comparing properties of the complexes synthesized by two different methods. The high affinity for negatively charged groups that is exhibited by PQ10 can be attributed to the presence of the quaternary amino groups. Our previous study revealed that this molecule formed a polyelectrolyte complex with HA, a macromolecule which is classified as an anionic polyelectrolyte. In this study, commercial brown HA and PQ10 of 656.1g/mol were utilized (Siyawamwaya *et al.*, 2016). It is essential to identify a simplified and cost-effective method of PEC fabrication applicable to contemporary dosage form design. Solid dispersions were synthesized using the complexation-precipitation (C-P) and extrusion-spheronization (E-S) approaches. Solid dispersions have been known to enhance the bioavailability of drugs (Kim *et al.*, 2009). Dispersion of the drug within a matrix prevents agglomeration of the drug while encouraging its solubility. These dispersions are also responsible for increasing the surface area of the drug therefore enhancing the wettability of the bioactive (Singh *et al.*, 2016). However, the main drawback of solid dispersions is the tendency of the drug to recrystallize due to the metastable properties of the amorphous formulation (Serajuddin 1999; Shergill *et al.*, 2016).

The aqueous solubility and intestinal tissue permeability of efavirenz (EFV) were measured and any differences to a selected marketed formulation were noted. Poor solubility occurs when the drug solubilization rate is slower than the rate of its passage in the gastrointestinal tract (GIT) (Kim *et al.*, 2009). Various methods of improving the hydro-solubility of drugs have been employed and these include, but are not limited to, the addition of surfactants into formulations, the reduction of drug particle size, delivery of the drug in emulsion vehicles and the use of solid dispersions (Usach *et al.*, 2013; Siyawamwaya *et al.*, 2015). The permeability of such drugs can also be enhanced by utilizing polymeric delivery systems that increase the residence time of the drugs or by encapsulating the drugs in microspheres and/or nanoparticles that have a high surface area to volume ratio.

The model anti-HIV drug, EFV, was loaded into HA-PQ10 PEC fabricated by the complexation-precipitation and the extrusion-spheronization techniques. According to the Biopharmaceutics Classification System (BCS), EFV is categorized in Class II (Fandaruff *et al.*, 2015). It is a non-nucleoside reverse transcriptase inhibitor (NNRTI) with a bioavailability estimated to be between 40-45% and a solubility of 3-9 μ g/mL (Rao and Shirsath 2016; Six *et al.*, 2004). Any drug with a solubility <10 μ g/mL is regarded as poorly soluble. NNRTIs bind to the reverse transcriptase in a non-competitive manner. RTV was added to the optimized PEC in order to validate applicability of the complex to BCS class IV drugs which exhibit both poor solubility and poor permeability. RTV is classified as a PI which inhibits the formation of mature infectious virions. It possesses a bioavailability of 5% and an aqueous solubility of 1.26 μ g/mL (Dengale *et al.*, 2015). Low aqueous solubility and permeability also results in low and variable bioavailability *in vivo* and consequentially, higher drug doses have to be dosed in order to achieve optimal biological effects (Jones *et al.*, 2013).

4.2. MATERIALS AND METHODS

4.2.1. Materials

Humic acid (HA) (brown), polyquaternium-10 (PQ10), microcrystalline cellulose (Avicel PH-101)(MCC) and sodium lauryl sulphate (SLS) were procured from Sigma-Aldrich® (St. Louis, MO, USA). Pure efavirenz (EFV) and ritonavir (RTV) powder (99.99% purity) were purchased from Xingcheng Chemphar Co., Ltd. (Taizhou, Zhejiang, China) and used as received. The commercially available comparator products were Sonke-Efavirenz® 200mg and soft elastic capsules of Norvir® 100mg (ritonavir). All other reagents used were of analytical grade.

4.2.2. Synthesis of the drug-loaded Polyelectrolyte Complex (PEC)

4.2.2.1. Complexation-Precipitation (C-P) via solution-blending of HA and PQ10

Synthesis of the drug-loaded PEC by C-P involved dissolving EFV (200mg) in methanol (20mL) prior to titrating one polymer solution into the other. The EFV solution was added to the HA solution (100mL of 5.75mg/mL) and agitated for 5 minutes. Thereafter, an aqueous solution of PQ10 (235mL of 2.4mg/mL) was slowly titrated into the HA/EFV solution to facilitate self-assembly of the drug-loaded PEC (PEC-E_(C-P)) within seconds. The precipitate was filtered and dried in a vacuum oven at 40°C for 12 hours after which it was milled and filled into hard gelatin capsules.

4.2.2.2. Extrusion-spheronization (E-S) via benchtop extruder and spheronizer

A combination of HA (1400mg), PQ10 (1410mg), EFV (650mg) and microcrystalline cellulose (MCC) (1000mg) were blended in a homogenizer for 5 minutes before synthesis of the EFV-loaded PEC (PEC-E_(E-S)). The same amount of HA and PQ10 used in the C-P method were employed in E-S as well. Deionized water was added to form wet granules of the powder mass. The homogenous wet granules were transferred into the barrel of a Mini-Screw Extruder (Caleva Ltd. Sturminster Newton, Dorset, UK) for extrusion at 100rpm. MCC absorbed the granulating fluid (water) which was then compressed onto the outer surface of the extrudates thus further lubricating the surface to render the extrusion process feasible. The extrudates were then collected and immediately spheronized in a Multi-Bowl Spheronizer (Caleva Ltd. Sturminster Newton, Dorset, UK).

4.2.3. Physicochemical and mechanical characterization of the drug-free HA-PQ10 PEC

4.2.3.1. Assessment of the surface morphology

SEM (FEI Nova NanoLab™ 600 DualBeam FIB/SEM, Hillsboro, OR, USA) was utilized for determining the surface morphology of the PEC samples. Analysis was conducted at 20 kV. Prior to mounting samples onto the SEM stage, they were thoroughly dried and sputter coated with chromium for 2 minutes. All images were taken at x2000 magnification.

4.2.3.2. Complexation validation via PEC solubility testing in varying solvents

Complete synthesis of the PECs was evaluated utilizing the solvent test. PECs were dispersed separately in ethyl acetate, dimethyl sulfoxide (DMSO), formic acid, ethanol, acetone, dichloromethane (DCM) and water at 80°C for 24 hours under constant stirring. The achromatic solutions were observed for any colour changes which would indicate the solubility of PECs in the solvent.

4.2.3.4. Determination of polyelectrolyte complex cytotoxicity

Ex vivo cytotoxicity of drug free HA/PQ-10 PEC was conducted on the human colorectal adenocarcinoma (Caco2) cell line. The growth medium consisted of Dulbecco's Modified Eagle's Medium (DMEM) with 4.0mM L-Glutamine and 10% sodium pyruvate foetal bovine serum (FBS). A 25cm² tissue culture flask was utilized to aseptically culture the cells which were placed in an incubator (RS Biotech Galaxy, Irvine, UK) at 37°C, 95% relative humidity and 5% CO₂. Culturing was continued until a desired cell density (70-80% confluency) was obtained. Cytotoxicity was measured with the aid of the methyl tetrazolium (MTT) cell proliferation assay. Caco2 cells (100µL) were cultured in a 96 well plate with a density of (6 x 10⁴)/100µL and incubated in a CO₂ incubator. After 24 hours, serial dilutions of HA, PQ10,

PEC_(E-S) and PEC_(C-P) samples (100µL) were prepared in the well plate in triplicate and incubated for 24 hours. The samples were then replaced with 10µL of MTT solution and growth medium (100µL) before incubation for 3 hours. Absorbance from the wells was measured with the aid of a microplate reader (Power Wave XS, BIO-TEK®, USA) at 570nm with a background absorbance of 690nm. The MTT assay was also carried out on cells that were treated with the optimized formulation and cell viability was measured after 24 hours. Measurement was repeated on cells that were left to recover for a further 24 hours.

4.2.4. Characterization of EFV-loaded HA-PQ10 PECs produced by E-S and C-P

4.2.4.1. Influence of PEC synthesis method on the interaction of HA and PQ10

Attenuated Total Reflectance-Fourier Transform Infrared, ATR-FTIR, with a single reflection diamond MIRTGS detector (PerkinElmer® Spectrum 100 Series FT-IR Spectrometer PerkinElmerLtd., Beaconsfield, UK) was employed to assess the interactions between the PEC, pure drug and native polymers. This was conducted over a wavenumber of 6000–450cm⁻¹ using 25 wavenumbers per spectrum and a force of 115N. A resolution of 4cm⁻¹ was utilized.

4.2.4.2. Determination of the thermal properties of PECs and physical mixture

Melting points of dry powder samples were comparatively deduced by using differential scanning calorimetry (DSC) (Mettler Toledo DSC-1 STARe System, Schwerzenback, ZH, Switzerland) over a temperature range of 20°C–300°C with a heating rate of 10°C/min. Nitrogen was used as the purge gas to avoid oxidation. A maximum of 10mg sample was placed in a 40µL aluminium pan and the lid was crimped and perforated. Analysis of the thermograms revealed the specific temperature that the samples melted at and the curves were plotted as heat flow (mW) against temperature.

4.2.4.3. Determining the extent of supersaturation and in vitro EFV release

Drug quantification was conducted utilizing the EFV calibration curve described in Chapter 3 and the one for RTV had to be constructed as well. Serial dilutions of RTV in simulated intestinal fluid (SIF) containing 1% sodium lauryl sulfate (SLS) were utilized. The percentage drug-loading (%DL) was ascertained by adding finely ground PEC powder (100mg) into SIF (40mL) at pH 6.8 containing SLS (1%) (according to USP monograph, USP 32-NF 27). The powders were dispersed in the SIF. After incubation in an orbital shaker bath, samples were filtered with a 0.22µm filter and drug concentrations determined spectrophotometrically (Lambda 25 UV/Vis spectrophotometer, PerkinElmer, MA, USA) at 247nm for EFV ($R^2=0.9926$) and 241nm for RTV ($R^2=0.9998$). The saturation solubilities were determined by adding formulations containing 2.5mg/mL of EFV in SIF. This was incubated in an orbital

shaker bath for 36 hours and drug concentrations were determined via UV absorbance measurements (Mabrouk *et al.*, 2015). Sampling was conducted every 12 hours and the highest quantity of drug concentration determined was considered the supersaturation amount. The EFV release rate from the capsules was determined using the USP Apparatus II paddle stirrer at 50rpm (USP 33) (Erweka DT 700, Erweka GmbH, Heusenstamm, Germany). Formulations were placed under a ring-mesh assembly to prevent floatation that may lead to unsteady and biased drug release profiles (Viral *et al.*, 2010). The temperature was maintained at 37°C and sample aliquots (5mL) were collected at predetermined times over a 24 hour test period. Sink conditions in the dissolution fluid (900mL) were maintained by replacing the samples withdrawn immediately with drug-free media. The dissolution medium consisted of SIF, which was necessary to perform the studies under physiologically relevant conditions since the solubility of poorly aqueous soluble drugs is affected by the presence of surfactants. Saturation solubility, EFV release and permeation studies for the optimized PEC's were undertaken in the fed state simulated intestinal fluid (FeSSIF). Preparation of FeSSIF comprised dissolving NaOH (20.2g), glacial acetic acid (43.25g) and NaCl (59.37g) in deionized water (5L) and thereafter adjusting the pH to 5.0. Native FeSSIF (500mL) was used to dissolve sodium taurocholate (59.08g) and 59.08mL of lecithin dissolved in methylene chloride (100mg/mL) was added to the blank FeSSIF. The methylene chloride was eliminated from the emulsion by evaporation and the volume of the media was adjusted to 2L (Sinha *et al.*, 2010). Collected sample aliquots were immediately filtered using a 0.22µm filter and diluted appropriately. Equation 4.1 was employed to calculate the %DL.

$$\%DL = \frac{\text{amount of drug in 100mg powder sample}}{\text{total amount of powder sample}} \times 100$$

Equation 4.1

4.2.4.4. Ex vivo permeability studies employing porcine small intestinal tissue

A Franz Diffusion Cell (FDC) apparatus (PermeGear Inc. Bethlehem, PA, USA) was utilized to measure the drug permeation across porcine small intestinal tissue from the PECs across a concentration gradient of 4mg/mL. Phosphate buffered saline (PBS) (12mL) at pH 7.4 was added to the acceptor compartment. An emulsion of capsule contents (4mg/mL) in SIF and FeSSIF for the optimized PECs was added to the donor compartment. The two compartments were separated by a portion of excised porcine small intestinal tissue (ileum). The intestinal tissue was freshly obtained from a large white pig and immediately snap-frozen for preservation. Prior to the permeation experiment, the tissue was thawed and allowed to equilibrate on the acceptor compartment to 37°C for 20 minutes. The adipose and muscular layers were carefully excised. The study was performed over a 24 hour period at

37°C. Sample aliquots (0.5 mL) were withdrawn and replaced by PBS of equal volume. The mean values of the quantity of EFV that permeated were used to compute the flux (J) and permeability coefficient (P) of the drug according to Equation 4.2 and Equation 4.3. Flux is the quantity of drug transported across the membrane over a certain period of time and was determined employing Equation 4.2.

$$J = \frac{M}{At}$$

Equation 4.2

Where, M is the mass of EFV present in the acceptor compartment at time t and A is the area available for permeation (Tang *et al.*, 2005). Permeability can be defined as the rate of EFV permeation per unit concentration (Dezani *et al.*, 2013) and the permeability coefficient was calculated according to Fick's first law.

$$P = \frac{C_2 \times V}{A \times t \times C_1}$$

Equation 4.3

Where: P (cm.h⁻¹) is the permeability coefficient; V (mL) is the volume of the acceptor compartment (12mL); A (cm²) is the effective permeation area (1.767cm²); t (h) is the time interval; C_1 (mg.mL⁻¹) is the concentration in donor compartment and C_2 (mg.mL⁻¹) is the concentration in the acceptor compartment (Lavon *et al.*, 2005). The transepithelial electrical resistance (TEER) of the porcine tissue was measured using a SevenMulti™ dual meter pH/conductivity (Mettler Toledo, Zurich, Switzerland) at 25°C to confirm tissue integrity.

4.2.5. PEC optimization via a Design of Experiments (DoE) approach

4.2.5.1. Implementation of a randomized Box-Benkehn experimental design

A series of PEC formulations were synthesized using a 2-factor, 2 tier Box-Benkehn statistical design. Minitab® V16 software (Minitab Inc. PA, USA) was used to generate the experimental design template constituting 13 formulations, 5 centre-points and 1 replicate with the ratio of HA:PQ10 and the quantity of granulation fluid (deionized water) being the independent variables as shown in Table 4.1. The mean dissolution time (MDT) from the drug release studies and the drug flux from porcine intestinal tissue permeability studies over 24 hours were the responses that were considered and maximized to obtain an optimized PEC formulation with enhanced solubility and permeability of the encapsulated drug. Maximum speeds of extrusion and spheronization were set as constants based on results

from preliminary studies that showed that maximum speeds were ideal to facilitate the required extrusion and spheronization. EFV was used as the model drug for the experimental design phase of this study.

4.2.5.2. Evaluation of extrudate flow properties of the HA-PQ10 PEC

The Hausner Ratio (HR) was calculated to determine the flow properties of the extrudates that were then encapsulated into gelatin capsules. In order to measure the bulk and tapped densities, initial and final volumes of specific extrudate weight was recorded. The volume was at least 60% of the cylinder volume (Method 1 -section 2.9.34 European Pharmacopoeia (EP8.0, 2014). The final volume was measured after tapping a 50mL glass cylinder onto a hard wood surface from a 20mm height (Jan *et al.*, 2015). Bulk density, tapped density and the HR were calculated according to Equations 4.4, 4.5 and 4.6.

$$\text{Bulk density} = \frac{w}{v_o}$$

Equation 4.4

$$\text{Tapped density} = \frac{w}{v_f}$$

Equation 4.5

$$\text{HR} = \frac{\text{Tapped density}}{\text{Bulk density}}$$

Equation 4.6

Where w is the weight of the extrudates (g), v_o is the initial volume of extrudates (mL) and v_f is the final volume of the extrudates (mL).

4.2.5.3. Establishing the surface morphology and porosity of the optimized PEC

Surface morphologies of the optimized formulations were determined by SEM as explained in 2.3.1. The porosity was measured using BET isotherms of nitrogen on a Porosity Analyzer (ASAP 2020, Micromeritics Instrument Co., GA, USA) (Kondiah *et al.*, 2013). The extrudates were degassed to remove surface moisture and impurities. In order to measure the surface area, pore size and pore volume of the samples, unspheronized pieces of extrudates which were at least 100mg in weight were analysed. Analysis involved two phases, the evacuation phase and the heating phase. Parameters for the evacuation phase included a temperature ramp rate of 10°C/min with a target temperature of 40°C and an evacuation rate of 50mmHg/sec. The temperature ramp rate for the heating phase was 10°C/min with a 30°C hold time. The analyzer generated the Brunauer-Emmett-Teller (BET) and Barrett-Joyner-Halenda (BJH) nitrogen adsorption and desorption analysis. BET analysis provided surface

area analysis while BJH provided pore size and pore volume analysis. Equations 4.7 and 4.8 were implemented for BET surface area determination.

$$A_s(BET) = n_m^a \times L \times a_m$$

Equation 4.7

$$a_s(BET) = \frac{A_s(BET)}{m}$$

Equation 4.8

Where, $A_s(BET)$ is the total surface area and $a_s(BET)$ is the specific surface area of the adsorbent mass (m). L is the Avogadro constant (Kondiah *et al.*, 2013).

4.3. RESULTS AND DISCUSSION

4.3.1. Outcome of PEC synthesis and physical variances between PEC(E-S) and PEC(C-P)

Synthesis of the PECs was successful using either the C-P or E-S approaches. With the C-P technique, complexation occurred instantaneously when the PQ10 solution was added to the HA drug solution. This was evidenced by the formation of strand-like precipitates as a result of the complexation process. Self-assembly of the polymers produced a dense supernatant that presented a challenge in filtration. For the E-S technique, it was imperative to add excipients that facilitated extrusion and subsequent spheronization.

4.3.1.1. Analysis of surface morphology of the PEC in compacted and powdered form

Scanning electron microscopy (SEM) images of the PECs synthesized by the two methods revealed that they notably differed morphologically (Figure 4.1). The compact $PEC_{(E-S)}$ (Figure 4.1(b)) displayed an irregular surface devoid of the large pores associated with the $PEC_{(C-P)}$ fibres. Powdered $PEC_{(C-P)}$ maintained its fibrous nature while the surface of $PEC_{(E-S)}$ was tightly packed together in the powdered form. Surface morphology may be utilized in predicting drug dissolution properties which are dependent on surface area (DiNunzio *et al.*, 2008). From the SEM images, the pores on the $PEC_{(C-P)}$ may facilitate faster interaction of the PEC with the dissolution fluid, thus enhancing solubility and the rate of drug release. However, $PEC_{(E-S)}$ would be expected to have a more extended drug release pattern.

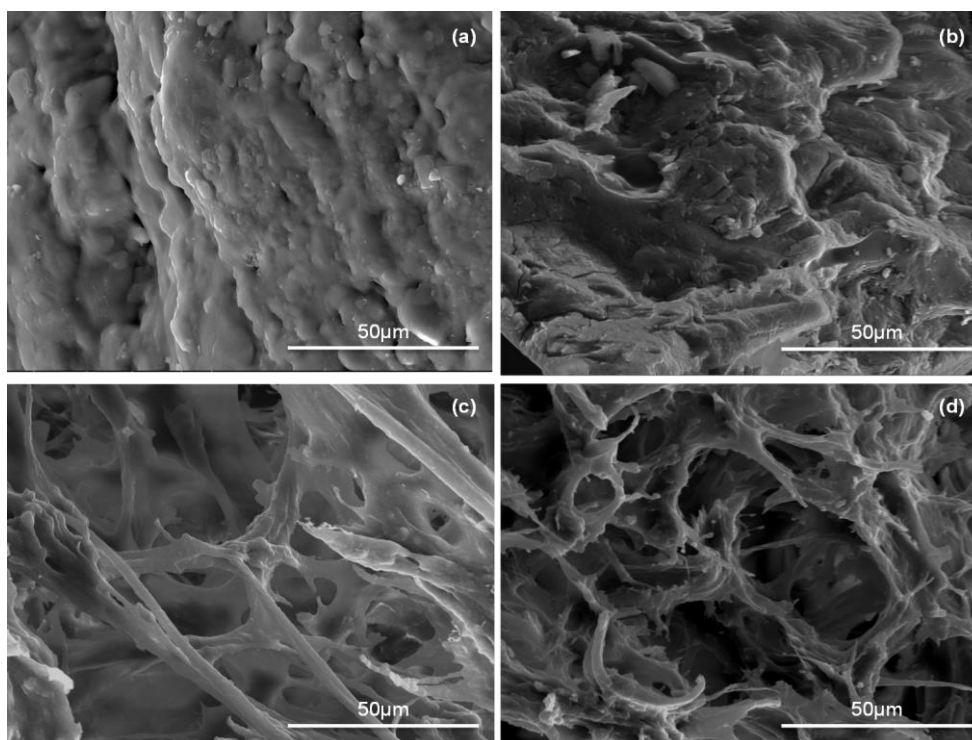


Figure 4.1: SEM images of drug-free PECs (a) $PEC_{(E-S)}$, (b) $PEC_{(E-S)}$ (powdered), (c) $PEC_{(C-P)}$ and (d) $PEC_{(C-P)}$ (powdered) at x2000 magnification

4.3.1.2. Validation of drug-free PEC complexation via solubility testing in varying solvents media

Stoichiometric PECs are generally insoluble in any known solvent (Shovsky *et al.*, 2009). The PECs were insoluble in all the representative solvents; ethyl acetate (electron donor), DMSO (electron acceptor), formic acid (proton donor), ethanol (proton donor), acetone (proton acceptor), DCM (dipole-dipole interaction) and deionized water (neutral). The slight solubility of $PEC_{(E-S)}$ in water was attributed to the partial complexation from E-S which resulted in the presence of uncomplexed polymers that were readily soluble in the water. Formic acid was included to validate the typical behaviour of PECs containing cellulose based polymers which dissolve completely in the acid (Ito *et al.*, 1986). Both formulations completely dissolved in formic acid.

4.3.1.3. Assessment of the cytotoxicity of the PEC

The MTT assay utilizes the reduction of the tetrazolium ring of 3-[4,5-dimethylthiazol-2-yl]-2,5-diphenyl tetrazolium bromide by the cell mitochondrial dehydrogenases yielding MTT formazan crystals which were then quantified spectrophotometrically with the aid of a microplate reader. This reduction of the tetrazolium ring is directly proportional to cell metabolism (Coimbra *et al.*, 2011). Studies previously conducted revealed that HA, PQ10 and $PEC_{(C-P)}$ were non-cytotoxic to Caco2 cells at 0.375mg/mL (Siyawamwaya *et al.*, 2016).

The assay in this study was conducted to ascertain the impact of each complexation technique on the cell viability and therefore biocompatibility of the PECs over 24 hours. According to the data presented in Figure 4.2 all the samples for the PECs and polymers exhibited non-cytotoxic behaviour (cell viability >90%) at all test concentrations barring $PEC_{(C-P)}$ at 1.5mg/mL which revealed slight cytotoxicity (cell viability = $89\pm 2.01\%$). It can be inferred that $PEC_{(E-S)}$ in comparison to $PEC_{(C-P)}$ is less likely to induce acute cytotoxicity at higher concentrations (1.5mg/mL).

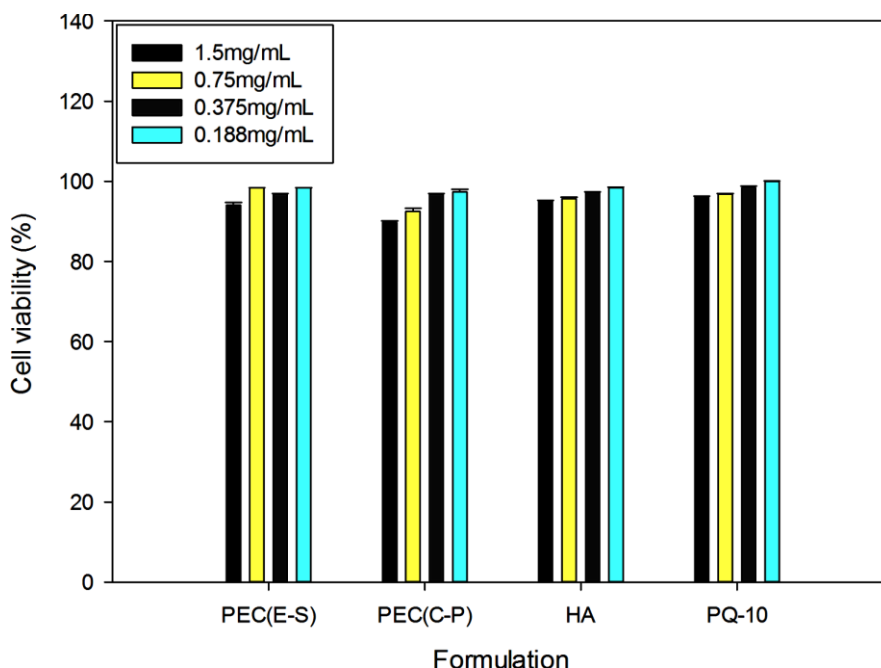


Figure 4.2: Cell viability analysis of HA, PQ10 and drug-free PECs

4.3.2. Characterization of EFV-loaded PEC synthesized by C-P and E-S

4.3.2.1. The influence of complexation method on EFV, HA and PQ10 interactions

The FTIR spectra (Figure 4.3) revealed that the dominant bond ($C=O$ cyclic, 1700cm^{-1}) from EFV was present in both PECs and the physical mixture (pE), with its position remaining constant in all formulations. However, its intensity was diminished significantly in the PECs and pE compared to the pure drug. Another EFV bond expressed in $PEC-E_{(E-S)}$, $PEC-E_{(C-P)}$ and pE was the exocyclic triple bond stretching (2248cm^{-1}). These characteristic peaks are consistent with the ones reported by da Costa and co-workers (da Costa *et al.*, 2012). Exhibition of these bonds in the drug loaded formulations confirmed presence of the unaltered drug in the drug/polymer complex or physical blend. The tertiary amide bond in EFV (1600cm^{-1}) overlaps with the new bond that is expected to form in PECs as previously reported (1). This is the point of complexation between NMe_3^+ and COO^- . Most of the groups in EFV are not available for bond formation with the polymers except for the N-H bond. This

is detected at 3500cm^{-1} – 3100cm^{-1} and would overlap with the polymeric O-H stretch detection at the same wavenumber. The interaction of the N-H bonds with hydrogen donor groups on the polymer chains may result in drug/polymer interaction which may improve drug entrapment and overall, enhance drug solubility as the bond would easily break in aqueous medium. The shape of the bond at 3500cm^{-1} – 3100cm^{-1} was sharper in the drug-loaded PECs than the drug-free PECs and pE. The resultant band around 3300cm^{-1} had a lower intensity than that of the drug free PEC signifying drug/polymer interaction (Sathigari *et al.*, 2012; Pawar *et al.*, 2016). FTIR is a quantitative analysis of the bonds found in the test sample, therefore the diminished absorbance of EFV bands in the formulations could have resulted from the masking effect of the polymers on the drug due to the high polymer : drug ratio.

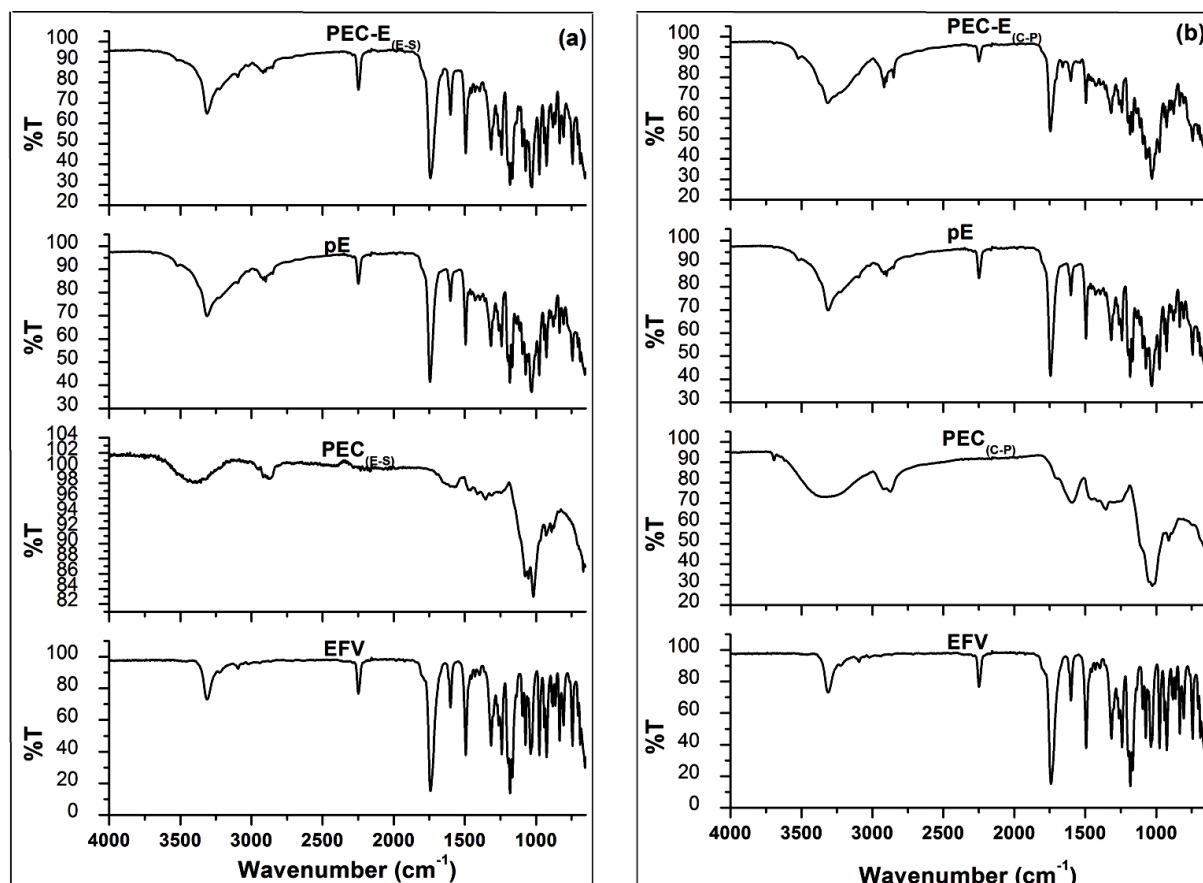


Figure 4.3: FTIR spectra for (a) PEC-E_(E-S) and (b) PEC-E_(C-P)

4.3.2.2. Elucidation of the thermodynamic properties of the EFV-loaded PEC compared to drug-free PEC and physical drug/polymer mixtures

The DSC thermograms in Figure 4.4 revealed the differences in thermal properties of the PECs produced by the two methods, pure EFV and physical blends. The physical blend shows various T_m values some of which correspond to the T_m of PEC_(E-S), PEC_(C-P) and EFV.

As expected, multiple endothermic events were noted for pE and one of them coincides with the melting point of pure EFV. The endotherm is reduced compared to that of the pure drug due to the high polymer : drug ratio. There was no sharp melting endotherm corresponding with that of the crystalline API in both drug-loaded PECs thus signifying the good miscibility of the API into the polymeric matrix. According to literature, the disappearance or shifting of the endotherm of a pure drug is indicative of lack of defined crystalline arrangements. This was probably a result of the API being partially miscible in the matrix and therefore forming a mixed solid dispersion system of amorphous and crystalline drug (Koh *et al.*, 2013). This is consistent with the FTIR results that revealed that drug/polymer interactions occurred. Ideal drug-polymer interactions are vital in order to prevent clumping of drug which is responsible for drug polymorphism. It can be inferred that the drug crystallinity was reduced upon dispersion into the HA-PQ10 and therefore led to enhanced drug solubility. A similar conclusion was reached by Mabrouk and co-workers (2015) who concluded that increase in solubility of efavirenz loaded into physically crosslinked hydroxyethylcellulose and polyacrylic acid hydrogel was as a result of a decrease in crystallinity of the drug as well as drug/polymer interactions. The endothermic peaks from 50°C-100°C were attributed to loss of moisture from the samples.

The peaks (around 150°C) adjacent to the one for EFV were attributed to the polymer thermal properties, this same peak is exhibited in the drug free extruded sample. This peak becomes broader in both complexes thus it can be concluded that the PECs are more amorphous in nature compared to the native polymers. PEC_(C-P) was expected to undergo complete complexation during synthesis in aqueous medium and hence would be more amorphous than PEC_(E-S). Complexation of PEC_(E-S) was probably partial after synthesis and only completed *in situ* during drug release and permeation when the system got in contact with the aqueous medium. PECs form in water or under temperatures which would cause the polymers to melt and neither of these conditions were met during the E-S process (Siyawamwaya *et al.*, 2016). The presence of the drug in the PEC resulted in remarkable changes in PEC-E_(C-P) which expressed significant endothermic events unlike PEC_(C-P) which hardly showed any changes during heat absorption. The behaviour of PEC-E_(E-S) was identical to its drug-free counterpart.

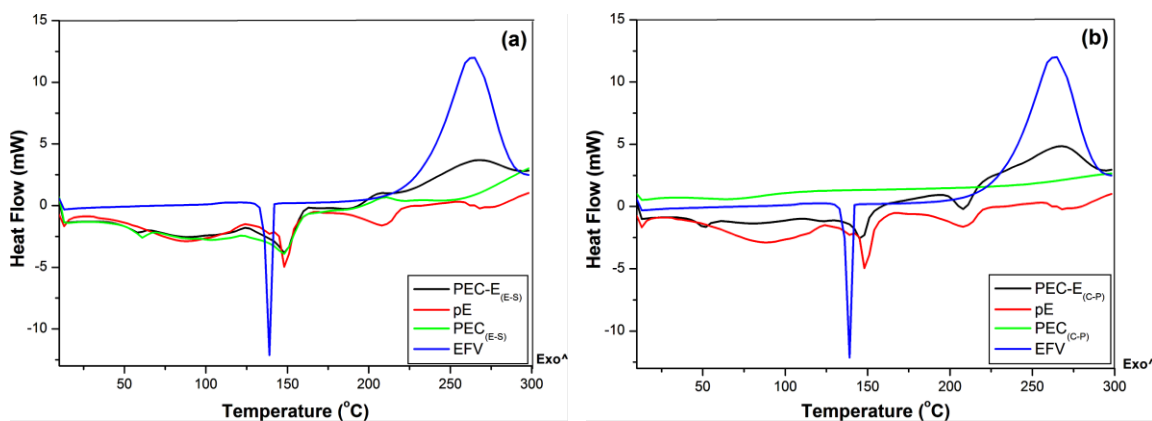


Figure 4.4: DSC thermograms for (a) PEC-E_(E-S) and (a) PEC-E_(C-P)

4.3.2.3. Evaluation of the extent of supersaturation and EFV release

Both PECs exhibited %DL >14% with PEC-E_(C-P) possessing higher EFV-loading ($20.82 \pm 2.03\%w/w$) than PEC-E_(E-S) ($14.19 \pm 0.49\%w/w$). This was due to the presence of excipients that were pertinent for the E-S process therefore lowering the %DL. The amount of MCC required to facilitate the E-S process was directly proportional to the amount of drug in the formulation (Kleinebudde 1997). Caution was exercised in determining the ideal drug-loading in order to avoid leaching of drug from the extrudates. PEC-E_(E-S) exhibited superior solubility properties ($5.1 \pm 5.39\%$) to PEC-E_(C-P) ($2.83 \pm 2.69\%$) and pE ($0.88 \pm 2.55\%$). The incorporation of EFV into the HA-PQ10 PEC greatly increased the wettability of EFV. Solubility enhancement was attributed to the partial conversion of the crystalline drug to the amorphous form which provided better interaction between the drug and dissolution medium due to the negation of lattice energy in the system. The PEC, due to the nature of the native polymers (HA and PQ10), was able to attract more dissolution medium which was trapped in the matrix for prolonged periods of time thus allowing sufficient contact between the drug and medium, leading to increase in wettability and consequently higher solubility. For PEC-E_(E-S), the extrusion process led to the dispersion and possible hydrogen bond interactions of EFV with the polymeric matrix thus enhancing drug solubility. After 36 hours, PEC-E_(E-S) still provided a saturated system and this demonstrated that a considerable degree of stability in protecting EFV from recrystallization within the dissolution time period was present. PEC-E_(C-P) did not maintain this stability since the highest EFV concentration was detected at the 24 hour sampling point. Supersaturation of the drug may not occur if an amorphous system rapidly reverts to the crystalline state (Prasad *et al.*, 2014). It was imperative to implement the additional step of complexation since the physical blend did not result in notable solubility amplification of EFV.

Figure 4.5(a) depicts the EFV release profiles over a 24 hour period. PEC-E_(E-S) and PEC-E_(C-P) both exhibited controlled release of EFV due to the entrapment of the drug in the novel complex. For satisfactory comparison of the drug-loaded PECs, MCC was added to the PEC-E_(C-P) before encapsulation into the hard gelatin capsules. The formulation that yielded superior solubility and permeability enhancement was selected for optimization and loading of the additional BCS class IV drug, RTV. Since the PECs do not easily dissolve in SIF, they were responsible for slowly releasing the drug from the system thus providing a controlled release system. Drug release from pE was poor (<40%) and this validated the need for using a PEC instead of the physical blend for optimal drug delivery. With the physical blend, upon dissolution of the capsule shell, the exposed blend formed a PEC *in situ*. However, the PEC formation occurred on the surface and was not uniformly distributed within the drug/polymer blend. Drug release from PECs is affected by the specific chemical structures of the native polymers hence different release profiles are expected from different polymer combinations (Shao *et al.*, 2015). The amphiphilic HA was responsible for lowering the solid/liquid interfacial tension therefore increasing the wettability of the lipophilic EFV which was trapped in the hydrophobic core of the polymer. This further prevented the agglomeration of EFV particles.

4.3.2.4. Assessment of ex vivo intestinal tissue permeability of EFV from the PEC

Transmembrane permeability profiles of the PECs were superior to those of the comparator products as illustrated in Figure 4.5(b). The constant EFV permeation from the PECs revealed that there was no saturation in the intestinal membrane. The permeability coefficient for PEC-E_(E-S) ($0.163 \pm 0.043 \text{ cm}^2 \cdot \text{h}^{-1}$) and PEC-E_(C-P) ($0.232 \pm 0.008 \text{ cm}^2 \cdot \text{h}^{-1}$), was elevated by the presence of larger amounts of free drug due to supersaturation. EFV-loading into the PEC system was responsible for this behavior. The consistent permeation coupled with higher permeability coefficients and flux values observed in the PEC-E_(C-P) were due to faster EFV release. PEC-E_(C-P) exhibited the highest flux of $0.054 \pm 0.024 \text{ mg} \cdot \text{cm}^{-2} \cdot \text{h}^{-1}$ while PEC-E_(E-S) had a flux of $0.033 \pm 0.052 \text{ mg} \cdot \text{cm}^{-2} \cdot \text{h}^{-1}$. The least flux was recorded for pE ($0.008 \pm 0.017 \text{ mg} \cdot \text{cm}^{-2} \cdot \text{h}^{-1}$).

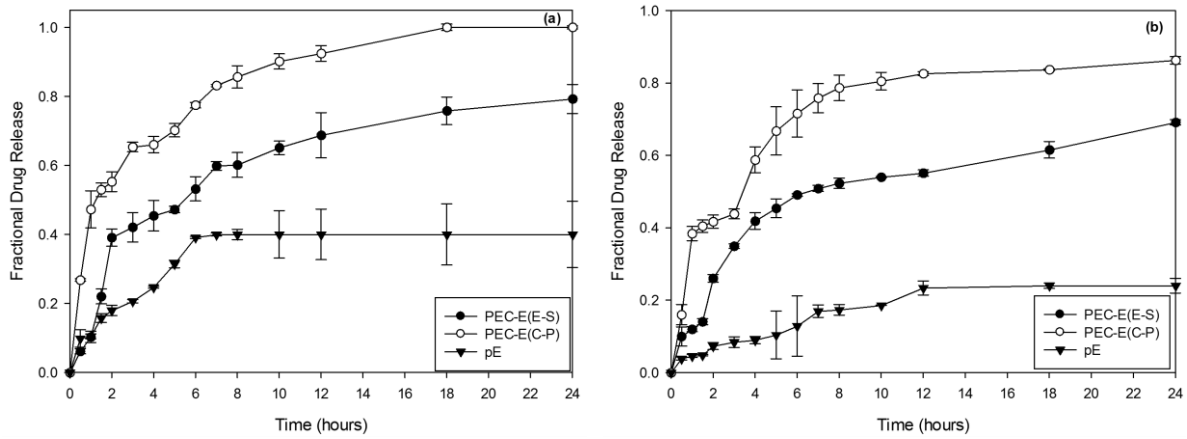


Figure 4.5: (a) Drug release profiles and (b) porcine intestinal tissue permeation profiles for EFV formulations

Figure 4.6 shows the TEER of the intestinal tissue before and after the permeation studies were undertaken. Results demonstrated any changes that might have occurred to the integrity of the tissue as a result of drug permeation. Both PECs had an increase in membrane charge contrary to pE which exhibited a decrease in membrane charge when EFV crossed the small intestinal tissue. It can be deduced that the EFV-loaded PECs did not cause any irreversible membrane damage and neither were there any leakages since EFV passage was constant. Controlled drug release was also responsible for the constant concentration gradient on the membrane. The improved permeation did not compromise the tissue viability as evidenced by the reversibility of TEER value after placement in distilled water at the end of the study. Permeation enhancement can be attributed to the interaction of the mucoadhesive PEC with the intestinal tissue. This led to prolonged duration of the drug at the absorption site in high concentrations due to enhanced solubility of the drug. The presence of mucus could have enhanced effectiveness of the complex. PEC-E_(c-p) did not have a stronger interaction with intestinal mucosa compared to the EFV-loaded extrudates. Permeation was affected by the PEC delivery system and not the physical mixture implying that the mechanism was not tight junction controlled but largely dependent on the resulting complex.

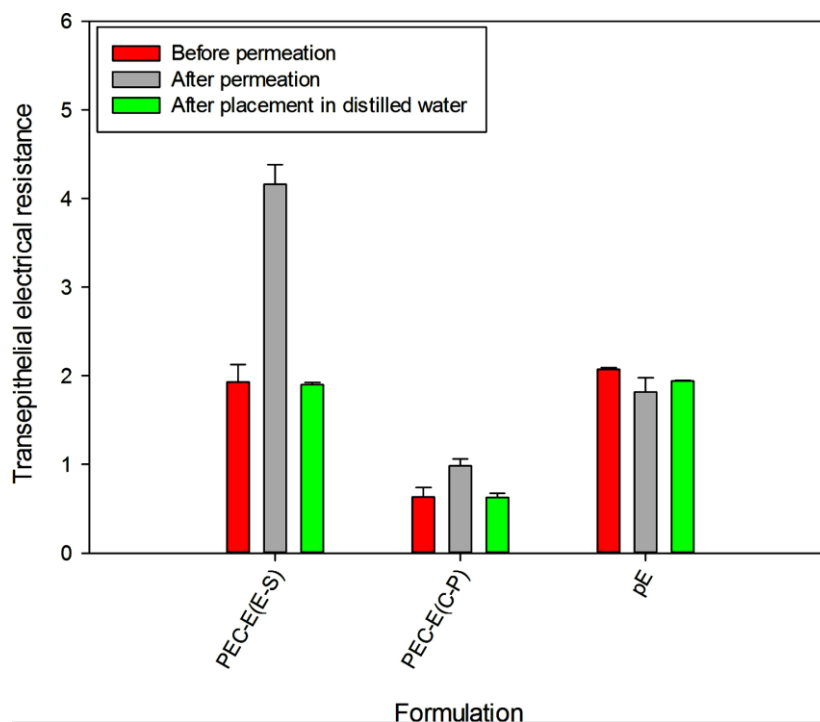


Figure 4.6: Intestinal integrity analysis of EFV-loaded formulations (TEER in $\Omega \cdot \text{cm}^2 \times 10^4$)

4.3.3. Analysis of the experimental design and optimized PEC formulations

4.3.3.1. Analysis of the physical properties of the experimental design formulations

PEC synthesis by E-S was chosen for optimization purposes since the complex showed superior solubility over 24 hours. All design formulations were effectively extruded and spheronized. At least $95 \pm 0.39\%$ of the extrudates fell within the ideal size range of 500-1000 μm as determined by Singh and co-workers (2012). The optimized PEC formulation had a composite desirability of 0.939. Loading of an alternative drug RTV into the optimized formulation (resulting in PEC-R_(E-S)) did not alter the E-S properties and RTV was also soluble in and compatible with the optimized polymer ratio. The HR value measures the interparticulate friction between extrudates and the test was implemented to determine suitability of the samples for encapsulation in a hard gelatin shell (Shah *et al.* 2008). The HR value was <1.25 (Table 4.1) for all formulations therefore F1-F13 had good flow properties. Generally, the smaller the HR value, the better the flow properties of the test sample (Shravani *et al.*, 2011; Singh and Kumar 2012). The small difference between the bulk (D_a) and tapped (D_c) densities further demonstrated that the extrudates had good flow properties.

Table 4.1: Flow properties of extrusion and spheronization of experimental design formulations

Formulation	HA : PQ10 molar ratio	Deionized Water (drops)	Bulk Density (D_a) (g/mL)	Tapped Density (D_c) (g/mL)	$D_a - D_c$ (g/mL)	Hausner Ratio (HR)
F1	5:3	4	0.79±0.0004	0.71±0.053	0.08±0.062	0.90±0.023
F2	5:3	4	0.79±0.019	0.71±0.037	0.08±0.031	0.90±0.092
F3	5:3	5	0.66±0.040	0.62±0.071	0.04±0.005	0.94±0.034
F4	1:3	4	0.85±0.073	0.68±0.004	0.17±0.009	0.80±0.003
F5	1:3	5	0.71±0.009	0.63±0.0009	0.08±0.084	0.89±0.003
F6	5:3	4	0.79±0.063	0.71±0.008	0.08±0.104	0.90±0.010
F7	3:1	3	0.79±0.039	0.65±0.083	0.14±0.075	0.82±0.097
F8	1:3	3	0.75±0.038	0.71±0.028	0.04±0.027	0.95±0.021
F9	5:3	4	0.79±0.082	0.71±0.026	0.08±0.026	0.90±0.063
F10	3:1	5	0.68±0.051	0.56±0.012	0.12±0.009	0.82±0.044
F11	3:1	4	0.80±0.093	0.67±0.014	0.13±0.017	0.84±0.050
F12	5:3	4	0.79±0.028	0.71±0.019	0.08±0.015	0.90±0.002
F13	5:3	3	0.73±0.004	0.68±0.049	0.05±0.035	0.93±0.008

Data expressed as mean (n=3)

Rapid contact of the extrudates with the aqueous medium facilitated the formation of the rate-controlling PEC due to *in situ* complexation. The highest MDTs were recorded for F4, F5 and F8 and these formulations contained the most PQ10 (1:3). This finding was due to the formation of a hydrated viscous layer around the extrudates as they absorbed the dissolution medium and this was consistent with the finding noted by Charoenthai and co-workers (2007). High molecular weight polymers are associated with sustained drug release from a system (Charoenthai *et al.*, 2007). The excess PQ10 provided the charge required for interaction with the aqueous environment thus attracting more aqueous fluid around the extrudates. It was observed that the extrudates from the formulations containing 5:3 polymeric ratios (F1-F3, F6, F9, F12 and F13) dissolved as the drug release progressed while the rest of the formulations remained intact during the study. For the three groups of polymeric ratios, the highest MDTs were noted for the formulations synthesized with 4 drops of distilled water for 446mg of drug/polymer powder mass therefore this was the ideal amount of granulating fluid for maximizing MDT. The presence of excess HA, a macromolecule, resulted in the drug release retardation seen in F7, F10 and F11. The amount of drug that permeated across the intestinal tissue was enhanced by the increase in the amount of HA in the formulation. The highest amount was recorded for F11 (Table 4.2), which was optimal.

Table 4.2: Flux and permeability coefficient results of experimental design and optimized formulations

Formulation	Flux (mg.cm ⁻² .h ⁻¹)	Permeability Coefficient (cm ² .h ⁻¹)	MDT (hours)	Extrudates within 710-1000µm size range (%)
F1	0.05±0.037	0.08±0.055	2.88±1.93	96.66±0.02
F2	0.05±0.029	0.08±0.059	2.94±5.03	96.66±0.49
F3	0.08±0.097	0.14±0.096	3.03±9.28	96.84±4.91
F4	0.01±0.082	0.02±0.016	8.63±0.17	98.92±6.44
F5	0.02±0.031	0.04±0.014	8.20±0.96	99.32±7.68
F6	0.05±0.060	0.07±0.032	3.48±0.49	96.66±0.94
F7	0.04±0.068	0.69±0.049	5.80±2.61	98.52±2.88
F8	0.04±0.010	0.08±0.087	6.39±7.30	99.22±0.26
F9	0.05±0.007	0.08±0.082	3.17±5.53	96.66±8.04
F10	0.09±0.009	0.56±0.035	5.64±8.17	95.50±10.92
F11	0.10±0.045	0.17±0.0007	5.76±1.16	97.28±1.92
F12	0.05±0.051	0.08±0.066	3.20±1.58	96.66±1.80
F13	0.08±0.060	0.15±0.040	3.03±3.37	96.42±4.97

Optimized formulations

Formulation	Flux (mg.cm ⁻² .h ⁻¹)	Permeability Coefficient (cm ² .h ⁻¹)	Total Drug Permeability (%)
PEC-E	0.033±0.040	1.85±0.088	96.34±0.49
cE	0.0078±0.015	0.00087±0.048	35.10±0.96
PEC-R	0.019±0.012	1.95±0.041	95.72±7.57
cR	0.086±0.007	0.012±0.071	56.94±3.53

Data expressed as mean (n=3)

4.3.3.2. Analysis of PEC formulation variables on MDT and ex vivo drug permeability

The optimal PEC formulation (having the composition of F11) consisted of a 3:1 HA:PQ10 polymeric ratio and synthesized with 4 drops of granulation fluid. Selection of the optimized system was based on the formulation that yielded both maximized MDT and flux values. Figure 4.7 is a schematic of the optimization desirability plots as determined by the Box-Benkehn experimental design.

Analysis of the regression coefficients for MDT revealed that p-values were significant (<0.05) therefore depicting good interaction of the polymers and granulating fluid. An R² of 97.8% was noted. Similarly, regression coefficients for flux showed significance for the interaction of HA and PQ10 with water and an R² value of 79.7%. The range for the p-values was 0,023-0,299. The residual plots for MDT and flux further validated a good fit of the model for the data. The plots indicated that there was a correlation between the observed and predicted data. The 2D response contour plots generated by Minitab® (Figure 4.8)

revealed that utilizing a formulation with either high or low level HA results in high MDT values. On the contrary, the use of the mid-level granulating fluid would be recommended to enhance the MDT. The contour plot for drug flux depicts that an increase of HA and water causes a simultaneous increase in amount of drug that permeated the intestinal tissue.

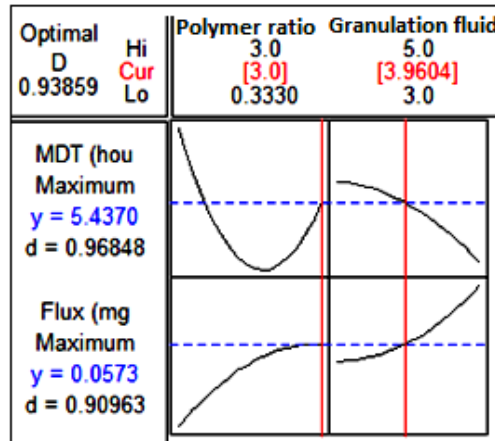


Figure 4.7: Schematic of the optimization desirability plots

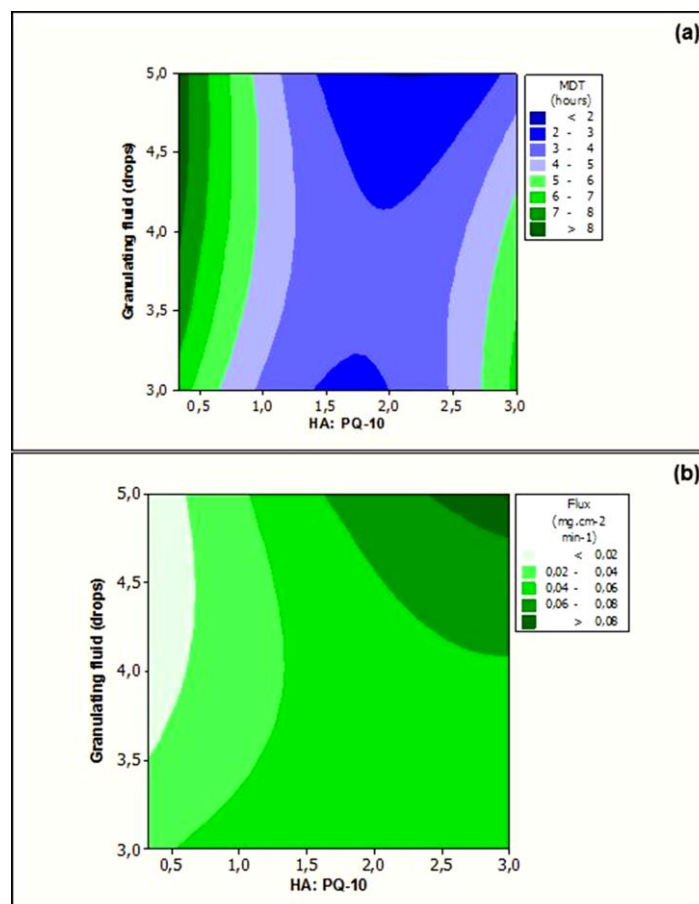


Figure 4.8: Contour plots depicting the influence of granulating fluid and HA: PQ10 on (a) MDT and (b) flux

4.3.4. Characterization of the optimized PEC formulation

4.3.4.1. Analysis of surface morphology and quantification of porosity of the extrudates

Spherical extrudates were obtained after spheronization as depicted in Figure 4.9. The technique was responsible for the smoothing of the extrudates (Figure 4.9(a) and 4.9(d)) devoid of the rough surface observed in the cross-sectional images of both PECs (Figure 4.9(b) and 4.9(e)). PEC-E_(E-S) had larger, interconnected and more numerous pores which were not observed in PEC-R_(E-S). Figure 4.9(c) and (f) are surface morphologies of the extrudates after 24 hour drug release studies. Both PECs exhibited a porous surface with PEC-R_(E-S) revealing larger pores than PEC-E_(E-S). It can be inferred that drug release from PEC-E_(E-S) occurred by diffusion while release from PEC-R_(E-S) involved erosion of the matrix.

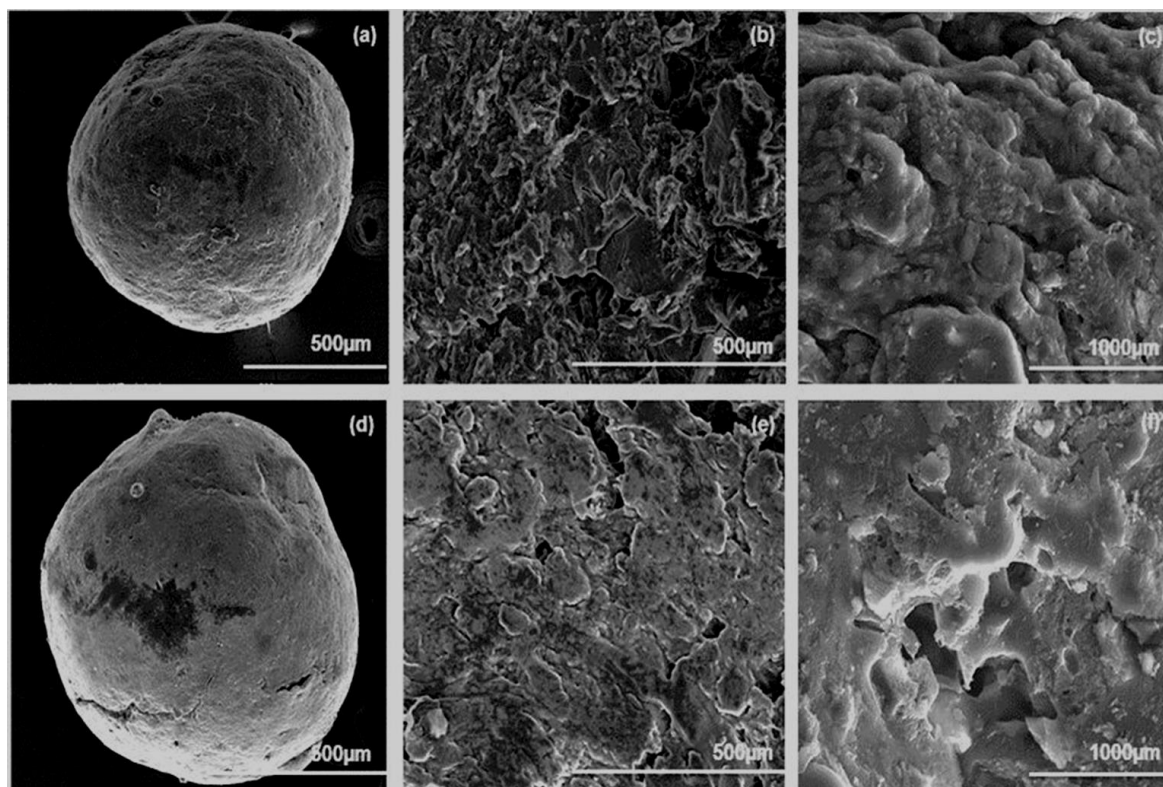


Figure 4.9: Surface morphology images of the EFV (a-c) and RTV (d-f) extrudates

Porosity is a measure of the quantity of nitrogen gas adsorbed onto the sample pores. Pore diameter may impact the rate of drug release due to the interaction of the drug-loaded matrix with the aqueous dissolution medium (Berger *et al.*, 2004). Evaluation of the BET results (Table 4.3) revealed that PEC-E_(E-S) had a significantly larger surface area (-249.7811) than PEC-R_(E-S) (-6.5412). This finding may be correlated with the SEM images, Figure 4.9(b) and 4.9(e). The BJH findings on pore sizes and volumes also maintained a similar trend of PEC-

E_(E-S) exhibiting a larger intraparticle porosity. Both formulations possessed mesopores since their pore sizes fell in the 2-50nm range.

Table 4.3: BET and BJH analysis of optimized PECs

Parameter	PEC-E _(E-S)	PEC-R _(E-S)
Surface area		
BET surface area (m ² /g)	-249.78±0.036	-6.54±0.079
Pore volume		
BJH Adsorption cumulative volume of pores	0.0032±0.0005 0.00029±0.009	0.00072±0.084 0.00071±0.007
BJH Desorption cumulative volume of pores		
Pore size		
BJH adsorption average pore diameter	103.02±0.023Å (10.30nm)	30.4±0.506Å (3.04nm)
BJH desorption average pore diameter	127.66±0.094Å (12.77nm)	31.64±0.019Å (3.16nm)

Data presented as mean (n=3)

4.3.4.2. Evaluation of saturation solubility, drug release and permeability of the optimized PEC formulation

Figure 4.10 shows the calibration curve used to quantify RTV. The solubility results revealed that both PECs exhibited more superior solubility properties to the commercially available comparator products (cE (EFV) and cR (RTV)). PEC-E possessed a much greater increase in supersaturation (14.16±2.81%) than PEC-R (4.39±0.57%). cR is a lipid-based formulation and such formulations have been the most popular for enhancing drug bioavailability over the last two decades (Jannin *et al.*, 2015).

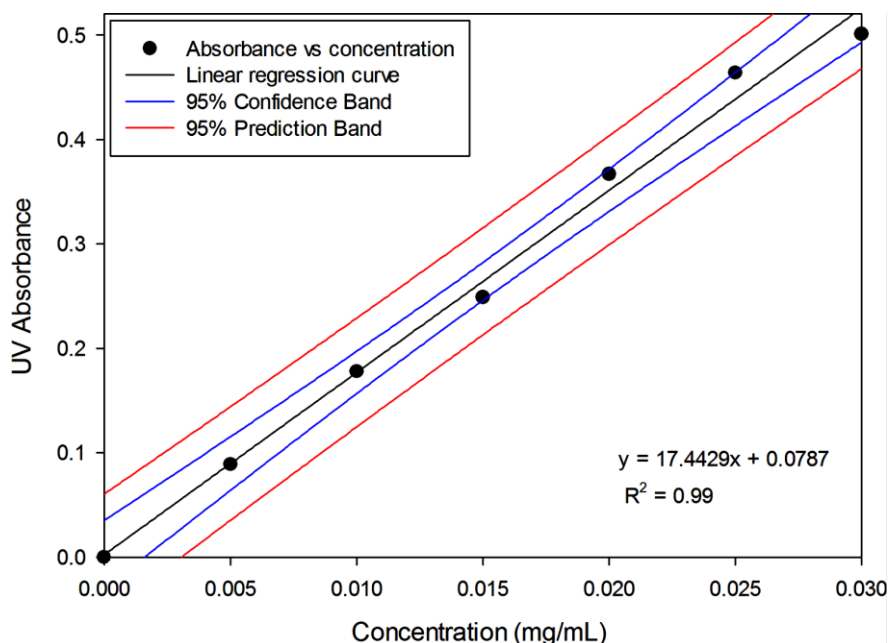


Figure 4.10: Calibration curve for RTV

In vitro dissolution studies were conducted in FeSSIF. The small intestine was selected as the target area of interest because most absorption occurs at this point. The upper intestine contains more bile salts and lecithin in the fed state therefore making it an important site for dissolution of poorly soluble drugs (Viral *et al.*, 2010). Figure 4.11(a) depicts profiles of the fractional drug release (FDR) against time for PEC-E_(E-S) and PEC-R_(E-S) over 24 hours. The comparator brands exhibited immediate drug release within 2 hours and the amount of drug released remained constant for the remainder of the 24 hours. Drug release for cE was incomplete (< 80%) and cR exhibited a total drug release within 2 hours. Solid dispersions have been known to prevent crystal growth of drugs as well as reduce the drug particle size and this property is responsible for the increase in concentration of the drug that undergoes dissolution (Betageri *et al.*, 1995). Solid dispersions are responsible for creating a microenvironment that promotes supersaturation of the drug in the dissolution medium (Brouwers *et al.*, 2009). These findings may be correlated to the Noyes Whitney equation (Equation 4.9) which is used to demonstrate how the dissolution rate of poorly soluble compounds may be improved so as to enhance oral bioavailability.

$$\frac{dC}{dt} = \frac{AD(C_s - C)}{h}$$

Equation 4.9

Where dC/dt is the rate of dissolution, A is the surface area available for dissolution, D is the diffusion coefficient of the compound, C_s is the saturation solubility of the compound in the

dissolution medium, C is the concentration of drug in the medium at time t and h is the thickness of the diffusion boundary layer (Dash *et al.*, 2010).

Loading the drugs into the PECs was beneficial in delaying the occurrence of any precipitation which is common in supersaturated solutions. This stability was achieved by the physical interaction of the drug with the polymers as validated by the FTIR results. Figure 4.11(b) highlights the permeability profiles of PEC-E_(E-S) and PEC-R_(E-S) and their respective comparator products. Permeation enhancement for PEC-E_(E-S) and PEC-R_(E-S) in comparison to the marketed formulations was $61.24 \pm 6.92\%$ and $38.78 \pm 0.50\%$, respectively. According to the collated data, there was a tremendous permeation flux and permeability enhancement of the BCS class II/IV drugs which were loaded in the novel PEC when measured against cE and cR. This enhancement was more pronounced in PEC-E_(E-S) and this may be attributed to EFV's ability to cross the intestinal tissue. The use of HA and PQ10 had a contributory effect on the permeation of EFV and RTV as both polymers have previously been reported to possess good mucoadhesive properties (Mazoniene *et al.*, 2011; Zhang *et al.*, 2003). A study by Mirza and co-workers (2011) revealed that the permeation of carbamazepine complexed to HA improved significantly compared to the permeation of the pure drug. This enhancement was attributed to HA being amphiphilic and more hydrophobic in aqueous media.

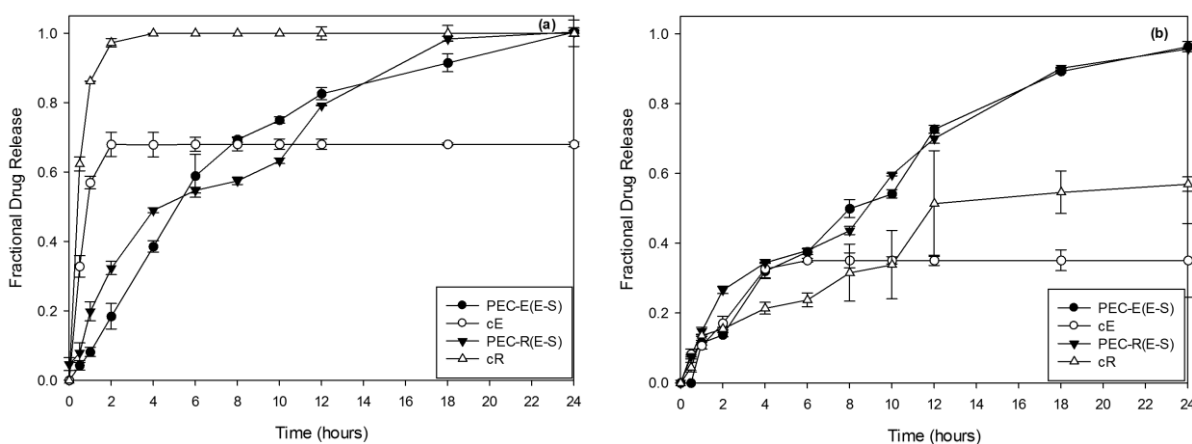


Figure 4.11: Graphs depicting (a) drug release profiles of EFV and RTV optimized formulations and (b) permeability profiles of EFV and RTV optimized formulations

4.4. CONCLUDING REMARKS

Extrusion-spheronization and complexation-precipitation techniques were successfully implemented for both drug-free and drug-loaded polyelectrolyte complex fabrication. Although they enhanced the delivery of the bioactive, synthesis by extrusion-spheronization

provided more desirable qualities in the resultant solid dispersions. The use of solid dispersions has been widely implemented as a solubilization technique, though there are limited studies on their implementation to enhance the solubility and permeability of anti-HIV drugs in BCS class II/IV. Solid dispersions of EFV and RTV in the optimized HA-PQ10 PEC showed promising results for targeted release to the small intestine and accelerated drug solubility and permeability. The formulation constituting the novel HA-PQ10 PEC may also be applied for targeted release of highly water soluble drugs. The quantity of HA used in this study was below the permissible 512mg/kg reported previously by Mirza and co-workers (2011). Therefore the PEC can be safely utilized for drug delivery purposes and the extruded PEC formulation was selected for optimization. Overall, these results indicated that the PEC enhanced the solubility and permeability of BCS class II/IV drugs that may have a positive impact on their bioavailability in a suitable *in vivo* model. Administration of full doses from the extruded PEC, particularly EFV, would result in sizable formulations hence it was imperative to further investigate formulation techniques that would allow higher drug loading and smaller formulation sizes.

4.5. REFERENCES

- Berger, J., Reist, M., Mayer, J.M., Felt, O., Gurny, R., 2004. Structure and interactions in chitosan hydrogels formed by complexation or aggregation for biomedical applications. *European Journal of Pharmaceutics and Biopharmaceutics*, 57(1), 35–52.
- Betageri, G.V., Makarla, K.R., 1995. Enhancement of dissolution of glyburide by solid dispersion and lyophilization techniques. *International Journal of Pharmaceutics*, 126(1), 155–60.
- Brouwers, J., Brewster, M.E., Augustijns, P., 2009. Supersaturating drug delivery systems: The answer to solubility-limited oral bioavailability? *Journal of Pharmaceutical Sciences*, 98(8), 2549–72.
- Charoenthai, N., Kleinebudde, P., Puttipipatkachorn, S., 2007. Use of chitosan-alginate as alternative pelletization aid to microcrystalline cellulose in extrusion/spheronization. *Journal of Pharmaceutical Sciences*, 96(9), 2469-84.
- Coimbra, P., Ferreira, P., De Sousa, H.C., Batista, P., Rodrigues, M.A., Correia, I.J., Gil, M.H., 2011. Preparation and chemical and biological characterization of a pectin/chitosan polyelectrolyte complex scaffold for possible bone tissue engineering applications. *International Journal of Biological Macromolecules*, 48(1), 112-118.

- da Costa, M.A., Seiceira, R.C., Rodrigues, C.R., Hoffmeister, C.R.D., Cabral, L.M., Rocha, H.V.A., 2012. Efavirenz Dissolution Enhancement I: Co-Micronization. *Pharmaceutics*, 5(1), 1–22.
- Dash, S., Padala, N.M., Lilakanta, N., Prasanta, C., 2010. Kinetic Modeling on Drug Release from Controlled Drug Delivery Systems. *Acta Poloniae Pharmaceutica*, 67(3), 217-223.
- Dengale, S.J., Hussen, S.S., Krishna, B.S.M., Musmade, P.B., Gautham Shenoy, G., Bhat, K., 2015. Fabrication, solid state characterization and bioavailability assessment of stable binary amorphous phases of Ritonavir with Quercetin. *European Journal of Pharmaceutics and Biopharmaceutics*, 89, 329–38.
- Dezani, A.B., Pereira, T.M., Caffaro, A.M., Reis, J.M., Serra, C.H., dos Reis Serra, C.H., 2013. Determination of lamivudine and zidovudine permeability using a different *ex vivo* method in Franz cells. *Journal of Pharmacology and Toxicological Methods*, 67(3), 194–202.
- DiNunzio, J.C., Miller, D.A., Yang, W., McGinity, J.W., Williams III, R.O., 2008. Amorphous compositions using concentration enhancing polymers for improved bioavailability of itraconazole. *Molecular Pharmaceutics*, 5(6), 968–80.
- Fandaruff, C., Segatto Silva, M.A., Galindo Bedor, D.C., de Santana, D.P., Rocha, H.V.A., Rebuffi, L., Azanza Ricardo, C.L., Scardi, P., Cuffini, SL., 2015. Correlation between microstructure and bioequivalence in anti-HIV drug efavirenz. *European Journal of Pharmaceutics and Biopharmaceutics*, 91, 52–8.
- Ito, H., Miyamoto, T., Inagaki, H., Noishiki, Y., Iwata, H., Matsuda, T., 1986. *In vivo* and *in vitro* blood compatibility of polyelectrolyte complexes formed between cellulose derivatives. *Journal of Applied Polymer Science*, 32(2), 3413–21.
- Jan, K., Riar, C.S., Saxena, D.C., 2015. Engineering and functional properties of biodegradable pellets developed from various agro-industrial wastes using extrusion technology. *International Journal of Food Science and Technology*, 52(12), 7625-39.
- Jannin, V., Chevrier, S., Michenaud, M., Dumont, C., Belotti, S., Chavant, Y., Demarne, F., 2015. Development of self emulsifying lipid formulations of BCS class II drugs with low to medium lipophilicity. *International Journal of Pharmaceutics*, 495(1), 385-92.
- Jones, E., Ojewole, E., Pillay, V., Kumar, P., Rambharose, S., Govender, T., 2013. Monolayered multipolymeric buccal films with drug and polymers of opposing solubilities for ARV therapy: Physico-mechanical evaluation and molecular mechanics modelling. *International Journal of Pharmaceutics*, 455(1), 197–212.

- Kim, J.Y., Zaoutis, T., Chu, J., Zhao, H., Rutstein, R., 2009. Effects of highly active antiretroviral therapy (HAART) on cholesterol in HIV-1 infected children: a retrospective cohort study. *Pharmacoepidemiology and Drug Safety*, 18(7), 589–94.
- Kleinebudde, P., 1997. The crystallite-gel-model for microcrystalline cellulose in wet-granulation, extrusion, and spheronization. *Pharmaceutical Research*, 14(6), 804-9.
- Koh, P.T., Chuah, J.N., Talekar, M., Gorajana, A., Garg, S., 2013. Formulation development and dissolution rate enhancement of efavirenz by solid dispersion systems. *Indian Journal of Pharmaceutical Sciences*, 75(3), 291.
- Kondiah, P.P., Tomar, L.K., Tyagi, C., Choonara, Y.E., Modi, G., du Toit, L.C., Pillay, V., 2013. A novel pH-sensitive interferon- β (INF- β) oral delivery system for application in multiple sclerosis. *International Journal of Pharmaceutics*, 456(2), 459-472.
- Lavon, I., Grossman, N., Kost, J., 2005. The nature of ultrasound–SLS synergism during enhanced transdermal transport. *Journal of Controlled Release*, 107(3), 484-94.
- Mabrouk, M., Chejara, D.R., Mulla, J.A.S., Badhe, R.V., Choonara, Y.E., Kumar, P., Pillay, V., 2015. Design of a novel crosslinked HEC-PAA porous hydrogel composite for dissolution rate and solubility enhancement of efavirenz. *International Journal of Pharmaceutics*, 490(1), 429-437.
- Mazoniene, E., Joceviciute, S., Kazlauske, J., Niemeyer, B., Liesiene, J. 2011. Interaction of cellulose-based cationic polyelectrolytes with mucin. *Colloids Surface B Biointerfaces*, 83(1), 160–4.
- Mirza, M.A., Ahmad, N., Agarwal, S.P., Mahmood, D., Anwer, M.K., Iqbal, Z., 2011. Comparative evaluation of humic substances in oral drug delivery. *Results in Pharma Sciences*, 1(1), 16–26.
- Pawar, J., Tayade, A., Gangurde, A., Moravkar, K., Amin, P., 2016. Solubility and dissolution enhancement of efavirenz hot melt extruded amorphous solid dispersions using combination of polymeric blends: A QbD approach. *European Journal of Pharmaceutical Sciences*, 88, 37-49.
- Prasad, D., Chauhan, H., Atef, E., 2014. Amorphous stabilization and dissolution enhancement of amorphous ternary solid dispersions: combination of polymers showing drug–polymer interaction for synergistic effects. *Journal of Pharmaceutical Sciences*, 103(11), 3511-23.
- Rao, M.R., Shirsath, C., 2016. Enhancement of Bioavailability of Non-nucleoside Reverse Transcriptase Inhibitor Using Nanosponges. *AAPS PharmSciTech*, 1-1.

- Sathigari, S.K., Radhakrishnan, V.K., Davis, V.A., Parsons, D.L., Babu, R.J., 2012. Amorphous-state characterization of efavirenz—polymer hot-melt extrusion systems for dissolution enhancement. *Journal of Pharmaceutical Sciences*, 101(9), 3456-64.
- Serajuddin, A., 1999. Solid dispersion of poorly water-soluble drugs: Early promises, subsequent problems, and recent breakthroughs. *Journal of Pharmaceutical Sciences*, 88(10), 1058-66.
- Shah, R.B., Tawakkul, M.A., Khan, M.A., 2008. Comparative evaluation of flow for pharmaceutical powders and granules. *AAPS PharmSciTech*, 9(1), 250-8.
- Shao, Y., Li, L., Gu, X., Wang, L., Mao, S., 2015. Evaluation of chitosan—anionic polymers based tablets for extended-release of highly water-soluble drugs. *Asian Journal of Pharmaceutical Sciences*, 10(1), 24–30.
- Shergill, M., Patel, M., Khan, S., Bashir, A., McConville, C., 2016. Development and characterisation of sustained release solid dispersion oral tablets containing the poorly water soluble drug disulfiram. *International Journal of Pharmaceutics*, 497(1), 3-11.
- Shovsky, A., Varga, I., Makuska, R., Claesson, P.M., 2009. Formation and stability of water-soluble, molecular polyelectrolyte complexes: effects of charge density, mixing ratio, and polyelectrolyte concentration. *Langmuir*. 25(11), 6113-21.
- Shrivani, D., Lakshmi, P.K., Balasubramaniam, J., 2011. Preparation and optimization of various parameters of enteric coated pellets using the Taguchi L9 orthogonal array design and their characterization. *Acta Pharmaceutica Sinica B*, 1(1), 56-63.
- Singh, G., Pai, R.S., Devi, V.K., 2012. Response surface methodology and process optimization of sustained release pellets using Taguchi orthogonal array design and central composite design. *Journal of Advanced Pharmaceutical Technology and Research*, 3(1), 30.
- Singh, G., Sharma, S., Gupta, G.D., 2016. Extensive Diminution of Particle Size and Amorphization of a Crystalline Drug Attained by Eminent Technology of Solid Dispersion: A Comparative Study. *AAPS PharmSciTech*, 1-5.
- Singh, I., Kumar, P., 2012. Preformulation studies for direct compression suitability of cefuroxime axetil and paracetamol: a graphical representation using SeDeM diagram. *Acta Poloniae Pharmaceutica*, 69(1), 87e93.
- Sinha, S., Ali, M., Baboota, S., Ahuja, A., Kumar, A., Ali, J., 2010. Solid dispersion as an approach for bioavailability enhancement of poorly water-soluble drug ritonavir. *AAPS PharmSciTech*, 11(2), 518–27.

- Six, K., Verreck, G., Peeters, J., Brewster, M., Mooter, G.V den., 2004. Increased physical stability and improved dissolution properties of itraconazole, a class II drug, by solid dispersions that combine fast-and slow-dissolving polymers. *Journal of Pharmaceutical Sciences*, 93(1), 124–31.
- Siyawamwaya, M., Choonara, Y.E., Bijukumar, D., Kumar, P., du Toit, L.C., Pillay, V., 2015. A review: overview of novel polyelectrolyte complexes as prospective drug bioavailability enhancers. *International Journal of Polymeric Materials and Polymeric Biomaterials*, 65(11), 955–68.
- Siyawamwaya, M., Choonara, Y.E., Kumar, P., Kondiah, P.P.D., du Toit, L.C., Pillay, V., 2016. A humic acid-polyquaternium-10 stoichiometric self-assembled fibrilla polyelectrolyte complex: Effect of pH on synthesis, characterization, and drug release. *Int Journal of Polymeric Materials and Polymeric Biomaterials*, 65(11), 550-60.
- Tang, M., Dettmar, P., Batchelor, H., 2005 Bioadhesive oesophageal bandages: protection against acid and pepsin injury. *International Journal of Pharmaceutics*, 292(1), 169–77.
- Usach, I., Melis, V., Peris, J.E., 2013. Non-nucleoside reverse transcriptase inhibitors: a review on pharmacokinetics, pharmacodynamics, safety and tolerability. *Journal of International AIDS Society*, 16(1), 18567.
- Viral, S., Dhiren, P., Mane, S., Umesh, U., 2010. Solubility and Dissolution Rate Enhancement of Licofelone by Using Modified Guar Gum. *International Journal of PharmTech Research*, 2, 1847-54.
- Zhang, X., Bai, R., 2003. Mechanisms and kinetics of humic acid adsorption onto chitosan-coated granules. *Journal of Colloid Interface Science*, 264(1), 30–8.

CHAPTER 5

SYNTHESIS AND COMPARISON OF HUMIC ACID-POLYQUATERNIUM 10 TABLETS IMPLEMENTING 3D-PRINTING AND DIRECT TABLET COMPRESSION

5.1. INTRODUCTION

Tablet formulations are the most popular and various techniques of tableting have been documented ranging from conventional methods such as direct compression to extensive cutting edge methods such as using 3D-Printing (3DP). The traditional approach is feasible and reproducible when powder samples have adequate flow and compressibility properties (Juban *et al.*, 2016).

3DP is revolutionizing the field of drug delivery. It involves the synthesis of customized and digitally controlled tablets in a layer-by-layer manner. Pharmaceutical industry has embraced 3DP for the synthesis of dosage forms and research is underway to make 3DP viable for manufacturing customized medicines. This technique is highly attractive allowing for precise and extensive drug-loading capacity (Goyanes *et al.*, 2015).

This study aimed at synthesizing a 3DP oral tablet, consisting of a humic acid (HA)-polyquaternium-10 (PQ10) polyelectrolyte complex (PEC) and with high drug-loading of efavirenz (EFV). To the best of our knowledge, no research has been undertaken on 3DP of tablets consisting of HA-PQ10 as the printing 'ink'. Manufacture of the oral tablet was undertaken with the aid of a 3D Bioplotter® (EnvisionTEC GmbH, Gladbeck, Germany) that is able to process a wide range of biomaterials such as polymer melts, polymer solutions and bioactive polymers (Pfister *et al.*, 2004). 3D bioplotting uses pressure to extrude material (API and polymers) from a sample holder in 3D onto a build platform. Each layer must solidify in order for the tablet to hold. This may be achieved by extruding molten polymers or a sludge that solidify at the build platform or by extruding the API-polymer melt into a liquid of equal viscosity (Goyanes *et al.*, 2015). Properties of the 3DP tablets were compared to tablets manufactured by direct compression to determine if the 3DP formulation performed superiorly.

5.2. MATERIALS AND METHODS

5.2.1. Materials

Brown humic acid sodium salt (HA), hydroxyethylcellulose ethoxylate, quaternized (PQ10 Mw=656.1g/mol), cellulose acetate phthalate (CAP Mw=2534.12g/mol), and sodium lauryl sulfate (SLS) were purchased from Sigma–Aldrich® (St. Louis, MO, USA). Efavirenz (EFV) was procured from Xingcheng Chemphar Co., Ltd. (Taizhou, Zhejiang, China). All other chemicals used were of analytical grade. Analytical grade methanol and acetone were used as solvents in sludge synthesis as well as to induce rapid solidification of the printed tablet due to their volatility. 3D-Printing was undertaken with the aid of a 3D-Bioplotter® (Bioplotter®, EnvisionTEC GmbH, Gladbeck, Germany). The sludge was transferred into a 30mL polyethylene cartridge attached to a 0.61mm cone needle (Nordson EFD, East Providence, Rhode Island, USA) on one end, and a feed tube connected to filtered and compressed air on the other end. The tablet shape and dimensions were designed with the aid of Magics® software Version 18.2 (Materialise, Leuven, Belgium) which created a rapid prototyping STereoLithography (.stl) file format with the desired cylindrical shape and dimensions (20mm diameter; 10mm thickness). Direct tablet compression was conducted on a Mini-Tablet Press (Rimek Minipress- II MT, Karnavati, Gujarat, India).

5.2.2. Preparation and characterization of a 3D-Printable (HA-PQ10)-EFV sludge

5.2.2.1. Determination of ideal excipients and solvents for 3DP sludge synthesis

EFV-loaded HA-PQ10 was rendered 3D-Printable by the addition of the enteric polymer and binding excipient, cellulose acetate phthalate (CAP) (12%w/v in acetone). Different excipients and solvents were explored to assess 3D-Printability of the EFV-loaded HA-PQ10 and it was determined that the CAP solution (12%w/v in acetone) could be effectively used as a binder solution. Preparation of the sludge involved the hydration of PQ10 (750mg) with deionized water (3mL). This was left to soak at room temperature for 15 minutes. EFV was partially dissolved in methanol (6mL) and the mixture added to the hydrated PQ10. Three different amounts of EFV (1500mg, 3000mg and 6000mg) were utilized to formulate sludges possessing the HA-PQ10 : EFV ratios of 1:2, 1:1 and 2:1, respectively. After adequate mixing, powdered HA (2250mg) was added followed by the CAP solution (1mL, 12%w/v in acetone). Methanol was also responsible for lowering the boiling point of acetone used to dissolve the CAP therefore maintaining the viscosity of the sludge while still in the printer cartridge, before extrusion. It was therefore determined that the critical material attributes (CMAs) for the 3D-Printable sludge were viscosity, printability without clogging the nozzle, operating temperature, concentration of CAP in acetone and quantity of methanol. The

resultant sludge was tested for 3D-Printability from the low temperature print head (0-70°C). The sludge formulation described yielded 5 tablets.

5.2.2.2. Determination of polymer-drug interactions in EFV and the 3D-Printable sludges

Interactions between the EFV and HA-PQ10 in the sludges were analyzed by Attenuated Total Reflectance Fourier Transform Infrared (ATR-FTIR) spectroscopy (PerkinElmer Spectrum 100, Llantrisant, Wales, UK). Powdered samples were placed onto an ATR top-plate containing a diamond crystal. Analysis was conducted within the wavenumber range of 650-4000 cm^{-1} with a direct contact force of 115N. The spectra from the EFV-loaded sludges were compared to the spectra for EFV and EFV-free 3D-Printable sludge (3DP_{HA-PQ10}).

5.2.2.3. Determination of thermal properties of EFV and 3D-Printable sludges

Thermal behaviour of pure EFV and the sludges was assessed by Differential Scanning Calorimetry (DSC, METTLER Toledo DSC1, STARe System, Switzerland). A known amount of the test sample was weighed in a 40 μl aluminium pan which was sealed and perforated before evaluation. The test was conducted at a temperature range of 25–325°C at 10°C/min. The melting points for each sample were determined and used to assess miscibility between EFV and HA-PQ10.

5.2.2.4. Determination of (HA-PQ10)-EFV sludge consistency

A texture analyzer (TAXT2i, Stable Microsystems Ltd., Surrey, England) equipped with a 10mm diameter acrylic cylindrical probe was used to infiltrate the sample and the force exerted to the probe was recorded. The EFV-loaded sludge was placed in a 30mm canister to minimize air exposure while the probe penetrated the sludge to a depth of 20mm. A pre-test speed of 1mm/s was implemented while a test and post-test speed of 0.5mm/s was set and assessment was repeated in triplicate. In order to determine the sludge hardness (maximum positive force after deformation) cohesiveness (maximum negative force after deformation) and springiness (distance that the sludge extended before separating from the probe), the one-deformation test was employed with the parameters being kept constant for all test samples (Tai *et al.*, 2014; Yildiz *et al.*, 2013; Sandhu and Singh, 2007).

5.2.3. Manufacture and physicochemical characterization of 3DP and direct compression tablets

5.2.3.1. Synthesis of cylindrical tablets using 3DP and direct compression

Slicing of the tablet had to be carried out in Magics® to ensure that there were no errors in the design. The STL file was converted to the BPL file format (Biplotter RP® Version 3.0) which could be used for 3DP in Visual Machine®. The 3DP critical process parameters (CPPs) for the EFV-loaded HA-PQ10 sludge were printing speed and extrusion pressure and these were controlled and set in Visual Machine®. The pressure and speed tuning option on the Visual Machine® software on the 3D Biplotter® was employed to optimize the strand width of the preferred sludge. The extruded sludge successfully formed a cylindrical tablet (20mm diameter, 10mm thickness) without layer collapse. The tablets were allowed to dry for 12 hours at 20°C. For direct compression, the sludge was left to dry before producing a homogenous powder with the aid of a mortar and pestle. Tablets were compressed on a Mini-Tablet Press under a pressure of 3 tonnes.

5.2.3.2. Measurement of mechanical strength and polymer-EFV packing of 3DP and direct compression tablets

The indentation tablet hardness was determined by calculating the Brinell hardness of the tablets synthesized from the sludges via 3DP and direct compression. A 3.175mm steel indenter was used to apply a 5kg load onto the surface of the tablets. The indenter had a maximum displacement of 0.1mm on the flat surface of the tablets. Tablet density was calculated to determine the influence of tableting method on the packing of polymer networks in the 3DP and direct compression tablets. Equation 5.1 was employed to calculate the Brinell Hardness Number (BHN) and Equation 5.2 was used to calculate the tablet density.

$$BHN = \frac{2F}{\pi D(D - \sqrt{D^2 - d^2})}$$

Equation 5.1

Where, F=load on the indenting tool (kg), D=diameter of the spherical probe indenter (3.175mm), and d=diameter at the rim of the impression made (depth 0.1mm) (Busignies *et al.*, 2006).

$$D(g/cm^3) = \frac{w}{\left(\frac{m}{2}\right)^2 \times \pi \times h}$$

Equation 5.2

Where w is the tablet weight (g), m is the tablet diameter (cm) and h is the tablet thickness (cm) (Hanif *et al.*, 2014).

5.2.3.3. Porositometric analysis undertaken on the 3DP and direct compression tablets

Porositometric analysis, utilizing Brunauer-Emmet-Teller (BET) and Barrett, Joyner and Halenda (BJH) isotherms of nitrogen, was undertaken. The adsorption and desorption profiles were generated to determine the surface area, pore diameter, total pore volume, and bulk and absolute densities of the 3DP and direct compression tablets. The ASAP 2020 Porositometer with ASAP 202 V3.01 software (Micromeritics Instrument Corp., Norcross, GA, USA) was employed for the analysis. Degassing of weighed samples (>100mg) placed in isothermal jackets was conducted for 24 hours before analysis.

5.2.3.4. Mapping of matrix hydration kinetics and gravimetric analysis of the 3DP and direct compression tablets

The dimensional changes associated with hydration kinetics of the 3DP and direct compression tablets in SIF were mapped using Magnetic Resonance Imaging (MRI) system (Oxford Instruments Magnetic Resonance, Oxon, UK). MRI has an in-line dissolution flow through cell (USP apparatus 4). SIF was circulated continuously at 4mL/min and a total of 64 scans were used. The physical properties of the 3DP tablet were compared to those of the direct compression tablet with the exact same (HA-PQ10)-EFV compositions. Gravimetric analysis was conducted to quantify the amount of moisture absorption and mass loss of the 3DP and direct compression tablets in SIF over 8 hours.

5.2.3.5. Analysis of *in vitro* drug release of 3DP and direct compression tablets

A USP 33 type II dissolution apparatus (Erweka DT 700, Erweka GmbH, Heusenstamm, Germany) was used to assess drug release profiles from 3DP and direct compression tablets. The test was conducted for 8 hours in 900 mL simulated intestinal fluid (SIF) (pH=6.8; 37°C; 50rpm) with 1% SLS. The small intestine, being the site of maximal absorption, was the target site for the delivery of EFV. At preset intervals, 5mL of the SIF was sampled and analyzed by ultraviolet (UV) spectrophotometer (LAMBDA 25 UV/Vis spectrophotometer, PerkinElmer, MA, USA).

5.3. RESULTS AND DISCUSSION

5.3.1. Analysis of the synthesized 3D-Printable (HA-PQ10)-EFV sludge

5.3.1.1. Assessment of the synthesis of a 3D-Printable sludge

Different excipients and solvents were explored to produce an EFV-loaded 3DP ink. Table 5.1 shows the results obtained from various printing ink screening formulations.

It was determined that CAP solution (12%^{w/v} in acetone) adequately plasticized the (HA-PQ10)-EFV sludge. Preparation of the sludge involved the hydration of 750mg of PQ10 by adding 3mL of distilled water. This was left to soak at room temperature for 15 minutes. EFV was partially dissolved in 6mL of methanol and the mixture added to the hydrated PQ10. Three different amounts of EFV (1500mg, 3000mg and 6000mg) were utilized to make sludges containing different (HA-PQ10):EFV ratios (1:2, 1:1 and 2:1). After adequate mixing, powdered HA (2250mg) was added followed by the CAP solution (1mL, 12%^{w/v} in acetone). CAP plasticized the sludge and provided enteric release properties (Asghar *et al.*, 2008). The extruded sludge successfully formed a cylindrical tablet (20mm diameter, 10mm thickness) without layer collapse (Figure 5.1).

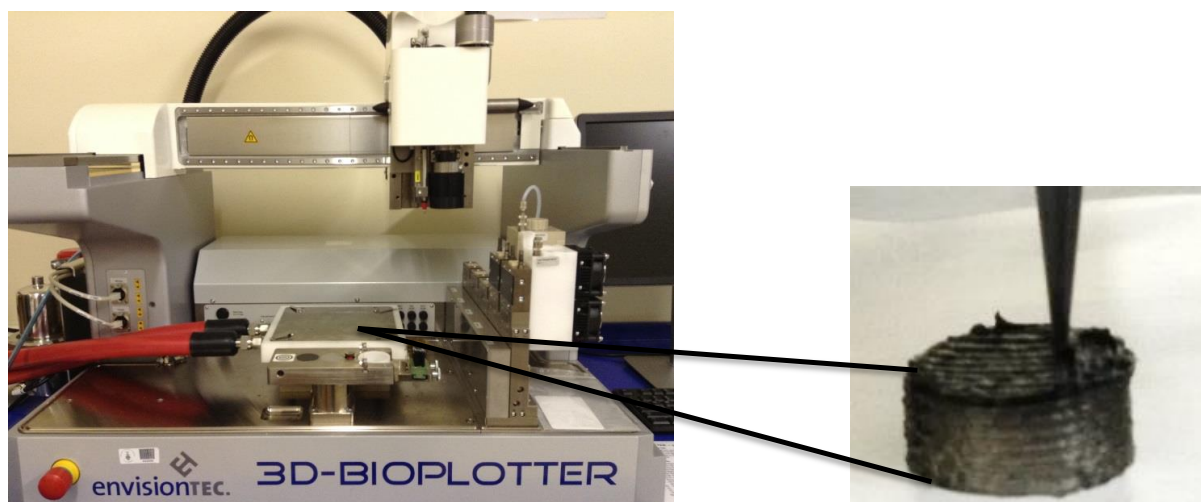


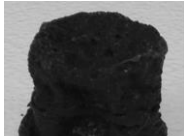








Figure 5.1: 3D-Printing of HA-PQ10 sludge using the 3D-Biplotter®

Minimal amount of methanol (1mL/500mg) was added to EFV to facilitate its dispersion in PQ10. Methanol was also responsible for lowering the boiling point of acetone used to dissolve the CAP therefore the sludge remained in a molten state while still in the printer cartridge, before extrusion. Limitations associated with 3DP are clogging of the sludge in the nozzle thus disturbing the extrusion process. In some cases, the surface of the printed product presents with imperfections, something which is uncommon in conventional tableting (Alhnan *et al.*, 2016).

Table 5.1: screening formulation template for 3D-Printable sludge

Polymer ink	Extrusion pressure (bar)	Printing speed (mm/s)	Injection nozzle (mm)	Result
PEI; lactose; methanol:water (1:1)	3	20	0.840	
PTBEM; PEI; methanol:chloroform (1:1)	1	30	0.610	
Eudragit L-55; PEGME; methanol:water (1:1)	1.5	30	0.610	
PEI:acetonitrile (1:5)	2	25	0.840	
Eudragit L-55; triacetin:methanol:water (1:4:5)	0.5	5	0.610	
Eudragit L-55; methanol:water (1:1)	0.4	5	0.610	
PEI; methanol:chloroform (1:1)	1.7	30	0.610	
MCC; PEI (5% in water); methanol:chloroform (1:1)	1.5	30	0.610	
MCC; PEI (5% in water); methanol:chloroform (1:1)	2.5	20	1.370	

5.3.1.1. Assessment of chemical and physical interactions in (HA-PQ10)-EFV sludge

The EFV functional groups were expressed in all the formulations and these included C-F stretch (1493cm^{-1}), tertiary amide (1601cm^{-1}), C=O cyclic (1742cm^{-1}), typical exocyclic triple bond stretching (2248cm^{-1}) and N-H stretching (3312cm^{-1}) (Figure 5.2). These peaks were similar with previously reported analysis by Alves and co-workers (2014). The addition of HA-PQ10 and CAP to EFV during sludge formation did not shift the skeleton stretching bands therefore (HA-PQ10)-EFV chemical interactions were not notable. The FTIR spectra for the $3\text{DP}_{2:1}$ and $3\text{DP}_{1:1}$ exhibited broad peaks corresponding with the EFV N-H stretching vibrations ($3500\text{-}3200\text{cm}^{-1}$). The N-H stretching absorbance is lower in $3\text{DP}_{2:1}$ (0.07) and remained unchanged in $3\text{DP}_{1:1}$ (0.1) compared to the absorbance of the same band in pure EFV (0.1). These observations are indicative of hydrogen bonding between the H donating groups in the N-H bands of EFV and H accepting groups in the O-H bands of $3\text{DP}_{\text{HA-PQ10}}$ (Sathigari *et al.*, 2012). The interaction was more pronounced in $3\text{DP}_{2:1}$ which had a decrease in the N-H peak absorbance in addition to peak broadening. $3\text{DP}_{2:1}$ possessed a higher HA-PQ10 concentration than $3\text{DP}_{1:1}$ and the presence of more numerous O-H groups led to higher chances of (HA-PQ10)-EFV H-bond formation. The broad peak exhibited in $3\text{DP}_{\text{HA-PQ10}}$ at 3380cm^{-1} was attributed to the water absorption band (Fule and Amin, 2014). The increase in absorbance of the $3\text{DP}_{1:1}$ tertiary amide band at 1601cm^{-1} suggests an elevation in the band vibrations at that (HA-PQ10)-EFV ratio.

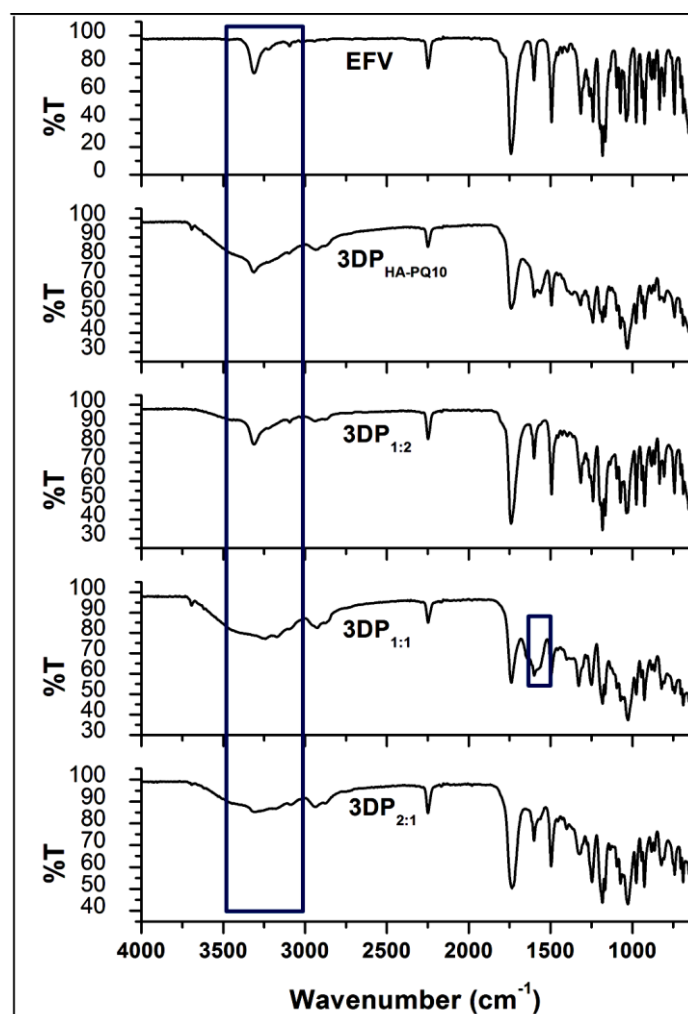


Figure 5.2: FTIR spectra depicting (HA-PQ10)-EFV interactions in 3D-Printable sludges at (HA-PQ10) : EFV ratios of 1:2, 1:1 and 2:1

5.3.1.2. Analysis of thermodynamic properties of (HA-PQ10)-EFV sludge

Figure 5.3 depicts the thermograms for EFV and the 3DP sludges at different (HA-PQ10) : EFV ratios. The broad endotherm at 75°C exhibited by 3DP_{HA-PQ10} was associated with water absorption as also is depicted in the 3DP_{HA-PQ10} FTIR spectrum (Fule and Amin, 2014). The endotherms for 3DP_{2:1} showed a disappearance of the EFV melting endotherm and this indicated that EFV was totally miscible in HA-PQ10 at this ratio. Two endotherms were shown for the 3DP_{1:1} formulation with the one occurring at 100°C being ascribed to loss of water. The EFV melting peak area was reduced in 3DP_{1:1} indicating partial conversion of the EFV to the amorphous state. A fraction of the drug was transformed from the crystalline to the amorphous state as it became miscible into the polymeric matrix (Alhijaj *et al.*, 2016).

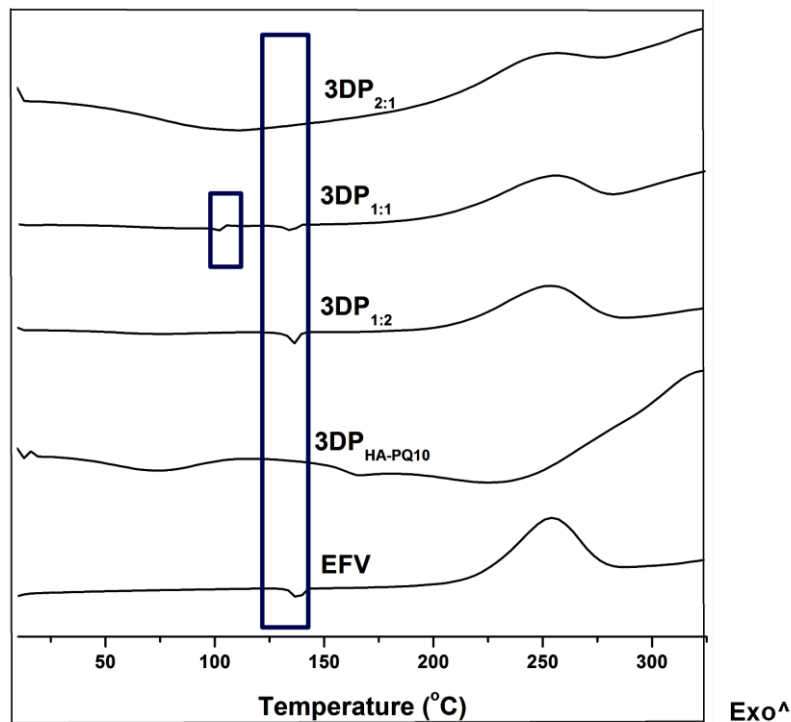


Figure 5.3: DSC thermograms of 3D-Printable sludges at (HA-PQ10) : EFV ratios of 1:2, 1:1 and 2:1

5.3.1.3. Assessment of the (HA-PQ10)-EFV sludge consistency

The hardness of the sludges was determined by recording the maximum force of deformation after the probe was applied. Figure 5.4 shows that 3DP_{1:2} sludge recorded the highest maximum force. During 3D-Printing, 3DP_{1:2} required the highest extrusion pressure and it was liable to clogging the injection nozzle. During texture analysis, 3DP_{1:2} sludge left a residue on the probe after deformation. The thick consistency was influenced by the high EFV concentration in the sludge. The increase in EFV concentration was also accompanied by an increase in cohesiveness. 3DP_{1:1} and 3DP_{2:1} recorded maximum negative forces of -0.054N and -0.04N respectively therefore indicating that 3DP_{1:1} and 3DP_{2:1} had similar cohesiveness. Sandhu and Singh (2007) reported that hardness can be impacted by the structure of the polymer in the substance tested. The 3DP_{2:1} was harder than 3DP_{1:1} exhibiting a higher value for maximum positive force of 0.122N while maximum positive force for 3DP_{1:1} was 0.12N. 3DP_{2:1} contained a higher concentration of the macromolecular HA-PQ10 (Siyawamwaya *et al.*, 2016). Springiness was directly proportional to the length of time taken to return to the original force (0N) after deformation. 3DP_{2:1} produced a tailing curve which took the longest to return to zero (>20s) and this was suggestive of superior springiness compared to 3DP_{1:2} and 3DP_{1:1}. 3DP_{2:1} exhibited the largest springiness due to an increase in concentration of the macromolecular polymers (Mua and Jackson 1998).

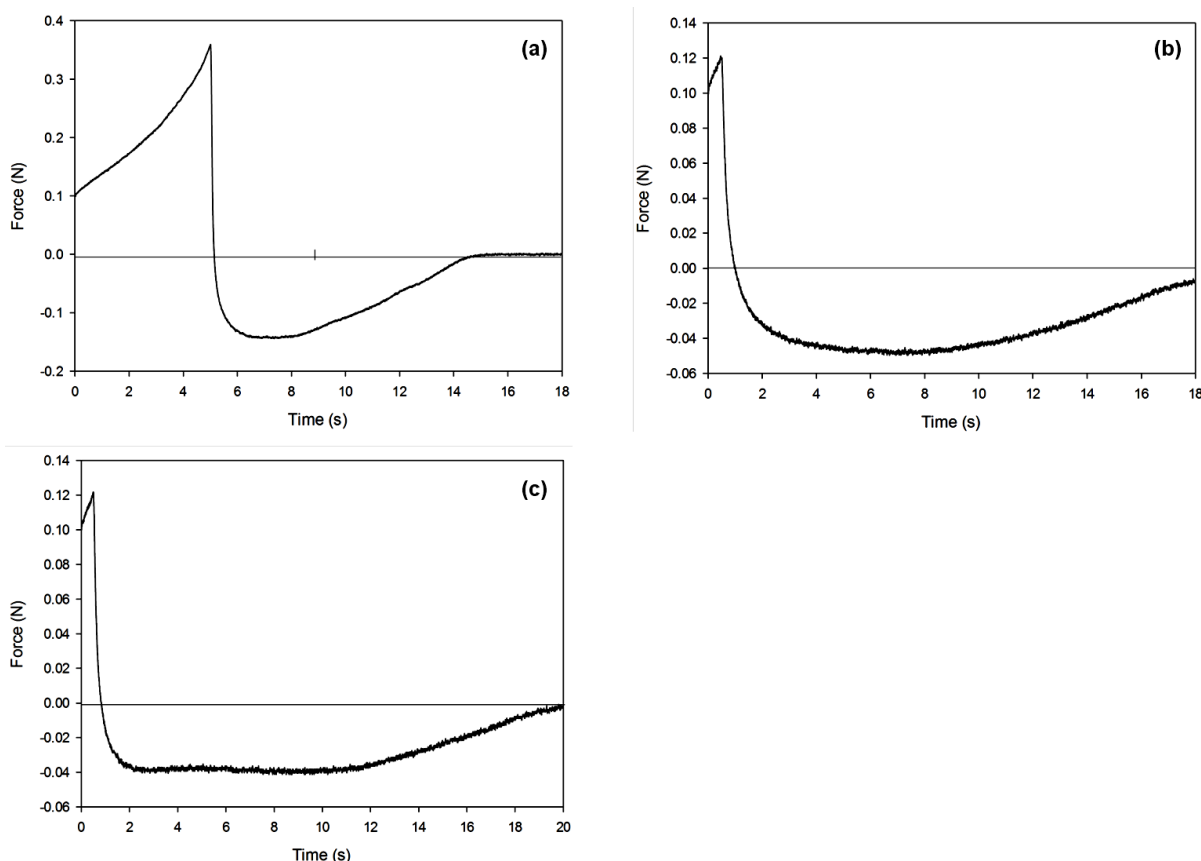


Figure 5.4: Graphs depicting one-deformation tests of sludges (a) 3DP_{1:2}, (b) 3DP_{1:1} and (c) 3DP_{2:1}

5.3.2. Analysis of the tablet manufacturing process and physicochemical characterization of 3DP and direct compression tablets

5.3.2.1. Determination of the tableting parameters for 3DP and direct compression

The preferred sludge for 3DP was determined to be 3DP_{1:1} after the assessment of FTIR, DSC and texture analysis results. 3DP_{1:1} contained equal proportions of HA-PQ10 and EFV. To maximize stability and uniformity throughout the 3DP process with this sludge, the printing speed and extrusion tuning option on Visual Machine® was employed (Figure 5.5). This function allowed for measurement of the strand widths at the respective extrusion pressure and printing speed. Optimal 3DP parameters (pressure=2bars and speed=25mm/s) were selected based on a strand width closer to the size of the injection nozzle as this was indicative of strands that would assemble a good solid object. The extrusion pressure and print speed were further validated in Visual Machine® by testing them at the ink purge station. Direct compression tablets were synthesized by compacting the dried sludge under 3 tonnes without additional excipients. The average tablet weights were 1085.7±2.81mg and 1571.5±3.7mg for 3DP and direct compression tablets respectively. The small variability in both tablets implies good reproducibility with either method of tableting.

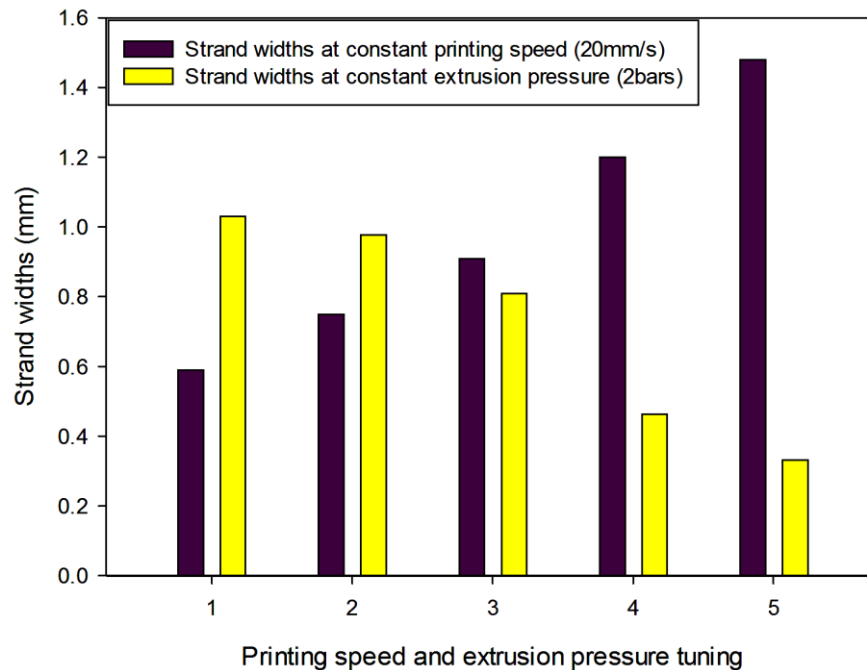


Figure 5.5: Printing speed and extrusion pressure tuning to detect strand width using a 0.61mm injection nozzle

5.3.2.2. Assessment of mechanical strength and (HA-PQ10)-EFV packing in 3DP and direct compression tablets

Assessment of the Brinell hardness test revealed that the direct compression tablets were significantly harder than the corresponding 3DP tablets. The calculated BHN numbers of 3DP tablet and direct compression tablet at the same ratio were 129.79N/mm² and 158.72N/mm² respectively. The measured tablet hardness is a reflection of the force exerted on the sludge or powder mass during tableting and the obtained values show that there was a greater force exerted onto the direct compression tablets than the 3DP tablets. Calculation of the tablet densities revealed that 3DP tablet was less dense (0.346g/cm³) compared to direct compression tablet (0.500g/cm³). The differences in BHN and tablet densities was due to the tableting technique used where axial forces were exerted on the powder for the direct compression tablet by the upper and lower dies of the tablet press. Powder compaction shifted intermolecular bonds (hydrogen and Van der Waals bonds) within the compressed (HA-PQ10)-EFV mass thus storing some energy within the tablet (Muley *et al.*, 2016). 3DP was subjected to restricted compression forces.

5.3.2.3. Assessment of porositometric analysis of the 3DP and direct compression tablets

This test provided a mechanistic understanding of the void spaces in the 3DP and direct compression tablets. 3DP tablets exhibited a higher surface area and pore volume than

direct compression tablets of the same composition (Table 5.2). The contrasting observations were due to the different intermolecular forces created within the internal tablet structure. Direct compression tablets were subjected to axial compression forces during synthesis and these were responsible for the significant reduction in the void spaces thus creating a continuous and dense (HA-PQ10)-EFV network (Andrews *et al.*, 2008 ;Westermarck *et al.*, 1998). This is congruent with the calculated density values in section 5.3.2.2. The degree of pores is expected to determine the extent of interaction of the matrix with the dissolution medium (Gonzalez *et al.*, 2013). It is worthwhile to note that correlation of pore surface and dissolution may not always be accurate due to the fact that porosity analysis relies on high pressure N₂ being forced into the pores of the sample whereas dissolution is dependent on tablet surface properties (Riippi *et al.*, 1998).

Table 5.2: Pore volume and BET surface areas of 3DP and direct compression formulations

	Parameter	3DP tablet	Direct compression tablet
Surface area	BET Surface Area	3.0141m ² /g	2.1084m ² /g
	Adsorption average pore width (4V/A by BET)	97.6188Å	51.0291Å
Pore volume	BJH Adsorption average pore diameter (4V/A):	125.343Å	85.614Å
	BJH Desorption average pore diameter (4V/A):	93.275Å	68.910Å

Assessment of the shapes of the isotherms revealed that the branches are mostly in a horizontal alignment and it can be deduced that all formulations exhibited type II isotherms characterized by H3 hysteresis loops. Figure 5.6 depicts the isotherms with the quantity of nitrogen adsorbed (cm³/g STP) plotted against relative pressure (P/P⁰). The increase in adsorption towards P/P⁰=1 is indicative of presence of pores in both tablets. Both tablets had an adsorption average pore width 2–50nm therefore this can be interpreted as that the formulations contained mesopores (Sing 1985). Mesoporous surfaces provide a large surface area to volume ratio that enhances wettability of the encapsulated drug. Such a surface is able to retain high drug doses in the pores for long periods thus they are beneficial in manufacturing controlled release formulations (Santos *et al.*, 2011).

Analysis of the microstructural images from SEM (Figure 5.6) revealed that the 3DP and direct compression tablets exhibited different surface features. The 3DP tablet had a smooth surface compared to direct compression tablet. 3D-Printing resulted in the formation of interconnected fibrils and pores (red circles) dispersed on the tablet surface. The features on

the direct compression tablet suggested that it had a more compact microstructure with a loose mesh of fibrils. These findings corroborated with the porositometric analysis which showed that 3DP was characterized by the presence of more numerous pores than the direct compression tablet.

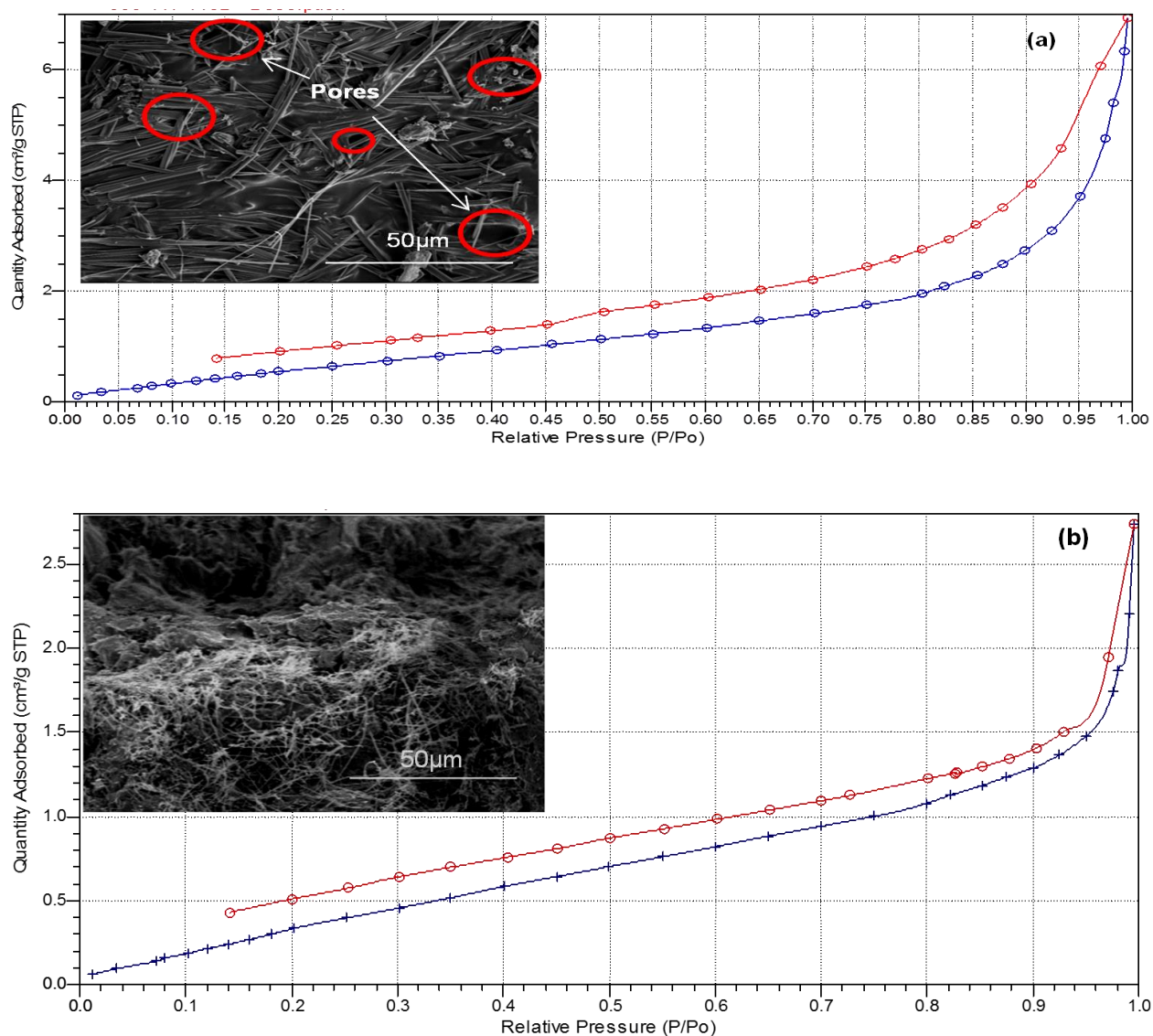


Figure 5.6: Isotherm linear plots of (a) 3DP_{1:1} tablet and (b) direct compression tablet depicting N₂ adsorption (blue) and desorption (red) with inserts of SEM micrographs of tablets at x2000 magnification

5.3.2.4. MRI mapping and gravimetric analysis of the 3DP and direct compression tablets

MRI was employed to map solvent mobility in 3DP and direct compression tablet. This approach highlighted the difference in hydration dynamics of the 3DP tablet with the direct compression tablet *in situ*. Fluid penetration into the matrix resulted in changes in the proton signal of the MRI which caused increase in tablet brightness (Shapiro *et al.*, 1996).

Observations similar to those made Kulinowski and co-workers (2011) were made where the uncompressed tablet (3DP tablet) swelled longitudinally and did not disintegrate in contrast to the compressed tablet (direct compression tablet) which formed voids as the study progressed.

Figure 5.7 shows that the 3DP tablet underwent gradual and homogenous hydration to form a hydrogel structure. The tablet swelled and maintained its dimensional integrity throughout the test period. With the progression of time, it formed a gel layer due to the absorption of SIF and consequent relaxation of the polymer network, thus allowing the release of EFV. Upon contact with SIF, the direct compression tablet was hydrated accompanied by tablet fragmentation which formed the free polymer layer. 3DP exhibited 3 phases of hydration kinetics characterized by the dry core, interface layer and gel layer. The direct compression tablet had an additional moiety, the free polymer chains layer (outermost layer), thus making it exhibit 4 phases of hydration kinetics. The dry core is the innermost part of the tablet with limited fluid mobility and this core was no longer visible after 2 hours in 3DP tablet and after 4 hours in the direct compression tablet.

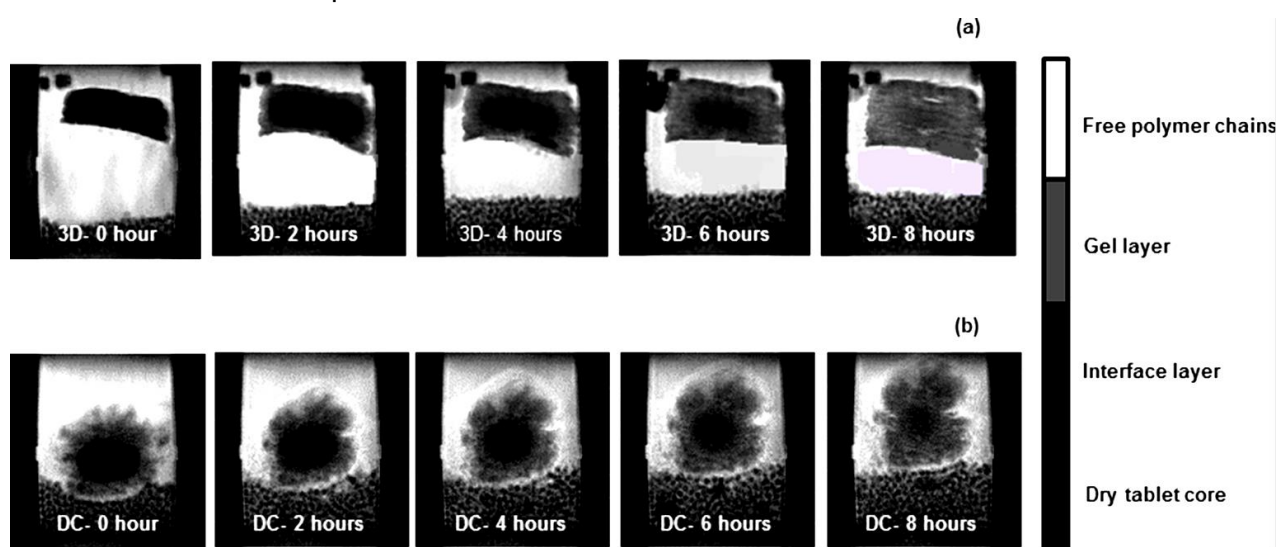


Figure 5.7: MRI coronal plane imaging of (a) 3DP tablet and (b) direct compression tablet in SIF over 8 hours

Although both tablets consisted of the same (HA-PQ10) : EFV compositions, striking differences were visualized between them with the 3DP tablet swelling, floating and remaining intact while the direct compression tablet also swelled to a limited extent but fragmented. Figure 5.8 shows differences in tablets before and after MRI was conducted. The 3DP tablet showed significant increase in size after the study thus confirming its swellability in SIF.

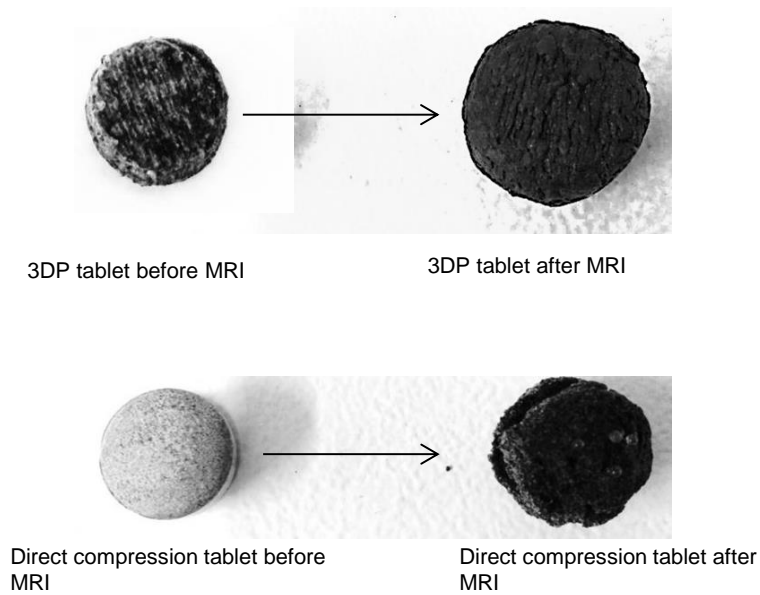


Figure 5.8: Digital images of the dry 3DP and direct compression tablets before MRI and the hydrated tablets after MRI analysis

Equations 5.3 was employed to calculate the total equilibrium swelling front as well as the dry mass loss at a particular time (t) and at the onset of the experiment (0) (Ali *et al.*, 2017).

$$Water\ content(\%)(t) = \frac{wet\ mass(t) - dry\ mass(t)}{wet\ mass(t)} \times 100$$

Equation 5.3

Gravimetric analysis in SIF revealed that SIF permeated into both 3DP and direct compression matrices leading to $57.7 \pm 0.15\%$ and $44.8 \pm 0.89\%$ fluid absorption respectively. Visual analysis of the medium in which this analysis was conducted (Figure 5.9), revealed that direct compression tablet lost fragments of the tablet during the study, something which was not observed with the 3DP tablet.

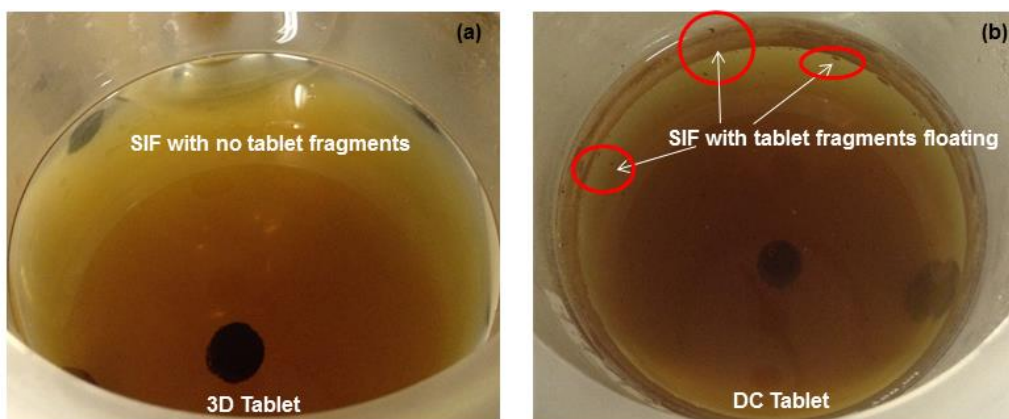


Figure 5.9: Gravimetric analysis of (a) 3DP and (b) direct compression tablets in SIF

5.3.2.5. *In vitro* drug release profiles

The rate of EFV release from the 3DP tablet was slightly higher than that of the direct compression tablet likely due to the rapid fluid ingress which caused loosening of the matrix (Figure 5.10). Hydrophilic polymers are known to retard drug release through formation of viscous gel barriers around the tablet (Ali *et al.*, 2017). EFV release was reduced by the CAP gel layer that formed at the tablet-dissolution fluid interface in SIF. Both 3DP and compressed tablets were expected to swell due to the presence of the enteric-responsive CAP which is known to swell upon exposure to SIF (Asghar and Mantha, 2008). Swelling was more significant in the 3DP tablet which served to impede drug release. The method of manufacture influenced the tablet formed, based on the pressure or compression applied (Moritz and Łaniecki, 2012). 3DP utilized pressure to force the sludge out of the sample holder with complete drying of the tablet to constant weight occurring over a 12 hour period. According to a study conducted by Markl and co-workers (2016) the particles are not distorted before interparticular interactions occur as is the case in direct compression of tablets, therefore drug release profiles for direct compression tablets cannot be expected to be similar to the 3DP tablets consisting of the same components.

The drug release profiles obtained in this study are inconsistent with the findings reported by Crowley and co-workers (2003) who showed that tablets from direct compression had a faster drug release than tablets that underwent extrusion during manufacture. (HA-PQ10)-EFV hydrogen bond interactions that occurred in the sludge as discovered in FTIR in section 5.3.1.1. From the MRI mapping analysis (section 5.3.2.4) and the presence of more pores, as shown in porositometric analysis (5.3.2.3), one would expect an immediate and faster release compared to that exhibited by the direct compression tablets. The HA-PQ10 electrostatic bonds would be expected to undergo hydrolysis leading to cleavage (Windheuser *et al.*, 1963). However, in this case the matrix was a PEC (HA-PQ10) which

behaved as an EFV reservoir, as expected, and that resulted in a robust 3D-Printed tablet slowly releasing the encapsulated drug as demonstrated by the release profiles (Siyawamwaya *et al.*, 2016). The DSC results in section 5.3.1.2 show that increasing HA-PQ10 amounts in the sludges resulted in enhanced (HA-PQ10)-EFV miscibility thus promoting the conversion of the crystalline EFV to the more soluble amorphous state. In order to control and extend the release of the encapsulated drug, the presence of both amorphous and crystalline forms of the drug in one formulation is beneficial (Al-Hamidi *et al.*, 2010). Furthermore, the large volume of pores in 3DP facilitated higher dissolution. Mixing and partial solubilization of EFV in methanol during the sludge synthesis contributed to solubility enhancement (Savjani *et al.*, 2012).

Exploring different shapes has proven to be one approach to tailoring drug release profiles. By modifying the structural patterns or strand widths printed, the porosity of the tablet may be changed and this may consequently be used to customize the drug release profiles (Goole and Amighi, 2016). A 3D-Bioplotter® offers the flexibility of using either a low (0-70°C) or high (30-250°C) temperature printing head. This allows for one tool to be employed in the manufacture of diverse formulations consisting of a wide range of materials.

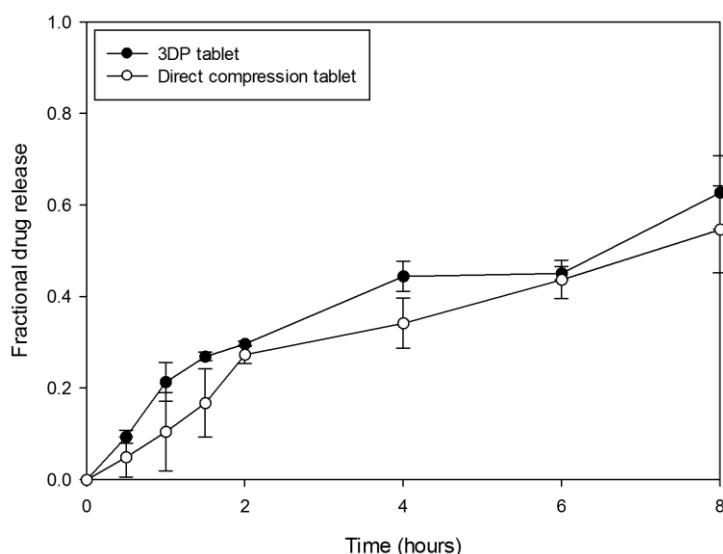


Figure 5.10: Drug release profiles of 3DP tablet and direct compression tablet in 900mL SIF at 37°C over 8 hours

Based on the findings in this study, the differences between 3DP and direct compression tablets are attributed to the arrangement of particles during tableting as illustrated in Figure 5.11. 3DP was undertaken on a wet sludge and drying occurred gradually over 12 hours after the tablet was synthesized. On the other hand, direct compression was carried out on the dried powder mass of the sludge. The two processes also apply pressure differently during the tableting process. 3DP utilized extrusion of the sludge while shaping it into the

predetermined cylindrical shape. With direct compression, the distortion observed with tablet hydration was caused by loose packing of the compressed material at the lateral surface of the tablet. Direct compression of solid materials is expected to result in the development of a lower perpendicular force in the die compared to the force applied on the material (Klose *et al.*, 2006). Keleb and co-workers (2001) reported that during cold extrusion process, solid bridges form between tablet particles as they dry and these are responsible for the higher porosity in extruded tablets than direct compression tablets. Since the direct compression tablet exhibited a higher BHN, the intermolecular forces created by compaction are more numerous than the solid bridges that formed in the 3DP tablet. These findings can be correlated with the porosity data that confirmed that the 3DP tablet had a larger number of pores than the direct compression tablet.

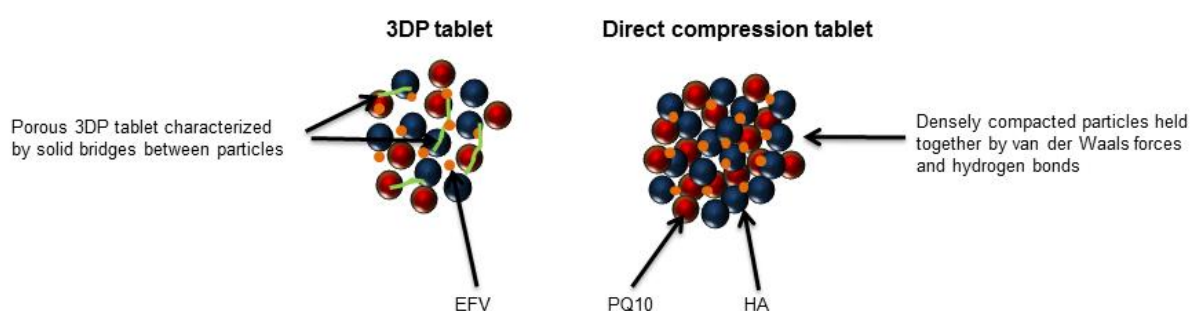


Figure 5.11: Proposed EFV-polymer particle arrangement in 3DP tablet and direct compression tablet

5.4. CONCLUDING REMARKS

The optimal sludge, 3DP_{1:1}, was selected based on its ease of printing and polymer-EFV interactions and miscibility noted in the FTIR and DSC findings. FTIR results revealed that there were (HA-PQ10)-EFV hydrogen bond interactions with 3DP_{1:1} and this makes it more attractive for enhancing drug solubility. Although both 3DP and direct compression are physical tableting methods, remarkable differences were seen in the manufactured tablets. Direct compression tableting method was responsible for the formation of denser and therefore more mechanically resilient tablets. The (HA-PQ10)-EFV mixture was subjected to particulate interactions during compaction and this contributed to the increase in tablet strength. The compaction force impacts on the strength of tablets synthesized. The 3DP tablet swelled more and released more EFV during drug release compared to the direct compression tablet. The implementation of 3DP offers flexibility in the design of formulations which is not restricted to the structure of moulds as is the case in conventional tableting. HA-PQ10 PEC has proved to be a flexible composite material with potential for the controlled oral delivery of drugs.

5.5. REFERENCES

- Alhnan, M.A., Okwuosa, T.C., Sadia, M., Wan, K.W., Ahmed, W., Arafat, B., 2016. Emergence of 3D printed dosage forms: opportunities and challenges. *Pharmaceutical Research*, 33(8), 1817-32.
- Ali, R., Dashevsky, A., Bodmeier, R., 2017. Poly vinyl acetate and ammonio methacrylate copolymer as unconventional polymer blends increase the mechanical robustness of HPMC matrix tablets. *International Journal of Pharmaceutics*, 516(1), 3-8.
- Al-Hamidi, H., Edwards, A.A., Mohammad, M.A., Nokhodchi, A., 2010. To enhance dissolution rate of poorly water-soluble drugs: glucosamine hydrochloride as a potential carrier in solid dispersion formulations. *Colloids Surfaces B*, 76(1), 170-8.
- Alhijaj, M., Yassin, S., Reading, M., Zeitler, J.A., Belton, P., Qi, S., 2016. Characterization of heterogeneity and spatial distribution of phases in complex solid dispersions by thermal analysis by structural characterization and X-ray micro computed tomography. *Pharmaceutical Research*, 1-9.
- Alves, L.D., Soares, M.F., de Albuquerque, C.T., da Silva, É.R., Vieira, A.C., Fontes, D.A., Figueirêdo, C.B., Sobrinho, J.L., Neto, P.J., 2014. Solid dispersion of efavirenz in PVP K-30 by conventional solvent and kneading methods. *Carbohydrate Polymers*, 104, 166-74.
- Andrews, G.P., Jones, D.S., Diak, O.A., McCoy, C.P., Watts, A.B., McGinity, J.W., 2008. The manufacture and characterisation of hot-melt extruded enteric tablets. *European Journal of Pharmaceutics and Biopharmaceutics*, 69(1), 264-73.
- Asghar, L.F., Mantha, N., 2008. Design and evaluation of ethyl cellulose based matrix tablets of ibuprofen with pH modulated release kinetics. *Indian Journal of Pharmaceutical Sciences*, 70(5), 596.
- Busignies, V., Leclerc, B., Porion, P., Evesque, P., Couarraze, G., Tchoreloff, P., 2006. Quantitative measurements of localized density variations in cylindrical tablets using X-ray microtomography. *European Journal of Pharmaceutics and Biopharmaceutics*, 64(1), 38-50.
- Chowdary, K.P.R., Ramya, K., 2013. RECENT RESEARCH ON CO-PROCESSED EXCIPIENTS FOR DIRECT COMPRESSION-A REVIEW. *Pharmacie Globale*, 4(2), 1-4.
- Crowley, M.M., Schroeder, B., Fredersdorf, A., Obara, S., Talarico, M., Kucera, S., McGinity, J.W., 2004. Physicochemical properties and mechanism of drug release from ethyl cellulose matrix tablets prepared by direct compression and hot-melt extrusion. *International Journal of Pharmaceutics*, 269(2), 509-22.

- Davies, P.N., Worthington, H.E., Podczeczek, F., Newton, J.M., 2007. The determination of the mechanical strength of tablets of different shapes. *European Journal of Pharmaceutics and Biopharmaceutics*, 67(1), 268-76.
- Fule, R., Amin, P., 2014. Hot melt extruded amorphous solid dispersion of posaconazole with improved bioavailability: investigating drug-polymer miscibility with advanced characterisation. *BioMed Research International*, 2014. <http://dx.doi.org/10.1155/2014/146781>
- Gaurav, A., Ashamol, A., Deepthi, M.V., Sailaja, R.R., 2012. Biodegradable nanocomposites of cellulose acetate phthalate and chitosan reinforced with functionalized nanoclay: mechanical, thermal, and biodegradability studies. *Journal of Applied Polymer Science*, 125(S1).
- Gonzalez, G., Sagarzazu, A., Zoltan, T., 2013. Influence of microstructure in drug release behavior of silica nanocapsules. *Journal of Drug Delivery*, 2013.
- Goole, J., Amighi, K., 2016. 3D printing in pharmaceutics: a new tool for designing customized drug delivery systems. *International Journal of Pharmaceutics*, 499, 376-94.
- Goyanes, A., Wang, J., Buanz, A., Martínez-Pacheco, R., Telford, R., Gaisford, S. and Basit, A.W., 2015. 3D printing of medicines: engineering novel oral devices with unique design and drug release characteristics. *Molecular Pharmaceutics*, 12(11), 4077-84.
- Hanif, M., Harris, M.H., Rabia, I.Y., Nadeem, M., Liaqat, H., 2014. Formulation development of intermediate release Nimesulide tablets by CCRD for IVIVC studies. *Pakistan Journal of Pharmaceutical Sciences*, 27(4), 785-92.
- Juban, A., Briançon, S. and Puel, F., 2016. Processing-induced-transformations (PITs) during direct compression: Impact of tablet composition and compression load on phase transition of caffeine. *International Journal of Pharmaceutics*, 501(1), 253-64.
- Keleb, E.I., Vermeire, A., Vervaet, C., Remon, J.P., 2001. Cold extrusion as a continuous single-step granulation and tableting process. *European Journal of Pharmaceutics and Biopharmaceutics*, 52(3), 359-68.
- Klose, D., Siepman, F., Elkharraz, K., Krenzlin, S., Siepman, J., 2006. How porosity and size affect the drug release mechanisms from PLGA-based microparticles. *International Journal of Pharmaceutics*, 314(2), 198-206.
- Kulinowski, P., Dorożyński, P., Młynarczyk, A., Węglarz, W.P., 2011. Magnetic resonance imaging and image analysis for assessment of HPMC matrix tablets structural evolution in USP apparatus 4. *Pharmaceutical Research*, 28(5), 1065-73.
- Markl, D., Zeitler, J.A., 2017. A Review of Disintegration Mechanisms and Measurement Techniques. *Pharmaceutical Research*, 1-28.

- Moritz, M., Łaniecki, M., 2012. Application of SBA-15 mesoporous material as the carrier for drug formulation systems. Papaverine hydrochloride adsorption and release study. *Powder Technology*, 230, 106-11.
- Mua, J.P., Jackson, D.S., 1998. Retrogradation and gel textural attributes of corn starch amylose and amylopectin fractions. *Journal of Cereal Science*, 27(2), 157-66.
- Muley, S., Nandgude, T., Poddar, S., 2016. Extrusion–spheronization a promising pelletization technique: In-depth review. *Asian Journal of Pharmaceutical Sciences*, 11(6), 684-99.
- Pfister, A., Landers, R., Laib, A., Hübner, U., Schmelzeisen, R., Mülhaupt, R., 2004. Biofunctional rapid prototyping for tissue-engineering applications: 3D biplotting versus 3D printing. *Journal of Polymer Science Part A: Polymer Chemistry*, 42(3), 624-38.
- Riippi, M., Yliruusi, J., Niskanen, T., Kiesvaara, J., 1998. Dependence between dissolution rate and porosity of compressed erythromycin acistrate tablets. *European Journal of Pharmaceutics and Biopharmaceutics*, 46(2), 169-75.
- Rojas, J., Ciro, Y., Correa, L., 2014. Functionality of chitin as a direct compression excipient: An acetaminophen comparative study. *Carbohydrate Polymers*, 103, 134-9.
- Sandhu, K.S., Singh, N., 2007. Some properties of corn starches II: Physicochemical, gelatinization, retrogradation, pasting and gel textural properties. *Food Chemistry*, 101(4), 1499-507.
- Santos, H.A., Salonen, J., Bimbo, L.M., Lehto, V.P., Peltonen, L., Hirvonen, J., 2011. Mesoporous materials as controlled drug delivery formulations. *Journal of Drug Delivery Science and Technology*, 21(2), 139-55.
- Sathigari, S.K., Radhakrishnan, V.K., Davis, V.A., Parsons, D.L., Babu, R.J., 2012. Amorphous-state characterization of efavirenz—polymer hot-melt extrusion systems for dissolution enhancement. *Journal of Pharmaceutical Sciences*, 101(9), 3456-64.
- Savjani, K.T., Gajjar, A.K., Savjani, J.K., 2012. Drug solubility: importance and enhancement techniques. *ISRN Pharmaceutics*, 5, 2012.
- Shapiro, M., Jarema, M.A., Gravina, S., 1996. Magnetic resonance imaging of an oral gastrointestinal-therapeutic-system (GITS) tablet. *Journal of Controlled Release*, 38(2-3), 123-7.
- Sing, K.S., 1985. Reporting physisorption data for gas/solid systems with special reference to the determination of surface area and porosity (Recommendations 1984). *Pure and Applied Chemistry*. 57(4), 603-19.
- Siyawamwaya, M., Choonara, Y.E., Kumar, P., Kondiah, P.P., du Toit, L.C., Pillay, V., 2016. A humic acid-polyquaternium-10 stoichiometric self-assembled fibrilla

polyelectrolyte complex: Effect of pH on synthesis, characterization, and drug release. *International Journal of Polymeric Material and Polymeric Biomaterials*, 65(11), 550-60.

- Tai, A., Bianchini, R., Jachowicz, J., 2014. Texture analysis of cosmetic/pharmaceutical raw materials and formulations. *International Journal of Cosmetic Science*, 36(4), 291-304.
- Westermarck, S., Juppo, A.M., Kervinen, L., Yliruusi, J., 1998. Pore structure and surface area of mannitol powder, granules and tablets determined with mercury porosimetry and nitrogen adsorption. *European Journal of Pharmaceutics and Biopharmaceutics*, 46(1), 61-8.
- Windheuser, J.J., Misra, J., Eriksen, S.P., Higuchi, T., 1963. Physics of tablet compression XIII. Development of die-wall pressure during compression of various materials. *Journal of Pharmaceutical Sciences*, 52(8), 767-72.
- Yildiz, Ö., Yurt, B., Baştürk, A., Toker, Ö.S., Yılmaz, M.T., Karaman, S., Dağlıoğlu, O., 2013. Pasting properties, texture profile and stress–relaxation behavior of wheat starch/dietary fiber systems. *Food Research International*, 53(1), 278-90.

CHAPTER 6

FORMULATION AND EVALUATION OF AN ANTI-HIV 3D-PRINTED 'CONTROLLED RELEASE TRITHERAPEUTIC TABLET'

6.1. INTRODUCTION

The major recurrent challenge faced with the enteral administration of drugs falling in the Biopharmaceutics Classification System (BCS) class I and class III is that they behave like liquid formulations *in vivo*. They rapidly dissolve at a faster rate than the gastric emptying time (Tsume and Amidon, 2010). One of the solutions to the problem is to formulate controlled release preparations. This ensures that therapeutic levels in the body can be maintained while unpleasant side effects associated with the drugs are prevented. However, for BCS class III active pharmaceutical ingredients, poor intestinal tissue permeation further limits their optimal bioavailability.

This study focused on the design, characterization and evaluation of a novel 3D-Printed Fixed-Dose Combination (FDC) tablet comprising a humic acid-polyquaternium 10 complex (HA-PQ10) as the 'pharma-ink' to achieve controlled release of three drugs namely efavirenz (EFV), tenofovir disoproxil fumarate (TDF) and emtricitabine (FTC) as the model drug regimen. The previously reported unique 'printable' properties of HA and PQ10 inspired the use of this complex for designing the 3DP FDC tablet in this study (Siyawamwaya *et al.*, 2016, 2015). It is crucial to control the release of these highly hydrophilic drugs (TDF and FTC) to circumvent their dose dependent toxicity in the human body as well as to maximize their absorption into the systemic circulation. Additionally, they are associated with short half-lives therefore making frequent administration of the drugs imperative in order to maintain the required plasma drug levels. The aim was to prolong their release beyond immediate and intermediate drug release. TDF is a fumarate salt of the bisisopropoxycarbonyloxymethyl ester derivative of tenofovir which has been shown to be more effective than other tenofovir derivatives. FTC is used for the prevention of perinatal HIV-1 reverse transcriptase. Both TDF and FTC are nucleoside reverse transcriptase inhibitors (NRTIs). EFV falls under the non-nucleoside reverse transcriptase inhibitor (NNRTI) group for HIV-1 drugs (Ray *et al.*, 2016).

Therefore this study aimed to utilize a single-step 3DP as an alternative manufacturing technique to produce a controlled release FDC tablet using pre-blended and partially self-assembled HA and PQ10 as the polyelectrolyte framework to control the release of EFV,

TDF and FTC as the recommended first-line treatment drugs for HIV-1 (Lamorde *et al.*, 2012). These drugs are also listed within different classes of the Biopharmaceutics Classification System (BCS) (EFV=class II, TDF=class III and FTC=class I) and thus useful to test the feasibility of the 3DP tablet to control the release of hydrophilic and lipophilic drug molecules. *In vitro* dissolution performance of CRTT was measured against that of Atripla® (Merck, Sharp & Dohme Corp, Kenilworth, NJ, US), a prescription FDC tablet currently available on the market. This combination of drugs was first approved in 2006, after showing evidence of bioequivalence with the individual drug (Lamorde *et al.*, 2012). FDCs, in comparison to monotherapy, offer benefits of encouraging patient adherence to treatment. The HA-PQ10 PEC was utilized to formulate an oral FDC which circumvents some of the rate limiting steps to effective drug absorption.

6.2. MATERIALS AND METHODS

6.2.1. Materials

Brown humic acid sodium salt (HA), hydroxyethylcellulose ethoxylate, quaternized (PQ10 $M_w=656.1\text{g/mol}$) and cellulose acetate phthalate (CAP $M_w=2534.12\text{g/mol}$) were purchased from Sigma-Aldrich® Inc. (St. Louis, Mo, USA). Efavirenz (EFV) (Wenzhou Zhongtai Chemical Co., Ltd, Wenzhou, China), tenofovir disoproxil fumarate (TDF) (Changzhou Yongrui Chemical Research Institute Co., Ltd, Jiangsu, China) and emtricitabine (FTC) (Beijing Zhongshuo Pharmaceutical Technology Development Co., Ltd, Beijing, China) were the model drugs used. UPLC grade water was purified by Milli-Q® gradient water purification system (Millipore SAS, Molsheim, France). Analytical grade methanol and acetone were used as solvents for the sludge synthesis. 3DP of the sludge was undertaken using a 3D-Bioplotter® (EnvisionTEC GmbH, Gladbeck, Germany) equipped with polyethylene cartridges.

6.2.2. Synthesis of 3DP fixed dose combination tablet

The optimal shape of the tablet was determined by printing various tablet shapes and ascertaining the shape that yielded better prototyping. The tablet shapes explored included, cylindrical, donut-shape, elliptical, cuboid and a rectangular prism (rounded box). Computer-aided design of these shapes was undertaken using the Magics® software. Afterwards, two strategies of printing a single tablet containing the three actives, EFV, TDF and FTC were investigated. These included 3DP of the sludge with all the drugs mixed in their respective proportions and the second method involved 3DP of each individual drug in its own sludge, in layers. For the second method, the initial layers consisted of EFV, followed by FTC and the top most layers would consist of TDF. All the sludges comprised of optimal HA-PQ10 :

drug ratios yielding 50% drug loading as determined in Chapter 5 section 5.3.7. A 0.61mm injection nozzle was utilized for all formulations. Printing parameters had to be slightly adjusted from those previously determined in Chapter 5 section 5.3.1 to suit the sludge consistency.

6.2.3. Determination of electrostatic stability between formulation components

The test for electrostatic interaction was undertaken to measure the extent of electromagnetic radiation absorption and vibrations resulting from chemical bonds between the drug molecules EFV/TDF/FTC and HA-PQ10 during the 3DP process. Powdered samples of the formulation components were placed on a diamond crystal of an Attenuated Total Reflectance-Fourier Transform Infrared (ATR-FTIR) spectrophotometer equipped with a single reflection diamond MIRTGS detector (PerkinElmer® Spectrum 100 Series FT-IR Spectrometer PerkinElmerLtd., Beaconsfield, UK). Analysis was conducted over a wavenumber of 6000cm^{-1} - 450cm^{-1} .

6.2.4. Surface morphology characterization of 3DP tablet

The surface morphology of the tablets was characterized with the aid of scanning electron microscopy (SEM) (FEI Nova NanoLab™ 600 DualBeam FIB/SEM, Hillsboro, OR, USA). The samples were coated with 10nm of carbon followed by 5nm of gold-palladium coating prior to mounting them on a double-sided carbon tape. The parameters employed were 30kV at $30\mu\text{s}$. Scanning of the samples provided insight into the exact strand widths and pore sizes created employing a 0.61mm injection nozzle at 60° and 90° angle inner structure pattern when 3D bioplotting.

6.2.5. Prediction of tablet matrix strength in simulated gastric and intestinal fluid

CRTT tablets were mounted on the BioTester 5000 test system (CellScale Biomaterials Testing, Waterloo, Ontario) using the BioRake tines (1.3mm tine spacing). The tablets were first hydrated in simulated gastric fluid (SGF, pH=1.2) and simulated intestinal fluid (SIF, pH=6.8) for 30 minutes to facilitate the mounting onto the BioRakes. The test was conducted to predict any remarkable changes in the tensile modulus of CRTT *in vivo* (Yin *et al.*, 2015). Samples were tested while submerged in the respective fluid, SGF or SIF, at 37°C . Y-axis uniaxial stretching was conducted with the BioRakes $2500\mu\text{m}$ apart. A load cell of 5N was utilized taking into account gastric mechanical destructive forces (1.9N fed state) as well as the intestinal force of 1.2N (Ali *et al.*, 2017). The image tracking tool was used to quantify in-plane motions and to directly measure the resultant strains that took place during the test. Parameters used for the displacement test included applying a stretch magnitude of 40% for 20 seconds and repeating the cycles 3 times. The data collated was utilized to construct

stress-strain curves and the initial linear portion was used to determine the Young's modulus in both SGF and SIF (Sriamornsak *et al.*, 2007). Stress is the force exerted per unit area and strain is the deformation observed due to the stress.

6.2.6. Determination of drug loading and the *in vitro* dissolution of CRTT and the conventional tablet

Calibration curves were prepared by making serial dilutions of the standard solutions for EFV (0.67mg/mL), TDF (1mg/mL) and FTC (1mg/mL). Drug loading was determined by printing two tablet layers which were then crushed, placed in 50mL of SIF and left in the orbital shaker bath for 24 hours to ensure complete drug release. Drug quantification was carried out with the aid of the UV spectrophotometer (LAMBDA 25 UV/Vis spectrophotometer, PerkinElmer, MA, USA).

Dissolution studies were carried out in a USP 33 type II apparatus (Erweka DT 700, Erweka GmbH, Heusenstamm, Germany) which was operated at 50rpm and 37°C over the 24 hour test period. For the first 2 hours, the test was run in 500mL fed state simulated gastric fluid (FeSSGF), pH 1.2 and this was changed to 900mL fed state simulated intestinal fluid (SIF), pH 6.8 for the rest of the study. Preparation of FeSSIF comprised of dissolving NaOH (20.2g), glacial acetic acid (43.25g) and NaCl (59.37g) in deionized water (5L) and thereafter adjusting the pH to 5.0. Native FeSSIF (500mL) was used to dissolve sodium taurocholate (59.08g) and 59.08mL of lecithin dissolved in methylene chloride (100mg/mL) was added to the blank FeSSIF. The methylene chloride was eliminated from the emulsion by evaporation and the volume of the media was adjusted to 2L (Viral *et al.*, 2010). Middle stage simulated gastric fluid was prepared by mixing 500mL of ultra high temperature milk (UHT-milk) with 480mL of acetate buffer. The solution was adjusted to pH 5.0 before adding the acetate buffer to 1L (Jantratid *et al.*, 2008). Sample aliquots (5mL) were withdrawn at predetermined times and these were filtered then dried before reconstituting them with methanol. Drug release was measured with the aid of a UV spectrophotometer at the respective wavenumbers for each drug (EFV=247nm, TDF=262nm and FTC=281nm).

6.3. RESULTS AND DISCUSSION

6.3.1. Assessment of synthesis of the 3DP tablet

One of the aims of this study was to improve 3DP of the drug loaded HA-PQ10 from Chapter 5. Different pharmaceutical materials give different results with the selected shapes and it was imperative to determine the optimal tablet shape that was most ideal for the selected materials. It was concluded that the rectangular prism shape worked best with the drug-

loaded HA-PQ10. Figure 6.1 shows digital images of CRTT obtained from printing using the two different designs and containing the same dosages. Printing the three drugs in separate layers is advantageous in customizing the release patterns for each drug. However, in this study separating the drug layers increased the formulation size. 3DP of the sludge containing a blend of EFV/TDF/FTC yielded reproducible tablets. The printing of TDF-loaded HA-PQ10 sludge distorted the overall shape and appearance of the tablet (Figure 6.1). Sludge modifications such as adding more polymers would be required to enhance the 3D-Printability of TDF-loaded HA-PQ10. Ultimately, this would increase the size of the tablet thus negatively impacting on patient compliance (Jimmy and Jose, 2011).



Figure 6.1: Digital images of results from two design attempts implemented

The optimal CRTT design was the rectangular prism which was manufactured from the ink containing EFV, TDF and FTC. Printing parameters for the FDC were an extrusion pressure of 1.3bars, at a print speed of 37mm/s. The addition of TDF and FTC to the EFV-loaded HA-PQ10 had an additional plasticizing effect on the sludge therefore lowering the extrusion pressure to that determine in Chapter 5. Pre and post flow delays of 0.05s were implemented and the wait time between layers was 30s. The inner pattern comprised of a strand distance of 1.2mm and to further optimize the formulation, 60° and 90° angles between each layer were explored.

6.3.2. Analysis of any electrostatic interactions between the HA-PQ10 and the drugs

Analysis of FTIR spectra (Figure 6.2) revealed that there was no evident interaction between the drugs and HA-PQ10. Due to its predominance, EFV displayed some of its dominant peak in CRTT while TDF and FTC bands were masked. The peaks from EFV (exocyclic triple bond= 2278cm^{-1} , C=O cyclic bond= 1742cm^{-1} and tertiary amide= 1601cm^{-1}) expressed in CRTT did not shifted but their absorbances were diminished due to the presence of the other drugs and polymers in the system. The formation of the two new peaks in the wavenumber region of $3250\text{-}3300\text{cm}^{-1}$ in CRTT suggests that hydrogen bond formation occurred due to the NH bonds from the drugs interacting with the OH functional groups in HA-PQ10 as described in Chapter 5 section 5.3.1.1. This region contains NH bonds from EFV, TDF and

FTC as well as OH functional groups from TDF, FTC and HA-PQ10. The difference in peak absorbance between CRTT and the drugs is insignificant indicating that weak hydrogen interactions took place.

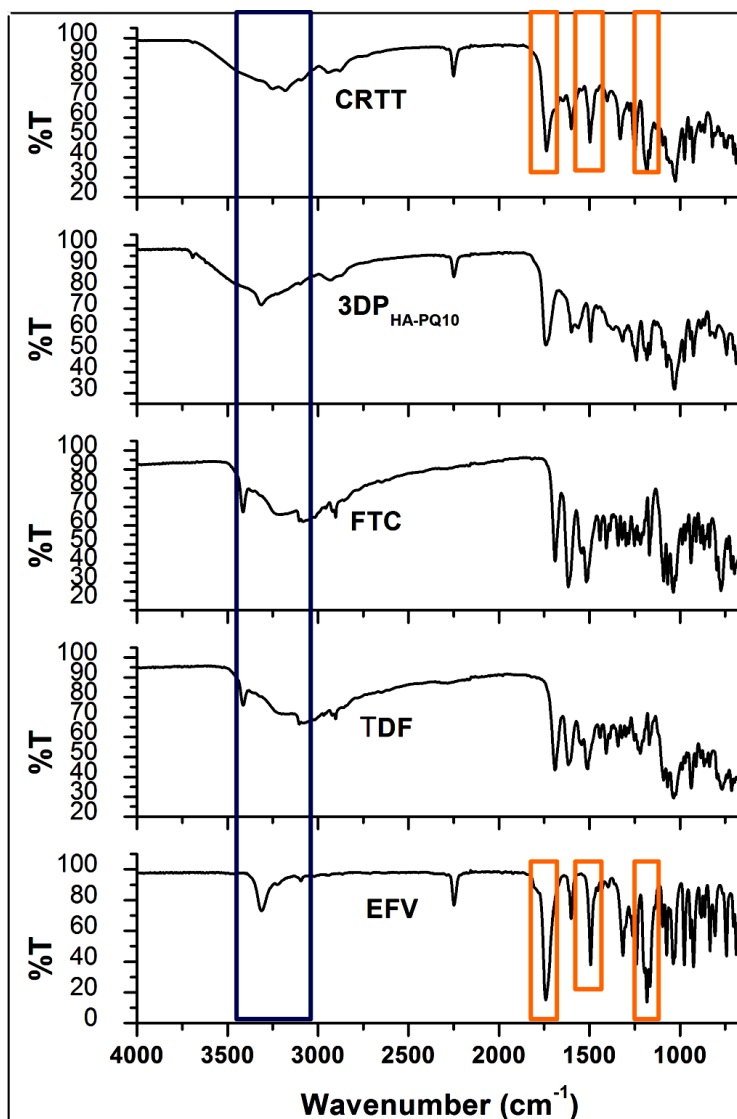


Figure 6.2: FTIR spectra of CRTT in relation to EFV, TDF, FTC and HA-PQ10

6.3.3. Analysis of CRTT surface morphology

SEM imagery provided insight into the exact strand widths and pore sizes created by 3DP with a 0.61mm injection nozzle creating 60° and 90° inner structure patterns (Figure 6.3). Surface morphology of the tablet at 100x magnification is depicted in Figure 6.3(a) and a closer analysis of the surface at higher magnification, 500x (Figure 6.3(b)), revealed that CRTT contained a fibrilla structure with pores spread on it. Such a surface would be expected to allow permeation of the dissolution fluid therefore increasing the wettability of the encapsulated drugs. Besides these smaller pores evident on the strands, the inner

patterns selected (90° and 60° with 1.2mm distance) also created pores through gaps between the strands. These patterns were intentionally chosen to increase the ingress of fluid into the system as confirmed by results from the drug release study. The final strand thickness and pores created after 3DP were measured from the SEM images. The CRTT with inner structure pattern of 90° (Figure 6.3(c)) gave better strand thickness (0.65mm) in relation to the nozzle size used (0.61mm). The 3DP tablet with the 60° inner pattern yielded thicker strands measured to be 0.88mm thick (Figure 6.3(d)). This indicated that smudging occurred during printing therefore the ideal inner structure pattern for drug-loaded HA-PQ10 was determined to be 90° between each tablet layer.

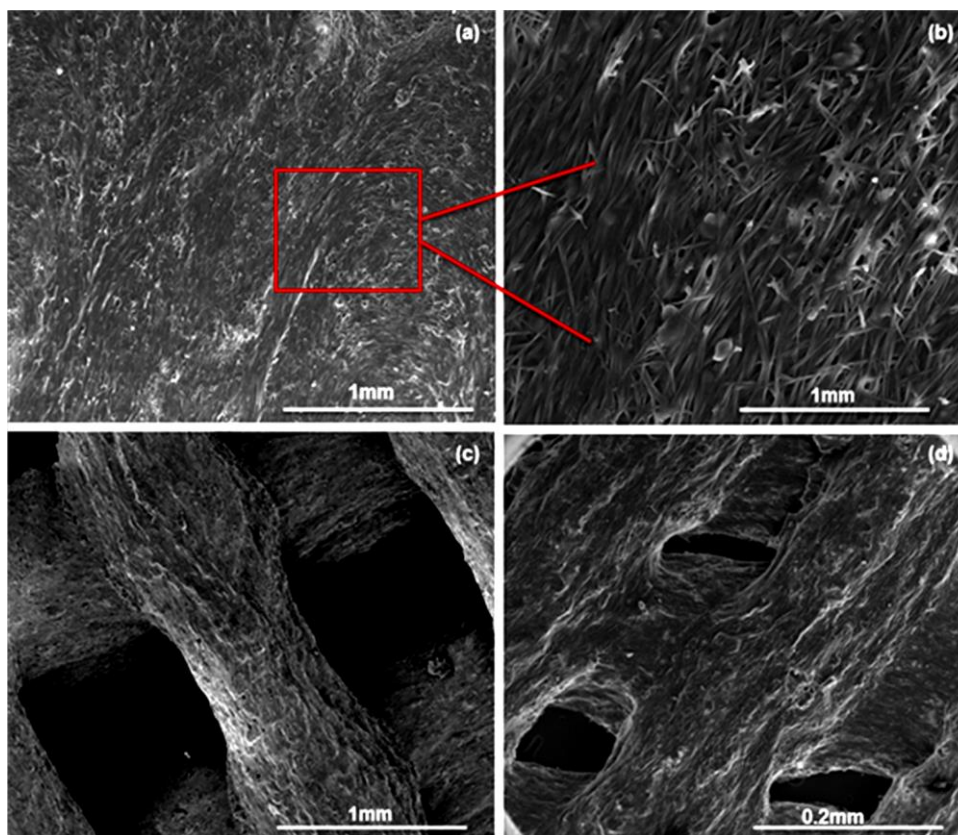


Figure 6.3: SEM images of CRTT at (a) surface of a strand at 80x magnification, (b) surface of a strand at 500x magnification, (c) inner pattern alignment of strands at 90° and (d) inner pattern alignment of strands at 60°

6.3.4. Evaluation of the CRTT matrix strength prediction in gastric and intestinal fluid

The image tracking option was implemented to calculate the exact values and spatial variation of the strains subjected to CRTT based on the motions of the BioRake tines. Figure 6.4 shows the digital images of CRTT set up in SGF and SIF with inserts of the image tracking as well as the Y-force graph. More strain was exerted towards the periphery of the tablet in both media (red areas). The higher strain values were demonstrated in SGF with

the highest strain of 52.8 recorded. CRTT exhibited more mechanical strength in SGF where it did not absorb the medium readily. This characteristic was expected since the FDC contains CAP which is insoluble in SGF. Once submerged in SIF, the tablet became 'softer' as evidenced by the lower strain values (maximum strain 21.3). CAP became solvated in SIF therefore allowing more matrix-fluid interaction. Tablets should resist mechanical stress in the GIT in order to prevent erratic tablet erosion. Assessment of mechanical strength was vital because it was a measure of CRTT's ability to withstand the mechanical forces likely to be exerted on it in the gastrointestinal tract (GIT). Formulation of tablets with good resistance maximizes the chance of obtaining more accurate *in vitro-in vivo* correlation. Solid dosage forms are liable to losing their tensile strengths when hydrated (Ali *et al.*, 2017). Despite the differences in behaviour of CRTT in SGF and SIF, the tablet maintained its tensile strength modulus and did not break during movement of the attached BioRakes.

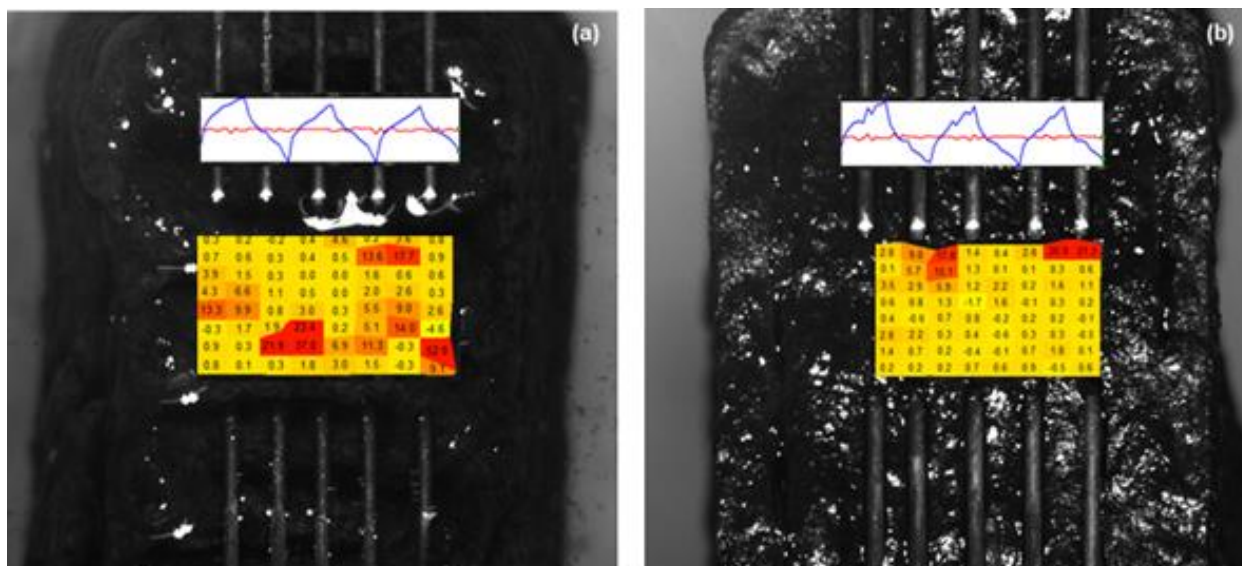


Figure 6.4: Digital Biotester images of CRTT, corresponding strains and Y-force graphs in (a) SGF and (b) SIF

Calculation of the Young's modulus revealed that CRTT was more elastic in SGF than SIF with values of 0.1167Pa (Figure 6.5) and 0.1129Pa (Figure 6.6) respectively. These values indicated that the nature of the tablet was amorphous overall as crystalline materials would have exhibited much higher Young's modulus values as studied by Eichhorn and Young (2001). It can be concluded that CRTT was more elastic in SIF as the pH was more favourable for fluid ingress into the tablet thus making the polymeric matrix more flexible. CRTT elasticity had an effect on the solubility of drugs as adequate fluid absorption into the system increases drug wettability (Sideridou *et al.*, 2003).

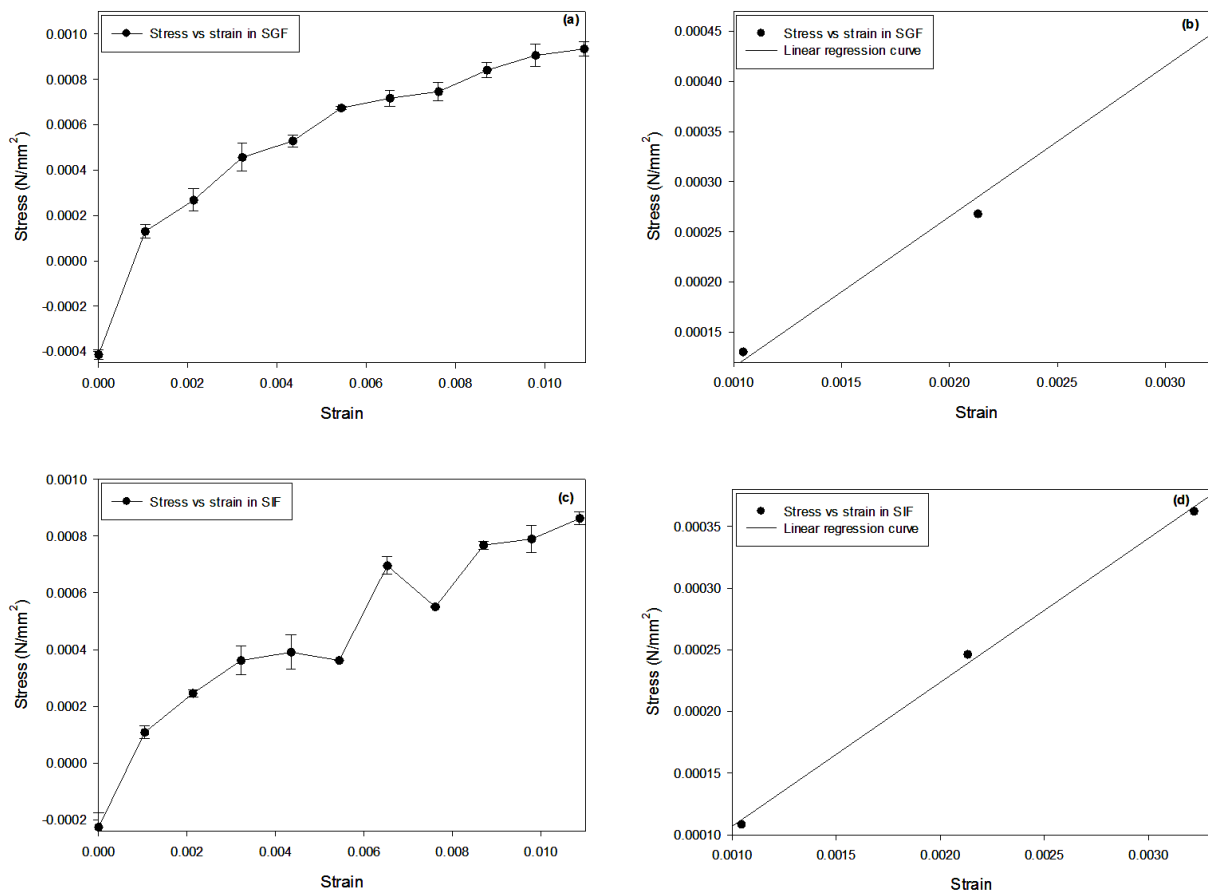


Figure 6.5: Stress-strain graphs of (a) CRTT submerged in SGF, (b) initial linear curve in SGF, (c) CRTT submerged in SIF and (d) initial linear curve in SIF

6.3.5. Analysis of drug loading and the *in vitro* drug release profiles of 3DP CRTT and the conventional tablet

The rectangular prism tablet dimensions were adjusted to accommodate the drug loading and the optimal size was found to be 2.3cmx0.8cmx1.2cm, constituting EFV/TDF/FTC at 300mg/150mg/100mg loading capacities. Drug loading in each layer was 12.5mg/6.3mg/4mg of EFV/TDF/FTC respectively. The calibration of EFV was repeated since the drug used was from a different to that previously used. Figure 6.7 shows the calibration curves used for the *in vitro* quantification of drugs in the study.

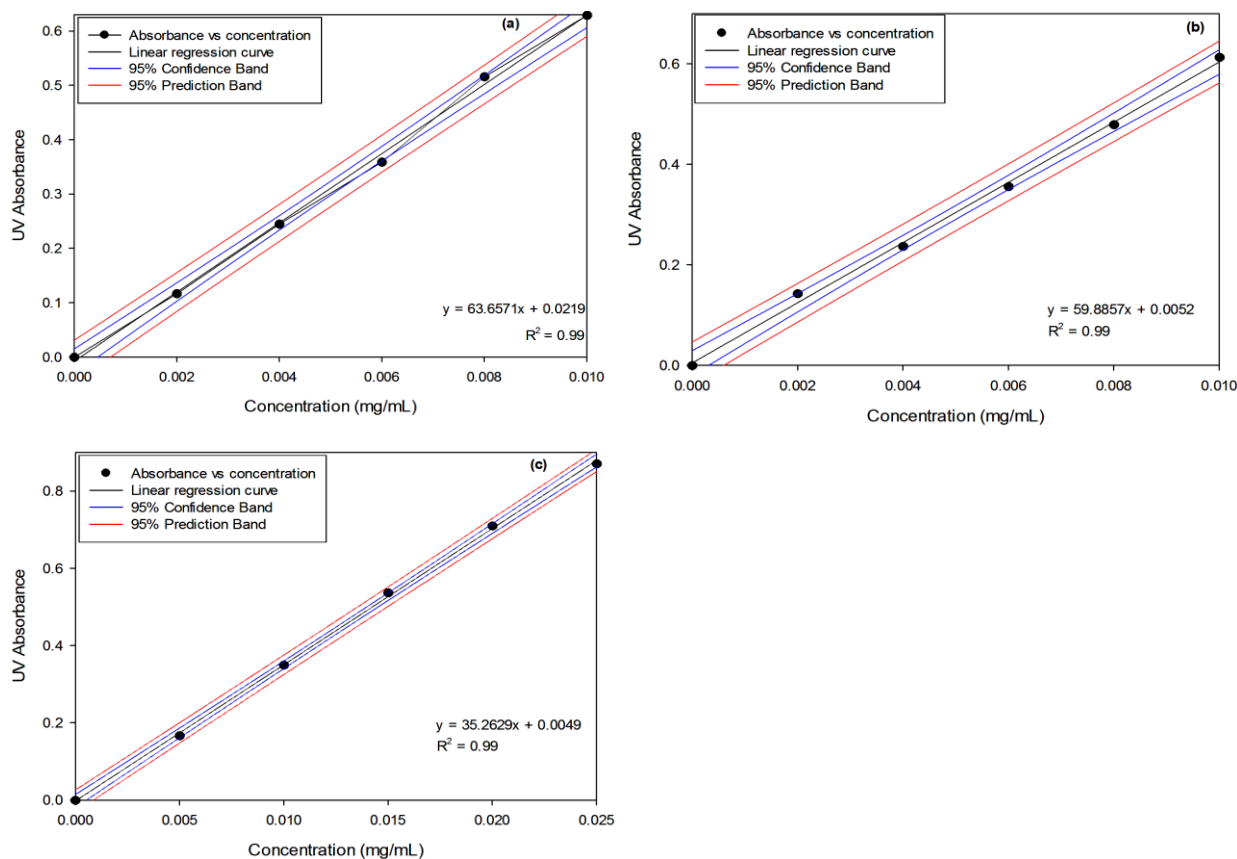


Figure 6.6: UV calibration curves of (a) EFV, (b) TDF and (c) FTC

The rate of release of TDF and FTC was proportional to the rate of hydration of the tablets (Figure 6.8). Release in SGF was almost insignificant due to the incorporation of CAP in the system which is insoluble in acidic media. The small amount of drug that dissolved was the amount that was on the tablet surface and not covered with the CAP since the tablet was not coated. Visual inspection of the media showed that the SGF had a slight tinge of yellow colour (due to HA) in SGF. The colour deepened to a more brown solution in SIF as a result of the permeation of more fluid into the tablet leading to dissolution of some of the polymers into the alkaline medium. Swelling of the complex into a hydrogel structure facilitated drug release by allowing the SIF to gain access to the entrapped drug (Harillal *et al.*, 2013).

Swelling occurs when the charge density in the drug-loaded PEC becomes low and the polyelectrolyte fails to maintain the complex. This process leads to subsequent dissolution, however in this study, the rate of release was retarded by the formation of a strong gel due to the macromolecular nature of polymers used (Buriuli and Verma, 2017; Sriamornsak *et al.*, 2007). The conventional tablet disintegrated within 30 minutes of being placed in SGF and this explains the high drug release within the duration of 2 hours. The sustained release exhibited by CRTT was attributed to the HA-PQ10 PEC which limited movement of the entrapped drugs into the dissolution medium. CAP served as a diffusion barrier to water

access into the matrix therefore restricting the bioactives within the tablet and slowly releasing them over time.

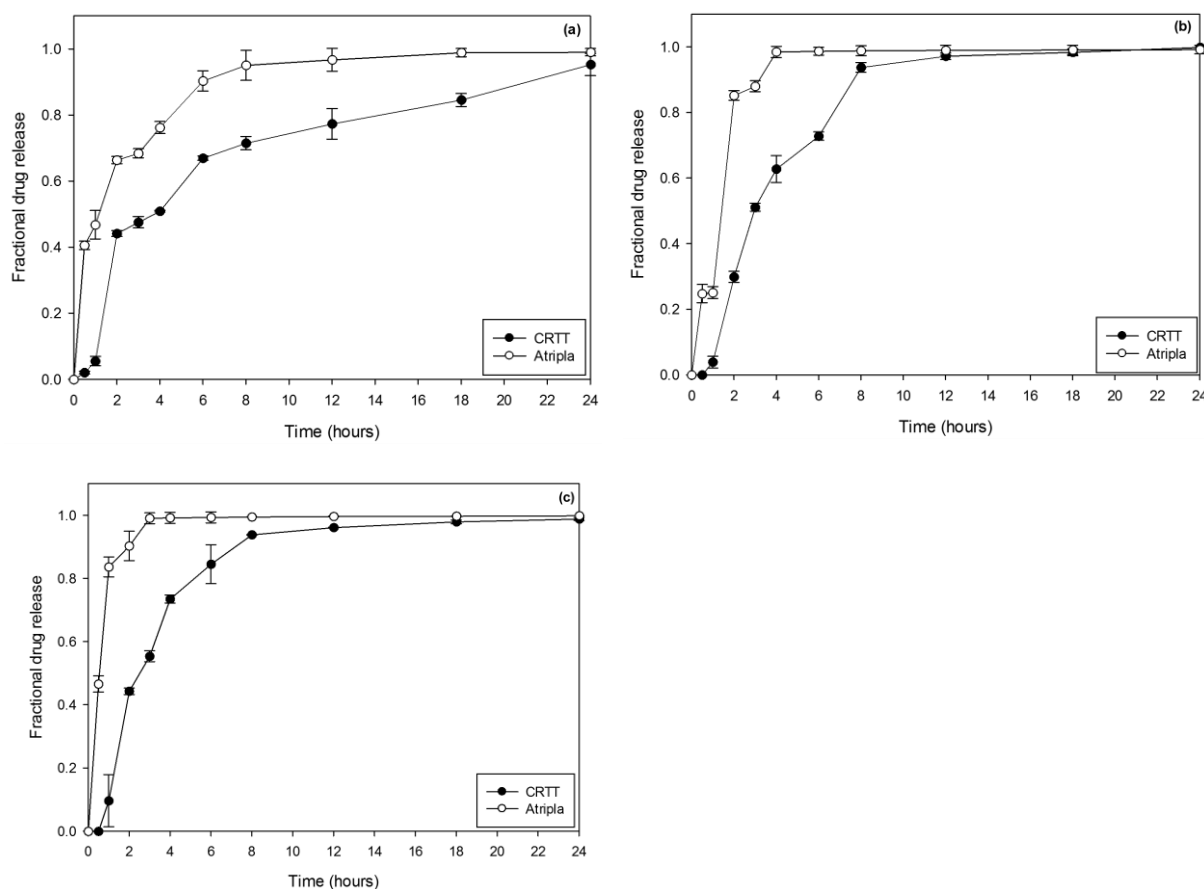


Figure 6.7: Drug release profiles of (a) EFV, (b) TDF and (c) FTC in CRTT compared to Atripla®

6.4. CONCLUDING REMARKS

The HA-PQ10 matrix is applicable for formulation of a 3DP FDC loaded with both lipophilic and hydrophilic drugs. Extrusion-based 3DP is a versatile tool that allows the control of object geometries to customize them for the 'printing ink' as well as for the intended purpose of the 3DP object. Optimization of CRTT involved printing different tablet shapes and exploring with inner structure patterns thus 3DP renders a lot of potential for the manufacture of novel drug delivery systems. Through SEM analysis, the exact size of the resultant printed strands could be measured and this further contributed to the tablet optimization process. This chapter also explored how CRTT would behave in simulated gastric and intestinal conditions by measuring the mechanical properties as well dissolution in the respective fluids. At this stage, it was pertinent to conduct *in vivo* studies of the system to verify the *in vitro* findings.

6.5. REFERENCES

- Ali, R., Dashevsky, A., Bodmeier, R., 2017. Poly vinyl acetate and ammonio methacrylate copolymer as unconventional polymer blends increase the mechanical robustness of HPMC matrix tablets. *International Journal of Pharmaceutics*, 516(1), 3-8.
- Buriuli, M., Verma, D., 2017. Polyelectrolyte Complexes (PECs) for Biomedical Applications. In *Advances in Biomaterials for Biomedical Applications*, Springer, Singapore 45-93.
- Eichhorn, S.J., Young, R.J., 2001. The Young's modulus of a microcrystalline cellulose. *Cellulose*, 8(3), 197-207.
- Harilall, S.L., Choonara, Y.E., Modi, G., Tomar, L.K., Tyagi, C., Kumar, P., du Toit, L.C., Iyuke, S.E., Danckwerts, M.P., Pillay, V., 2013. Design and pharmaceutical evaluation of a nano-enabled crosslinked multipolymeric scaffold for prolonged intracranial release of zidovudine. *Journal of Pharmacy and Pharmaceutical Sciences*, 16(3), 470-85.
- Jantratid, E., Janssen, N., Reppas, C., Dressman, J.B., Dissolution media simulating conditions in the proximal human gastrointestinal tract: an update. *Pharmaceutical Research*, 25(7), 1663.
- Jimmy, B., Jose, J., 2011. Patient medication adherence: measures in daily practice. *Oman Medical Journal*, 26(3), 155-9.
- Lamorde, M., Byakika-Kibwika, P., Tamale, W.S., Kiweewa, F., Ryan, M., Amara, A., Tjia, J., Back, D., Khoo, S., Boffito, M., Kityo, C., 2012. Effect of food on the steady-state pharmacokinetics of tenofovir and emtricitabine plus efavirenz in Ugandan adults. *AIDS Research and Treatment*, 2012: 105980.
- Ray, A.S., Fordyce, M.W., Hitchcock, M.J., 2016. Tenofovir alafenamide: a novel prodrug of tenofovir for the treatment of human immunodeficiency virus. *Antiviral Research*, 125, 63-70.
- Sideridou, I., Tserki, V., Papanastasiou, G., 2003. Study of water sorption, solubility and modulus of elasticity of light-cured dimethacrylate-based dental resins. *Biomaterials*, 24(4), 655-65.
- Siyawamwaya, M., Choonara, Y.E., Kumar, P., Kondiah, P.P.D., du Toit, L.C., Pillay, V., 2016. A humic acid-polyquaternium-10 stoichiometric self-assembled fibrilla polyelectrolyte complex: Effect of pH on synthesis, characterization, and drug release. *International Journal of Polymeric Material and Polymeric Biomaterials*, 65(11), 550-60.
- Sriamornsak, P., Thirawong, N., Weerapol, Y., Nunthanid, J., Sungthongjeen, S., 2007. Swelling and erosion of pectin matrix tablets and their impact on drug release behavior. *European Journal of Pharmaceutics and Biopharmaceutics*, 67(1), 211-9.

- Tsume, Y., Amidon, G.L., 2010. The biowaiver extension for BCS class III drugs: the effect of dissolution rate on the bioequivalence of BCS class III immediate-release drugs predicted by computer simulation. *Molecular Pharmaceutics*, 7(4), 1235-43.
- Viral, S., Dhiren, P., Mane, S., Umesh, U., 2010. Solubility and Dissolution Rate Enhancement of Licofelone by Using Modified Guar Gum. *International Journal of PharmTech Research*, 2, 1847-54.

CHAPTER 7

IN VIVO ANALYSIS OF THE 3D-PRINTED FIXED DOSE COMBINATION TABLET IN LARGE WHITE PIGS

The animal ethics clearance for this study was obtained from the Animal Ethics Screening Committee (AESC) at the University of the Witwatersrand, Johannesburg, South Africa (AESC clearance number: 2014/38/C).

7.1. INTRODUCTION

New drug delivery systems warrant the need to perform *in vivo* studies to assess their efficacy as well as to predict their pharmacokinetic and pharmacodynamic properties when used in human beings. *In vitro* studies are conducted under simulated *in vivo* conditions but more accurate results are obtained when systems are tested in living organisms. The bioavailability of drugs is affected by various factors including physicochemical, biological, food ingested and formulation factors (Yasuji *et al.*, 2012). *In vivo* toxicity as a result of anti-HIV therapy remains a major cause for concern and the toxicity has been found to be dose-dependent (Pinti *et al.*, 2006). This indicates the need to enhance the effectiveness and bioavailability of the anti-HIV drugs. Implementing effective, yet, convenient therapies such as the fixed dose combination (FDC) plan will boost the likelihood of patients adhering to the treatment and therefore leading to success of the treatment.

Pigs are cost-effective animal models in studies that require repeated blood sampling. Frequent sampling enables one to attain more in-depth quantifiable indications of drug release and absorption of drugs from the gastrointestinal tract (GIT) into the systemic circulation. The anatomy of the GIT in the selected pig model resembles that of the human being. Rabbits and rodents, though common animal models, are not ideal due to the size of oral dosage forms (Jensen-Waern *et al.*, 2009). Previous studies have validated the safety and biocompatibility of humic acid (HA) and polyquaternium-10 (PQ10) (Siyawamwaya *et al.*, 2016), it was still pertinent to further corroborate such findings with animal studies. This was done to establish the efficacy of the two polymers in a 3D-Printed FDC yielding a polyelectrolyte complex (PEC) loaded with known first line HIV drugs (efavirenz (EFV), tenofovir disoproxil fumarate (TDF) and emtricitabine (FTC)).

7.2. MATERIALS AND METHODS

7.2.1. Materials

Brown humic acid sodium salt (HA), hydroxyethylcellulose ethoxylate, quaternized (PQ10 $M_w \sim 656.1 \text{g/mol}$), cellulose acetate phthalate (CAP $M_w = 2534.12 \text{g/mol}$) and diclofenac sodium salt were purchased from Sigma-Aldrich® (St. Louis, USA). Efavirenz (EFV), tenofovir disoproxil fumarate (TDF) and emtricitabine (FTC) were purchased from DB Fine Chemicals/Specialities (Pty) Ltd (Woodmead, Johannesburg, South Africa). A comparator product, Atripla®, was commercially available. UPLC grade water was purified by Milli-Q® gradient water purification system (Millipore SAS, Molsheim, France). All other chemicals used were of analytical grade.

7.2.2. Habituation of pigs at the animal unit

Upon arrival at the Central Animal Services (CAS), University of the Witwatersrand, the six large female white pigs were housed in the farm animal unit where a 12 hour light/dark cycle was maintained. Initially, they were all kept in one pen while they adapted to a new environment, the researchers and standard procedures. Habituation was achieved by brushing and feeding them with raisins. After insertion of jugular catheters, they were housed in separate smooth walled pens for easier monitoring.

7.2.3. Experimental design and procedures on the white pigs

For easier withdrawal of blood as well to avoid pain in the pigs, catheters (7 French gauge double lumen 35cm catheter (CS-28702); Arrow Deutschland GmdH, Erding, Germany) were inserted into the jugular veins through a subcutaneous incision (Figure 7.1(a-d)). Catheterization was performed by the staff at CAS under aseptic conditions. The pigs were anaesthetized using ketamine (11mg/kg I.M), midazolam (0.3mg/kg I.M) and topical procaine HCl (0.5%). An antibiotic (Buprenorphine 0.05mg/kg I.M) and an analgesic (Carpofen 4mg/kg I.M) were also administered prior to surgery and anaesthesia was maintained by 2% isoflurane and 100% oxygen gas. The vital signs were monitored throughout the procedure. The external injection ports of the catheters were sutured to the skin to prevent disturbing the catheter when the pig moved (Figure 7.1(e)). Functioning of the catheter was tested by withdrawal of a blood sample followed by flushing of the brown external ports using heparinized saline (1000i.u/L 0.9% saline) (Figure 7.1(f)). The pigs were allowed 10 days of full recovery before commencement of dosing with the synthesized delivery system and conventional tablets (Jørgensen et al., 2010). Meanwhile, the ports were maintained by flushing twice daily during feeding time. An antiseptic solution was sprayed on both ports

before withdrawing blood using a needle and syringe. An equal amount of heparinized saline (5mL) was injected into the port to prevent any blockages from blood clots.

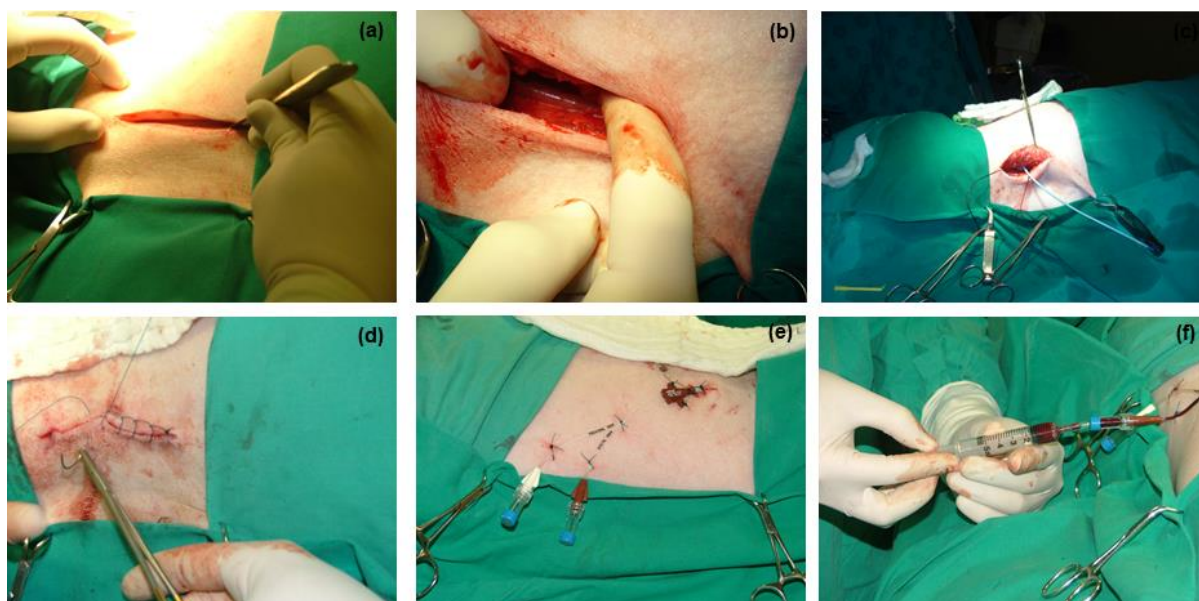


Figure 7.1: Digital images depicting the surgical procedure followed during catheterization

7.2.4. Administration of the 3DP CRTT and conventional via gastric gavage

Five pigs (± 45 kg) were dosed with either CRTT or Atripla® tablets during a crossover study where 1 week washout period was allowed between the dosage forms. A full standard dose of EFV/TDF/FTC (600mg/300mg/200mg respectively) was administered. Two CRTT tablets (EFV=300mg, TDF=150mg and FTC=100mg in each tablet) had to be administered to meet the daily dosage for an adult human. One pig was used as the control for each study. A baseline sample was withdrawn prior to gastric administration which was conducted while the pigs were fasting. The animals were sedated as explained in section 7.2.3 before the insertion of the intragastric tube through which the formulations were administered (Figure 7.2(a-c)). Water (50mL) was poured down the tube to ensure that the tablet was not stuck in the intragastric tube. The pigs were monitored in the housing unit during recovery after the gastric administration.

The same procedure for flushing described in section 7.2.3 was also used in blood sampling (Figure 7.2(d)). Blood sampling was conducted at: 0, 1, 2, 3, 4, 6, 8, 12, 18 and 24 hour intervals and food was used to distract the pigs while blood sampling was conducted. The collected blood samples were put into heparinized vacutainers (Improvacuter®, Guangzhou Improve Medical Instruments, Guangzhou, China), centrifuged at 3000rpm for 15 minutes

before aspirating the plasma supernatant which was then stored in a freezer (-80°C) for further analysis.



Figure 7.2: Digital images of gastric administration of CRTT and Atripia®

Figure 7.3 highlights the outline of the *in vivo* study.

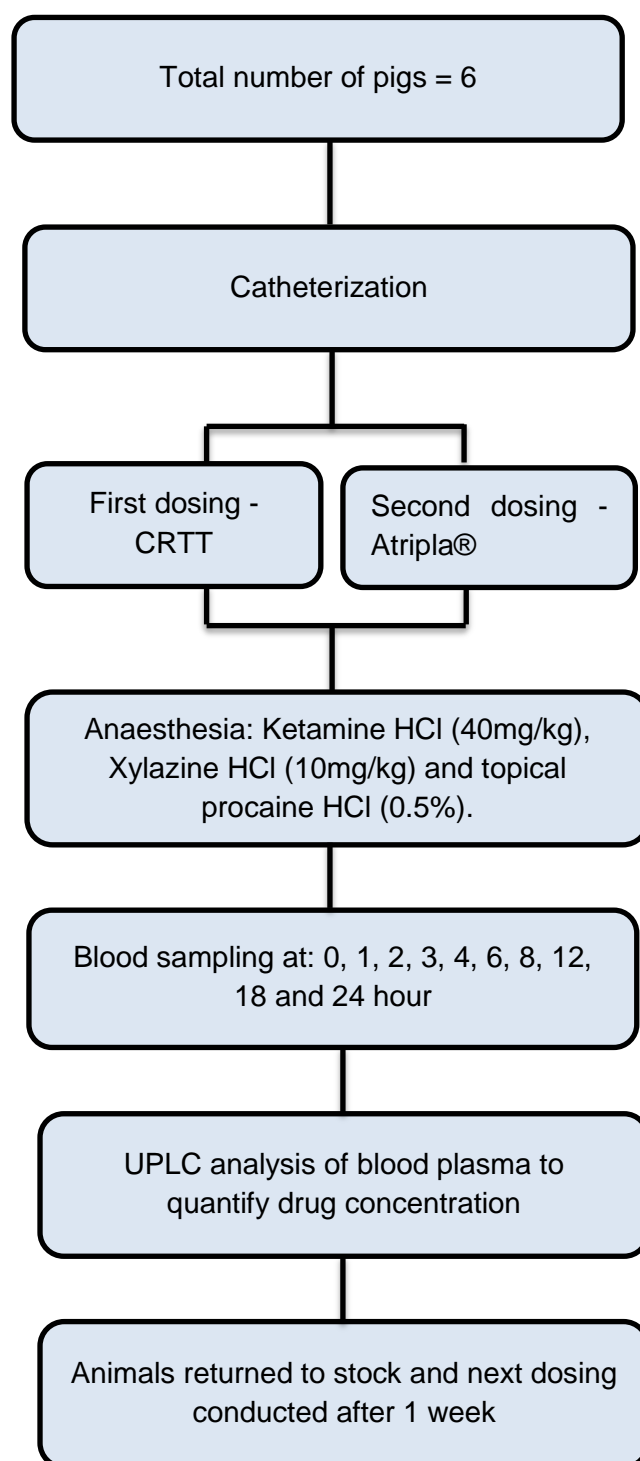


Figure 7.3: Flow diagram showing the outline of the *in vivo* study

7.2.5. Drug Quantification by Ultra Performance Liquid Chromatography Analysis

The collected blood samples were analyzed with the aid of an Ultra Performance Liquid Chromatography (UPLC). The Waters® Acquity™ UPLC system (Waters®, Milford, MA,

USA) contains a binary solvent manager, sample manager and is coupled with a photodiode array (PDA) detector. The output signal is monitored by Empower[®] Pro Software (Waters[®], Milford, MA, USA). The instrument was run using an Acquity[®] UPLC BEH shield RP18 (1.7 μ m; 2.1x100mm) analytical column. A modified method for quantifying EFV, TDF and FTC to that proposed by Induri and co-workers (2016) was employed.

7.2.6. Ultra Performance Liquid Chromatography Parameters

Optimized conditions involved utilizing gradient elution conditions (Table 7.1) at 0.4mL/min flow rate and room temperature. Mobile Phase A (MPA) consisted of orthophosphoric acid in deionized water (0.1%) while Mobile Phase B (MPB) was 100% HPLC grade acetonitrile. Ultraviolet (UV) detection of all drugs and the internal standard, diclofenac sodium (DS), was optimal at a wavelength of 257nm. All samples were filtered through a 0.2 μ m filter (GHP Acrodisc[®] 13mm Syringe Filters, Pall Corporation, New York, USA) prior to insertion into a 2mL ANSI48 vial. Injection volume was set at 10 μ L with a total run time of 3 minutes.

Table 7.1: Ultra Performance Liquid Chromatography gradient elution conditions

Elution time (min)	Flow rate (mL/min)	MPA (%)	MPB (%)
0.0	0.4	88	12
0.8	0.4	15	85
2.0	0.4	88	12
3.0	0.4	88	12

7.2.7. Preparation of Standard Calibration Curve and the Liquid-Liquid Extraction Process

Standard solutions in drug-free porcine blood plasma were prepared from the stock solution of EFV/TDF/FTC (30mg/15mg/10mg in 100mL diluent). The diluent comprised of 70% MPA and 30% MPB. The plasma (0.49mL) was spiked with the standard drug solution (0.01mL) as well DS (0.01mL of 0.03mg/mL) before mixing with the aid of a vortex for 2 minutes. EFV/TDF/FTC were extracted from the blood plasma prior sample injection by adding 0.5ml of hexane : ethyl acetate (1:1) to an equal volume of plasma (Avery 2010). This was centrifuged for 3 minutes at 3000rpm. The top layer was allowed to dry before reconstitution with methanol (0.5ml) and this was centrifuged for another 3 minutes. A standard curve was obtained by plotting area under the curve (AUC_{drug}/AUC_{DS}) against the specific concentration. The extraction method was validated by comparing the peak areas of a known drug concentration spiked in blank plasma (AUC_{plasma}) with the area of the same concentration of standard solution ($AUC_{standard}$). Equation 7.1 was employed for the percentage extraction calculation (Rezk *et al.*, 2005).

$$\% \text{ Extraction} = \frac{AUC_{\text{plasma}}}{AUC_{\text{standard}}} \times 100$$

Equation 7.1

The same procedure was followed for assessment of plasma drug concentration during the *in vivo* study.

7.2.8. Determination of the pharmacokinetic profiles of drugs and 3DP CRTT IVIVC

A Microsoft Excel add-in program written in Visual Basic for Applications (VBA), PKSolver, was employed to conduct pharmacokinetic analysis of the release profiles (Zhang *et al.*, 2010). Since the system under investigation was an oral one, compartmental analysis was undertaken and appropriate parameters obtained.

To further optimize the FDC, WinNonLin® software (V5.3 with IVIVC Toolkit Build 20091211139, Pharsight Software, Statistical Consultants Inc., Apex, NC, USA) was instituted to predict *in vitro-in vivo* correlation (IVIVC) of the *in vitro* and *in vivo* release data from all drugs. A Level A IVIVC is a mathematical model that establishes a point to point correlation of the *in vitro* dissolution and *in vivo* plasma drug concentration. IVIVC was determined by using the deconvolution and convolution processes. With deconvolution, the Wagner-Nelson (Wang and Nedelman, 2002) method is employed to detect an approximate amount of drug absorbed which together with the concentration of drug dissolved is used to develop the appropriate IVIVC model. The convolution method is then implemented to convolve the predicted amount of drug absorbed to the predicted plasma drug concentrations.

7.3. RESULTS AND DISCUSSION

7.3.1. Post-surgical and post-gavage evaluation of pigs

All pigs were monitored during recovery from anaesthesia which was administered for both the jugular catheter insertion as well as the gastric administration of the tablets. Administration of both CRTT and Atripla® resulted in good recovery and resumption of normal activities in the pigs. No major adverse effects were observed besides the pigs becoming lethargic at 4 hours after administration of Atripla® tablets. This lasted for about 1 hour after which they behaved normally. Blood sampling was successful without any sign of distress from the pigs.

7.3.2. *In vivo* drug release profiles of 3DP CRTT and Atripla®

EFV, TDF, FTC and the internal standard (DS) were eluted within 3 minutes and their retention times were 1.709min (EFV), 1.513min (TDF), 0.977min (FTC) and 2.513 min (DS)

(2.513 min) (Figure 7.4). Validation of the extraction process revealed that all the analytes had a percentage extraction above 80% (84.46% EFV, 93.79% TDF and 97% FTC). The use of methanol resulted in higher percentage extraction through the liquid-liquid extraction process compared to acetonitrile.

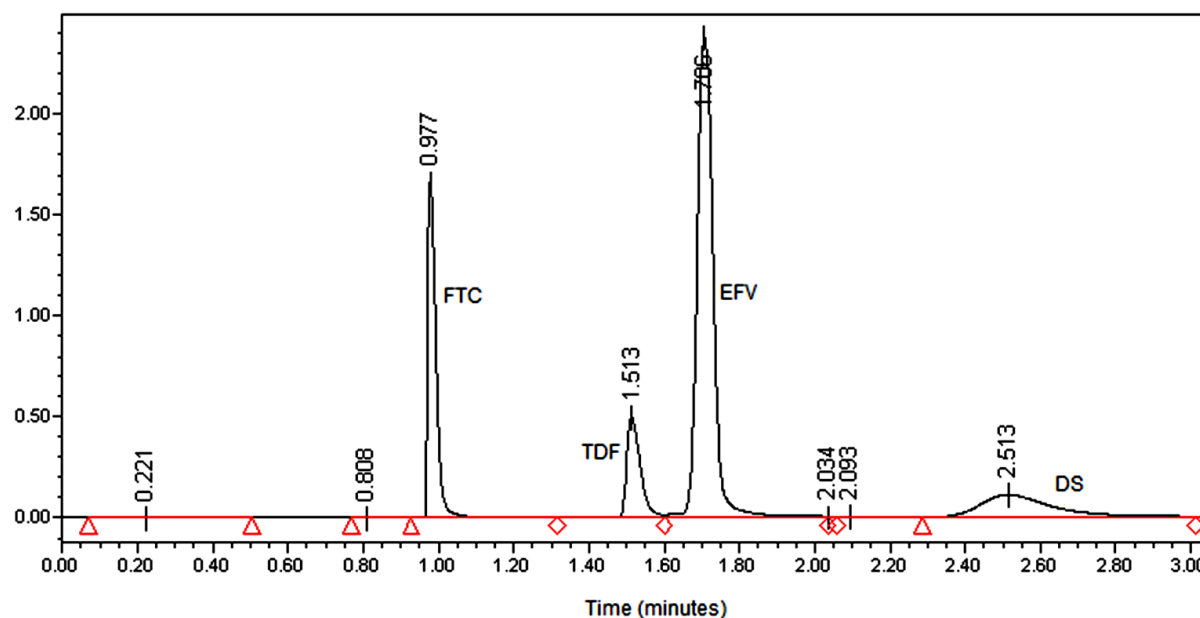


Figure 7.4: Representative chromatogram of stock solution showing the UPLC detection and selectivity of EFV, TDF, FTC and DS

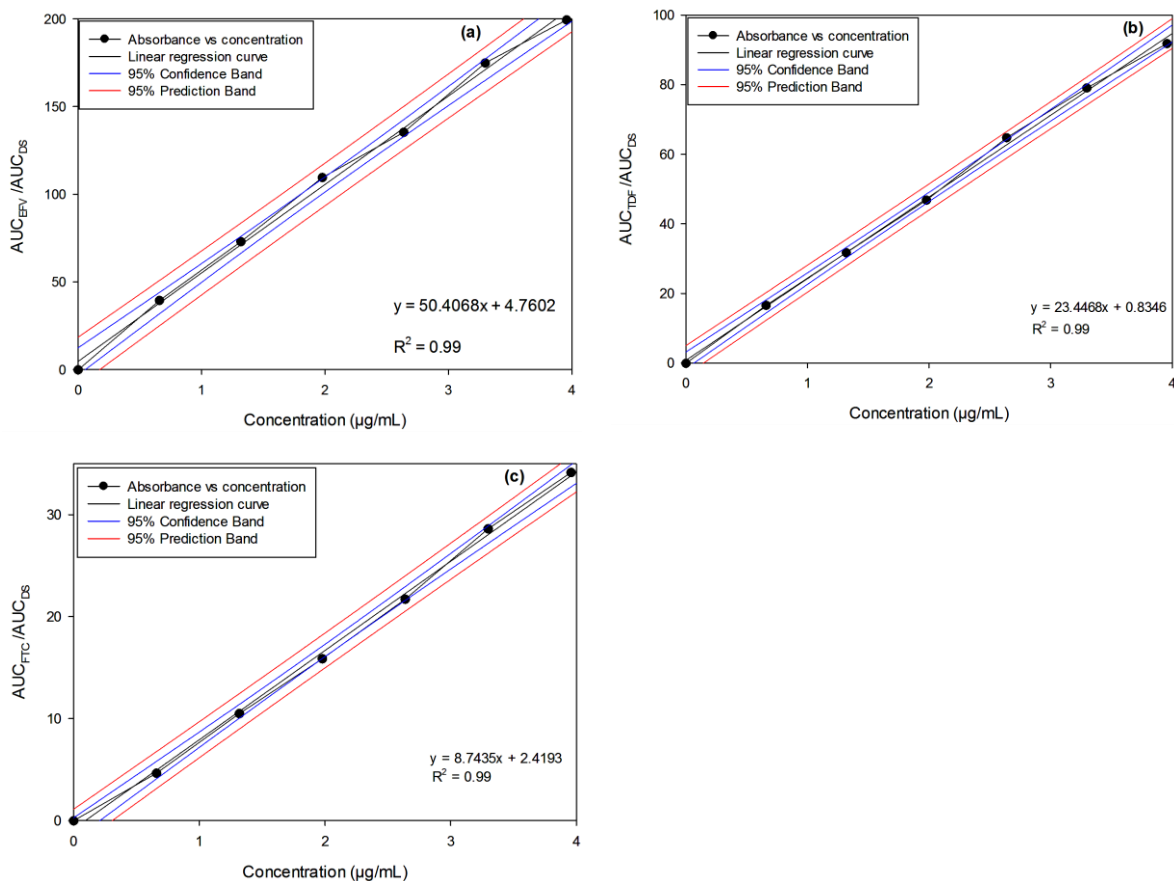


Figure 7.5: Calibration curves for (a) EFV, (a) TDF and (c) FTC

The plasma drug release profiles for CRTT and Atripla® are depicted in Figure 7.6. The maximum plasma drug concentrations (C_{max}) for all drugs were reached after 6 hours, in CRTT. The lethargy that exerted inaction in the pigs 4 hours after Atripla® administration was likely due to the faster release of EFV, TDF and FTC. The C_{max} recorded for EFV release from Atripla® exceeded the EFV C_{max} from CRTT. Slow release of EFV is beneficial given that the drug has a narrow therapeutic index and is associated with neuropsychiatric effects when plasma drug concentrations are increased. The therapeutic interval of EFV has been set at 1-4µg/mL (Ståhle *et al.*, 2004) and the EFV plasma levels from CRTT were sustained within this index from 4-24 hours. CRTT successfully increased the bioavailability of TDF and FTC both of which had higher C_{max} values than the same drugs in Atripla®. The CRTT release profiles suggested that drug release occurred mostly in the intestines regardless of the Biopharmaceutics Classification System (BCS) class of the drug.

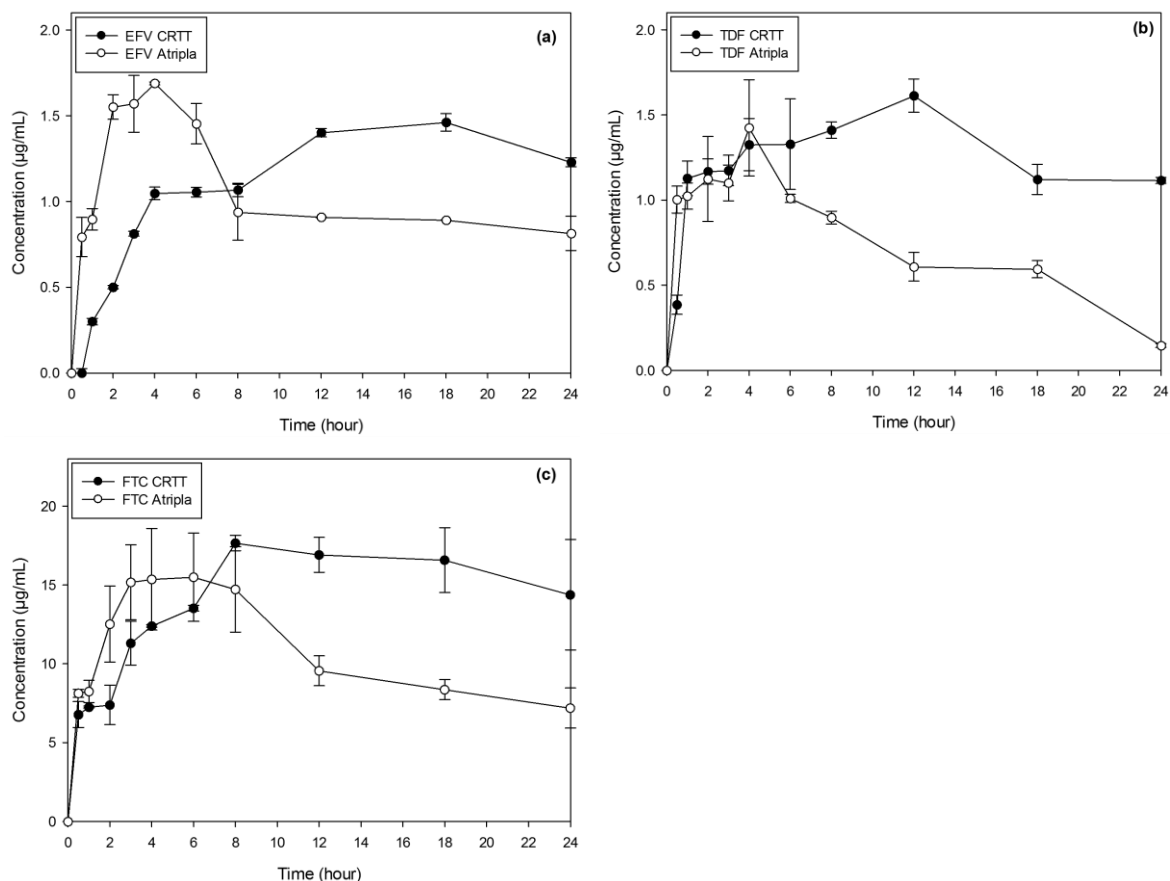


Figure 7.6: *In vivo* plasma drug concentrations for (a) EFV, (b) TDF and (c) FTC

7.3.3. Evaluation of *in vivo* pharmacokinetics of EFV, TDF and FTC and their IVIVC analysis

Modelling was conducted with the one compartmental algorithm with and without lag. Pharmacokinetics analysis revealed that release for EFV, TDF and FTC was best described by the one compartmental analysis with Tlag (Table 7.2, Table 7.3 and Table 7.4). This algorithm with the Tlag presented with the most favourable SE, SS, AIC and SC values for the optimized CRTT therefore providing a more accurate dose exposure-response relationship. The need for the absorption time lag emphasizes that the active pharmaceutical ingredients (APIs) are distributed in the systemic circulation after crossing the gastrointestinal barrier. For comparative purposes, one compartmental modelling with lag was also conducted for Atripla®.

Table 7.2: Efavirenz extravascular compartmental model with Tlag

Parameter	Units	Average value	
		CRTT	Atripla®
A	µg/mL	1.632	1.812
K _a	1/h	0.223	1.053
K ₁₀	1/h	0.009	0.043
Tlag	h	1x10 ⁻⁶	0.000216
t _{½ka}	h	3.112	0.658
t _{½k10}	h	74.071	15.953
V/F	(mg)/(µg/mL)	383.770	345.457
CL/F	(mg)/(µg/mL)/h	3.591	15.010
T _{max}	h	14.854	3.158
C _{max}	µg/mL	1.361	1.514
AUC _{0-t}	µg/mL*h	27.790	25.278
AUC _{0-inf}	µg/mL*h	167.072	39.973
AUMC	µg/mL*h ²	18603.613	957.920
MRT	h	111.351	23.964
Diagnostics			
R obs-pre		0.980	0.939
SS		0.0813	0.287
WSS		0.0813	0.287
R ²		0.992	0.980
WR ²		0.992	0.980
SE		0.116	0.202
AIC		-17.090	-5.748
SC		-15.880	-4.156

Table 7.3: Tenofovir disoproxil fumarate extravascular compartmental model with Tlag

Parameter	Units	Average value	
		CRTT	Atripla®
A	µg/mL	1.451	102.443
K _a	1/h	0.975	0.277
K ₁₀	1/h	0.009	0.267
Tlag	h	0.014	1x10 ⁻⁶
t _{½ka}	h	0.711	2.506
t _{½k10}	h	78.330	2.599
V/F	(mg)/(µg/mL)	417.241	81.441
CL/F	(mg)/(µg/mL)/h	3.692	21.719
T _{max}	h	4.879	3.682
C _{max}	µg/mL	1.377	1.380
AUC _{0-t}	µg/mL*h	29.891	13.659
AUC _{0-inf}	µg/mL*h	162.505	13.813
AUMC	µg/mL*h ²	18530.713	101.730
MRT	h	114.032	7.365
Diagnostics			
R obs-pre		0.945	0.883
SS		0.232	0.718
WSS		0.232	0.718
R ²		0.984	0.921
WR ²		0.984	0.921
SE		0.182	0.320
AIC		-8.094	4.350
SC		-6.502	5.941

Table 7.4: Emtricitabine extravascular compartmental model with Tlag

Parameter	Units	Average value	
		CRTT	Atripla®
A	µg/mL	18.471	19.978
K _a	1/h	0.347	0.722
K ₁₀	1/h	0.008	0.0472
Tlag	h	1x10 ⁻⁶	1x10 ⁻⁶
t _{½ka}	h	1.996	0.960
t _{½k10}	h	83.295	14.687
V/F	(mg)/(µg/mL)	11.094	10.712
CL/F	(mg)/(µg/mL)/h	0.092	0.505
T _{max}	h	11.009	4.041
C _{max}	µg/mL	16.450	15.430
AUC _{0-t}	µg/mL*h	348.658	259.273
AUC _{0-inf}	µg/mL*h	2166.431	395.649
AUMC	µg/mL*h ²	266578.470	8930.989
MRT	h	123.050	22.573
Diagnostics			
R obs-pre		0.959	0.970
SS		29.133	14.038
WSS		29.133	14.038
R ²		0.983	0.990
WR ²		0.983	0.990
SE		2.040	1.416
AIC		45.091	37.059
SC		46.682	38.651

A: the zero time intercept associated with the Alpha phase (an initial phase of rapid decrease in plasma concentration due distribution)

K_a: 1st order absorption rate constant

K₁₀: Elimination rate constant

Tlag: Finite time taken for a drug to appear in systemic circulation following extravascular administration

t_{½ka}: Absorption half-life rate constant

t_{½k10}: Elimination half-life rate constants

V/F: The volume of distribution of the absorbed fraction

CL/F: The observed total body clearance for extravascular administration

T_{max}: Time at which the maximum concentration (C_{max}) is observed

C_{max}: Maximum observed concentration occurring at T_{max}

AUC_{0-t}: Area Under the Curve (AUC) from the dosing time to the last measurable concentration

AUC_{0-inf}: AUC from dosing time extrapolated to infinity

AUMC: Area Under the Moment Curve

MRT: Mean Residence Time is the average amount of time the drug remains in a compartment or system

3DP CRTT can be deemed capable of extending drug release over a prolonged period of time as indicated by the elevated MRT values for all drugs (111.351 hours for EFV, 114.032 hours for TDF and 123.050 hours for FTC) and their respective lower elimination rate constants. Residence time values for Atripla® were 23.964 hours (EFV), 7.365 hours (TDF) and 22.573 hours (FTC). Consequently, there was a significant difference in the time taken to reach maximum plasma drug concentration (T_{max}) in CRTT than in the comparator product (EFV=11.696 hours, TDF=1.197 hours and FTC=6.968 hours). The T_{max} for EFV, TDF and FTC was higher in CRTT and these values were significantly higher than those recorded by Lamorde and co-workers (2012) for the same FDC. The CRTT maximum drug concentrations at T_{max} (C_{max}) were lower with the lipophilic drugs EFV and TDF and higher with FTC than for the same drugs in Atripla®. Overall, higher plasma drug concentrations were recorded for all drugs in CRTT than in Atripla® based on the AUC_{0-t} and AUC_{0-inf} values therefore implying superior therapeutic efficacy of CRTT. These results may be linked to the high swellability and solubility enhancing effects of CRTT with minimal tablet erosion.

7.3.4. Assessment of IVIVC of EFV, TDF and FTC in CRTT

Level A assessment of CRTT release profiles led to the development of a correlation between the *in vitro* and *in vivo* results. The results provided insight on the predictive accuracy of the *in vitro* drug release study employed. Deconvolution was achieved by using the Wagner Nelson method to calculate the concentration of the drugs absorbed using the linear trapezoidal rule (Figure 7.7). Although *in vitro* drug release studies were conducted in biologically relevant media, high shear rates in physiological conditions are responsible for more rapid tablet disintegration (Mudie *et al.*, 2010). These conditions cannot be accurately simulated during the *in vitro* dissolution. EFV and TDF reached maximum concentrations much later than was predicted from the *in vitro* studies. Both these APIs exhibit bioavailability limitations with EFV being poorly soluble (lipophilic) and TDF contains a diester derivative responsible for its lipophilicity, rendering it a poorly permeable drug. The lipophilicity of both EFV and TDF meant that these drugs were trapped in the hydrophobic core of amphiphilic HA of HA-PQ10 and this enhanced their dissolution and absorption across the intestinal membrane. Absorption of EFV and TDF was further improved when the pigs were fed leading to a higher amount of drug absorbed, compared to that recorded in the dissolution studies.

TDF and FTC are subject to intracellular phosphorylation and this largely determines absorption of the drugs. Phosphorylation would take place *in vivo* therefore both TDF and FTC showed markedly higher concentrations than the maximum reached *in vitro* (Lamorde *et al.*, 2012). The IVIVC results suggest that the *in vitro* test conducted resulted in a slower

initial drug release but reached the maximum concentration faster. After convolution, EFV release was best described using the correlation plot which yielded an 85.17% level of accuracy of correlation of the fraction of drug absorbed in relation to that released. TDF and FTC showed best correlation with the levy plot (percentage absorbed against percentage dissolution) with 87.32% and 96.96% accuracies respectively.

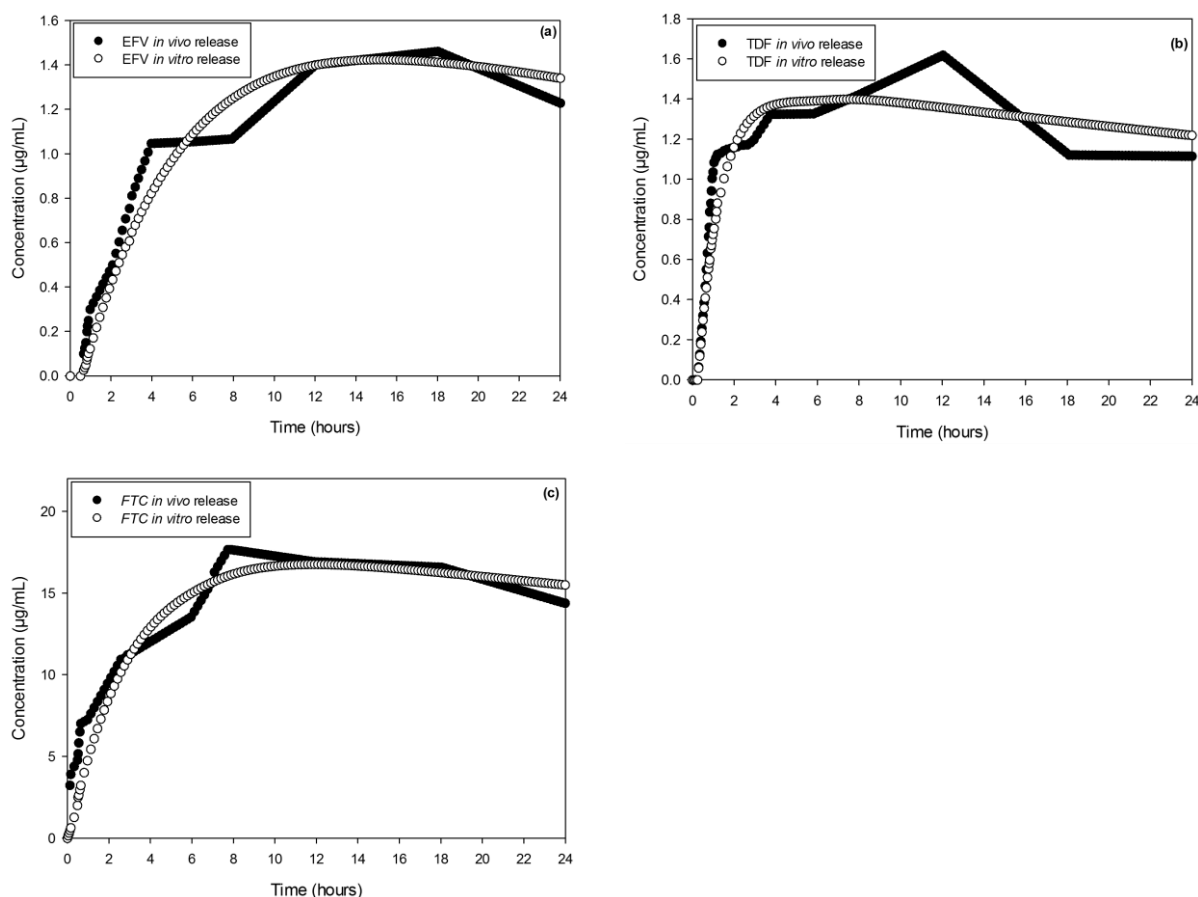


Figure 7.7: Predicted *in vitro* release profiles and mean observed *in vivo* CRTT drug release profiles of (a) EFV, (b) TDF and (c) FTC

7.4. CONCLUDING REMARKS

In vivo analysis of the drugs loaded in the 3DP FDC tablet confirmed successful controlled and targeted drug release mechanism from the delivery system. The system allowed for the delivery and simultaneous release of three drugs belonging to different BCS classes (EFV=class II, TDF=class III and FTC=class I). The maximum drug concentrations absorbed were superior in TDF and FTC compared to the release of the same drugs in Atripla®. Though EFV absorption from CRTT was lower, the release was sustained within the therapeutic index throughout the 24 hour test period. Administration of delivery systems capable of slowly releasing anti-HIV bioactives is commendable since it leads to the minimum side effects.

7.5. REFERENCES

- Induri, M., Mantripragada, B.R., Yejella, R.P., 2016. Development and validation of UPLC method for simultaneous estimation of Efavirenz and Lamivudine in pharmaceutical formulations. *Journal of Applied Pharmaceutical Science*, 6(03), 029-33.
- Jensen-Waern, M., Andersson, M., Kruse, R., Nilsson, B., Larsson, R., Korsgren, O., Essén-Gustavsson, B., 2009. Effects of streptozotocin-induced diabetes in domestic pigs with focus on the amino acid metabolism. *Laboratory Animals*, 43(3), 249-54.
- Jørgensen, H., Serena, A., Theil, P.K., Engberg, R.M., 2010. Surgical techniques for quantitative nutrient digestion and absorption studies in the pig. *Livestock Science*, 133(1), 57-60.
- Lamorde, M., Byakika-Kibwika, P., Tamale, W.S., Kiweewa, F., Ryan, M., Amara, A., Tjia, J., Back, D., Khoo, S., Boffito, M., Kityo, C., 2012. Effect of food on the steady-state pharmacokinetics of tenofovir and emtricitabine plus efavirenz in Ugandan adults. *AIDS Research and Treatment*.
- Mudie, D.M., Amidon, G.L., Amidon, G.E., 2010. Physiological parameters for oral delivery and in *vitro* testing. *Molecular Pharmaceutics*, 7(5), 1388-405.
- Pinti, M., Salomoni, P., Cossarizza, A., 2006. Anti-HIV drugs and the mitochondria. *Biochimica et Biophysica Acta (BBA)-Bioenergetics*, 1757(5), 700-7.
- Rezk, N.L., Crutchley, R.D., Kashuba, A.D., 2005. Simultaneous quantification of emtricitabine and tenofovir in human plasma using high-performance liquid chromatography after solid phase extraction. *Journal of Chromatography B*, 822(1), 201-8.
- Siyawanwaya, M., Choonara, Y.E., Kumar, P., Kondiah, P.P.D., du Toit, L.C., Pillay, V., 2016. A humic acid-polyquaternium-10 stoichiometric self-assembled fibrilla polyelectrolyte complex: Effect of pH on synthesis, characterization, and drug release. *International Journal of Polymeric Material and Polymeric Biomaterials*, 65(11), 550-60.
- Ståhle, L., Moberg, L., Svensson, J.O., Sönnernborg, A., 2004. Efavirenz plasma concentrations in HIV-infected patients: inter-and intraindividual variability and clinical effects. *Therapeutic Drug Monitoring*, 26(3), 267-70.
- Wang, Y., Nedelman, J., 2002. Bias in the Wagner-Nelson estimate of the fraction of drug absorbed. *Pharmaceutical Research*, 19(4), 470-476.
- Yasuji, T., Kondo, H., Sako, K., 2012. The effect of food on the oral bioavailability of drugs: a review of current developments and pharmaceutical technologies for pharmacokinetic control. *Therapeutic Delivery*, 3(1), 81-90.

- Zhang, Y., Huo, M., Zhou, J., Xie, S., 2010. PKSolver: An add-in program for pharmacokinetic and pharmacodynamic data analysis in Microsoft Excel. *Computer Methods and Programs in Biomedicine*, 99(3), 306-14.

CHAPTER 8

CONCLUSIONS, RECOMMENDATIONS AND FUTURE OUTLOOK

8.1. CONCLUSIONS

It is highly beneficial to design systems that not only enhance the effectiveness of bioactives, but also seeks to make the treatment plan successful by reducing the pill burden. Complex dosing regimens usually result in poor patient compliance leading to the onset of drug resistance.

This study validated that complexation between humic acid and polyquaternium-10 is possible using the complexation-precipitation (C-P) technique yielding an amorphous polyelectrolyte complex. Drug loading with a BCS class II drug, EFV, was successfully achieved and the C-P method was extended to extrusion-spheronization (E-S) yielding impressive solubility, permeability and biocompatibility results which were preferable to those obtained from C-P. Similarly, encapsulation of RTV into the extruded and spheronized HA-PQ10 produced spheroidal extrudates accompanied by solubility and permeability enhancement compared to the comparator product.

The third technique implemented was 3DP of drug-loaded HA-PQ10 into an oral tablet with an extrusion-based Biplotter®. With this technology, a higher drug loading (50%) was attained. Characterization of the EFV-loaded 3DP tablet revealed that the swelling and drug release kinetics of the 3DP tablet were superior to those synthesized by direct compression. The larger and more numerous pores on the 3DP tablet allowed sufficient fluid-matrix interaction which enhanced the wettability of the encapsulated drug. These differences were attributed to the differences in tableting techniques implemented thus rendering 3DP a cutting edge and promising technique for novel formulations.

The optimal 3DP tablet was a fixed dose combination (FDC) of efavirenz (EFV), tenofovir (TDF) and emtricitabine (FTC) which swelled significantly in simulated intestinal fluid than gastric fluid. The pH responsiveness of the FDC was attributed to the presence of cellulose acetate phthalate (CAP). A versatile drug delivery system, capable of encapsulating and enhancing bioavailability of drugs from all BCS classes, was successfully 3D-Printed into a tablet with higher drug loading than the spheronized extrudates. *In vivo* studies further corroborated the potential for bioavailability enhancement from the FDC. EFV, TDF and FTC

were released in a sustained manner. TDF and FTC had higher plasma concentrations than the conventional FDC, Atripla®.

3DP successfully minimized problems associated with lower drug loading, as well as drug and polymer wastage experienced with the benchtop extrusion process. The shape and size of the formulation could be predetermined and customized. Drug release properties were modified by changing the inner structure pattern to 'enlarge' the tablet porosity. The loading of EFV, TDF and FTC, which belong in different BCS classes, was successful with each drug exhibiting high intestinal absorption properties.

8.2. RECOMMENDATIONS AND FUTURE OUTLOOK

This thesis reports on how a pH responsive tablet was successfully fabricated from the novel HA-PQ10 PEC. The 3D-Printed tablet from cost-effective and biocompatible materials gave impressive outcomes however minor improvements could be made following modifications to the system:

- TDF and FTC had higher maximum drug concentrations reached than from the conventional, after more research, dose reduction could be considered.
- The pig model provided gainful insight into the *in vivo* performance of the 3DP tablet, however, more analysis would need to be conducted in a human model to obtain accurate indications of how the system would work for anti-HIV drug administration.
- The sludge for printing can be further modified to allow individual drugs to be printed in different layers whilst avoiding synthesis of sizable formulations. This would be beneficial in synthesizing FDCs of incompatible drugs, modifying their release kinetics.
- The research reported in this thesis provides techniques that are applicable to other areas of drug delivery. The novel HA-PQ10 PEC can be applied for other drug delivery systems, other than the oral route due to swellability and maintenance of structural integrity subsequently prolonging their drug release profiles.

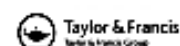
9.1. APPENDIX A

9.1.1. Research Publications

9.1.1.1. Review Paper

Published in ISI rated journal (International Journal of Polymeric Materials and Polymeric Biomaterials)

International Journal of Polymeric Materials and Polymeric Biomaterials, 64: 955–968
 Copyright © 2015 Taylor & Francis Group, LLC
 ISSN: 0091-4037 print/1563-515X online
 DOI: 10.1080/00914037.2015.1058816



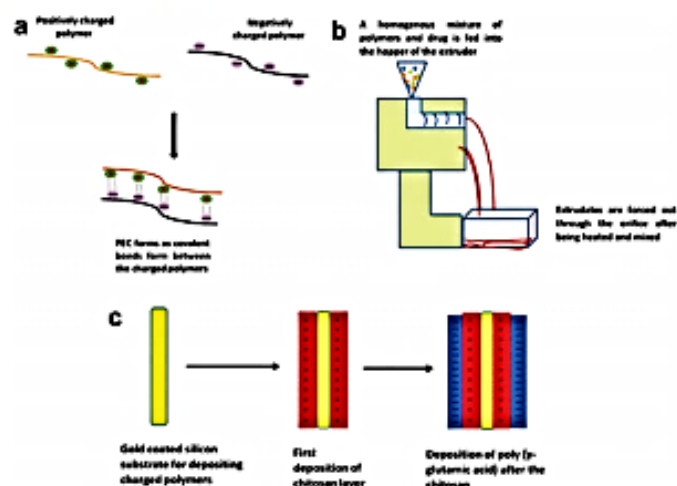
A Review: Overview of Novel Polyelectrolyte Complexes as Prospective Drug Bioavailability Enhancers

MARGARET SIYAWAMWAYA, YAHYA E. CHOONARA, DIVYA BIJUKUMAR, PRADEEP KUMAR, LISA C. DU TOIT, and VINESS PILLAY

Wits Advanced Drug Delivery Platform Research Unit, Department of Pharmacy and Pharmacology, School of Therapeutic Sciences, Faculty of Health Sciences, University of the Witwatersrand, Johannesburg, South Africa

Received 4 December 2014, Accepted 5 April 2015

Polyelectrolyte complexes are novel, emerging polymeric combinations that can impart a variety of applications in the pharmaceutical and biomedical fields. This article reviews various approaches to improve oral bioavailability in systems that utilize polymeric polyelectrolyte complexes (PECs). The present review focuses on various strategies used for the synthesis of PECs, the conditions that have to be met to facilitate their formation and the types of polymers that can be employed in order to synthesize the complexes. This article also offers a concise overview of the mechanisms of drug release and the advancement in drug bioavailability provided by polymeric polyelectrolyte complexes.



Keywords: Bioavailability, controlled drug release, polyelectrolyte complex

Address correspondence to: Viness Pillay, Wits Advanced Drug Delivery Platform Research Unit, Department of Pharmacy and Pharmacology, School of Therapeutic Sciences, Faculty of Health Sciences, University of the Witwatersrand, Johannesburg, 7 York Road, Parktown 2193, South Africa. E-mail: viness.pillay@wits.ac.za

Color versions of one or more of the figures in the article can be found online at www.tandfonline.com/jgpm.

1. Introduction

Polymeric materials which are sensitive to specific conditions such pH, temperature, magnetic and electric fields have become highly attractive in the field of drug delivery [1] and [2]. These transitions are primarily due to the alterations in the charged groups by the interaction of oppositely charged polymers, changes in the efficiency of hydrogen bonding at higher temperature or ionic strength, and they

9.1.1.2. Research Paper 1

Published in ISI rated journal (International Journal of Polymeric Materials and Polymeric Biomaterials)

INTERNATIONAL JOURNAL OF POLYMERIC MATERIALS AND POLYMERIC BIOMATERIALS
2016, VOL. 65, NO. 11, 550–560
<https://dx.doi.org/10.1080/00914037.2016.1149843>



A humic acid-polyquaternium-10 stoichiometric self-assembled fibrilla polyelectrolyte complex: Effect of pH on synthesis, characterization, and drug release

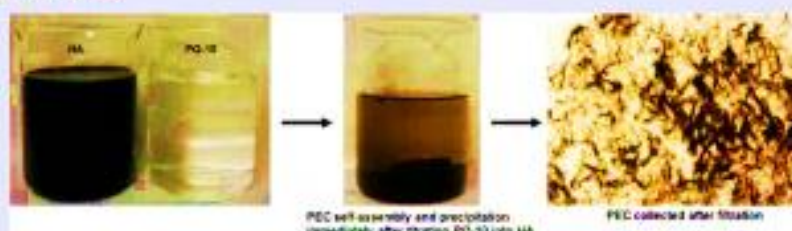
Margaret Siyawamwaya, Yahya E. Choonara, Pradeep Kumar, Pierre P. D. Kondiah, Lisa C. du Toit and Viness Pillay

Wits Advanced Drug Delivery Platform Research Unit, Department of Pharmacy and Pharmacology, School of Therapeutic Sciences, Faculty of Health Sciences, University of the Witwatersrand, Johannesburg, South Africa

ABSTRACT

A polyelectrolyte complex (PEC) was produced and validated from humic acid and polyquaternium-10 using a solution-blend method. Humic acid was used based on its properties of encapsulating hydrophilic and hydrophobic drugs while polyquaternium-10 provided high swellability in aqueous media. PECs at varying pH values were prepared and characterized for their physicochemical properties. Efavirenz (model drug) was used to assess the performance of the PEC. Results revealed that drug-loading ranged between 11.9–23.91% and PEC formation was due to ionic reactions between the amino (polyquaternium-10) and carboxylic (humic acid) groups. This formed a fibrilla PEC complex that provided controlled release of efavirenz.

GRAPHICAL ABSTRACT



ARTICLE HISTORY

Received 3 September 2015
Accepted 31 January 2016

KEYWORDS

Humic acid;
polyquaternium-10;
polyelectrolyte complex;
self-assembly; targeted drug
release

1. Introduction

Polyelectrolyte complexes (PECs) utilize unique properties of polymers involved in the complex and are formed by electrostatic binding between a cation and an anion [1,2]. As previously reported by our group [3], polymers that are readily charged or those that become charged under specific conditions such as certain pH values are a prerequisite for PEC formation. This study utilized the solution mixing method to investigate the possibility of a stoichiometric PEC formation between humic acid (HA) and polyquaternium-10 (PQ-10) with emphasis on the effect of pH of the solution medium on synthesis. It is a well-known fact that pH of the solution medium is one of the parameters which significantly impacts on the PEC formation [4,5]. Stoichiometric polymeric ratios yield insoluble and neutrally charged PECs [6,7].

PQ-10 is a cationic cellulose derivative, which is also known as quaternized hydroxyethylcellulose ethoxylate. It is stipulated that polymers containing quaternary amino groups are promising candidates for biomedical applications since they exhibit diverse chemical properties [8]. They are soluble in both

aqueous and aqueous-alcoholic media. The ammonium group in PQ-10 is situated at the end of the poly (ethylene glycol) chains therefore it possesses a very high affinity for negatively charged groups. During the aggregation process, as the PEC forms, these hydroxyethyl substituents may be included in the complex and thereby contributing to the self-assembly process [9].

Advantages of using PQ-10 include nontoxicity, mucoadhesion, biocompatibility, stability against gastrointestinal enzymes, and the ability to attain a high viscosity upon swelling [10]. An example of a similar polymer is chitosan by which the cationic nature is also attributed to the presence of the ammonium substituents. The ionization of PQ-10 is pH independent unlike that of chitosan. PQ-10 exhibits efficient solubility properties in water and upon dissolving, there is thickening of the medium [9,11]. PQ-10 has been known to form stable complexes with anionic surfactants and this combination is believed to possibly enhance the solubility of hydrophobic drugs [11,12]. Additionally, PQ compounds exhibit antibacterial properties which are facilitated by their penetration enhancing effects [11,13].

CONTACT Viness Pillay viness.pillay@wits.ac.za Wits Advanced Drug Delivery Platform Research Unit, Department of Pharmacy and Pharmacology, School of Therapeutic Sciences, Faculty of Health Sciences, University of the Witwatersrand, Johannesburg, 7 York Road, Parktown 2193, South Africa. Color versions of one or more of the figures in the article can be found online at www.tandfonline.com/gpon.

9.1.1.3. Research Paper 2

Published in ISI rated journal (AAPS PharmSciTech)

AAPS PharmSciTech (© 2017)
DOI: 10.1208/s12249-017-0803-4



Research Article

Synthesis, Comparison, and Optimization of a Humic Acid-Quat10 Polyelectrolyte Complex by Complexation-Precipitation versus Extrusion-Spheronization

Margaret Siyawanwaya,¹ Yahya E. Choonara,¹ Pradeep Kumar,¹ Pierre P. D. Kondiah,¹ Lisa C. du Toit,¹ and Viness Pillay^{1,2}

Received 21 November 2016; accepted 3 May 2017

Abstract. A novel humic acid and polyquaternium-10 polyelectrolyte complex (PEC) was synthesized utilizing two methods and the solubility and permeability of efavirenz (EFV) were established. Complexation-precipitation and extrusion-spheronization were used to synthesize and compare the drug-loaded PECs. The chemical integrity, thermo-mechanical differences, and morphology between the drug-loaded PECs produced by the two methods were assessed by attenuated total reflectance-Fourier transform infrared, differential scanning calorimetry, and SEM. The extent of drug solubilization was determined using the saturation solubility test while the biocompatibility of both PECs was confirmed by cytotoxicity studies on human adenocarcinoma cells (caco2). Bio-relevant media was used for the solubility and permeability analysis of the optimized PEC formulations for accurate assessment of formulation performance. Ritonavir (RTV) was loaded into the optimized formulation to further corroborate the impact of the PEC on the solubility and permeability properties of a poorly soluble and poorly permeable drug. The optimized EFV-loaded PEC and the RTV-loaded PEC exhibited $14.16 \pm 2.81\%$ and $4.39 \pm 0.57\%$ increase in solubility, respectively. Both PECs were compared to currently marketed formulations. Intestinal permeation results revealed an enhancement of $61.24 \pm 6.92\%$ for EFV and $38.78 \pm 0.50\%$ for RTV. Although both fabrication methods produced PECs that enhanced the solubility and permeability of the model Biopharmaceutics Classification System Class II and IV drugs, extrusion-spheronization was selected as most optimal based on the higher solubility and permeability improvement and the impact on caco2 cell viability.

KEY WORDS: polyelectrolyte complex; humic acid and polyquaternium-10; complexation-precipitation; extrusion-spheronization; efavirenz; ritonavir.

INTRODUCTION

The humic acid (HA) and polyquaternium-10 (PQ10) polyelectrolyte complex (PEC) was explored in order to benefit from the synergistic effect of using a polymeric complex contrary to the individual polymers. The novel HA-PQ10 PEC, previously reported (1), was investigated further for the purposes of comparing properties of the complexes synthesized by two different methods. The high

affinity for negatively charged groups that is exhibited by PQ10 can be attributed to the presence of the quaternary amino groups. Our previous study revealed that this molecule formed a polyelectrolyte complex with HA, a macromolecule which is classified as an anionic polyelectrolyte. In this study, commercial brown HA and PQ10 of 656.1 g/mol were utilized (1). It is essential to identify a simplified and cost-effective method of PEC fabrication applicable to contemporary dosage form design. Solid dispersions were synthesized using the complexation-precipitation (C-P) and extrusion-spheronization (E-S) approaches. Solid dispersions have been known to enhance the bioavailability of drugs (2). Dispersion of the drug within a matrix prevents agglomeration of the drug while encouraging its solubility. These dispersions are also responsible for increasing the surface area of the drug, therefore enhancing the wettability of the bioactive (3). However, the main drawback of solid dispersions is the tendency of the drug to recrystallize due to the metastable properties of the amorphous formulation (4,5).

Electronic supplementary material The online version of this article (doi:10.1208/s12249-017-0803-4) contains supplementary material, which is available to authorized users.

¹ Wits Advanced Drug Delivery Platform Research Unit, Department of Pharmacy and Pharmacology, School of Therapeutic Sciences, Faculty of Health Sciences, University of the Witwatersrand, Johannesburg, 7 York Road, Parktown, 2193, South Africa.

² To whom correspondence should be addressed. (e-mail: viness.pillay@wits.ac.za)

9.2. APPENDIX B

9.2.1. Abstracts of Research Outputs at Conference Proceedings

9.2.1.1. *The Academy of Pharmaceutical Sciences of the Pharmaceutical Society of South Africa (APSSA) Conference, Cedar Woods of Sandton, Conference Centre, Johannesburg, South Africa, 2015. (Poster Presentation).*

Humic acid/polyquaternium-10 novel stoichiometric self-assembled fibrous polyelectrolyte complex

Margaret Siyawamwaya, Viness Pillay, Yahya E. Choonara, Pradeep Kumar, Pierre P.D Kondiah and Lisa C. Du Toit.

Department of Pharmacy and Pharmacology, Faculty of Health Sciences, University of the Witwatersrand, 7 York Road, Parktown, 2193, Johannesburg, South Africa.

The formation of a novel polyelectrolyte complex (PEC) between humic acid (HA) and polyquaternium-10 (PQ-10) was investigated and validated. The solution mixing method was utilized to investigate the impact of the formation of a PEC at pH 6.0, 7.0 and 8.0. The stoichiometric self-assembly between the polymers occurred when 140 mg of HA reacted with 141 mg of PQ-10. Attenuated Total Reflectance-Fourier Transform Infrared (ATR-FTIR), powder X-ray diffraction (XRD), scanning electron microscopy (SEM), differential scanning calorimetry (DSC) and thermogravimetric analysis (TGA) were pertinent methods employed for characterization. The drug release potential of the complex was investigated after a drug falling in Biopharmaceutics Classification System (BCS) class II was loaded into the complexes. The complexation ability of the two polymers can be attributed to their complementary charges that facilitated spontaneous formation of the electrostatic bonds between amino groups in PQ-10 and carboxylic groups in HA leading to the formation of a self-assembled “fibrilla” architecture. The % drug loading for the PECs at pH 6.0, 7.0 and 8.0 were 23.91%, 14.27% and 11.9% respectively. The complex is applicable for the delivery of lipophilic drugs such as EFV through entrapping them in the hydrophobic core of HA. The study conclusively revealed that ionic interactions occurred between HA and PQ-10 leading to the formation of a new “fibrilla” complex that can be implemented for targeted drug release purposes.

9.2.1.2. The 7th Cross Faculty Post Graduate Symposium, University of the Witwatersrand, Johannesburg, South Africa, 2016. (Poster Presentation).

Humic acid/polyquaternium-10 novel stoichiometric self-assembled fibrous polyelectrolyte complex: synthesis, characterization and drug release

Margaret Siyawamwaya, Viness Pillay, Yahya E. Choonara, Pradeep Kumar, Pierre P.D Kondiah and Lisa C. Du Toit.

Department of Pharmacy and Pharmacology, Faculty of Health Sciences, University of the Witwatersrand, 7 York Road, Parktown, 2193, Johannesburg, South Africa.

The formation of a novel polyelectrolyte complex (PEC) between humic acid (HA) and polyquaternium-10 (PQ-10) was investigated and validated. The solution mixing method was utilized to investigate the formation of a PEC at pH 6.0, 7.0 and 8.0. The stoichiometric self-assembly between the polymers occurred when 140 mg of HA reacted with 141 mg of PQ-10. Attenuated Total Reflectance-Fourier Transform Infrared (ATR-FTIR), powder X-ray diffraction (XRD), scanning electron microscopy (SEM), differential scanning calorimetry (DSC) and thermogravimetric analysis (TGA) were pertinent methods employed for characterization. The drug release potential of the complex was investigated after a drug falling in Biopharmaceutics Classification System (BCS) class II was loaded into the complexes. The % drug loading for the PECs at pH 6.0, 7.0 and 8.0 were 23.91%, 14.27% and 11.9% respectively. The study conclusively revealed that ionic interactions occurred between the HA and PQ-10 leading to the formation of a new “fibrilla” complex that can be utilized for the enhancement of bioavailability of drugs as well as for their targeted release purposes.

9.2.1.3. The Faculty of Health Sciences Research Day, University of the Witwatersrand, Johannesburg, South Africa, 2016. (Poster Presentation).

The use of a novel polyelectrolyte complex to enhance the aqueous solubility of a BCS class II anti-HIV drug

Margaret Siyawamwaya, Viness Pillay, Yahya E. Choonara, Pradeep Kumar, Pierre P.D Kondiah and Lisa C. Du Toit.

Department of Pharmacy and Pharmacology, Faculty of Health Sciences, University of the Witwatersrand, 7 York Road, Parktown, 2193, Johannesburg, South Africa.

Poor *in vivo* bioavailability of drugs in Biopharmaceutics Classification System (BCS) class II remains a cause for concern in anti-HIV therapy. It is imperative to enhance the bioavailability of these drugs in order to circumvent the need for large doses which leads to toxicity in the body. A novel polyelectrolyte complex was utilized to improve the solubility and therefore, the bioavailability, of a poorly water soluble anti-HIV drug, efavirenz, which has a bioavailability of 40-45%. Solid dispersions of the drug in the polyelectrolyte complex were synthesized. Characterization of the drug and polymeric complex were undertaken with the aid of Attenuated Total Reflectance-Fourier Transform Infrared (ATR-FTIR), scanning electron microscopy (SEM) and differential scanning calorimetry (DSC). Human colorectal adenocarcinoma (Caco2) cell line viability test was conducted to determine the biocompatibility of the system. Any cytotoxicity caused by the efavirenz loaded complex over the 24 hour test period was measured and quantified. In order to determine any increase in solubility and therefore bioavailability of the drug entrapped in the complex, a saturation solubility study was carried out. The complexation ability of the two polymers was attributed to their complementary charges that resulted in the formation of the electrostatic bonds between the polymers. Efavirenz was successfully dispersed and entrapped in the polyelectrolyte complex. The study conclusively revealed that the solubility of efavirenz loaded into the optimized polyelectrolyte complex was superior by 14.16% to that of the comparator product tested in simulated human gastrointestinal fluid.

9.2.1.4. The International AAPS Annual Meeting and Exposition, Colorado Convention Centre, Denver, Colorado, USA, 2016. (Poster Presentation).

3D Printing of a Novel Humic Acid and Polyquaternium-10 Polyelectrolyte Complex for Oral Controlled Drug Release Application

Margaret Siyawamwaya, Viness Pillay, Yahya E. Choonara, Pradeep Kumar, Pierre P.D Kondiah and Lisa C. Du Toit.

Department of Pharmacy and Pharmacology, Faculty of Health Sciences, University of the Witwatersrand, 7 York Road, Parktown, 2193, Johannesburg, South Africa.

3D printing is revolutionizing the design of drug delivery systems. The purpose of this study was to utilize 3D printing to fabricate a novel humic acid-polyquaternium-10 polyelectrolyte complex (HA/PQ-10 PEC) to increase the bioavailability of efavirenz. Optimal 3D printing parameters for the HA/PQ-10 PEC were identified. By using the 3D Bioplotter®, the stability of the amorphous solid dispersion system and efavirenz loading was enhanced. The *in vitro* drug release properties could be altered by changing the porosity of the tablet via varying the printing design. 3D printing of the HA/PQ-10 PEC was achieved by initially allowing the native polymers to complex thus forming a printable sludge that was extruded from the low temperature sample holder of the 3D Bioplotter® (EnvisionTEC GmbH, Gladbeck, Germany). Microcrystalline cellulose (MCC) was added as a binder to the HA/PQ-10 PEC sludge to facilitate solidification after extrusion. Swelling of the PEC was evaluated by placing the pre-weighed efavirenz tablets in 900mL of simulated intestinal fluid (SIF)(pH 6.8).

The USP apparatus II paddle stirrer (Erweka DT 700, Erweka GmbH, Heusenstamm, Germany) (50rpm) was utilized and temperature was maintained at 37°C. Tablets were reweighed periodically over 24 hours to determine the extent of swelling. Other pertinent tests undertaken included measurement of the viscosity of the optimal printable sludge by rheological analysis (ThermoHaake MARS Modular Advanced Rheometer, Thermo Electron, Karlsruhe, Germany). The mechanical strength of the 3D printed tablets was measured using a BioTester 5000 test system (CellScale Biomaterials Testing, ON, Canada). Drug release studies were conducted to further corroborate the controlled release properties of the drug-loaded 3D printed HA/PQ-10 PEC. The HA/PQ-10 PEC was successfully printed in 3D at 25°C. Suitable operation parameters were a speed of 20mm/s and a pressure of 2.5 bars. It was pertinent to first form a highly viscous sludge of the PQ-10 before adding the HA powder. Complexation occurred immediately. The tablet swelled in SIF to a maximum of 353.3% after 4 hours and the swelling slowly decreased over the 24 hour test period. Rheological studies revealed an elevated viscosity of the PEC sludge (45 950mPa.s) compared to that for the initial PQ-10 paste (2904mPa.s). This increase in viscosity was attributed to the HA/PQ-10 electro-association leading to complexation. These results validate the potential of the drug delivery system to control drug release over 24 hours. The results obtained indicate that the novel HA/PQ-10 PEC can undergo 3D printing with potential for application in controlled drug release systems. Findings of this study also suggest that highly soluble drugs from BCS class I and III may also be loaded into the HA/PQ-10 PEC for controlled release due to the synthesis of a swellable system.

9.3. APPENDIX C

9.3.1. Animal Ethics Approval



STRICTLY CONFIDENTIAL

ANIMAL ETHICS SCREENING COMMITTEE (AESC)

CLEARANCE CERTIFICATE NO. 2014/38/C

INVESTIGATORS: Prof V Pillay

CO-INVESTIGATORS (For postgraduate degree purposes): Ms B Choonara
Ms M Siyawamwaya
Mr M Sithole

SCHOOL: Pharmacy & Pharmacology

LOCATION: Faculty of Health Sciences

PROJECT TITLE: *In vivo assessment of innovative polymeric oral drug delivery systems in large White Pigs*

Number and Species

18 Large White Pigs

Approval was given for to the use of animals for the project described above at an AESC meeting held on 24 June 2014 . This approval remains valid until 23 June 2016.

The use of these animals is subject to AESC guidelines for the use and care of animals, is limited to the procedures described in the application form and is subject to any additional conditions listed below.

None.

Signed: _____ Date: 1/7/2014
(Chairperson, AESC)

I am satisfied that the persons listed in this application are competent to perform the procedures therein, in terms of Section 23 (1) (c) of the Veterinary and Para-Veterinary Professions Act (19 of 1982)

Signed: _____ Date: 27 June 2014
(Registered Veterinarian)

cc: Supervisor: N/A
Director: CAS

Works 2000/1air0015/AESCCert.wps